

ISSN - 0132-1447

საქართველოს
მეცნიერებათა
აкадеმიის
ბიულეტენი

GEORGIAN NATIONAL ACADEMY OF SCIENCES

საქართველოს მეცნიერებათა ეროვნული აკადემია



Bulletin

524 / 2
2012

ბულეტენი

New Series

vol. 6, no. 2

MAY-JUNE-JULY-AUGUST

2012

ტ. 6, № 2

მაისი-ივნისი-ივლისი-აგვისტო



GEORGIAN ACADEMY PRESS
TBILISI



«საქართველოს მეცნიერებათა ეროვნული აკადემიის მოამბე»

«BULLETIN OF THE GEORGIAN NATIONAL ACADEMY OF SCIENCES»

Scientific Journal Appearing in English & Georgian in Three Issues Annually

Founded in 1940

Editor-in-Chief

Th. V. Gamkrelidze
President

Associate Editors:

Vice Presidents

G. Tevzadze, Fr. Todua,
Academician-Secretary
O. Natishvili



სარედაქციო საბჭო EDITORIAL COUNCIL

Zhores I Alfërov, *St. Petersburg*
(Physics)
Winfried EH Blum *Vienna*
(Soil Science)
Leonid A Bokeria, *Moscow*
(Cardiovascular Surgery)
Mikhail Davydov *Moscow*
(Oncology)
Georgi Dvali *New York, NY*
(Theoretical Physics)
Revaz Gamkrelidze *Moscow*
(Mathematics)
Jost Gippert *Frankfurt*
(Comparative Linguistics)
Alice C Harris, *Stony Brook NY USA*
(Linguistics)
György Hazai *Budapest*
(Oriental Studies)
Friedrich Hirzebruch *Bonn*
(Mathematics)
Günter Hotz *Saarbrücken*
(Computer & Information Sciences)
Vyacheslav V Ivanov *Los Angeles Cal USA*
(Semiotics, Cultural History)
Nicholas Kipshidze, *New York, NY*
(Experimental Medicine)
Theo Kobusch *Bonn*
(Philosophy)
Herbert Mang, *Vienna*
(Engineering & Technical Sciences)

Mortimer Mishkin *Bethesda, Md., USA*
(Cognitive Neuroscience)
Georgi Muskhelishvili, *Bremen*
(Molecular Genetics)
Boris Paton *Kiev*
(Metallurgy & Metal Technologies)
David Prangishvili, *Paris*
(Microbiology, Virology)
Peter L. Privalov, *Baltimore, Md., USA*
(Molecular Biology, Biophysics)
Peter H. Raven *St. Louis, Mo., USA*
(Plant Biology)
Colin Renfrew *Cambridge, UK*
(Archaeological Science)
Roald Z. Sagdeev *College Park, Md., USA*
(Geophysics)
Karl Horst Schmidt *Bonn*
(Indo-European & Caucasian Studies)
Gela G. Tevzadze† *Chicago*
(Molecular Genetics)
Zurab Tsereteli, *Moscow*
(Arts)
Aslan Tsivadze, *Moscow*
(Chemical Sciences)
Richard Villems, *Tallinn*
(Molecular Biology, Genetics)

სარედაქციო კოლეგია EDITORIAL BOARD

Members of the Academy:

L. Aleksidze, T. Andronikashvili, T. Beridze, N. Berikashvili, G. Chogovadze, I. Gamkrelidze, T. Ioseliani, K. Japaridze, O. Japaridze, N. Javakhishvili, E. Kemertelidze, M. Khananashvili, G. Kharadze, I. Kiguradze, N. Kipshidze, T. Kopaleishvili, G. Kvesitadze, M. Lordkipanidze, R. Metreveli, D. Muskhelishvili, T. Oniani, M. Salukvadze, G. Sanadze, N. Tsintsadze, G. Tsitsishvili, N. Vakhania, M. Zaalishvili, I. Zhordania

Publisher: Loudmila Gverdtsteli



Text Editor: Arrian Tchanturia

Bulletin of the Georgian National Academy of Sciences presents the Proceedings of the Georgian Academy in different fields of Science and Technology: Mathematical & Physical Sciences, Geology & Chemical Sciences, Biological & Medical Sciences, Engineering & Applied Sciences, Agricultural & Environmental Sciences, Humanities & Social Sciences, etc.

Copyright © by the Georgian National Academy of Sciences

TABLE OF CONTENTS

შინაარსი

Mathematics & Physical Sciences

მათემატიკა & ფიზიკური მეცნიერებანი

MATHEMATICS

მათემატიკა

Elizbar Nadaraya, Petre Babilua, Mzevinar Patsatsia
On One Nonparametric Estimate of a Bernoulli Regression Function

ე. ნადარაია, პ. ბაბილუა, მ. ფაცაცია
ბერნულის რეგრესიის ფუნქციის ერთი არაპარამეტრული შეფასების შესახებ

Nina Danelia and Vakhtang Kokilashvili
On the Approximation of Periodic Functions within the Frame of Grand Lebesgue Spaces

ნ. დანელია, ვ. კოკილაშვილი
პერიოდული ფუნქციების მიაზლოების შესახებ გრანდ ლეგესის სივრცეების ჩარჩოებში

Giorgi Khimshiashvili
Maxwell Conjecture and Polygonal Linkages

გ. ხიმშიაშვილი
მაქსველის ჰიპოთეზა და სახსრული მრავალკუთხედები

Gigla Oniani and Giorgi Tervadze
On Analytic and Harmonic Functions with a Dirichlet Finite Integral in the Unit Circle

გ. ა. ონიანი, გ. თეთვაძე
დრიხლეს სასრული ინტეგრალის მქონე ანალიზური და პარმონიული ფუნქციების შესახებ ერთეულიდან წრეში

Giorgi Oniani
On the Regular Convergence by Rectangles of Multiple Fourier-Haar Series

გ. ონიანი
ფურიე-ჰარის ჯერადი მწკრივების მართკუთხედების მიხედვით რეგულარული კრებალობის შესახებ

Pikria Ghurtskaia and Dazmir Shulaia
Singular Integral Equation Arising from the Theory of the Penetration of Gamma Rays

ფ. ლურწყაია, დ. შულაია
გამა სხივების გაჭოლის თეორიიდან წარმოქმნილი სინგულარული ინტეგრალური განტოლება

STRUCTURAL MECHANICS
სამშენებლო მექანიკა

Guram Gabrichidze
One Mathematical Model and Algorithm of the Microtremor Use for Structure Real Seismic Resource Assessment

გ. გაბრიჩიძე
ნაკებობის რეალური სეისმური რესურსის შესაფასებლად სუსტი რყევების გამოყენების ერთი მათემატიკური მოდელი და ალგორითმი

PHYSICS
ფიზიკა

Giorgi Baramidze and Giorgi Kharadze
On Quantum Description of Parametric Instability of Coherently Precessing Spin Mode of Superfluid ⁴He-A

გ. ბარამიძე, გ. ხარაძე
ზუღუნად ⁴He-A-ში კოპერენტული სპინური პრეცესიის პარამეტრული არამდგრადობის კვანტური აღწერა

Niko Avalishvili, George I. Japaridze, David Nozadze, Saeed Mahdaviyar
Magnetization Plateau in the Spin S=1/2 Two-Leg Ladder with Trimer Modulation of the Rung-Exchange

Contents

ნ. ავალიშვილი, გ. ვაფარაძე, დ. ნოზაძე,
ს. მაკდაფეიფარი
დამაკონტებულობის პლატოები კიბის
სტრუქტურის მქონე $S=1/2$ სპინურ ჯაჭვში
“საფებურის” გასწვრივ გაცვლის ტრიმერული
მოლეულაციის შემთხვევაში

Natela Namoradze and Ioseb Ratishvili
**Ordering Effects in the Heat Capacity of
Light Rare-Earth Superstoichiometric
Dihydrides. $CeH_{2.36}$**

ნ. ნამორაძე, ი. რატიშვილი
მონწერიგების ეფექტები მსუბუქ იშვიათ მიწათა
ზესტეციომეტრიულ დიბიდრიდების
სითბოტეკადობაში. $CeH_{2.36}$

*Badri Chiladze, Nodar Lomidze,
Mikhail Nioradze, Alexandr Sidelnikov,
Igor Trekov*

**Application of Cherenkov Effect to Increase
the Safety of Nuclear Plants**

ბ. ჭილაძე, ნ. ლომიძე, მ. ნიორაძე,
ა. სიდელნიკოვი, ი. ტრეკოვი
ჩერენკოვის ეფექტის გამოყენება ბირთვული
ენერგეტიკის უსაფრთხოების ასამაღლებლად

GEOFYSICS
გეოფიზიკა

Irakli G. Shekrladze
**Preventing Severe Convective Storm:
Anticipatory Restratification of
Lower Atmosphere**

ი. შეკრილაძე
მძლავრი კონვექციური შტორმის პრევენცია:
ატმოსფეროს ქვედაფენის წინმსწრები
გადასტრათიფიცირება

Demuri Demetrashvili and Diana Kvaratskhelia
**Numerical Study of the Vertical Hydrological
Structure of the Black Sea under Transitive
Climatic Forcing Conditions**

დ. დემეტრაშვილი, დ. კვარაცხელია
შავი ზღვის ჰიდროლოგიური ვერტიკალური
სტრუქტურის რიცხვითი გამოკვლევა
გარდამავალი ატმოსფერული კლიმატური
ზემოქმედების პირობებში

PHYSICAL CHEMISTRY
ფიზიკური ქიმია

*George Chubinidze, Ia Kurashvili,
Guram Bokuchava, Zurab Chachkhiani,
George Darsavelidze*

**Dynamical Mechanical Properties of
Boron-Doped Monocrystalline Germanium** 89
გ. ჩუბინიძე, ი. კურაშვილი, გ. ბოკუჩავა,
ზ. ჩაჩხიანი, გ. დარსაველიძე
ბორით ლეგირებული მონოკრისტალური
გერმანიუმის დინამიური მექანიკური
თვისებები 92

CHEMICAL TECHNOLOGY
ქიმიური ტექნოლოგია

*Zurab Mirijanashvili, Giorgi Tavadze,
Vazha Gharibashvili, Alexandre Kandelaki*
**Study of the Process of Obtaining Metal
Chlorides from Materials Containing Tungsten** 94

ზ. მირიჯანაშვილი, გ. თაყაძე,
ვ. ღარიბაშვილი, ა. კანდელაკი
ვოლფრამის შემცველი მასალებიდან
შემადგენელ ლითონთა ქლორიდების
მიღების პროცესის კვლევა 99

GEOLOGY
გეოლოგია

Ferando D. Maisadze
**Duration of Mesozoic Orogenies
(on the Example of Georgia)** 100

ფ. მაისაძე
მეზოზოური ოროგენული ფაზისების
ხანგრძლივობა (საქართველოს მაგალითზე) 109

Biological Sciences
ბიოლოგიური მეცნიერებანი

PLANT GROWING
მეცენარეობა

*Teimuraz Andronikashvili, Marine Zautashvili,
Luba Eprikashvili, Nino Burkiashvili,
Nino Pirtskhalava*
**Natural Zeolite – One of the Possibilities
of Transition from Chemical to Biological
Agronomy** 111

Contents

თ. ანდრონიკაშვილი, მ. ზაუტაშვილი,
ლ. ეპრიკაშვილი, ნ. ბურკიაშვილი,
ნ. ფორცხაღაჯა
ბუნებრივი ცეოლითები - ქიმიური
აგრონომიიდან ბიოლოგიურზე
გადასვლის ერთ-ერთი შესაძლებლობა

GENETICS AND SELECTION
ბენეტიკა და სელექცია

*Petre Naskidashvili, Gulnari Chkhutashvili,
David Bedoshvili, Maka Naskidashvili*
"Gorda" - a New Short-Stemmed Botanical
and Genetic Variety of Soft Wheat (*Triticum
aestivum* L.) Developed by Induced
Mutagenesis

117

პ. ნასყიდაშვილი, ვ. ჩხუტაშვილი,
დ. ბედოშვილი, მ. ნასყიდაშვილი
რბილი ზორბლის (*T. aestivum* L.) ინდუცირებული
მოკლეღეროიანი ახალი ბოტანიკური და
გენეტიკური ფორმა „გორდა“

134

137

BIOCHEMISTRY
ბიოქიმია

*Nino Dumbadze, Nugzar Aleksidze,
Giorgi Alexidze*
Isolation and Biochemical Characterization
of Mannose-Specific Lectin from Georgian
Endemic Plant *Polygonatum obtusifolium*
Misc. rhizomes

119

ნ. დუმბაძე, ნ. ალექსიძე, ვ. ალექსიძე
საქართველოს ენდემური მცენარე
სვინტრიდან (*Polygonatum obtusifolium* Misc.)
მანოზა-სპეციფიკური ლექტინის გამოყოფა და
ბიოქიმიური დახასიათება

124

PALAEOBIOLOGY
პალეობიოლოგია

*Irina Shatilova, Lamara Maissuradze,
Irma Kokolashvili, Kakhaber Koiava*
The Comparison of the Results of
Palynological and Microfaunistic
Investigations of the Sarmatian
Deposits of Eastern Georgia

138

ZOOLOGY
ზოოლოგია

*Oleg Gorgadze, Andreas Schmidt-Rhaesa,
Numu Kintsurashvili*
New Data on Georgian Species of Freshwater
Horsehair Worms (Nematomorpha: Gordiida)

125

ო. გორგაძე, ა. შმიდტ-რეზა, ნ. კინსურაშვილი
ახალი მონაცემები საქართველოს მტკნარი
წვლის ბწევრების (Nematomorpha: Gordiida)
შესახებ

128

ი. შატილოვა, ლ. მაისურაძე,
ი. კოკოლაშვილი, კ. კოიავა
აღმოსავლეთ საქართველოს სარმატული
ნალექების პალეობიოლოგიური და
მიკროფაუნისტური კვლევის შედეგების
შეპირისპირება

143

PARASITOLOGY AND HELMINTHOLOGY
პარაზიტოლოგია და ჰელმინთოლოგია

*Ketevan Nikolaishvili, Tsitsino Lomidze,
Lali Murvanidze*
Arginase in the Organs of Water Snake
(*Natrix tessellata*, Laurenti, 1768) and Cestode
(*Ophiothaenia europaea*, Odening, 1963)
Parasitizing in it

129

ქ. ნიკოლაიშვილი, ც. ლომიძე, ლ. მურვანიძე
წვლის ანკარას (*Natrix tessellata*, Laurenti, 1768)
ორგანოებში და ცესტოდაში (*Ophiothaenia
europaea*, Odening, 1963) ფერმენტ არგინაზას
აქტიუობის შესახებ

132

MEDICAL SCIENCES
სამედიცინო მეცნიერება

Fridon Todua and Dudana Gachechiladze
Brain Structural-Hemodynamic Changes
in Patients with Potential Cardiac Source
of Embolism

145

ფ. თოდუა, დ. გაჩეჩილაძე
თავის ტვინის სტრუქტურულ-ჰემოდინამიკური
ცვლილებები კარდიოგენული ემბოლიის
წყაროს მქონე პირებში

151

Humanities & Social Studies

ჰუმანიტარული და სოციალური მეცნიერებანი

ARCHAEOLOGY

არქეოლოგია

Konstantine Pitshkelauri

Uruk Migrants in the Caucasus

153

კ. ფიცხელაური

ურუქელი მიგრანტები კავკასიაში

159

ECONOMICS

ეკონომიკა

Iuri Ananiashvili and Vladimer Papava

**Impact of the Average Tax Rate
on the Aggregate Demand**

(Keynesian Models)

162

ი. ანანიაშვილი, ვ. პაპავა

**გასაშუალოებული საგადასახადო ტვირთის
ზეგუელენა ერთობლივ მოთხოვნაზე
(კეინზიანური მოდელები)**

169

Alexander Tvalchrelidze and Avtandil Silagadze

**Capitalization of Mineral Commodities
– World and Georgian Experiences**

170

ა. თვალჭრელიძე, ა. სილაგაძე

**მინერალური ნედლეულის კაპიტალიზაცია –
მსოფლიო და ქართული გამოცდილება**

173

HISTORY

ისტორია

Werner Seibt

**The Byzantine Thema of Soteroupolis-Anakopia
in the 11th Century**

174

ვ. ზაიბტი

**სოტერუპოლის-ანაკოფის ბიზანტიური თემა
XI საუკუნეში**

176

Mathematics

On One Nonparametric Estimate of a Bernoulli Regression Function

Elizbar Nadaraya*, Petre Babilua**, Mzevinar Patsatsia†

* Academy Member, Department of Exact and Natural Sciences, I. Javakishvili Tbilisi State University

**Department of Exact and Natural Sciences, I. Javakishvili Tbilisi State University

† Sokhumi State University, Department of Mathematics and Computer Sciences, Tbilisi

ABSTRACT. We consider the class of nonparametric estimates of a Bernoulli regression function. We establish the conditions of uniform consistency and give the limit theorems for continuous functionals connected with the functions on $C[a,1-a]$, $0 < a < 1/2$. © 2012 Bull. Georg. Natl. Acad. Sci.

Key words: Bernoulli regression function, kernel type estimate, asymptotic unbiasedness, consistency, Wiener process.

Let a random variable Y take two values 1 and 0 with probabilities p ("success") and $1-p$ ("failure"). Assume that the probability of "success" p is a function of an independent variable $x \in [0,1]$, i.e. $p = p(x) = P\{Y = 1 | x\}$ ([1-3]). Let x_i , $i = \overline{1, n}$ be the division points of the interval $[0,1]$ which are chosen from the relation

$$H(x_i) = \int_0^{x_i} h(u) du = \frac{2i-1}{2n}, \quad i = \overline{1, n},$$

where $h(x)$ is the known positive distribution density on $[0,1]$. Let further Y_i , $i = \overline{1, n}$, be independent Bernoulli random variables with $P\{Y_i = 1 | x_i\} = p(x_i)$, $P\{Y_i = 0 | x_i\} = 1 - p(x_i)$. The problem consists in estimating the function $p(x)$, $x \in [0,1]$, by the sampling Y_1, Y_2, \dots, Y_n . Such problems arise in particular in biology ([1, 3]), in corrosion studies [4] and so on.

As an estimate for $p(x)$ we consider a statistic ([5, 6]) of the form

$$\hat{p}_n(x) = p_{1n}(x) p_{2n}^{-1}(x), \quad (1)$$

$$p_{\nu n}(x) = \frac{1}{nb_n} \sum_{i=1}^n h^{-1}(x_i) K\left(\frac{x-x_i}{b_n}\right) Y_i^{2-\nu}, \quad \nu = 1, 2,$$

where $K(x) \geq 0$ is some distribution density (kernel), $K(x) = K(-x)$, $x \in (-\infty, \infty)$, $\{b_n\}$ is a sequence of positive numbers converging to zero.



Lemma 1. Assume that

1^o. $K(x)$ is a function of bounded variation.

2^o. $p(x)$ and $h(x)$ are also functions of bounded variation on $[0,1]$, and $h(x) \geq \mu > 0$, $x \in [0,1]$.

If $nb_n \rightarrow \infty$, then

$$\frac{1}{nb_n} \sum_{i=1}^n K^{v_i} \left(\frac{x-x_i}{b_n} \right) p^{v_i}(x_i) h^{-v_i}(x_i) = \frac{1}{b_n} \int_0^1 K^{v_i} \left(\frac{x-u}{b_n} \right) p^{v_i}(u) h^{-v_i+1}(u) du + O\left(\frac{1}{nb_n} \right), \quad (2)$$

uniformly with respect to $x \in [0,1]$, $v_i \in N \cup \{0\}$, $i = \overline{1,3}$.

Proof. Let $H_n(x)$ be an empirical distribution function of the "sampling" x_1, x_2, \dots, x_n , i.e.

$$H_n(x) = n^{-1} \sum_{i=1}^n I(x_i < x)$$

It can be easily verified that

$$\sup_{0 \leq x \leq 1} |H_n(x) - H(x)| = \sup_{0 \leq x \leq 1} \left| \frac{1}{n} \left[nH\left(x + \frac{1}{2}\right) - H(x) \right] \right| \leq \frac{1}{2n}. \quad (3)$$

We have

$$\begin{aligned} \frac{1}{nb_n} \sum_{i=1}^n K^{v_i} \left(\frac{x-x_i}{b_n} \right) p^{v_i}(x_i) h^{-v_i}(x_i) - \frac{1}{b_n} \int_0^1 K^{v_i} \left(\frac{x-u}{b_n} \right) p^{v_i}(u) h^{-v_i+1}(u) du = \\ = \frac{1}{b_n} \int_0^1 K^{v_i} \left(\frac{x-u}{b_n} \right) p^{v_i}(u) h^{-v_i}(u) d[H_n(u) - H(u)]. \end{aligned} \quad (4)$$

Applying the integration by parts formula to the right-hand part of (4) and taking (3) into account, we obtain (2).

Theorem 1. Let the conditions of Lemma 1 be fulfilled. Then the estimate (1) is asymptotically unbiased and consistent at all points $x \in [0,1]$, where $p(x)$ is continuous. Moreover, it has an asymptotically normal distribution, i.e.

$$\begin{aligned} \sqrt{nb_n} (\hat{p}_n(x) - E\hat{p}_n(x)) \sigma^{-1}(x) \xrightarrow{d} N(0,1), \\ \sigma^2(x) = \frac{p(x)(1-p(x))}{h(x)} \int K^2(u) du, \end{aligned}$$

where $p(x)$ is continuous.

The proof of the theorem with the aid of Lemma 1 is analogous to the proof of Theorem 1 in [7].

Theorem 2. Let $K(x)$ satisfy condition 1^o of Lemma 1 and, besides, $\varphi(t) = \int e^{itx} K(x) dx$ be absolutely integrable; then the functions $p(x)$ and $h(x)$ are continuous and satisfy condition 2^o of Lemma 1.

(a) Let $nb_n^2 \rightarrow \infty$, then

$$D_n = \sup_{x \in \Omega_n} |\hat{p}_n(x) - p(x)| \xrightarrow{P} 0, \quad \Omega_n = [b_n^\alpha, 1 - b_n^\alpha], \quad 0 < \alpha < 1.$$

(b) If $\sum_{n=1}^{\infty} n^{-s/2} b_n^{-s} < \infty$, $s > 2$, then $D_n \rightarrow 0$ a.s.

Proof. Using Whittle's inequality [8] for moments of quadratic form, it can be shown [7] that

$$P \left\{ \sup_{x \in \Omega_n} |\hat{p}_n(x) - E\hat{p}_n(x)| \geq \varepsilon \right\} \leq \frac{c_1}{\varepsilon^s (\sqrt{n} b_n)^s}, \quad s > 2, \quad \varepsilon > 0. \quad (5)$$

Furthermore, by virtue of Lemma 1,

$$p_{2n}(x) = \frac{1}{b_n} \int_0^1 K \left(\frac{x-u}{b_n} \right) du + O \left(\frac{1}{nb_n} \right),$$

and since

$$\sup_{x \in \Omega_n} \left(1 - \frac{1}{b_n} \int_0^1 K \left(\frac{x-u}{b_n} \right) du \right) \leq \int_{-\infty}^{-b_n^{n-1}} K(u) du + \int_{b_n^{n-1}}^{\infty} K(u) du \longrightarrow 0,$$

we can write that $\sup_{x \in \Omega_n} |p_{2n}(x) - 1| \rightarrow 0$ as $n \rightarrow \infty$, i.e. $p_{2n}(x) \geq 1 - \varepsilon_0$, $0 < \varepsilon_0 < 1$, for sufficiently large $n \geq n_0$, uniformly with respect to $x \in \Omega_n$. Therefore from the definition of $\hat{p}_n(x)$ it follows that

$$\sup_{x \in \Omega_n} |E\hat{p}_n(x) - p(x)| \leq (1 - \varepsilon_0)^{-1} \left[\sup_{x \in \Omega_n} |Ep_{1n}(x) - p(x)| + \sup_{x \in \Omega_n} |1 - p_{2n}(x)| \right], \quad (6)$$

where the second summand in the right-hand part of (6) converges to 0, and the first summand is estimated as follows. It is not difficult to show that

$$\begin{aligned} \sup_{x \in \Omega_n} |Ep_{1n}(x) - p(x)| &\leq S_n + o(1) + O \left(\frac{1}{nb_n} \right), \\ S_n &= \sup_{0 \leq x \leq 1} \left| \frac{1}{b_n} \int_0^1 (p(y) - p(x)) K \left(\frac{x-y}{b_n} \right) dy \right|. \end{aligned}$$

Extend the function $p(x)$ continuously up to the interval $[-1, 2]$. Let $p^*(x)$ be the extended function and assume that $p^*(x) \geq 0$ and $\sup_{0 \leq x \leq 1} p(x) = \sup_{[-1, 2]} p^*(x)$. We easily conclude that

$$\begin{aligned} S_n &\leq \sup_{0 \leq x \leq 1} \int_{-1}^1 |p^*(x-y) - p^*(x)| \frac{1}{b_n} K \left(\frac{y}{b_n} \right) dy \leq \\ &\leq \sup_{0 \leq x \leq 1} \sup_{|y| \leq \delta} |p^*(x-y) - p^*(x)| \int K(y) dy + 2 \sup_{-1 \leq x \leq 2} p^*(x) \int_{|y| \geq \delta/b_n} K(y) dy, \quad \delta > 0. \quad (7) \end{aligned}$$

The first summand in the right-hand part of (7) can be made arbitrarily small by a choice of $\delta > 0$. After choosing $\delta > 0$ and assuming that $n \rightarrow \infty$, we obtain that the second summand tends to 0. From this and the relations (5) and (6), the proof of the theorem follows.

Theorem 3. Let the kernel $K(x) \geq 0$ be chosen so that it would be a function of finite variation and satisfy the conditions $K(-u) = K(u)$, $K(u) = 0$ for $|u| \geq 1$, $\int K(u) du = 1$. Let $g(x) \geq 0$, $x \in [a, 1-a]$,

$0 < a < 1/2$, be a measurable and bounded function. Let, further,

$0 < \inf p(x) \leq \sup p(x) < 1$, $x \in [0, 1]$.

(a) If $p(x)$ is continuous and $nb_n^2 \rightarrow \infty$, then

$$T_n = \sqrt{n} \int_a^{1-a} g_1(x) [\hat{p}_n(x) - E\hat{p}_n(x)] dx \xrightarrow{d} N(0, \sigma^2),$$

$$g_1(x) = g(x)\psi(x), \quad \psi(x) = \left(\frac{h(x)}{p(x)(1-p(x))} \right)^{1/2}.$$

(b) If $nb_n^2 \rightarrow \infty$, $nb_n^4 \rightarrow 0$ and $p(x)$ has bounded derivatives up to second order, then for $n \rightarrow \infty$

$$T_n = \sqrt{n} \int_a^{1-a} g_1(x) [\hat{p}_n(x) - p(x)] dx \xrightarrow{d} N(0, \sigma^2),$$

$$\sigma^2 = \int_a^{1-a} g^2(x) dx.$$

Proof. We have

$$\sigma_n^2 = \text{Var } \bar{T}_n = n^{-1} \sum_{j=1}^n \psi^{-2}(x_j) \left(\frac{1}{b_n} \int_a^{1-a} K\left(\frac{u-x_j}{b_n}\right) g_{2n}(u) du \right)^2,$$

$$g_{2n}(x) = g_1(x) p_{2n}^{-1}(x).$$

By virtue of Lemma 1, it is not difficult to establish that

$$\sigma_n^2 = \int_a^{1-a} \psi^{-2}(t) dt \left(\frac{1}{b_n} \int_a^{1-a} K\left(\frac{u-t}{b_n}\right) g_1(u) du \right)^2 + o(1) + O\left(\frac{1}{nb_n^2}\right),$$

and also

$$\left| \int_a^{1-a} \psi^{-2}(t) dt \left(\frac{1}{b_n} \int_a^{1-a} K\left(\frac{u-t}{b_n}\right) g_1(u) du \right)^2 - \int_a^{1-a} g^2(u) du \right| \leq$$

$$\leq c_2 \int_a^{1-a} dt \left| \frac{1}{b_n} \int_a^{1-a} g_1(u) K\left(\frac{u-t}{b_n}\right) du - g_1(t) \int_a^{1-a} \frac{1}{b_n} K\left(\frac{u-t}{b_n}\right) du \right| + c_3 \int_a^{1-a} \left| \int_a^{1-a} \frac{1}{b_n} K\left(\frac{u-t}{b_n}\right) du - 1 \right| dt = A_{1n} + A_{2n}.$$

Since $\int_a^{1-a} \frac{1}{b_n} K\left(\frac{u-t}{b_n}\right) du \rightarrow 1$ for all $t \in (a, 1-a)$, we see that $A_{2n} \rightarrow 0$. Further, extend the function $g_1(u)$

in the exterior of $[a, 1-a]$ by zero and denote the extended function by $g_1^*(x)$. Then

$$A_{1n} \leq c_4 \int_0^1 \left(\int_{-\infty}^{\infty} |g_1^*(x+y) - g_1^*(y)| dy \right) \frac{1}{b_n} K\left(\frac{x}{b_n}\right) dx \leq$$

$$\leq c_5 \int_{-1}^1 \left(\int_{-\infty}^{\infty} |g_1^*(y+ub_n) - g_1^*(y)| dy \right) K(u) du = c_5 \int_{-1}^1 \omega(ub_n) K(u) du \rightarrow 0 \quad \text{as } n \rightarrow \infty. \quad (8)$$

where

$$\omega(y) = \int_{-\infty}^{\infty} |g_1^*(y+x) - g_1^*(x)| dx.$$

The inequality (8) holds by virtue of the Lebesgue theorem on majorized convergence and the fact that $\omega(ub_n) \leq 2 \|g_1^*\|_{L_1(-\infty, \infty)}$ and $\omega(ub_n) \rightarrow 0$ as $n \rightarrow \infty$. We have thereby proved that $\sigma_n^2 \rightarrow \sigma^2$.

Let us now verify the fulfillment of the conditions of the Central Limit Theorem for the sums

$$\bar{T}_n = \frac{1}{\sqrt{n}} \sum_{j=1}^n a_{jn} (Y_j - p(x_j)), \quad a_{jn} = \int_a^{1-a} \frac{1}{b_n} K\left(\frac{x-x_j}{b_n}\right) g_{2n}(x) dx$$

Since $a_{jn} \leq c_6$, $E|Y_j - p(x_j)|^{2+\delta} \leq 1$, $j = \overline{1, n}$ and $\sigma_n^2 \rightarrow \sigma^2$, the Lyapunov fraction $L_n = O(n^{-\delta/2})$, $\delta > 0$.

Finally, the condition (b) of the theorem follows from (a) if we take into account that

$$\sqrt{n} \int_a^{1-a} g_1(x) [E\hat{p}_n(x) - p(x)] dx = O(\sqrt{n} b_n^2) + O\left(\frac{1}{\sqrt{n} b_n}\right) \quad (9)$$

Lemma 2. Under the conditions (a) and (b) of Theorem 3 we respectively have

$$E|\bar{T}_n|^s \leq c_7 \left(\int_a^{1-a} g(u) du \right)^{s/2}, \quad s > 2 \quad (10)$$

and

$$E|T_n|^s \leq c_8 \left(\int_a^{1-a} g(u) du \right)^{s/2}, \quad s > 2. \quad (11)$$

Proof. \bar{T}_n is the linear form of $\xi_j = Y_j - p(x_j)$, $E\xi_j = 0$, $1 \leq j \leq n$. It is obvious that $E|\xi_j|^s \leq 1$, $j = \overline{1, n}$.

Therefore, by virtue of Whittle's inequality [8] and Lemma 1, we obtain

$$E|\bar{T}_n|^s \leq c(s) 2^s \left[\int_0^1 \left(\frac{1}{b_n} \int_a^{1-a} K\left(\frac{u-t}{b_n}\right) g_{2n}(u) du \right)^2 dt + O\left(\frac{1}{nb_n^2}\right) \left(\int_a^{1-a} g_{2n}(u) du \right)^2 \right]^{s/2},$$

$$c(s) = \frac{2^{s/2}}{\sqrt{\pi}} \Gamma\left(\frac{s+1}{2}\right). \quad (12)$$

Further, taking into account that

$$g_{2n}(u) \leq g(u) \left[\frac{(\max h(x))^{1/2}}{\sqrt{p_1(1-p_2)}} \left(1 + O\left(\frac{1}{nb_n}\right) \right) \right] \leq c_9 g(u),$$

$$a \leq u \leq 1-a, \quad p_1 = \inf p(x), \quad p_2 = \sup p(x), \quad x \in [0, 1],$$

from (12) we obtain (10). Finally, this and (9) imply (11).

Let us introduce the following random processes:

$$\bar{T}_n(t) = \sqrt{n} \int_a^t (\hat{p}_n(u) - E\hat{p}_n(u)) \psi(u) du, \quad T_n(t) = \sqrt{n} \int_a^t (\hat{p}_n(u) - p(u)) \psi(u) du.$$

Theorem 4. Let the conditions (a) and (b) of Theorem 3 be fulfilled. Then for all functional $f(\cdot)$ continuous on $C[a, 1-a]$, $0 < a < 1/2$, the distributions $f(\bar{T}_n(t))$ and $f(T_n(t))$ converge to the distribution $f(w(t-a))$, where $w(t-a)$, $a \leq t \leq 1-a$, is a Wiener process with the correlation function $r(s, t) = \min(t-a, s-a)$, $w(t-a) = 0$, $t = a$.

The proof of the theorem by Theorem 3 and Lemma 2 is analogous to the proof of Theorem 2 in [9].

მათემატიკა

ბერნულის რეგრესიის ფუნქციის ერთი არაპარამეტრული შეფასების შესახებ

ე. ნადარაია*, პ. ბაბილუა**, მ. ფაცაცია†

* აკადემიის წევრი, ი. ჯავახიშვილის სახ. თბილისის სახელმწიფო უნივერსიტეტი, ზუსტ და საბუნებისმეტყველო მეცნიერებათა ფაკულტეტი

** ი. ჯავახიშვილის სახ. თბილისის სახელმწიფო უნივერსიტეტი, ზუსტ და საბუნებისმეტყველო მეცნიერებათა ფაკულტეტი

† სოხუმის სახელმწიფო უნივერსიტეტი, მათემატიკისა და კომპიუტერულ მეცნიერებათა ფაკულტეტი, თბილისი

განხილულია ბერნულის რეგრესიის ფუნქციის არაპარამეტრული გულოვან შეფასებათა კლასი. შესწავლილია თანაბრად ძალდებულობის საკითხი. გარდა ამისა, განხილულია ამ შეფასებასთან დაკავშირებული უწყვეტ ფუნქციათა $C[a, 1-a]$, $0 < a < 1/2$ კლასში განსაზღვრული ზოგიერთი ფუნქციონალის ზღვართი განაწილების საკითხი.

REFERENCES

1. S. Efromovich (1999), Nonparametric Curve Estimation. Methods, Theory, and Applications. Springer Series in Statistics. New York.
2. J. B. Copas (1983), Appl. Statist., **32**, 1: 25-31.
3. H. Okumora, K. Naito (2004), J. Nonparametr. Stat., **16**, 1-2: 39-62.
4. K. B. Mangaladze (1986), Soobshch. AN GSSR, 124: 261-263.
5. E. A. Nadaraya (1964), Teor. Veroyatn. Primen., 9: 157-159.
6. G. Watson (1964), Sankhya, Ser. A, 26: 359-372.
7. E. Nadaraya, P. Babilua, G. Sokhadze (2010), Bull. Georg. Natl. Acad. Sci., **4**, 3: 5-12.
8. P. Whittle (1960), Teor. Veroyatnost. i Primenen., 5: 331-335.
9. E. Nadaraya, P. Babilua, G. Sokhadze (2011), Bull. Georg. Natl. Acad. Sci., **5**, 2: 11-18.

Received March, 2012

Mathematics

On the Approximation of Periodic Functions within the Frame of Grand Lebesgue Spaces

Nina Danelia* and Vakhtang Kokilashvili**

* Department of Exact and Natural Sciences, I. Javakishvili Tbilisi State University

** Academy Member, Andrea Razmadze Mathematical Institute of I. Javakishvili Tbilisi State University

ABSTRACT. The paper announces the boundedness criteria of majorants for β -order ($\beta > 0$) Cesàro and Abel-Poisson means in weighted grand Lebesgue spaces $L^{p,\theta}$ ($1 < p < \infty$, $\theta > 0$). It is claimed that in these spaces the mean continuity property fails to hold. The fractional order moduli of smoothness are introduced in a subspace of $L^{p,\theta}$ where the set of smooth functions is dense. Using these characteristics, direct and inverse inequalities of the constructive theory of functions are obtained. The rate of approximation by β -order ($\beta > 0$) Cesàro means is estimated for a function from the above-mentioned subspace. In weighted grand Lebesgue spaces, an analog of the well-known Bernstein inequality is established for the derivatives of trigonometric polynomials. © 2012 Bull. Georg. Natl. Acad. Sci.

Key words: Grand Lebesgue space, majorants of linear summability means, trigonometric polynomials, direct and inverse inequalities, mean continuity, Bernstein type inequality, logarithmic-fractional order derivative.

The present paper announces the authors' recent results on the approximation of functions by Fourier operators in some new function spaces.

Let $\mathbb{T} = (-\pi, \pi)$ and $1 < p < \infty$, $\theta > 0$. The weighted grand Lebesgue space of 2π -periodic functions is defined by the norm

$$\|f\|_{L^{p,\theta}_w} = \sup_{0 < \varepsilon < p-1} \left(\frac{\varepsilon^\theta}{2\pi} \int_{\mathbb{T}} |f(x)|^{p-\varepsilon} w(x) dx \right)^{\frac{1}{p-\varepsilon}}.$$

Here w is a weight function, i.e. an a. e. positive function which is integrable on \mathbb{T} . When $w \equiv 1$, we set $L^{p,\theta}_w = L^{p,\theta}$.

In the weighted case, grand Lebesgue spaces on the bounded sets of a Euclidean space were introduced by T. Iwaniec and C. Sbordone [1] for $\theta = 1$, and by L. Greco, T. Iwaniec and C. Sbordone [2] for $\theta > 1$. It is a well-established fact that these spaces are non-reflexive non-separable ones.



For the boundedness problems in $L_w^{p,\theta}$ for various integral operators we refer the reader to [3-6].

It is well known that the following continuous embeddings hold:

$$L_w^p \rightarrow L_w^{p,\theta} \rightarrow L_w^{p-\varepsilon}, \quad 0 < \varepsilon < p-1.$$

Let $f \in L^1(\mathbb{T})$ and

$$f(x) \sim \frac{a_0}{2} + \sum_{k=1}^{\infty} (a_k(f) \cos kx + b_k(f) \sin kx) \quad (1)$$

be its Fourier series.

We denote by $\sigma_n^\beta(f, x)$ ($\beta > 0$) and $u_r(f, x)$ the Cesàro and Abel-Poisson summability means, respectively.

A weight function w is said to be of the Muckenhoupt class A_p ($1 < p < \infty$) if

$$\sup \left(\frac{1}{|I|} \int_I w(x) dx \right) \left(\frac{1}{|I|} \int_I w^{1-p'}(x) dx \right)^{p-1} < \infty,$$

where the supremum is taken over all intervals whose length is less than 2π .

Theorem 1. Let $1 < p < \infty$ and $\theta > 1$. The following statements are equivalent:

i) There exists a positive constant $c_1 > 0$ such that

$$\left\| \sup_n \left| \sigma_n^\beta(f, x) \right| \right\|_{L_w^{p,\theta}} \leq c_1 \|f\|_{L_w^{p,\theta}}$$

for an arbitrary function $f \in L_w^{p,\theta}$,

ii) There exists a positive constant $c_2 > 0$ such that $\left\| \sup |u_r(f, x)| \right\|_{L^{p,\theta}} \leq c_2 \|f\|_{L^{p,\theta}}$;

for an arbitrary function $f \in L_w^{p,\theta}$,

iii) $w \in A_p(\mathbb{T})$.

Note that an analogous statement is valid for more general means of the linear method of summability.

As has been mentioned above, the space $L_w^{p,\theta}$ is a non-separable one. The closure of L^p by the norm of $L_w^{p,\theta}$ does not coincide with the latter space.

We denote by $\dot{L}_w^{p,\theta}$ the closure of L^p with respect to the norm of $L_w^{p,\theta}$. As is known [7], $\dot{L}_w^{p,\theta}$ is a subspace of the space $L_w^{p,\theta}$ of functions satisfying

$$\lim_{\varepsilon \rightarrow 0} \varepsilon^\theta \int_{\mathbb{T}} |f(x)|^{p-\varepsilon} w(x) dx = 0.$$

For functions from $\dot{L}_w^{p,\theta}$ we obtain in a standard manner

Corollary. Let $1 < p < \infty$ and $\theta > 1$. Let $w \in A_p(\mathbb{T})$. Then for $f \in \dot{L}_w^{p,\theta}$ we have

$$\lim_{n \rightarrow \infty} \left\| \sigma_n^\beta(f, \cdot) - f \right\|_{L_w^{p,\theta}} = 0$$

and

$$\lim_{n \rightarrow \infty} \|u_r(f, \cdot) - f\|_{L_w^{p,\theta}} = 0.$$

Theorem 3. Let $1 < p < \infty$ and $\theta > 1$. The mean continuity property fails to hold in the space $L^{p,\theta}$, i.e. there exists a function $f \in L^{p,\theta}$ such that

$$\lim_{h \rightarrow 0} \|f(\cdot + h) - f(\cdot)\|_{L^{p,\theta}} \neq 0.$$

Theorem 3 shows that in the space $L^{p,\theta}$ it is impossible to define the moduli of smoothness by the translation operator but in $\dot{L}^{p,\theta}$ the moduli of smoothness can be introduced in the traditional way.

Here we employ the moduli of smoothness of fractional order. Assume that $r \geq 0$. Let Δ_r^h denote

$$\Delta_r^h f(x) = \sum_{k=0}^r (-1)^k \binom{r}{k} f(x + (r-k)h)$$

which is the r -th order difference of the function f .

Here

$$\binom{r}{k} = \frac{r(r-1)\cdots(r-k+1)}{k!}$$

for $k > 1$, and

$$\binom{r}{k} = 0$$

for $k = 1$.

For $f \in \dot{L}^{p,\theta}(\mathbb{T})$ we set

$$\omega_r(f, \delta)_{L^{p,\theta}} = \sup_{|h| \leq \delta} \|\Delta_r^h f(\cdot)\|_{L^{p,\theta}}$$

and

$$E_n(f)_{L^{p,\theta}} = \inf \|f - T_n\|_{L^{p,\theta}},$$

where the infimum is taken over all trigonometric polynomials of degree not greater than n .

For a further presentation of our results we need the definition of power-logarithmic order derivative. Let $\lambda_n = n^\alpha \ln^\gamma(n+1)$. Assume that α, γ and β are some positive numbers. We say that a function $f \in L_w^{p,\theta}$, $1 < p < \infty$, $\theta > 0$ and $w \in A_p(T)$, has a (λ, β) derivative $f^{(\lambda, \beta)}$ if the series

$$\sum_{k=1}^{\infty} \lambda_k \left(a_k(f) \cos k \left(x + \frac{\beta\pi}{2k} \right) + b_k(f) \sin k \left(x + \frac{\beta\pi}{2k} \right) \right)$$

is the Fourier series of function $f^{(\lambda, \beta)}$.

For the logarithmic-fractional order derivatives of periodic functions we refer to L.D.Kudryavtsev [8]

The following analog of the well-known Bernstein inequality is valid.



Theorem 4. Let $1 < p < \infty$, $\theta > 1$. Let $w \in A_p(T)$. There exists a constant $c > 0$ such that

$$\|T_n^{(\lambda, \beta)}\|_{L^{p, \theta}} \leq c \lambda_n \|T_n\|_{L^{p, \theta}}$$

for an arbitrary trigonometric polynomial T_n .

We emphasize the results of A.I. Stepanets [9, 10], who proved the Bernstein type inequality in unweighted classical Lebesgue spaces for the derivatives in general sense.

Theorem 5. Let $1 < p < \infty$ and $\theta > 1$. Assume that $f \in \dot{L}^{p, \theta}$ has a derivative $f^{(\lambda, \beta)} \in \dot{L}^{p, \theta}$. Then for arbitrary $r > 0$ we have

$$E_n(f)_{L^{p, \theta}} \leq c \frac{1}{\lambda_n} \omega_r\left(f^{(\lambda, \beta)}, \frac{1}{n+1}\right)$$

with a positive constant c independent of f and n .

Theorem 6. Let $1 < p < \infty$ and $\theta > 1$. Then for $f \in \dot{L}^{p, \theta}$ and $r > 0$ the inequality

$$\omega_r\left(f, \frac{1}{n}\right)_{L^{p, \theta}} \leq \frac{c_r}{n^r} \sum_{k=1}^n k^{r-1} E_{k-1}(f)_{L^{p, \theta}}$$

holds with a positive constant c_r independent of f and n .

Theorem 7. Let $1 < p < \infty$ and $\theta > 1$. Let the condition

$$\sum_{k=1}^{\infty} \frac{\lambda_k}{k} E_{k-1}(f)_{L^{p, \theta}} < \infty$$

be satisfied for a function $f \in \dot{L}^{p, \theta}$. Then there exists $f^{(\lambda, \beta)} \in \dot{L}^{p, \theta}$ and the inequality

$$\omega_r\left(f^{(\lambda, \beta)}, \frac{1}{n}\right)_{L^{p, \theta}} \leq c \left(\frac{1}{n^r} \sum_{k=1}^n \lambda_k \cdot k^{r-1} E_{k-1}(f)_{L^{p, \theta}} + \sum_{k=n+1}^{\infty} \frac{\lambda_k}{k} E_{k-1}(f)_{L^{p, \theta}} \right)$$

holds with a constant c independent of f and n .

In the Lebesgue spaces L^p ($1 < p < \infty$), results analogous to Theorems 5, 6 and 7 are presented in [11] for the moduli of smoothness of k -th order ($k \in \mathbb{N}$).

Our next result concerns the rate of approximation by linear summability means in $\dot{L}^{p, \theta}$.

Theorem 8. Let $1 < p < \infty$ and $\theta > 1$. For $f \in \dot{L}^{p, \theta}$ and $\beta > 0$ the inequality

$$\|f(\cdot) - \sigma_n^\beta(f, \cdot)\|_{L^{p, \theta}} \leq c \omega_r\left(f, \frac{1}{n+1}\right)_{L^{p, \theta}}$$

holds for a positive constant c independent of f and n .

A similar estimate holds for the deviation by the Abel-Poisson means.

The proof of Theorem 8 is based on the analog of the Marcinkiewicz multiplier theorem for $L_w^{p, \theta}(\mathbb{T})$.

Theorem 9. Let $1 < p < \infty$ and $\theta > 1$, and let $w \in A_p$. Assume that $f \in L_w^{p, \theta}$ and its Fourier series is (1).

Let the sequence $(\lambda_n)_{n=0}^{\infty}$ satisfy the conditions

$$|\lambda_n| \leq M, \quad \sum_{k=2^{n-1}}^{2^n-1} |\lambda_k - \lambda_{k+1}| \leq M$$

for some $M > 0$ and arbitrary $n \in \mathbb{N}$.

Then the trigonometric series

$$\frac{\lambda_0 a_0}{2} + \sum_{n=1}^{\infty} \lambda_n (a_n \cos nx + b_n \sin nx)$$

is the Fourier series of some $F \in L_w^{p,\theta}$ with a constant c independent of f and the inequality

$$\|F\|_{L_w^{p,\theta}} \leq Mc \|f\|_{L^{p,\theta}}$$

holds with a constant c independent of f .

In their further paper the authors intend to throw light on the approximation problems both in weighted grand Lebesgue spaces and in multidimensional cases.

მათემატიკა

პერიოდული ფუნქციების მიახლოების შესახებ გრანდ ლებეგის სივრცეების ჩარჩოებში

ნ. დანელია*, ვ. კოკილაშვილი**

* ი. ჯავახიშვილის სახ. თბილისის სახელმწიფო უნივერსიტეტი, ზუსტ და საბუნებისმეტყველო მეცნიერებათა ფაკულტეტი

** აკადემიის წევრი, ი. ჯავახიშვილის სახ. თბილისის სახელმწიფო უნივერსიტეტის ანდრია რაზმაძის მათემატიკის ინსტიტუტი

ნაშრომში მოყვანილია წონიანი გრანდ ლებეგის $L^{p,\theta}$ ($1 < p < \infty$, $\theta > 0$) სივრცეების ფუნქციების β -რიგის ($\beta > 0$) ჩეზაროსა და აბელ-პუასონის საშუალოების მასორანტების შემოსაზღვრულობის კრიტერიუმები. ნაჩვენებია, რომ გრანდ ლებეგის სივრცეებში ფუნქციათა საშუალოდ უწვევტობის თვისებას, განსხვავებით კლასიკური ლებეგის სივრცეებიდან, აღარ აქვს ადგილი. აღნიშნული სივრცის იმ ქვესივრცისათვის, სადაც გლუვი ფუნქციები ყველგან მკვერთია გრანდ ლებეგის სივრცის ნორმით, შემოღებულია წილადური რიგის სიგლუვის მოდული და მის ტერმინებში დამტკიცებულია ფუნქციათა კონსტრუქციული თეორიის პირდაპირი და შებრუნებული თეორემები. ზემოხსენებული ქვესივრცის ფუნქციებისათვის დადგენილია β -რიგის ($\beta > 0$) ჩეზაროსა და აბელ-პუასონის საშუალოებით მიახლოების რიგი. წონიანი გრანდ ლებეგის სივრცეებში მიღებულია ტრიგონომეტრიული პოლინომების წარმოებულების შესახებ ს. ბერნშტეინის ცნობილი თეორემის ანალოგი.



REFERENCES

1. T. Iwaniec, C. Sbordone (1992), Arch. Rational Mech. Anal., **119**, 2: 129-143.
2. L. Greco, T. Iwaniec, C. Sbordone (1997), Manuscripta Math., **92**, 2: 249-258.
3. A. Fiorenza, B. Gupta, P. Jain (2008), Studia Math., **188**, 2: 123-133.
4. V. Kokilashvili, A. Meskhi (2009), Georgian Math. J., **16**, 3: 547-551.
5. V. Kokilashvili (2010), J. Math. Sci. (Springer, New York), **170**, 2.
6. V. Kokilashvili (2011), Singular integrals and strong fractional maximal functions in grand Lebesgue spaces. Nonlinear Analysis, Function Spaces and Applications, Vol. 9, 261-269, Proceedings of the International School held in Třešt', September 11-17, 2010, Ed. By J. Rakosnik. Institute of Mathematics, Academy of Sciences of the Czech Republic, Praha, 2011.
7. C. Sbordone (1997), Ann. Scuola Norm. Sup. Pisa Cl. Sci., **25**(4), 3-4: 739-756.
8. L.D. Kudryavtsev (1982), Dokl. Akad. Nauk SSSR, 266: 274-276, English transl. Sov. Math. Dokl. 25: 311-313.
9. A.I. Stepanets (1987), Classification and approximation of periodic functions (in Russian), Naukova Dumka, Kiev.
10. A.I. Stepanets (1995), Ukr. Math. Zh., 47(9): 1441-1448.
11. A. F. Timan (1963), Theory of approximation of functions of a real variable. Translated from the Russian by J. Berry. International Series of Monographs in Pure and Applied Mathematics, Vol. 34. A Pergamon Press Book. The Macmillan Co., New York, 1963; Russian original: (1960), Gosudarstv. Izdat. Fiz.-Mat. Lit., Moscow.

Received April, 2012

Mathematics

Maxwell Conjecture and Polygonal Linkages

Giorgi Khimshiashvili

Department of Arts and Sciences, Ilia State University, Tbilisi

(Presented by Academy Member Nikoloz Vakhania)

ABSTRACT. Motivated by the famous Maxwell conjecture on the number of equilibria of point charges, we discuss the electrostatic potential of point charges placed at the vertices of polygonal linkage. In particular, we establish that electrostatic potential is a Morse function on the moduli space of a generic polygonal linkage, which yields estimates for the number of its equilibria. For quadrilateral linkage, we present a number of results on the structure of electrostatic equilibria and, as a by-product, prove that its shape is completely controllable by changing the charge at just one vertex. © 2012 Bull. Georg. Natl. Acad. Sci.

Key words: point charge, electrostatic potential, equilibrium, polygonal linkage, moduli space, Morse function, critical point.

1. The famous conjecture of J.C. Maxwell states that the number of equilibria of n equal point charges in \mathbb{R}^3 does not exceed $(n-1)^2$ [1]. This conjecture remains unproven even for $n=3$ and the best established estimate for $n=3$ is 12 [2]. Being classical and intriguing, this conjecture gained a lot of attention of researchers (see, e.g., [2]). In particular, various modifications and special cases of Maxwell conjecture have been considered, which led to a number of interesting mathematical results obtained by topological (see, e.g., [3]) and analytical methods (cf. [4]).

Along these lines, we suggest an analog of Maxwell conjecture in the context of polygonal linkages, present several related results for linkages with a small number of vertices and discuss a few promising topics naturally arising in the framework of our setting. Our approach relies on the topological results on moduli spaces of linkages [5] and signature formulae for the topological invariants of functions on moduli spaces [6].

2. Let us first recall some definitions and facts concerned with electrostatic potentials. By definition, the electrostatic (Coulomb) potential of a system V of unit charges $q=1$ placed at the points $v_i \in \mathbb{R}^3$ is a rational function on \mathbb{R}^3 defined by the formula $\Psi_V(P) = \sum (d(P, v_i))^{-1}$, where $P \in \mathbb{R}^3$ and $d(P, v_i)$ denotes the Euclidean distance between P and v_i . The electrostatic energy of V is defined by the formula $E_V(V) = \sum (d(v_i, v_j))^{-1}$, where the sum is taken over all pairs of nonequal indices.

28861

We will also consider the planar analog of G called *planar electrostatic potential* Φ which is defined for a system V of unit charges placed at the points $z_i \in \mathbb{R}^2$ by the formula $\Phi_V(z) = \sum \text{Ln}(d(z, z_i))$, where Ln denotes the natural logarithm and $z \in \mathbb{R}^2$. The *planar electrostatic energy* of V is defined as $E_p(V) = \sum \text{Ln}(d(z_i, z_j))$, where the sum is taken over all pairs of nonequal indices.

For a system V of points $z_i \in \mathbb{R}^2$ we also introduce a polynomial $P_V(z) = \prod (z - z_i)$ having the points z_i as its zeroes.

Notice that the natural planar analog of Maxwell conjecture holds true in virtue of a classical observation of C. Gauss. Indeed, Gauss showed that the critical points of Φ_V coincide with the zeroes of derivative $(P_V)'$ of polynomial P_V (cf. [4], Ch.1). This immediately yields the exact estimate for the number of equilibria of planar electrostatic potential.

Fact 1. The number of critical points of planar electrostatic potential of n unit charges in the plane does not exceed $n - 1$.

For $n=3$, using this observation of Gauss and a well-known theorem on zeroes of derivatives of cubic polynomial ([4], Ch.1) one obtains an explicit geometric description of equilibria of planar electrostatic potential.

Fact 2. The critical points of planar electrostatic potential of three unit charges placed at the vertices of triangle Δ lie at the foci of the ellipse tangent to the sides of Δ at their midpoints.

Such an ellipse always exists and is often called the *Steiner ellipse* of Δ [7]. It is known that it has the maximal area among all ellipses contained in Δ , which suggests that the equilibria of potentials might be connected with certain extremal properties of arising configurations of equilibria. Both these facts serve as paradigms for our considerations.

3. We present now some definitions and facts concerned with polygonal linkages. Recall that a polygonal linkage (or a closed polygonal k -chain) L is defined by a k -tuple of positive numbers l_i called *sidelengths* of L . In the case of a closed polygonal chain it is always assumed that each of the sidelengths is not greater than the sum of all other ones [5]. A polygonal linkage is called *regular* if all sidelengths are equal. The *planar configuration space* $C(L)$ of a polygonal k -chain L is defined as the collection of all k -tuples of points v_i in Euclidean plane such that the distance between v_i and v_{i+1} is equal to l_i , where it is assumed that $v_{k+1} = v_1$. Each such collection of points is called a *configuration* of L . A configuration is called *convex* if the corresponding polygon is convex. Factoring $C(L)$ over the natural diagonal action of $\text{SO}(2)$ one obtains the *(planar) moduli space* $M(L) = M_k(L)$ [5]. The subset of $M(L)$ formed by the convex configurations will be denoted $M^c(L)$. Analogously, one can define higher configuration spaces $M_N(L)$ of which we will only consider $M_3(L)$ and denote it $S(L)$. Moduli spaces, as well as configuration spaces, are endowed with natural topologies induced by Euclidean metric.

It is easy to see that the planar moduli space can be identified with the subset of configurations such that $v_1 = (0,0)$, $v_2 = (l_1, 0)$. It is well known that, for a closed k -chain, the moduli space has a natural structure of compact orientable real-algebraic set of dimension $k - 3$. Let us say that a polygonal linkage is *degenerate* if it has an *aligned configuration*, i.e., a configuration where all vertices lie on the same straight line. It is well known that this happens if and only if there exists a k -tuple of "signs" $s_i = \pm 1$ such that $\sum s_i l_i = 0$. The moduli spaces $M_N(L)$ of polygonal linkage L is smooth (does not have singular points) if and only if L is nondegenerate (see, e.g., [5]).

4. We are now able to describe the settings discussed in the sequel. The main idea is to fix a polygonal linkage L as above and consider E_p and E_s as functions on the corresponding moduli spaces $M(L)$ and $S(L)$ respectively. We present now a rigorous description of this setting in the case of *quadrilateral linkage*.

So let $Q = Q(a, b, c, d)$ be a nondegenerate quadrilateral linkage with pairwise non-equal lengths of the sides. For brevity, such a linkage will be called *admissible*. For each configuration V of Q , let us consider its energies $E_p(V)$ and $E_s(V)$. Since Q does not have configurations with coinciding vertices, both these energies are smooth (infinitely differentiable) functions on $M(Q)$ and $S(Q)$ respectively. So one may consider their critical points in these moduli spaces which in fact correspond to the *physical equilibria* of linkage Q subject only to electrostatic forces between its vertices.

We can now formulate the two problems we are interested in: (P1) find the number of equilibria of E_p and E_s for a given linkage, and (P2) find the maximal possible number of equilibria of E_p and E_s over the set of all admissible quadrilateral linkages.

Notice a conceptual analogy of (P2) with Maxwell conjecture. However, an essential **difference** is that here we consider the **equilibria of the linkage itself** and not the equilibria of its electrostatic potential in the ambient space. In such a setting the problem acquires several new aspects, which lead to the following results in the spirit of [6]. First of all, problem (P1) can be solved using our general approach based on signature formulae for topological invariants [6].

Theorem 1. *For an admissible quadrilateral linkage Q , the number of equilibria of any of energies E_p and E_s can be calculated as the signature of a quadratic form with the coefficients algebraically expressible through the sidelengths of Q .*

Outline of the proof. The result follows by applying the signature formula for Euler characteristic to the polynomial system for the equilibria obtained by the method of Lagrange multipliers. We give first an outline of the proof in the case of planar potential E_p .

The main idea in this case is to simplify the expression for E_p by considering the length of diagonals of configuration V as coordinates on $M(L)$. More precisely, we put $x = d(v_1, v_3)$, $y = d(v_2, v_4)$ and notice that the pair (x, y) completely determines the shape of configuration V , i.e. its class in $M(Q)$. In these coordinates one has: $E_p = x^4 + y^4 + C$, where C is the constant equal to the sum of the terms corresponding to the sides of V . Obviously, C has no influence on the critical points of E_p .

Now, from a classical result known as the *Euler four points formula* [7] follows that the moduli space $M(Q)$ is defined by the following polynomial equation in coordinates (x, y) :

$$x^2y^4 + y^2x^4 - (a^2 + b^2 + c^2 + d^2)x^2y^2 + (a^2 - d^2)(b^2 - c^2)x^2 + (a^2 - b^2)(d^2 - c^2)y^2 + C_1 = 0, \quad (*)$$

where $C_1 = (b^2d^2 - a^2c^2)(b^2 + d^2 - a^2 - c^2)$ is a constant.

Denoting by T the left hand side of this equation we see that point V is critical for E_p if and only if the gradients of E_p and T with respect to (x, y) coordinates are proportional at this point which gives another polynomial equation $T_1 = 0$. In this way we obtain a (2×2) -system of polynomial equations and it is easy to verify that its jacobian is not identically equal to zero. This means that one can express the number of real solutions to this system by the signature formula [6], which yields the desired result.

In case of E_s the proof is in a sense easier since the lengths of diagonals (x, y) are independent local coordinates on $S(Q)$ in the interior of a certain box $B = [x_m, x_M] \times [y_m, y_M]$ defined by the regions of values of x and y on $S(Q)$. This follows from the existence of diagonal bendings [5] which change one of the diagonals leaving the second one unchanged. So the equilibria are given by counting the zeroes of gradient E_s inside

the box B and checking the degenerate configurations of Q with extremal values of x or y . Both these procedures can be done effectively using signature formulae and the result follows.

The above considerations and methods used in [6], [8] enable one to show that the equilibria are in fact nondegenerate in the sense of Morse theory.

Theorem 2. *For a generic admissible quadrilateral linkage Q , E_p and E_s are Morse functions on $M(Q)$ and $S(Q)$ respectively.*

The proof is obtained by analyzing the constrained extremal problem for the potential in question. To this end we consider the extended Hessian matrix of Lagrange function in coordinates (x, y) introduced above. Due to the simple form of E_p and E_s in these coordinates, the determinant of Hessian T_2 can be computed explicitly. We compute next the resultant of polynomials T, T_1, T_2 and verify that it does not vanish identically, which implies that the zeroes of the determinant generically cannot coincide with the solutions to the Lagrange system for equilibria.

Results of such kind are useful because they enable one to estimate the number of equilibria using Morse inequalities and similar topological tools [3], [9]. For quadrilateral linkages, this is not indeed interesting since both $M(L)$ and $S(L)$ have very simple topology but this idea may yield a useful paradigm in the general case of linkage with arbitrary number of sides $n > 4$.

After having found the polynomial system real solutions to which give the equilibria of potential in moduli space one can try to describe the bifurcation diagram of this system in the space of parameters (a, b, c, d) and find the number of equilibria in each component of its complement by the aforementioned signature formulas. We were only able to do this for the planar potential E_p which yielded a solution to problem (P2) in this case.

Theorem 3. *For any admissible linkage Q , E_p has no more than 8 critical points on $M(Q)$.*

A detailed proof of this result will be published elsewhere. Analogous results for linkages with the number of sides bigger than four would be difficult to prove by the same method since the arising polynomial systems involve not less than three variables in which cases computers are usually unable to calculate the result using signature formulae.

5. The above results on electrostatic equilibria of linkages have the following curious application in the spirit of control theory. Consider an admissible quadrilateral linkage Q as above and place positive charges at its vertices. Among the critical points of E_p and E_s the global minima are especially important since they give the *stable equilibria* of the linkage subject to only electrostatic forces.

It is easy to see that the global minimum of E_s can only be attained at a planar configuration of quadrilateral Q . Indeed, for each nonplanar configuration one can increase the length of at least one of the diagonals without changing another one which clearly decreases the value of E_s . Thus in this context it is sufficient to consider both potentials as functions on $M(Q)$.

As is geometrically obvious and can be easily verified, given a non-convex planar configuration, one can increase both of its diagonals simultaneously by deforming the linkage [7]. Thus the global minima of both potentials always belong to $M^c(Q)$. In fact, one can prove a stronger result.

Theorem 4. *For an admissible quadrilateral linkage Q with arbitrary positive charges at its vertices, the global minimum of E_s on $M(Q)$ is unique, and the same is true for E_p .*

This result suggests the idea of controlling the shape of Q by changing the charge at one of the vertices of Q . More precisely, we fix the positions of the first two vertices of Q , place unit positive charges at all vertices except the first one placed at the origin, and permit ourselves to change the value $q > 0$ of charge at the first vertex. By Theorem 4, for each $q > 0$ we have a single stable equilibrium of E_s , i.e. a well-defined point

in $M^+(Q)$ which we denote by $V(q)$. A natural question now is whether this mapping is surjective as a mapping from R_1 into $M^+(Q)$. A positive answer to this question would mean that we may force the linkage to take any convex shape from $M^+(Q)$ by choosing a proper value of q .

Theorem 5. *The mapping from R_1 into $M^+(Q)$ defined by sending q to $V(q)$ is surjective on the interior of $M^+(Q)$.*

Outline of the proof. First of all, using Lagrange method it is easy to see that the configuration with the lengths of diagonals equal to (x_0, y_0) is the global minimum of E_q when the charge at the first vertex is equal to $q = (x_0)^2 (y_0)^{-2} T_x (T_y)^{-1}$, (**)

where the subscripts denote partial derivatives and both y_0 and T_y are non-zero.

If $y_0 = 0$ one has an analogous relation with the roles of x and y exchanged. It only remains to show that the obtained value of q is indeed positive. This can be proven by analyzing the implicit functions of the form $y(x)$ and $x(y)$ obtained from equation (*). A simple argument implies that in convex position both partial derivatives have the same sign, which completes the proof.

Using the ideology and terminology of control theory [10] this result means that convex configurations of charged quadrilateral Q as above can be completely controlled by the value of charge at just one of its vertices. The same result holds for E_p and its proof can be obtained by a slight modification of the relation (**) in the above argument. In this context the result for E_x is more important since in real life one always deals with the Coulomb potential

It is now obvious that similar problems make sense for linkages with arbitrary number of sides. Discussion of arising generalizations and applications will be continued in forthcoming publications of the author.

მათემატიკა

მაქსველის ჰიპოთეზა და სახსრული მრავალკუთხედები

გ. ხიმშიაშვილი

ილიას სახელმწიფო უნივერსიტეტი, მეცნიერებათა და ტელეკომუნიკაციების ფაკულტეტი, თბილისი
 (წარმოდგენილია აკადემიკოს ნ. ვახანიას მიერ)

ნაშრომში განხილულია მაქსველის ცნობილი ჰიპოთეზის ანალოგები სახსრული მრავალკუთხედების კონტექსტში და მოყვანილია საკმაოდ დეტალური შედეგები სახსრული ოთხკუთხედის შემთხვევაში. დამტკიცებულია აგრეთვე, რომ დამუხტული სახსრული ოთხკუთხედის სრული კონტროლი შესაძლებელია მხოლოდ ერთი მუხტის მნიშვნელობის შეცვლით.

REFERENCES

1. *J.C. Maxwell* (1873), *A Treatise on Electricity and Magnetism*, London.
2. *A. Gabriellov, D. Novikov, B. Shapiro* (2007), *Proc. Lond. Math. Soc.* **95**: 443-472.
3. *M. Morse, S. Cairns* (1969), *Critical Point Theory in Global Analysis and Differential Topology*. Academic Press, 389 p.
4. *V. Prasolov* (2008), *Polynomials*, AMS Transl. Math. Monographs.
5. *M. Kapovich, J. Millson* (1995), *J. Diff. Geom.* **42**: 133-164.
6. *G. Khimshiashvili* (2009), *J.Math. Sci.*, **160**, 10: 127-136.
7. *M. Berger* (1982), *Geometry*. Vol.1. Paris.
8. *G. Panina, A. Zhukova* (2011), *Centr. Eur. J. Math.* **9**, 2: 364-377.
9. *V. Arnold, A. Varchenko, S. Gusein-Zade* (2004), *Singularities of Differentiable Mappings*. MCCME, M. (in Russian).
10. *A. Agrachev, Yu. Sachkov* (2004), *Control Theory from the Geometric Viewpoint*. Springer.

Received February, 2012

Mathematics

On Analytic and Harmonic Functions with a Dirichlet Finite Integral in the Unit Circle

Gigla Oniani* and Giorgi Tetvadze*

* Department of Exact and Natural Sciences, Akaki Tsereteli State University, Kutaisi

(Presented by Academy Member Revaz Bantsuri)

ABSTRACT. The paper deals with the study of integral representations and boundary properties of harmonic functions having an analytical and summable gradient with a summable derivative in the unit circle. One theorem of S.M. Nikolski on the existence of a boundary value of a harmonic function is formulated more precisely. © 2012 Bull. Georg. Natl. Acad. Sci.

Key words: analytic function, majorant function, gradient, Bergman space.

Denote by D the open unit circle on the \mathbb{C} -complex plane, and by T the unit circumference with centre at the origin, i.e.

$$D = \{z \in \mathbb{C} : |z| < 1\},$$
$$T = \{t \in \mathbb{C} : |t| = 1\}.$$

Assume that $H(D)$ is a set of all analytical functions in D . Let $p > 0$ be some fixed number. Denote by A_p' the space of all those functions $f \in H(D)$ which satisfy the condition

$$\iint_D |f'(z)|^p d\sigma(z) < +\infty, \quad (1)$$

where $d\sigma(z) = dx dy$ is a usual plane Lebesgue measure in D and $z = x + iy$, $x, y \in \mathbb{R} = (-\infty, +\infty)$.

If $p = 2$, then the space A_2' is called the Dirichlet space or the space of analytic functions with a finite integral (see [1]).

Denote by $H_p'(D)$ the Bergman space of analytic functions in the circle D , i.e.

$$H_p' = \left\{ f \in H(D) : \iint_D |f(z)|^p d\sigma(z) < \infty \right\}.$$



Assume that $f(z) = u(z) + iv(z)$, where $u = \operatorname{Re} f$ and $v = \operatorname{Im} f$, then since $\forall z \in D$

$$f'(z) = \frac{\partial u}{\partial x} - i \frac{\partial u}{\partial y} = \frac{\partial v}{\partial y} + i \frac{\partial v}{\partial x},$$

we have

$$|\operatorname{grad} u| = \sqrt{\left(\frac{\partial u}{\partial x}\right)^2 + \left(\frac{\partial u}{\partial y}\right)^2} = \sqrt{\left(\frac{\partial v}{\partial y}\right)^2 + \left(\frac{\partial v}{\partial x}\right)^2} = |\operatorname{grad} v| = |f'(z)|.$$

This implies

$$f \in A_p' \Leftrightarrow \int_D |\operatorname{grad} u|^p d\sigma(z) < \infty,$$

$$f \in A_p' \Leftrightarrow \int_D |\operatorname{grad} v|^p d\sigma(z) < \infty.$$

The theorems below are valid.

Theorem 1. $f \in A_1'(D)$ if and only if the equality

$$f(z) = f(0) + \frac{z}{\pi} \int_D \frac{f'(t) d\sigma(t)}{1-zt} \quad (2)$$

holds $\forall z \in D$.

Proof. Since

$$\int_D |f'(z)| d\sigma(z) < \infty,$$

we have $f' \in H_1'(D)$. According to Kabaila's theorem (see [2]), $\forall z \in D$ we obtain

$$\begin{aligned} f'(z) &= \frac{1}{\pi} \int_D \frac{f'(t) d\sigma(t)}{(1-zt)^2} \Leftrightarrow f(z) = f(0) + \int_0^z f'(\xi) d\xi = f(0) + \frac{1}{\pi} \int_0^z \left[\int_D \frac{f'(t) d\sigma(t)}{(1-\xi t)^2} \right] d\xi = \\ &= f(0) + \frac{1}{\pi} \int_D f'(t) d\sigma(t) \cdot \int_0^z \frac{d\xi}{(1-\xi t)^2} = f(0) + \frac{1}{\pi} \int_D f'(t) d\sigma(t) \left[\frac{1}{1-zt} - 1 \right] = f(0) + \frac{z}{\pi} \int_D \frac{f'(t) d\sigma(t)}{1-zt}. \end{aligned}$$

The theorem is proved.

Theorem 2. If $f \in A_1'(D)$, then $\forall z \in D$

$$\frac{1}{\pi} \int_D \frac{f'(t) d\sigma(t)}{1-zt} = \overline{f'(0)}.$$

Proof. Indeed, assume $C(z, t) = (1-zt)^{-1}$ and

$$C[f'](z) = \frac{1}{\pi} \int_D C(z, t) f'(t) d\sigma(t).$$

It is obvious that $C(z, t) = \sum_{n=0}^{\infty} z^n t^n$. This series converges uniformly to $t \bar{D}$ because $|z| < 1$. Also, using the function f' we have

$$\frac{1}{\pi} \int_D f'(t) d\sigma(t) = f'(0)$$

and $\forall n \in \mathbb{N}$

$$\int_D f'(t) t^n d\sigma(t) = 0.$$

Therefore

$$\begin{aligned} C[\overline{f'}](z) &= \frac{1}{\pi} \int_D \overline{f'}(z) C(z, t) d\sigma(t) = \frac{1}{\pi} \int_D \overline{f'(t) C(z, t)} d\sigma(t) = \frac{1}{\pi} \int_D \overline{f'(t) \left[\sum_{n=0}^{\infty} z^n t^n \right]} d\sigma(t) = \\ &= \frac{1}{\pi} \int_D \overline{f'(t) d\sigma(t)} + \frac{1}{\pi} \sum_{n=1}^{\infty} z^n \int_D \overline{f'(t) t^n d\sigma(t)} = \overline{f'(0)} + 0 = \overline{f'(0)}. \end{aligned}$$

The theorem is proved.

Theorem 3. If $f \in A_1'(D)$ and $f(0) = 0$, then $\forall z \in D$

$$f(z) = \frac{z}{\pi} \int_D \frac{1+z\bar{t}}{1-z\bar{t}} u(t) d\sigma(t),$$

where $u = \operatorname{Re} f'$.

Proof. It is obvious that

$$\frac{1+z\bar{t}}{1-z\bar{t}} = 2C(z, t) - 1 = \frac{2}{1-z\bar{t}} - 1.$$

Since $f' \in H_1'(D)$, we have (see [3])

$$\begin{aligned} f'(z) &= \frac{1}{\pi} \int_D \operatorname{Re} f'(t) \left[\frac{2}{(1-z\bar{t})^2} - 1 \right] d\sigma(t) \Leftrightarrow \\ \Leftrightarrow f(z) &= \frac{1}{\pi} \int_D \left[\int_D u(t) \left(\frac{2}{(1-\xi\bar{t})^2} - 1 \right) d\sigma(t) \right] d\xi = \\ &= \frac{1}{\pi} \int_D u(t) d\sigma(t) \int_0^1 \left[\frac{2}{(1-\xi\bar{t})^2} - 1 \right] d\xi = \frac{1}{\pi} \int_D \left[\frac{2z}{1-z\bar{t}} - z \right] u(t) d\sigma(t) = \frac{z}{\pi} \int_D \frac{1+z\bar{t}}{1-z\bar{t}} u(t) d\sigma(t). \end{aligned}$$

The theorem is proved.

Theorem 4. *The following propositions are equivalent:*

- 1) $f \in A_1'(D)$,
- 2) $\forall z \in D, f(z) = \frac{z}{\pi} \int_D f'(t) C(z, t) d\sigma(t)$,
- 3) $f(z) = \frac{z}{\pi} \int_D f'(t) [2 \operatorname{Re} C(z, t) - 1] d\sigma(t)$.

Proof. Theorem 1 implies that 1) \Leftrightarrow 2). Let us show that 2) \Rightarrow 3). Indeed, using Theorem 2 we obtain

$$\begin{aligned} \frac{z}{\pi} \int_D f'(t) [2 \operatorname{Re} C(z, t) - 1] d\sigma(t) &= \frac{z}{\pi} \int_D 2 \operatorname{Re} C(z, t) f'(t) d\sigma(t) - \frac{z}{\pi} \int_D f'(t) d\sigma(t) = \\ &= \frac{z}{\pi} \int_D [C(z, t) + \overline{C}(z, t)] f'(t) d\sigma(t) - \frac{z}{\pi} \int_D f'(t) d\sigma(t) = \frac{z}{\pi} \int_D C(z, t) f'(t) d\sigma(t) + \\ &\quad + \frac{z}{\pi} \int_D \overline{C}(z, t) f'(t) d\sigma(t) = f(z) - \frac{z}{\pi} \int_D f'(t) d\sigma(t) + \\ &\quad + \frac{z}{\pi} \int_D f'(t) d\sigma(t) + \frac{z}{\pi} \sum_{n=1}^{\infty} z^n \int_D f'(t) t^n d\sigma(t) = f(z) + 0 = f(z). \end{aligned}$$

If

$$f(z) = \frac{z}{\pi} \int_D f'(t) [2 \operatorname{Re} C(z, t) - 1] d\sigma(t),$$

then we have

$$f'(0) = \frac{1}{\pi} \int_D f'(t) d\sigma(t) \quad \text{as } z \rightarrow 0.$$

Hence we conclude that $f \in A_1'(D)$, i.e. 3) \Rightarrow 1). The theorem is proved.

Assume $f \in L^1(D)$, where $L^1(D)$ is the Lebesgue space, and consider the operator

$$C[f](z) = \frac{1}{\pi} \int_D \frac{f(t) d\sigma(t)}{1 - zt}.$$

Theorem 5. *If $f \in L^1(D)$, then the function $F : D \rightarrow \mathbb{C}$ defined $\forall z \in D$ by the equality*

$$F(z) = C[f](z) \tag{3}$$

belongs to the Hardy-Riesz class $H^p(D) \forall p \in (0, 1)$.

Proof. It is clear that F is an analytic function in D . We can assume without loss of generality that f is a real-valued non-negative function. Let us separate the real part of function (3). For this, we write the variables z and t in the explicit form: $z = re^{i\varphi}$, $t = \rho e^{i\theta}$, where $0 < r < 1$, $0 < \rho < 1$, $0 \leq \theta \leq 2\pi$, $0 \leq \varphi \leq 2\pi$. Thus

$$\begin{aligned}
 F(z) &= \frac{1}{\pi} \int_D \frac{f(\rho e^{i\theta}) \rho d\rho d\theta}{1 - r\rho e^{i(\theta-\varphi)}} = \frac{1}{\pi} \int_0^{1-2r} \int_0^{2\pi} \frac{(1-r\rho e^{i(\theta-\varphi)}) f(\rho e^{i\theta}) \rho d\rho d\theta}{|1 - r\rho e^{i(\theta-\varphi)}|^2} = \\
 &= \frac{1}{\pi} \int_0^{1-2r} \int_0^{2\pi} \frac{(1-r\rho \cos(\theta-\varphi)) f(\rho e^{i\theta}) \rho d\rho d\theta}{1+r^2\rho^2-2r\rho \cos(\theta-\varphi)} + \frac{i}{\pi} \int_0^{1-2r} \int_0^{2\pi} \frac{r\rho \sin(\varphi-\theta) f(\rho e^{i\theta}) \rho d\rho d\theta}{1+r^2\rho^2-2r\rho \cos(\theta-\varphi)},
 \end{aligned}$$

whence we obtain

$$\begin{aligned}
 u(z) = \operatorname{Re} F(z) &= \frac{1}{\pi} \int_0^{1-2r} \int_0^{2\pi} \frac{(1-r\rho \cos(\theta-\varphi)) f(\rho e^{i\theta}) \rho d\rho d\theta}{1+r^2\rho^2-2r\rho \cos(\theta-\varphi)} \geq \\
 &\geq \frac{1}{\pi} \int_0^{1-2r} \int_0^{2\pi} \frac{(1-r\rho) f(\rho e^{i\theta}) \rho d\rho d\theta}{(1+r\rho)^2} \geq \frac{1-r}{\pi(1+r)^2} \int_0^{1-2r} \int_0^{2\pi} f(\rho e^{i\theta}) \rho d\rho d\theta = \frac{1-r}{\pi(1+r)^2} \|f\| \geq 0.
 \end{aligned}$$

Therefore since the real part of the function F is non-negative, by virtue of Smirnov's theorem (see [4]),

$$F \in H^p(D), \quad \forall p \in (0, 1).$$

Theorem 6. If $f \in A_1'(D)$, then

$$f \in \bigcap_{0 < p < 1} H^p(D).$$

Proof. According to Theorem 1, $\forall z \in D$ we have

$$f(z) = f(0) + \frac{z}{\pi} \int_D \frac{f'(t) d\sigma(t)}{1-zt},$$

thus, by virtue of Theorem 5, $f \in H^p(D)$, $\forall p \in (0, 1)$, i.e. $A_1'(D) \subset H^p(D)$, $\forall p \in (0, 1)$.

Corollary 1. If $f \in A_1'(D)$, then there exists an angular limit of the function f

$$f^* \in L^p(T), \quad \forall p \in (0, 1)$$

a.e. on the circumference T .

Corollary 2. If $f \in A_2'(D)$, where $A_2'(D)$ is the Dirichlet space, i.e.

$$\iint_D |f'(t)|^2 d\sigma(t) < \infty,$$

then the function f has an angular limit

$$f^*(t) = \lim_{z \rightarrow t} f(z) \text{ and } f^* \in L^p(D), \quad \forall p \in (0, 1)$$

a.e. on T .

S. M. Nikolski (see [5]) showed that if the harmonic function $u : D \rightarrow \mathbb{R}$ satisfies the conditions:

$$1) \int_D |u(z)| d\sigma(z) < \infty,$$

$$2) \int_D (\text{grad } u)^2 d\sigma(z) < \infty,$$

then there exists a radial limit of the function u

$$f(\theta) = \lim_{r \rightarrow 1} u(re^{i\theta})$$

a.e. on the circumference T and $f \in L^2(T)$.

Let us assume that $f(z) = u(z) + iv(z)$, where v is a continuous conjugate harmonic function of u . Then

$$|f'(z)|^2 = (\text{grad } u)^2 = (\text{grad } v)^2,$$

and therefore, by condition 2), the function f has a.e. on T the angular boundary values $f^*(t)$ and $f^* \in L^p(T)$, $\forall p \in (0, 1)$. Hence we conclude that the following statement is true.

Corollary 1. If the harmonic function $u: D \rightarrow \mathbb{R}$ satisfies the condition

$$|f'(z)|^2 = (\text{grad } u)^2 = (\text{grad } v)^2,$$

then the function u has a.e. on the circumference T the angular limit $u^*(e^{i\theta}) = \lim_{z \rightarrow e^{i\theta}} u(z)$ and $u^* \in L^p(T)$, $\forall p \in (0, 1)$.

If the harmonic function $u: D \rightarrow \mathbb{R}$ satisfies both conditions of Nikolski's theorem, then the analytic function $f(z) = u(z) + iv(z)$, where $u(z) = \text{Re } f(z)$, will satisfy the conditions:

$$1) \int_D |f(z)| d\sigma(z) < \infty,$$

$$2) \int_D |f'(z)|^2 d\sigma(z) < +\infty.$$

Indeed, by the Riesz inequality (see [1]) we have

$$\|f\| = \int_D |f(z)| d\sigma(z) \leq c \int_D |u(z)| d\sigma(z) = c \|u\|,$$

where c is a positive constant, whence we obtain

$$\|v\| \leq \|f\| \leq c \|u\|.$$

This means that the function v satisfies condition 1) of Nikolski's theorem.

Therefore, since

$$|f'(z)|^2 = \left(\frac{\partial u}{\partial x}\right)^2 + \left(\frac{\partial u}{\partial y}\right)^2 = \left(\frac{\partial v}{\partial x}\right)^2 + \left(\frac{\partial v}{\partial y}\right)^2 = (\text{grad } u)^2,$$

the functions f and v satisfy condition 2) of Nikolski's theorem.

According to Theorem 6, there exist a.e. on the circumference T the angular limits:

$$f^*(t) = \lim_{z \rightarrow t} f(z),$$

$$u^*(t) = \lim_{z \rightarrow t} u(z),$$

$$v^*(t) = \lim_{z \rightarrow t} v(z).$$

Moreover, $f^* \in L^p(T)$, $u^* \in L^p(T)$ and $v^* \in L^p(T)$, $\forall p \in (0,1)$. By Nikolski's theorem (see [5]), $f^* \in L^2(T)$, $u^* \in L^2(T)$ and $v^* \in L^2(T)$. Hence, by Smirnov's theorem (see [4]) $f \in H^2(D)$ and therefore $u, v \in h^2(D)$.

We have thereby proved the validity of

Theorem 7. *If the harmonic function $u : D \rightarrow R$ satisfies the conditions:*

- 1) $\int_D |u(z)| d\sigma(z) < \infty$,
- 2) $\int_D (\text{grad } u)^2 d\sigma(z) < +\infty$,

then $u \in h^2(D)$ or

$$\|u\| = \sup_{0 < r < 1} \int_0^{2\pi} |u(re^{i\theta})|^2 d\theta < \infty.$$

Theorem 8. *If the real part of the analytic function $f(z) = u(z) + iv(z)$ satisfies the conditions:*

- 1) $\int_D |u(z)| d\sigma(z) < \infty$,
- 2) $\int_D (\text{grad } u)^2 d\sigma(z) < \infty$,

then $f \in H^2(D)$, i.e.

$$\sup_{0 < r < 1} \int_0^{2\pi} |f(re^{i\theta})|^2 d\theta < \infty.$$

მათემატიკა

დირიხლეს სასრული ინტეგრალის მქონე ანალიზური და ჰარმონიული ფუნქციების შესახებ ერთეულოვან წრეში

გ. ა. ონიანი*, გ. თეთვაძე†

* აკაკი წერეთლის სახელმწიფო უნივერსიტეტი, ზუსტ და საბუნებისმეტყველო მეცნიერებათა ფაკულტეტი, ქუთაისი

(წარმოდგენილია აკადემიის წევრის რ. პანცურის მიერ)

სტატიაში შესწავლილია ერთეულოვან წრეში ჯამებადი წარმოებულის მქონე ანალიზური და ჯამებადი გრადიენტის მქონე ჰარმონიული ფუნქციების ინტეგრალური წარმოდგენები და სასაზღვრო თვისებები. დაზუსტებულია ჰარმონიული ფუნქციის სასაზღვრო მნიშვნელობის არსებობის შესახებ ს.მ. ნიკოლსკის ერთი თეორემა.

REFERENCES

1. S. V. Shvedenko (1985), *Mathematical Analysis*, 23: 3-124, VINITI, M. (in Russian).
2. V. Kabaila (1970), *Litovsk. Mat. Sb.*, 10: 471-490 (in Russian).
3. G. A. Oniani (1978), *Soobshch. AN GSSR*, 89, 2: 301-304 (in Russian).
4. I. I. Privalov (1950), *Boundary properties of analytic functions*, 2nd ed. M.-L. (in Russian).
5. S. M. Nikolski (1959), *Boundary values of functions*. In: *USSR during 40 years: 1917-1957*, Moscow (in Russian).

Received December, 2011

Mathematics

On the Regular Convergence by Rectangles of Multiple Fourier-Haar Series

Giorgi Oniani

Department of Exact and Natural Sciences, Akaki Tsereteli State University, Kutaisi

(Presented by Academy Member Vakhtang Kokilashvili)

ABSTRACT. It is sharpened the known result on almost everywhere convergence by rectangles of Fourier-Haar series of functions from $L(\ln^+ L)^{n-1}([0,1]^n)$. Namely, it is proved that the condition $f \in L(\ln^+ L)^k([0,1]^n)$, where $0 \leq k \leq n-1$, implies almost everywhere convergence of each subseries of Fourier-Haar series of f having dimension not more than $k+1$. © 2012 Bull. Georg. Natl. Acad. Sci

Key words: Fourier-Haar series, multiple series, convergence, subseries.

Definitions and notation. Below everywhere if something else is not said we will assume that $n \in \mathbb{N}$ and $n \geq 2$. For a given n -tuple Haar series

$$\sigma = \sum_{k \in \mathbb{N}^n} c_k h_k$$

by $S_m(\sigma)(x)$, $S_r(\sigma)(x)$, and $G_m(\sigma)(x)$, where $x \in \mathbb{I}^n = [0,1]^n$, $m \in \mathbb{N}^n$ and $r > 0$, denote, respectively, a rectangular partial sum, a spherical partial sum, and a rectangular general term of σ , i.e.,

$$S_m(\sigma)(x) = \sum_{k_1=1}^{m_1} \cdots \sum_{k_n=1}^{m_n} c_k h_k(x),$$

$$S_r(\sigma)(x) = \sum_{k_1^2 + \cdots + k_n^2 \leq r} c_k h_k(x),$$

$$G_m(\sigma)(x) = c_m h_m(x),$$

where $m = (m_1, \dots, m_n)$, $k = (k_1, \dots, k_n)$. If σ is the Fourier-Haar series of a function $f \in L(\mathbb{I}^n)$, then we will use f instead of σ in the above notation.

Fourier-Haar series of a function $f \in L(\mathbb{I}^n)$ at a point $x \in \mathbb{I}^n$ denote by $\sigma(f)(x)$.

Let $1 \leq k \leq n-1$. Any sequence obtained from $(a_m)_{m \in \mathbb{N}^n}$ by fixing some $n-k$ among n coordinates of the index $m = (m_1, \dots, m_n)$ is called a k -dimensional section of a sequence $(a_m)_{m \in \mathbb{N}^n}$. By n -dimensional section of $(a_m)_{m \in \mathbb{N}^n}$ we mean $(a_m)_{m \in \mathbb{N}^n}$.

Let $1 \leq k \leq n$. Any series composed by some k -dimensional section of the sequence $(a_m)_{m \in \mathbb{N}^n}$ is called k -dimensional subseries of the series $\sum_{m \in \mathbb{N}^n} a_m$.

Let us say that a series $\sum_{m \in \mathbb{N}^n} a_m$ regularly converge by rectangles if its every subseries converges by rectangles (here convergence by rectangles of single series is understood as its ordinary convergence). Note that such type of convergence of multiple series was considered by Móricz [1, 2].

Saying that a sequence $(a_m)_{m \in \mathbb{N}^n}$ converges (strongly converges) we mean the convergence of a_m to the limit as $\min\{m_1, \dots, m_n\} \rightarrow \infty$ ($\max\{m_1, \dots, m_n\} \rightarrow \infty$).

Note that for a sequence $(a_m)_{m \in \mathbb{N}^n}$ the following statements are equivalent: 1) $(a_m)_{m \in \mathbb{N}^n}$ strongly converges to a ; 2) $(a_m)_{m \in \mathbb{N}^n}$ converges to a and every $(n-1)$ -dimensional section of $(a_m)_{m \in \mathbb{N}^n}$ strongly converges to a ; 3) every section of $(a_m)_{m \in \mathbb{N}^n}$ converges to a .

It is clear that if series $\sum_{m \in \mathbb{N}^n} a_m$ regularly converges by rectangles, then its general term $(a_m)_{m \in \mathbb{N}^n}$ strongly converges to 0.

Result. It is known that for every $n \geq 2$, $L(\ln^+ L)^{n-1}(\mathbb{I}^n)$ is the widest integral class in which the almost everywhere convergence of Fourier-Haar series is provided both for rectangular partial sums (see [3,4]) and for spherical partial sums (see [5-7]). Here we note that cubic partial sums of Fourier-Haar series of every summable function f (i.e. $S_m(f)(x)$ with $m_1 = m_2 = \dots = m_n$) converge almost everywhere to f (see e.g. [4] for details).

The following theorem is true.

Theorem. If $0 \leq k \leq n-1$ and $f \in L(\ln^+ L)^k(\mathbb{I}^n)$, then every $(k+1)$ -dimensional subseries of $\sigma(f)(x)$ regularly converges by rectangles for almost every $x \in \mathbb{I}^n$.

Corollary 1. If $f \in L(\ln^+ L)^{n-1}(\mathbb{I}^n)$, then $\sigma(f)(x)$ regularly converges by rectangles for almost every $x \in \mathbb{I}^n$.

Corollary 2 ([3,4]). If $f \in L(\ln^+ L)^{n-1}(\mathbb{I}^n)$, then $\sigma(f)(x)$ converges by rectangles for almost every $x \in \mathbb{I}^n$.

Corollary 3 ([8]). If $f \in L(\ln^+ L)^{n-2}(\mathbb{I}^n)$, then every $(n-1)$ -dimensional section of the sequence $(G_m(f)(x))_{m \in \mathbb{N}^n}$ strongly converges to 0 for almost every $x \in \mathbb{I}^n$.

Remark. In [8] it was proved that: If an n -tuple Haar series σ converges by rectangles at a diadic-irrational point x and the rectangular general term $(G_m(\sigma)(x))_{m \in \mathbb{N}^n}$ strongly converges to 0, then σ

spherically converges at x to $\lim_{m \rightarrow \infty} S_m(\sigma)(x)$.

From this result follows the corollary: *If an n -tuple Haar series σ regularly converges by rectangles at a diadic-irrational point x , then σ spherically converges at x to $\lim_{m \rightarrow \infty} S_m(\sigma)(x)$.*

მათემატიკა

ფურიე-ჰაარის ჯერადი მწკრივების მართკუთხედების მიხედვით რეგულარული კრებალობის შესახებ

გ. ონიანი

აკაცი წერეთლის სახელმწიფო უნივერსიტეტი, შუსტ და საბუნებისმეტყველო მეცნიერებათა ფაკულტეტი, ქუთაისი

(წარმოდგენილია აკადემიის წევრის ე. კოკილაშვილის მიერ)

გაძლიერებულია ცნობილი შედეგი $L(\ln^+ L)^{n-1}([0,1]^n)$ ფუნქციის ფურიე-ჰაარის მწკრივის მართკუთხედების მიხედვით თითქმის ყველგან კრებალობის შესახებ. სახელდობრ, დამტკიცებულია, რომ $f \in L(\ln^+ L)^k([0,1]^n)$ პირობა, სადაც $0 \leq k \leq n-1$, იწვევს f -ის ფურიე-ჰაარის მწკრივის, $k+1$ -ზე არაუმეტესი განზომილების მქონე ყოველი ქვემწკრივის თითქმის ყველგან კრებალობას.

REFERENCES

1. F. Móricz (1979), Analysis Math., 5, 3: 135-147.
2. F. Móricz (1983), Acta Math. Hungar., 41:161-168.
3. O. P. Dzagnidze (1964), Soobshch. AN. GSSR, 34: 277-282.
4. T. S. Zerekidze (1985), Trudy Razmadze Mat. Inst. Tbilisi, 76: 80-99 (in Russian).
5. G. G. Kemkhadze (1977), Trudy Razmadze Mat. Inst. Tbilisi, 55: 27-38 (in Russian).
6. G. E. Tkebuchava (1994), Analysis Math., 20, 2: 147-153.
7. G. G. Oniani (2008), Dokl. Akad. Nauk Rossii, 419, 2: 169-170 (in Russian); translation in: (2008) Dokl. Math., 77, 2: 203-204.
8. G. G. Oniani (2012), Uspekhi Mat. Nauk, 67, 1: 185-186 (in Russian); translation in: (2012) Russian Math. Surveys, 67, 1.

Received February, 2012

Mathematics

Singular Integral Equation Arising from the Theory of the Penetration of Gamma Rays

Pikria Ghurtskaia* and Dazmir Shulaia**

* Department of Computer Engineering, Georgian Technical University, Tbilisi

** I. Vekua Institute of Applied Mathematics of I. Javakishvili Tbilisi State University

(Presented by Academy Member Revaz Bantsuri)

ABSTRACT. The aim of this paper is to study, in the class of Hölder functions, the linear integral equation arising from the theory of the penetration of gamma rays. Using the theory of singular integral equations, the solution of this equation is reduced to the Volterra equation. © 2012 Bull. Georg. Natl. Acad. Sci.

Key words: singular equation, piecewise holomorphic function, limiting values.

We present a method for solving singular integral equations which frequently occur when investigating many important problems of mathematical physics, namely in the fundamental problems of nuclear transport theory [1-3]. This equation has the form

$$(Lu)(x,t) = \int_{a-1}^{x+1} \frac{sK(x,y)}{s-t} u(y,s) ds dy + u(x,t) + \int_{a-1}^{x+1} \frac{tK(x,y)}{t-s} u(y,t) ds dy = f(x,t), \quad (1)$$

$$x \in [a,b], \quad t \in (-1,+1),$$

where $K(x,y)$ is the real-valued continuous function, the right part $f(x,t)$ is the real-valued function satisfying H^* condition (Muskhelishvili class) [4] with respect to t and we look for the solution of a continuous function satisfying H^* condition with respect to t .

Let Ω_z be the integral operator defined by

$$(\Omega_z g_z)(x,t) = g_z(x,t) + z \int_{a-1}^{x+1} \frac{K(x,y)}{z-t} g_z(y,t) dt dy, \quad x \in [a,b], \quad t \in (-1,+1), \quad (2)$$

where the parameter z is any point on the plane. This operator operating on any continuous function $g_z(x,t)$

piecewise holomorphic in z with a cut on the real axis $[-1, +1]$ and satisfying the H^* condition in t , will define a piecewise holomorphic function with a cut on $[-1, +1]$. By using the Plemelj-Sokhotskii formulas, we can calculate the limiting values of Ω_z as

$$(\Omega_z^\pm g_\zeta^\pm)(x, t) \equiv g_\zeta^\pm(x, t) + \zeta \int_a^{x+1} \frac{K(x, y)}{\zeta - s} g_\zeta^\pm(y, s) ds dy \pm i\pi \int_a^x K(x, y) g_\zeta^\pm(y, t) dy, \quad (3)$$

$$\zeta \in (-1, +1), \quad x \in [a, b], \quad t \in (-1, +1).$$

The basic result for L is the following theorem.

Theorem 1. *The equation*

$$(Lu)(x, t) = f(x, t) \quad (4)$$

admits only a unique continuous solution $u(x, t)$ satisfying the H^* condition with respect to t .

Proof. Let u be a solution of (1) and consider the function

$$\Psi_z(x) = \frac{1}{2i\pi} \int_a^{x+1} \int_{s-z}^1 \frac{sK(x, y)}{s-z} u(y, s) ds dy.$$

This function possesses the following properties:

(P₁) In the plane with the cut $[-1, +1]$ it is piecewise holomorphic with respect to z .

(P₂) As $z \rightarrow \infty$ it vanishes uniformly in x .

(P₃) By using the Plemelj-Sokhotskii formulas

$$\Psi_t^\pm(x) = \frac{1}{2i\pi} \int_a^{x+1} \int_{s-t}^1 \frac{sK(x, y)}{s-t} u(y, t) dt dy \pm \frac{t}{2} \int_a^x K(x, y) u(y, t) dy.$$

Combining the above equalities with (3), we get

$$\begin{aligned} (\Omega_t^+ \Psi_t^+)(x) - (\Omega_t^- \Psi_t^-)(x) &\equiv t \int_a^x K(x, y) u(y, t) dy + \int_a^{x+1} \int_{s-t}^1 \frac{sK(x, y)}{s-t} \int_a^y K(y, y') u(y, s) dy' ds dy + \\ &+ \int_a^x K(x, y) \int_a^{y-1} \int_{s-t}^1 \frac{tK(y, y')}{s-t} u(y, s) ds dy' dy. \end{aligned}$$

In view of (1) we obtain

$$(\Omega_t^+ \Psi_t^+)(x) - (\Omega_t^- \Psi_t^-)(x) = t \int_a^x K(x, y) f(y, t) dy.$$

Consequently, taking the Plemelj-Sokhotskii formulas into account, we can write

$$(\Omega_z \Psi_z)(x) = \int_a^{x+1} \int_{s-z}^1 \frac{sK(x, y) f(y, t)}{s-z} ds dy. \quad (5)$$

By virtue of Tamarkin's theorem [5] it follows that there is a unique solution of (5). This solution possesses the properties:

(R₁) In the plane with a cut $[-1, +1]$ it is piecewise holomorphic with respect to z .

(R₂) As $z \rightarrow \infty$ it vanishes uniformly in x .

(R₃) It may be represented in the form

$$\Psi_z(x) = \frac{1}{2i\pi} \int_{-1}^{+1} \frac{k(x,t)}{s-z} ds, \quad z \notin [-1, +1], \quad x \in [a, b],$$

where $k(x, t)$ is a certain uniquely determined function.

In view of the Plemelj-Sokhotskii formulas, the following equality is valid for the limiting values:

$$\Psi_t^+(x) + \Psi_t^-(x) = \frac{1}{i\pi} \int_{-1}^{+1} \frac{\Psi_s^+(x) - \Psi_s^-(x)}{s-t} ds. \quad (6)$$

By using (3), from (6) we are able to write

$$\overline{\Psi}_t(x) + \int_{a-1}^{x+1} \frac{sK(x,y)}{s-t} \overline{\Psi}_t(y) ds dy + \int_{a-1}^{x+1} \frac{sK(x,y)}{s-t} \overline{\Psi}_s(y) ds dy = \int_a^x K(x,y) f(y,t) dy, \quad (7)$$

where

$$\overline{\Psi}_t(x) = \Psi_t^+(x) - \Psi_t^-(x).$$

Let us consider now the following equation

$$u(x,t) + \int_{a-1}^{x+1} \frac{tK(x,y)}{s-t} ds u(x,t) dy = \int_{-1}^{+1} \frac{s\overline{\Psi}_t(x)}{t-s} ds + f(x,t), \quad (8)$$

which has a unique solution. Denote by

$$P(x,t) = \overline{\Psi}_t(x) - \int_a^x K(x,y) u(y,t) dy.$$

In view of (7) from (8) it follows that

$$P(x,t) + \int_{a-1}^{x+1} \frac{tK(x,y)}{s-t} P(y,s) ds dy = 0.$$

But Ω_z has no eigenvalues on $[-1, +1]$ and consequently

$$\overline{\Psi}_t(x) = \int_a^x K(x,y) u(y,t) dy.$$

Taking into account this last assertion, from (8) we obtain

$$u(x,t) + \int_{a-1}^{x+1} \frac{tK(x,y)}{t-s} ds u(x,t) dy = \int_{a-1}^{x+1} \frac{sK(x,y)}{t-s} u(y,s) ds dy + f(x,t),$$

which means that (4) holds and the proof is complete.

Now, our aim is a deeper study of the singular operator L . We wish to find the reduction operator of L and

hence reduction of the considered equation to a regular equation. For this purpose, we need to introduce the following singular operator

$$(Su)(x,t) \equiv \int_{a-1}^{x+1} \frac{sK(x,y)}{t-s} u(y,s) ds dy + u(x,t) + \int_{a-1}^{x+1} \frac{tK(x,y)}{t-s} u(y,t) ds dy.$$

We shall note the following property of the introduced operator. For any two continuous functions $u(x,t)$ and $v(x,t)$, satisfying the H^* conditions with respect to t

$$\int_{a-1}^{b+1} \int_{a-1}^{b+1} uSv dt dx = \int_{a-1}^{b+1} \int_{a-1}^{b+1} vLu dt dx.$$

Consequently, if equation (1) has a solution, then necessarily

$$\int_{a-1}^{b+1} \int_{a-1}^{b+1} v f dt dx = 0,$$

where v is any solution of the homogeneous equation

$$Sv = 0. \tag{9}$$

But the equation (1) admits only a unique solution, therefore equation (9) also admits a unique zero solution.

In our further consideration we will need also the following identity:

$$\begin{aligned} & \int_{a-1}^{x+1} \frac{sK(x,y)}{t-s} \int_{a-1}^y \frac{s'K(y,y')}{s'-s} u(y',s') ds' dy' ds dy = \\ & = \int_{a-1}^{x+1} \frac{u(y',t)}{s'-t} \left(\int_{y-1}^{x+1} \frac{tK(x,y)s'K(y,y')}{t-s} ds' dy' - \int_{y-1}^{x+1} \frac{tK(x,y)s'K(y,y')}{s'-s} ds' dy' \right) ds dy + \\ & \quad + \pi^2 t^2 \int_a^x \int_y^x K(x,y)K(y,y')u(y',t) dy' dy. \end{aligned} \tag{10}$$

This identity can be obtained by using the Bertrand-Poincaré formula [4].

We can show the important property of the operator S in the Theorem below.

Denote

$$\begin{aligned} R(x,y,t) = & -\pi^2 t^2 \int_y^x K(x,y')K(y',x)dy' + \int_{-1}^{+1} \frac{tK(x,y)}{t-s} ds + \int_{-1}^{+1} \frac{tK(y,x)}{t-s} ds - \\ & - \int_{y-1}^{x+1} \frac{tK(x,y)}{t-s} ds \int_{-1}^{+1} \frac{tK(y',x)}{t-s} ds dy'. \end{aligned}$$

Theorem 2. *The composition SL contains no singular part and the equality*

$$(SL)(x,t) = u(x,t) + \int_a^x R(x,y,t)u(y,t) dy \tag{11}$$

holds.

Proof. Performing the operations indicated on the left-hand side of (11) using identity (10) we obtain that Eq. (11) is true.

Thus, we may say that S reduces operator of L .

***Acknowledgement.** The first author is supported by the Shota Rustaveli National Science Foundation (Projects # GNSF/ST08/3-383).

მათემატიკა

გამა სხივების გაჭოლვის თეორიიდან წარმოქმნილი სინგულარული ინტეგრალური განტოლება

ფ. ღურწყაია*, დ. შულაია**

* საქართველოს ტექნიკური უნივერსიტეტი, კომპიუტერული ინჟინერიის დეპარტამენტი, თბილისი

** ი. ჯავახიშვილის სახ. თბილისის სახელმწიფო უნივერსიტეტის ი. ვაკუას გამყოფენობით მათემატიკის ინსტიტუტი, თბილისი

ნაშრომში წარმოდგენილია გამა სხივების გაჭოლვის თეორიიდან წარმოქმნილი სინგულარული ინტეგრალური განტოლების ამოხსნის მეთოდი ჰელდერის სივრცეში. განტოლების ამოხსნა დაიყვანება ვოლტერას ტიპის მეორე გეარის ერთგანზომილებიანი რეგულარული ინტეგრალური განტოლების ამოხსნამდე.

REFERENCES

1. *U. Fano, L. V. Spenser, M. J. Berger* (1959), Penetration and diffusion of X rays. Handbuch der Physik. Band XXXVIII/2, Berlin-Göttingen-Heidelberg.
2. *D. A. Shulata* (1990), DAN SSSR, **310**, 4: 844-849 (in Russian).
3. *D. A. Shulata* (1983), J. Vych. Math. i Math. Phys. **23**, 5: 1125-1140 (in Russian).
4. *N. Muskhelishvili* (1953), Singular Integral Equations, Groningen: P. Noordhoff.
5. *J. Tamarkin* (1927), Ann. Math., **28**, 2: 127-152.

Received April, 2012

Structural Mechanics

One Mathematical Model and Algorithm of the Microtremor Use for Structure Real Seismic Resource Assessment

Guram Gabrichidze

Academy Member, K. Zavriv Structural Mechanics, Earthquake Resistance and Engineering Examination Center, Tbilisi

ABSTRACT. Study of the structure behavior under microtremors to assess its real operating condition or to ascertain its dynamic characteristics is a widespread method in the world. It is distinguished for its cheapness, mobility, though it has also certain limitations. It is that transition process from microtremor to real is not univocal and relies on certain assumptions. Therefore, when we use this approach in practice, we are offered different algorithms and technologies of material processing obtained as the result of the experimental observation of the structure under microtremor, which creates probability of structure operational condition, particularly, its earthquake resistance distinctive assessment. Mathematical model and algorithm constructed on its basis, which univocally ascertains how to process displacements recorded under microtremors that to speak substantially about structure behavior when real seismic wave (seismogram) passes its foundation are suggested in the present article. © 2012 Bull. Georg. Natl. Acad. Sci.

Key words: *microtremors, seismic resistance of structures, earthquake.*

At present the acute problem of the whole world is seismic resistance assessment of structures located in seismically active regions. Complexity of this problem solution is determined by the fact that enormous number of structures are subject to such assessment, not only those that are built without observing antisismic design standards, but also those that are built considering the requirements of these standards. This is due to the fact that standards of earthquake resistance design periodically change and structures, built “yesterday”, do not correspond to today’s beliefs.

In practice very often it is necessary to examine a great number of structures in a short term in an operational situation. Such necessity often arises after a strong earthquake, or in the cases when the existing view concerning real seismic danger assessment changes and seismic danger assessment of a large populated region is required.

In such cases it is very difficult, or even impossible to carry out detailed inspection of the structures operational condition, following the recommendations of the corresponding normative documents, and incomplete examination of buildings in many cases is

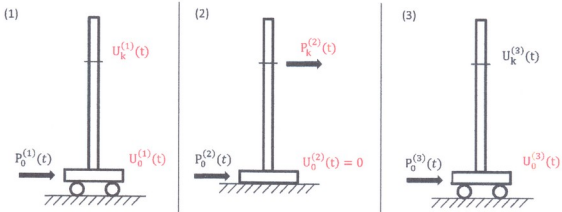


Fig. Dynamic states of structures.

unreliable or even dangerous.

In practice often an experimental method is used for structures behavior assessment under earthquake, connected with carrying out full-scale dynamic tests. In such cases structural elements of the structure reveal their real physical-mechanical properties and define the structure behavior as a whole.

Carrying out of full-scale dynamic tests of structures is an expensive and laborious process and cannot be used as an express-method. It should be mentioned also that as a result of full-scale dynamic tests basic dynamic parameters of the structure are defined, such as vibrations frequencies and forms, damping factor and so on. To ascertain structure behavior under earthquake it is also required to construct a mathematical model according to the results obtained experimentally and to carry out special calculations that are associated with certain conditionality.

In the engineering practice a number of simplified methods of structures seismic resource definition by full-scale dynamic tests are developed and applied. Some of them are characterized by refusal to apply complex, expensive means of excitation of strong vibrations of the structure and study structure behavior under microtremors or even ambient noise of the earth's surface. On the basis of the obtained data structure behavior under stronger excitations, particularly earthquakes, is assessed.

Transition from structure behavior under microtremor to behavior under strong influence is not univo-

cal process and relies on certain assumptions that make possible to develop different algorithms and, hence, different assessments of the seismic resource of the structure under test [1-4].

A mathematical model is suggested in the present article and on its basis an algorithm is constructed, which defines univocally how to process experimental information, obtained from structure under microtremor, to speak substantially about structure behavior under real, stronger and other kind of influence, in particular, under seismic waves passage.

Let us consider a structure (Fig.) in the foundation of which (at point 0) and at some level (at point K) seismographs are placed and displacements of these points synchronously caused by microtremor in the foundation of the structure are recorded.

This dynamic state of the structure, acting forces in the foundation and generated displacements conditionally are shown in the first column of the Fig. All the parameters of this dynamic state are marked by (1).

In the second column of the Fig. the second dynamic state of the structure is shown. It is imaginary and actually is not realized. The structure is rigidly fastened in the foundation and arbitrary force $P_k^{(2)}(t)$ is applied at the point K. All the parameters of this dynamic state are marked by (2).

In the third column of the Fig. the structure is shown, in the foundation of which seismic wave (seismogram) of the real earthquake spreads. All the

parameters of this dynamic state are marked by (3).

To simplify the perception of the further lay-outs in Fig. and in the obtained expressions, given (known) functions are represented in red color.

Let us apply to the known principle of the works reciprocity $A^{(i)(k)}(t) = A^{(k)(i)}(t)$ which states that the work of the forces of i dynamic state on the displacements of the k dynamic state is equal to the work of the forces of k state on the displacements of the i state.

Let us apply this principle to the dynamic states (1) and (2):

Considering the directions of the Fig. we write:

$$A^{(1)(k)}(t) = \int_0^t P_0^{(1)}(t-\tau) \times U_0^{(2)}(\tau) d\tau = 0.$$

Hence, the principle of the work reciprocity $A^{(1)(k)}(t) = A^{(k)(1)}(t)$, will take the form $A^{(2)(1)}(t) = 0$ and will be written as an integral equation:

$$\int_0^t P_0^{(2)}(t-\tau) \times U_0^{(1)}(\tau) d\tau + \int_0^t P_k^{(2)}(t-\tau) \times U_k^{(1)}(\tau) d\tau = 0. \quad (a)$$

Solving the equation (a) we define the function $P_0^{(2)}(t)$.

Let us apply the principle of the work reciprocity

to the dynamic systems (2) and (3). Let us remember that we have already defined function $P_0^{(2)}(t)$ and it is known (it is red). Considering the mentioned and directions of the Fig. we write:

$$A^{(3)(2)}(t) = \int_0^t P_0^{(3)}(t-\tau) \times U_0^{(2)}(\tau) d\tau = 0.$$

Hence, the principle of the work reciprocity $A^{(2)(3)}(t) = A^{(3)(2)}(t)$ will take the form

$A^{(2)(3)}(t) = 0$ and will be written as an integral equation:

$$\int_0^t P_0^{(2)}(t-\tau) \times U_0^{(3)}(\tau) d\tau + \int_0^t P_k^{(2)}(t-\tau) \times U_k^{(3)}(\tau) d\tau = 0. \quad (b)$$

Solving the integral equation (b) we define $U_k^{(3)}(t)$, displacement of the point K under real seismic wave passage in the foundation of the structure.

Such method allows possible to define displacements of any point and hence, behavior of the entire structure, all of its structural and non-structural elements and components under real earthquake. Modern possibilities of measuring technology, existence of wireless sensory nets and telecommunication systems open wide possibilities for the solution of various problems, using the suggested method.

სამშენებლო მექანიკა

ნაგებობის რეალური სეისმური რესურსის შესაფასებლად სუსტი რყევების გამოყენების ერთი მათემატიკური მოდელი და ალგორითმი

გ. გაბრიჩიძე

აკადემიის წევრი, კ.ზურაბიძის სამშენებლო მექანიკის, სეისმოლოგიის და ხანძარბრუნვის კვლევების ცენტრი, თბილისი

სუსტი რყევებისას ნაგებობის ქცევის შესწავლა მისი რეალური ტექნიკური მდგომარეობის შესაფასებლად, ან მისი დინამიკური მახასიათებლების დასადგენად, ფართოდ გავრცელებული მეთოდია მთელს მსოფლიოში. იგი გამოირჩევა თავისი სიიარაღით, მობილურობით, თუმცა გააჩნია გარკვეული შეზღუდვებიც. საქმე იმაშია, რომ სუსტიდან რეალურზე გადასვლის პროცედურა არ არის ცალსახად განპირობებული და გარკვეულ დაშვებებს ემყარება. ამის გამოა, რომ პრაქტიკაში ამ მიდგომის გამოყენებისას, სუსტი რყევებისას ნაგებობაზე ექსპერიმენტული დაკვირვებისას მოპოვებული მასალის გადამუშავებისას სხვადასხვა ალგორითმებსა და ტექნოლოგიებს გეთყაზობენ, რაც ნაგებობათა ტექნიკური მდგომარეობის, კერძოდ, მისი სეისმოლოგიის განსხვავებული შეფასების ალბათობას ქმნის. წარმოდგენილ სტატიამში შემოთავაზებულია მათემატიკური მოდელი და მის საფუძველზე ჩამოყალიბებული ალგორითმი, რომელიც ცალსახად განსაზღვრავს, თუ როგორ უნდა გადამუშავდეს სუსტი ზემოქმედებისას ჩაწერილი გადაადგილებები, რომ დასაბუთებულად ვიმსჯელოთ შენობის ქცევაზე მის ფუძეში რეალური სეისმური ტალღის (სეისმოგრამის) გავლისას.

REFERENCES

1. *Yutaka Nakamura, E.Dilek Gurler, Jun Saita* (1999), Dynamic Characteristics of Leaning Tower of Piza Using Microtremor-Preliminary Results. 25th Japan Congress on Earthquake Engineering. Tokyo. 7: 29-31.
2. *Yutaka Nakamura* (2001), Inventory Development for Natural and Built Environments: Use of Seismic Motion and Microtremor for Vulnerability Assessment. 4th EQTAP Workshop in Kamakura, December. 6p.
3. *Jun Saita, Yutaka Nakamura* (2010), Vulnerability Assessment for Ground and Structures Using Ambient Noise. System and Data Research, Co., Ltd., 3-25-3 Fujimidai, Kunitachi, Tokyo, 186-0003, Japan. 2p.
4. *G. Gabrichidze* (2005), Proceedings of the Institute of Structural Mechanics and Earthquake Engineering, 5: 31-35. Tbilisi.

Received May, 2012

Physics

On Quantum Description of Parametric Instability of Coherently Precessing Spin Mode of Superfluid $^3\text{He-A}$

Giorgi Baramidze* and Giorgi Kharadze**

* E. Andronikashvili Institute of Physics, I. Javakhishvili Tbilisi State University.

** Academy Member, E. Andronikashvili Institute of Physics, I. Javakhishvili Tbilisi State University

ABSTRACT. Among actual problems of the spin dynamics of superfluid ^3He the anomalously fast (catastrophic) decay of coherently spin-precessing mode is under active investigation. Experimentally this low-temperature phenomenon is observed in $^3\text{He-B}$. One of the possible mechanisms of the fast relaxation of the phase-coherent spin precession was attributed to the parametric instability realized in the background of a non-Leggett spin-orbital configuration of the Cooper condensate. An analogous process of the decay of coherent spin precession can be realized in $^3\text{He-A}$. The quantum description of this event is considered in some detail. © 2012 Bull. Georg. Natl. Acad. Sci.

Key words: superfluidity of ^3He , coherently precessing spin modes, catastrophic relaxation.

After the discovery [1, 2] of superfluid phases of liquid ^3He in the millikelvin temperature range a huge amount of information about the properties of this exotic ordered state of condensed matter has been collected. It was firmly established that superfluid phases of ^3He are characterized by the formation at $T < T_c(P)$ of the spin-triplet p -wave Cooper pair's condensate. The main body of experimental information on the properties of superfluid phases was obtained by means of CW and pulsed NMR techniques. Of fundamental importance is Leggett's theoretical approach [3] which proved to be extremely efficient in interpreting many peculiarities of observed spin-dynamical phenomena of superfluid A and B phases.

An important role in Leggett's theory is played by the coupling between magnetic dipole moments of ^3He nuclei which in the presence of the Cooper condensate acquires a coherent contribution with far-reaching consequences. One of the manifestations of this coherent part of the dipole-dipole (spin-orbital) coupling in superfluid ^3He is observed as a shift of the transverse NMR frequency from the Larmor value gH . Another exotic behaviour (also due to coherent dipole-dipole coupling) is manifested as a linear (and non-linear) longitudinal ringing of the magnetization.

A very informative experimental tool is the pulsed NMR by which the spin-dynamical regime is generated by the application of a short RF pulse (of suitable duration) deviating the spin by an angle β from its initial equilibrium orientation and free induction signal is registered. The measurements of the dependence of

dipole-shift of the transverse NMR frequency from the Larmor value was the main goal of pioneering experiments [4, 5]. Unusually long-lived induction decay signal (LLIDS) was registered in $^3\text{He-B}$ in spite of the presence of (uncontrolled) inhomogeneity of the applied steady magnetic field which induces the dephasing of the coherent spin-precessing mode.

The mechanism of the formation of LLIDS in $^3\text{He-B}$ was established due to joint experimental and theoretical efforts [6-9]. The experiments were performed by using a long cylindrical cell with the magnetic field $\vec{H} = H(z)\hat{z}$ oriented along cylinder axis \hat{z} . The controlled field inhomogeneity was given as $H(z) = H(z_0) + (\nabla H)(z - z_0)$ with constant gradient. The scenario which develops after the application of magnetization tipping RF pulse is based on the observation that due to the specific character of the dipole-dipole coupling potential of $^3\text{He-B}$ on the angle β the spin dynamics follows the route where the dipole forces are effectively eliminated. This is an important condition of the appearance of the magnetization-carrying spin current against the background of the Cooper condensate [10,11] which redistributes the magnetization in a way as to restore the phase coherency lost immediately after the RF tipping pulse. As a result, after the longitudinal spin current dies away, in the closed experimental cell the two-domain structure is stabilized where the static domain (SD) with equilibrium magnetization is separated by a narrow wall from the homogeneously precessing domain (HPD). The two-domain structure is subject to relaxation effects taking place in the volume of HPD due to an intrinsic Leggett-Takagi mechanism [12] active in bulk superfluid ^3He and spin diffusion across the domain boundary. It is evident that the decay of the two-domain spin structure should be observed as the growth of SD at the expense of the shrinking of HPD. In this way the parameters of Leggett-Takagi mechanism and spin-diffusion coefficient have been measured.

In [13] an attempt was made to continue the investigation of relaxation effects in the two-domain structure at low temperatures. Down to $T \cong 0.4T_c$ the experimental data changed with temperature rather slowly and were in accordance with known theoretical predictions. At a further lowering of the temperature the induction decay signal abruptly became so short that the induction signal typical of HPD could not be measured. Subsequently new measurements were carried out [14] in order to verify whether the above-mentioned low temperature instability of coherent spin precession was a specific feature of the presence of HPD in the experimental cell. The measurements were carried out in the pulsed NMR regime in the absence of HPD structure and the low-temperature instability was still found. This result clearly showed that the catastrophic relaxation found in [13] is just a particular example of a more general phenomenon. The adequate mechanism of this puzzling low-temperature catastrophic relaxation could not be found for a long period of time.

An important contribution in elucidating the mechanism of the catastrophic relaxation of coherent spin precession observed in $^3\text{He-B}$ at low temperatures was made in [15, 16]. In [15] it was proposed that an abrupt shortening of the relaxation time is due to the parametric instability of the spin-precessing mode with respect to the excitation of a pair of the longitudinal spin-wave quanta. This process is governed by the dipole-dipole forces acting against the background of a non-Leggett spin-orbital configuration of the Cooper condensate in the restricted geometry case. Another channel of the sudden decay of coherently precessing spin mode was attributed to the anisotropy of the spin-wave velocity [16].

An attempt to describe the parametric instability of spin-precessing mode in superfluid ^3He was undertaken in [17] where this process is considered for the case of $^3\text{He-A}$. Although this ordered state considerably differs from $^3\text{He-B}$, the mechanism of the decay of coherently precessing mode seems to be quite general in the presence of a non-Leggett spin-orbital background of the Cooper condensate. The essence of the parametric instability in $^3\text{He-A}$ is connected with the excitation of the longitudinal spin-waves due to the non-

linear coupling of the components of magnetic anisotropy axis \hat{d} provided by the dipole-dipole forces against the background of non-Leggett spin-orbital configuration. This scenario was considered in the framework of the Mathieu equation. In what follows we are going to investigate, somewhat retrospectively, the quantum approach to the process of disintegration of coherently precessing mode (long-wavelength transverse magnon) via the decay onto a pair of the short-wavelength longitudinal magnons.

The spin dynamics of superfluid ^3He in the presence of an external magnetic field \vec{H} is governed by the Leggett Hamiltonian

$$H = \frac{1}{2} g^2 (\hat{\chi}^{-1})_{\mu\nu} S_\mu S_\nu - g \vec{S} \cdot \vec{H} + U_D, \quad (1)$$

where \vec{S} (measured in the units of \hbar) stands for the total spin of the system, $\hat{\chi}$ – for the magnetic susceptibility tensor and g – for the gyromagnetic ratio of ^3He nucleus. An important contribution to the Hamiltonian (1) is the spin-orbital coupling (of dipole-dipole origin) which for $^3\text{He-A}$ is described by the potential

$$U_D(\hat{d}) = -\frac{1}{2} \left(\frac{\chi_\perp}{g^2} \right) \Omega_4^2 (\hat{d} \cdot \hat{l})^2, \quad (2)$$

where Ω_4 is linear longitudinal NMR frequency and the unit vectors \hat{d} and \hat{l} mark the anisotropy axis of the spin-triplet Cooper condensate in the spin and orbital spaces, respectively. The axis \hat{d} appears in the magnetic susceptibility tensor components

$$\chi_{\mu\nu} = \chi_\perp (\delta_{\mu\nu} - a d_\mu d_\nu), \quad a = \frac{\chi_\perp - \chi_{\parallel}}{\chi_\perp} > 0. \quad (3)$$

Decomposing the spin vector \vec{S} onto the transverse and longitudinal components with respect to \hat{d} as

$$g \vec{S}_\perp = \chi_\perp [\vec{H} - (\hat{d} \cdot \vec{H}) \hat{d}], \quad (4a)$$

$$g \vec{S}_\parallel = \chi_\parallel (\hat{d} \cdot \vec{H}) \hat{d} = S_\parallel \hat{d}, \quad (4b)$$

the Hamiltonian (1) is reduced to

$$H = H_\perp + H_\parallel + U_D(\hat{d}), \quad (5)$$

where

$$H_\perp = \frac{g^2}{2\chi_\perp} \vec{S}_\perp^2 - g \vec{S}_\perp \cdot \vec{H}, \quad (6a)$$

$$H_\parallel = \frac{g^2}{2\chi_\parallel} \left[\vec{S}_\parallel^2 + \frac{a}{1-a} (\hat{d} \cdot \vec{S}_\parallel)^2 \right] - g \vec{S}_\parallel \cdot \vec{H}. \quad (6b)$$

Now, it is convenient to transform Eqs. (6a, b) in passing to new representation for \vec{S}_\perp and $S_\parallel = \hat{d} \cdot \vec{S}_\parallel$.

Since $\vec{S}_\perp \perp \hat{d}$ one can introduce a new set of 2D variables $\vec{\xi}$ following the formula [18]

$$\vec{S}_\perp = \hat{d} \times \vec{\xi}. \quad (7)$$

On the other hand, taking into account that $(\hat{d} \cdot \vec{S})$ is a conserved quantity, it is concluded that

$S_{||} = S_{||}^{(0)} = \frac{\chi_{||}}{g} (\hat{d}_0 \cdot \vec{H})$, where \hat{d}_0 is the equilibrium value of \hat{d} . As a result it is found that

$$H_\perp = \frac{g^2}{2\chi_\perp} \left[\vec{\xi}^2 - (\hat{d} \cdot \vec{\xi})^2 \right] - g (\hat{d} \times \vec{\xi}) \cdot \vec{H}, \quad (8a)$$

$$H_{||} = -\chi_{||} \left[(\hat{d}_0 \cdot \vec{H}) (\hat{d} \cdot \vec{H}) - \frac{1}{2} (\hat{d}_0 \cdot \vec{H})^2 \right]. \quad (8b)$$

In what follows we choose the coordinate frame with $\vec{H} = H \hat{z}$ and consider the case of an externally fixed orientation of the orbital axis $\hat{l} = (0, \cos \alpha, \sin \alpha)$. At $\alpha \neq 0$ the equilibrium orientation of the spin axis \hat{d}_0 is not confined to (x, y) plane because the equilibrium configuration is established at the balance of the torque imposed on \hat{d} from the anisotropic part of the magnetic energy and the torque acting on \hat{d} from a fixed orbital field \hat{l} via the dipole-dipole potential:

$$a (\hat{d}_0 \cdot \vec{H}) (\hat{d}_0 \times \vec{H}) = \left(\frac{\Omega_A}{g} \right)^2 (\hat{d}_0 \cdot \hat{l}) (\hat{d}_0 \times \hat{l}), \quad (9)$$

from which it is concluded that $\hat{d}_0 = (0, \cos \beta, \sin \beta)$ with $\beta = \beta(\alpha)$ given by an equation (here and in what follows the Larmor frequency $\omega_L = gH$ is introduced):

$$\tan 2\beta = \frac{\left(\frac{\Omega_A}{\omega_L} \right)^2 \sin 2\alpha}{a + \left(\frac{\Omega_A}{\omega_L} \right)^2 \cos 2\alpha}. \quad (10)$$

It can be shown that $\vec{\xi}_0 = -\left(\frac{\chi_\perp}{g^2} \right) \omega_L \cos \beta \hat{x}$.

Finally, in choosing $\vec{\xi} = (\xi_x, 0, \xi_z)$ and remembering that $\hat{d}^2 = 1$ the Leggett Hamiltonian can be transcribed in terms of conjugated pairs of variables (ξ_x, d_x) and (ξ_z, d_z) as

$$H = \frac{g^2}{2\chi_\perp} \left[\xi_x^2 + \xi_z^2 - (\xi_x d_x + \xi_z d_z)^2 \right] + \omega_L \xi_x \sqrt{1 - (d_x^2 + d_z^2)} - \chi_{||} \left[(\hat{d}_0 \cdot \vec{H}) (\hat{d} \cdot \vec{H}) - \frac{1}{2} (\hat{d}_0 \cdot \vec{H})^2 \right] - \frac{\chi_\perp}{2g^2} \Omega_A^2 \left[(1 - d_x^2) \cos^2 \alpha - d_z^2 \cos 2\alpha + d_z \sqrt{1 - (d_x^2 + d_z^2)} \sin 2\alpha \right]. \quad (11)$$

Starting from Eq. (11) the set of the Hamilton equations follows:

$$\dot{\xi}_x = -\frac{\partial H}{\partial d_x}, \quad \dot{d}_x = \frac{\partial H}{\partial \xi_x}; \quad (12a)$$

$$\dot{\xi}_z = -\frac{\partial H}{\partial d_z}, \quad \dot{d}_z = \frac{\partial H}{\partial \xi_z}. \quad (12b)$$

From Eqs. (12a, b) in detailed form it is obtained:

$$\dot{\xi}_x = \frac{g^2}{\chi_1} (\xi_x^2 d_x + \xi_x \xi_z d_z) + \omega_L \frac{\xi_x d_x}{\sqrt{1-(d_x^2+d_z^2)}} - \frac{\chi_1}{g^2} \Omega_A^2 \left[\cos^2 \alpha d_x + \frac{1}{2} \sin 2\alpha \frac{dx dz}{\sqrt{1-(d_x^2+d_z^2)}} \right], \quad (13a)$$

$$\dot{d}_x = \frac{g^2}{\chi_1} [\xi_x (1-d_x^2) - \xi_x d_x d_z] + \omega_L \sqrt{1-(d_x^2+d_z^2)}; \quad (13b)$$

$$\begin{aligned} \dot{\xi}_z = \frac{g^2}{\chi_1} (\xi_z^2 d_z + \xi_x \xi_z d_x) + \omega_L \frac{\xi_z d_z}{\sqrt{1-(d_x^2+d_z^2)}} - \frac{\chi_1}{g^2} \Omega_A^2 [\cos 2\alpha d_z - \\ - \frac{1}{2} \sin 2\alpha \frac{1-d_x^2-2d_z^2}{\sqrt{1-(d_x^2+d_z^2)}}] + \frac{\chi_{II}}{g^2} \omega_L^2 \sin \beta, \end{aligned} \quad (14a)$$

$$\dot{d}_z = \frac{g^2}{\chi_1} [\xi_z (1-d_z^2) - \xi_x d_x d_z]. \quad (14b)$$

Expanding the right-hand side of Eqs. (13a, b) and Eqs (14a, b) in the small deviations $\delta \bar{\xi} (= \bar{\rho})$ and $\delta \bar{d} (= \bar{q})$ from their equilibrium values up to the second order it is found that

$$\begin{aligned} \dot{p}_x = -m\omega_x^2 q_x - \kappa_1 p_x + \left[\frac{\sin \beta}{m} p_x p_x - \frac{\omega_L}{\cos \beta} (\cos 2\beta p_x q_x + \cos^2 \beta p_x q_x) - \right. \\ \left. - \frac{m}{2\cos^3 \beta} (\omega_L^2 \sin 2\beta + \Omega_A^2 \sin 2\alpha) q_x q_x \right], \end{aligned} \quad (15a)$$

$$\dot{q}_x = \frac{p_x}{m} - \kappa_2 q_x + \left[-\frac{\sin \beta}{m} p_x q_x + \frac{\omega_L}{2\cos \beta} \left(\cos 2\beta q_x^2 - \frac{q_x^2}{\cos^2 \beta} \right) \right]; \quad (15b)$$

$$\begin{aligned} \dot{p}_z = -\frac{m}{\cos^2 \beta} \omega_z^2 q_z + \kappa_2 p_z + \left[\frac{\sin \beta}{m} p_z^2 - \frac{\omega_L}{\cos \beta} \left(\cos^2 \beta p_z q_x - \frac{p_z q_x}{\cos^2 \beta} \right) - \right. \\ \left. - \frac{m}{4\cos^3 \beta} (\omega_L^2 \sin 2\beta + \Omega_A^2 \sin 2\alpha) \left(q_x^2 + \frac{3q_x^2}{\cos^2 \beta} \right) \right], \end{aligned} \quad (16a)$$



$$\dot{q}_z = \frac{\cos^2 \beta}{m} p_z + \kappa_1 q_x + \left[-\frac{\sin \beta}{m} (2p_z q_z + p_x q_x) + \omega_L \cos \beta q_x q_z \right]. \quad (16b)$$

In Eqs. (15a, b) and (16a, b) the following abbreviations are used:

$$m = \frac{\chi_{\perp}}{g^2}, \quad \kappa_1 = \omega_L \sin \beta \cos \beta, \quad \kappa_2 = \omega_L \tan \beta, \quad (17a)$$

$$\omega_z^2 = \omega_L^2 \sin^2 \beta + \Omega_A^2 \left(\cos^2 \alpha + \frac{1}{2} \sin 2\alpha \tan \beta \right) \quad (17b)$$

$$\omega_z^2 = \omega_L^2 + \Omega_A^2 \left(\cos 2\alpha \cos^2 \beta + \sin 2\alpha \frac{1 + 2\cos^2 \beta}{2} \tan \beta \right). \quad (17c)$$

The same set of equations can be reproduced by means of Taylor expansion [19] of the Hamiltonian (11) to the corresponding order in $\delta \vec{\xi}$ and $\delta \vec{d}$. It can be verified that the linear part of Eqs. (15a, b) and (16a, b) is governed by

$$H_2 = \left(\frac{1}{2m} p_x^2 + \frac{m}{2} \omega_z^2 q_z^2 \right) + \left(\frac{\cos^2 \beta}{m} p_z^2 + \frac{m\omega_z^2}{2\cos^2 \beta} q_z^2 \right) + \kappa_1 p_z q_x - \kappa_2 p_x q_z, \quad (18)$$

and the non-linear contribution stems from

$$\begin{aligned} H_3 = & -\frac{\sin \beta}{m} (p_x q_x + p_z q_z) p_z + \omega_L \left[\cos \beta p_z q_x q_z + \frac{1}{2\cos \beta} \left(\cos 2\beta q_x^2 - \frac{q_z^2}{\cos^2 \beta} \right) p_x \right] + \\ & + \frac{m\omega_L^2}{2\cos^2 \beta} \left[\sin \beta + \frac{1}{2} \left(\frac{\Omega_A}{\omega_L} \right)^2 \frac{\sin 2\alpha}{\cos \beta} \right] \left(q_x^2 + \frac{q_z^2}{\cos^2 \beta} \right) q_z. \end{aligned} \quad (19)$$

Eq. (19) contains the information on the mechanism of the interaction between various spin-excitation modes of ${}^3\text{He-A}$. In order to specify this eigen-modes it is necessary to go back to the linear level and address Eqs. (18) from which it is evident that in the case of the non-Leggett spin-orbital configuration the coefficients κ_1 and κ_2 are non-zero and H_2 is non-diagonal in the initial variables \vec{p} and \vec{q} . The diagonalization of Eq. (18) can be achieved by passing to new pairs (\mathcal{P}_x, Q_x) and (\mathcal{P}_z, Q_z) according to the transformation

$$p_x = \mathcal{P}_x \cos \lambda - Q_x \frac{\sin \lambda}{f}, \quad q_x = Q_x \cos \lambda + \mathcal{P}_x f \sin \lambda; \quad (20a)$$

$$p_z = \mathcal{P}_z \cos \lambda - Q_z \frac{\sin \lambda}{f}, \quad q_z = Q_z \cos \lambda + \mathcal{P}_z f \sin \lambda. \quad (20b)$$

The diagonalization is realized by a suitable choice of the rotation angle λ and an amplitude f as

$$\tan 2\lambda = 2\sqrt{2}\omega_L \sin \beta \frac{\sqrt{\omega_z^2 + \omega_x^2}}{\omega_z^2 - \omega_x^2}, \quad f^2 = \frac{1}{m^2} \frac{2 \cos^2 \beta}{\omega_z^2 + \omega_x^2}. \quad (21)$$

As a result of this procedure the second order Hamiltonian (18) acquires the following form:

$$H_2 = \left(\frac{1}{2m} I_x \mathcal{P}_x^2 + \frac{1}{2} m \Omega_x^2 Q_x^2 \right) + \left(\frac{\cos^2 \beta}{2m} I_z \mathcal{P}_z^2 + \frac{m \Omega_z^2}{2 \cos^2 \beta} Q_z^2 \right), \quad (22)$$

where

$$I_x = 1 + \frac{\omega_z^2 - \omega_x^2 - \sqrt{\omega_z^2 + \omega_x^2}}{2(\omega_z^2 + \omega_x^2)}, \quad I_z = 1 - \frac{\omega_z^2 - \omega_x^2 - \sqrt{\omega_z^2 + \omega_x^2}}{2(\omega_z^2 + \omega_x^2)}, \quad (23)$$

$$\Omega_x^2 = \frac{1}{2} \left[\omega_z^2 + \omega_x^2 - \frac{1}{2} (\omega_z^2 - \omega_x^2 + \sqrt{\omega_z^2 + \omega_x^2}) \right], \quad \Omega_z^2 = \frac{1}{2} \left[\omega_z^2 + \omega_x^2 + \frac{1}{2} (\omega_z^2 - \omega_x^2 + \sqrt{\omega_z^2 + \omega_x^2}) \right], \quad (24)$$

with

$$\sqrt{\omega_z^2 + \omega_x^2} = \sqrt{(\omega_z^2 - \omega_x^2)^2 + 8 \omega_z^2 (\omega_z^2 + \omega_x^2) \sin^2 \beta}. \quad (25)$$

Let us pass to the normal coordinate representation according to the prescription:

$$\mathcal{P}_x = \sqrt{\frac{m \Omega_x}{2 \cos^2 \beta}} (\hat{a} + \hat{a}^*), \quad Q_x = i \sqrt{\frac{I_x \cos^2 \beta}{2 m \Omega_x}} (\hat{a} - \hat{a}^*); \quad (26a)$$

$$\mathcal{P}_z = \sqrt{\frac{m \Omega_z}{2}} (\hat{b} + \hat{b}^*), \quad Q_z = i \sqrt{\frac{I_z}{2 m \Omega_z}} (\hat{b} - \hat{b}^*), \quad (26b)$$

where the commutators $[\hat{a}, \hat{a}^*] = [\hat{b}, \hat{b}^*] = 1$. As a result it is concluded that

$$H_2 = I_z \Omega_z \hat{a}^* \hat{a} + I_x \Omega_x \hat{b}^* \hat{b} + \text{const}. \quad (27)$$

This is an answer for the spectrum of the eigen-oscillations of $^3\text{He-A}$ developing against the background of the non-Leggett equilibrium spin-orbital configuration described by $\vec{l} = (0, \cos \alpha, \sin \alpha)$ and $\vec{d}_0 = (0, \cos \beta, \sin \beta)$ with $\beta = \beta(\alpha)$ found according to Eq.(10).

Now we are ready to transcribe the non-linear part of the Leggett Hamiltonian (Eq.19) in the terms of normal coordinates. Before considering the non-Leggett equilibrium configuration case (which is our main concern), it is instructive to analyze first the Leggett configuration with $\alpha = \beta = 0$ appropriate to bulk $^3\text{He-A}$. In this case $\Omega_z^2 = \omega_z^2 + \Omega_A^2 = \omega_z^2$, $\Omega_x^2 = \Omega_A^2 = \omega_y^2$ and the second order contribution to Leggett Hamiltonian (Eq.18) is diagonal in the initial variables \vec{p} and \vec{q} . As a result it is concluded that in the normal coordinates (here $\omega_x \gg \omega_y$)

$$p_z = \sqrt{\frac{m\omega_z}{2}} (\hat{a} + \hat{a}^*), \quad q_z = i \sqrt{\frac{1}{2m\omega_z}} (\hat{a} - \hat{a}^*), \quad (28a)$$

$$p_x = \sqrt{\frac{m\omega_H}{2}} (\hat{b} + \hat{b}^*), \quad q_x = i \sqrt{\frac{1}{2m\omega_H}} (\hat{b} - \hat{b}^*). \quad (28b)$$

In order to construct the non-linear contribution H_3 , Eqs. (28a, b) are to be used in Eq. (19). In this way it can be shown that for the Leggett spin-orbital configuration

$$H_3 = \omega_z \left[p_z q_x q_z + \frac{1}{2} p_x (q_x^2 - q_z^2) \right] = -\frac{\omega_z}{2\sqrt{2m\omega_H}} \left[(\hat{a} - \hat{a}^*) (\hat{a} + \hat{a}^*) (\hat{b} - \hat{b}^*) + \frac{1}{2} (\hat{b} - \hat{b}^*)^2 (\hat{b} + \hat{b}^*) - \frac{1}{2} \frac{\omega_H}{\omega_z} (\hat{a} - \hat{a}^*)^2 (\hat{b} + \hat{b}^*) \right]. \quad (29)$$

It is seen that in bulk ${}^3\text{He-A}$ (with the Leggett equilibrium configuration) the interaction term $\hat{a}\hat{b}^*\hat{b}^*$ corresponding to the decay of a -type excitation onto the pair of the b -type modes is absent.

On the other hand, in [17] it was shown that in a strong magnetic field ($\omega_z \gg \Omega_A$) the high frequency coherently precessing transverse mode of the magnetization experiences parametric instability signaling the decay of this mode at sufficiently low temperatures. An important observation is that the decay onto a pair of longitudinal spin-waves happens against the background of a non-Leggett equilibrium spin-orbital configuration with externally fixed $\hat{l} = (0, \cos \alpha, \sin \alpha)$. In order to reproduce this process in terms of the Hamiltonian (19) we have to address the general case described by the variables (\mathcal{P}_x, Q_x) and (\mathcal{P}_z, Q_z) . According to the transformations (20a, b) it can be shown that in the strong magnetic field case

$$H_2 = \omega_z \hat{a}^* \hat{a} + \omega_H \hat{b}^* \hat{b}, \quad (30)$$

where now

$$\begin{aligned} \omega_z^2 &= \omega_L^2 + \Omega_A^2 \cos 2\alpha, \\ \omega_H^2 &= \Omega_A^2 \cos^2 \alpha, \end{aligned} \quad (31)$$

and the contribution to H_3 corresponding to the process $\hat{a}\hat{b}^*\hat{b}^*$ is

$$H_3 = -iV(\alpha) \hat{b}^* \hat{b}^* \hat{a} \quad (32)$$

with the amplitude

$$V(\alpha) = \frac{1}{12\sqrt{2}} \sqrt{\frac{\omega_z}{m}} \frac{1+\alpha}{a} \left(\frac{\Omega_A}{\omega_z} \right)^2 \sin 2\alpha. \quad (33)$$

In order to describe the decay of the transverse magnon onto the pair of longitudinal magnons it is necessary to take into account the contribution of the spin currents. This is achieved in supplementing the Leggett Hamiltonian (19) by the term

$$U_{\nabla} = \frac{1}{2} mc_{\parallel}^2 (\nabla_i \hat{d}) \cdot (\nabla_j \hat{d}), \quad (34)$$

where

$$c_{\parallel}^2 = c_{\perp}^2 (\delta_{ij} - l_i l_j) + c_{\parallel}^2 l_i l_j, \quad (35)$$

with c_{\perp} and c_{\parallel} being the transverse and longitudinal spin-wave velocities. The gradient energy (34) generates a torque acting on \vec{S} given as

$$m \hat{d} \times (c_{\perp}^2 \nabla_{\perp}^2 \hat{d} + c_{\parallel}^2 \nabla_{\parallel}^2 \hat{d}). \quad (36)$$

The results of this modification are simple. In the Fourier representation

$$H_2(\vec{k}) = \omega_{\perp}(\vec{k}) \hat{a}^*(\vec{k}) \hat{a}(\vec{k}) + \omega_{\parallel}(\vec{k}) \hat{b}^*(\vec{k}) \hat{b}(\vec{k}), \quad (37)$$

where the magnon frequencies (squared) are given as

$$\begin{aligned} \omega_{\perp}^2(\vec{k}) &= \omega_L^2 + \Omega_A^2 \cos 2\alpha + c_{\parallel}^2 k_i k_j, \\ \omega_{\parallel}^2(\vec{k}) &= \Omega_A^2 \cos^2 \alpha + c_{\parallel}^2 k_i k_j. \end{aligned} \quad (38)$$

As to the third order term H_3 , it takes the form

$$H_3(\vec{k}) = -iV(\alpha) \hat{b}^*(-\vec{k}) \hat{b}^*(\vec{k}) \hat{a}(0), \quad (39)$$

and describes the decay of transverse magnon (with $\vec{k}_{\perp} = 0$) into a pair of longitudinal magnons traveling in the opposite directions, so that the conservation law of the energy and momentum is fulfilled:

$$\begin{aligned} \omega_{\perp}(0) &= \omega_{\parallel}(\vec{k}) + \omega_{\parallel}(-\vec{k}), \\ \vec{k} = 0 &= \vec{k} + (-\vec{k}). \end{aligned} \quad (40)$$

As can be seen from Eq. (33), the amplitude of this process is non-zero in the case of the non-Leggett spin-orbital configuration in accordance with the conclusion made in [17].

As a general conclusion it can be stated that, in spite of the fundamental difference in the structure of the order parameters of superfluid A and B phases, the catastrophic low temperature instability of homogeneously spin-precessing modes in both cases is developing in the background of the non-leggett orbital textures present in the restricted geometry.

ფიზიკა

ზედენად ${}^3\text{He-A}$ -ში კოჰერენტული სპინური პრეცესიის პარამეტრული არამდგრადობის კვანტური აღწერა

გ. ბარამიძე*, გ. ხარაძე**

* ი. ჯავახიშვილის სახ. თბილისის სახელმწიფო უნივერსიტეტის ე. ანდრონიკაშვილის სახ. ფიზიკის ინსტიტუტი, თბილისი

** აკადემიკოსი, ი. ჯავახიშვილის სახ. თბილისის სახელმწიფო უნივერსიტეტის ე. ანდრონიკაშვილის სახ. ფიზიკის ინსტიტუტი, თბილისი

ზედენად ${}^3\text{He}$ -ში სპინური დინამიკის თავისებურებათა შორის აქტიურად შეისწავლება კოჰერენტული სპინ-პრეცესიული მდგომარეობების ანომალურად სწრაფი (კატასტროფული) რელაქსაციის პროცესები. ექსპერიმენტულად ეს მოვლენა დეტალურად იქნა გამოკვლეული ${}^3\text{He}$ -ის B ფაზაში. ამ უჩვეულო მოვლენის შესაძლო ახსნა ეფუძნება მოსაზრებას, რომ სპინ-პრეცესიული მდგომარეობის სწრაფი რელაქსაცია დაკავშირებულია მის დაშლასთან გასწვრივ სპინურ ტალღებზე. მსგავსი პროცესი შესაძლებელია ${}^3\text{He}$ -ის A ფაზაშიც. ნაშრომში ჩატარებულია ამ მექანიზმის კვანტური აღწერა.

REFERENCES

1. D.D. Osheroff et al. (1972), Phys. Rev. Lett., **28**: 885.
2. D.D. Osheroff et al. (1972), Phys. Rev. Lett., **29**: 920.
3. A.J. Leggett (1975), Rev. Mod. Phys., **47**: 331.
4. L.R. Corruccini, D.D. Osheroff (1978), Phys. Rev., **B17**: 126.
5. R.W. Giannetta et al. (1981), J.Low Temp. Phys., **45**: 295.
6. A.S. Borovik-Romanov et al. (1984), JETP Lett., **40**: 1033.
7. I.A. Fomin (1984), JETP Lett. **40**: 1037.
8. A.S. Borovik-Romanov et al. (1985), Sov.Phys. JETP, **61**: 1199.
9. I.A. Fomin (1985), Sov. Phys. JETP, **61**: 1207.
10. I.A. Fomin (1991), Physica, **B169**: 153.
11. V.V. Dmitriev, I.A. Fomin (2009), J. Phys. Cond. Matter, **21**: 164202.
12. A.J. Leggett, Shin Takagi (1977), Ann. Phys., **106**:79.
13. Yu.M. Bunkov et al. (1989), Europhys. Lett., **8**: 645.
14. Yu.M. Bunkov et al. (1990), Physica, **B165&166**: 675.
15. Yu.M. Bunkov et al. (2006), JETP Lett., **83**:530.
16. E.V. Surovtsev, I.A. Fomin (2009), arXiv, 0907.2119.
17. A.D. Gongadze et al. (1980), Sov. Phys. JETP, **51**: 310.
18. V.V. Lebedev, I.M. Khalatnikov (1977), ZhETF, **73**: 1537.
19. G.E. Gurgenisvili (1983), Doctoral Thesis, TSU, Tbilisi (in Russian).

Received May, 2012

Physics

Magnetization Plateau in the Spin $S=1/2$ Two-Leg Ladder with Trimerized Modulation of the Rung Exchange

Niko Avalishvili*, George I. Japaridze**, David Nozadze†, Saeed Mahdavifar††

* Department of Engineering, Ilia State University, Tbilisi

** Academy Member, Ilia State University, Andronikashvili Institute of Physics, Tbilisi

† Department of Physics, Missouri University of Science and Technology, Rolla, Missouri, 65409, USA

†† Department of Physics, University of Gulan, P.O.Box 41335-1914, Rasht, Iran

ABSTRACT. The ground-state magnetic phase diagram of a two-leg spin ladder with trimerized modulated rung exchange is studied using the continuum-limit bosonization approach. In the limit where the rung exchange is dominant, the model is mapped onto the effective quantum sine-Gordon model with topological term. Six quantum phase transitions at different critical magnetic fields are identified. We have shown that the magnetization curve of the system exhibits two plateaus at magnetization equal to the $1/3$ and $2/3$ of the saturation value. The width of the plateaus is proportional to the excitation gap at given magnetization and scales as δ^ν , where δ is the amplitude of rung exchange modulation and the critical exponent is obtained as $\nu = 1.13$ in the case of a ladder with antiferromagnetic legs and $\nu = 1.50$ in the case of ladder with ferromagnetic legs. © 2012 Bull. Georg. Natl. Acad. Sci.

Key words: quantum spin ladders, magnetization plateaus.

Introduction. Low-dimensional quantum magnetism has been the subject of intense research for decades. Perpetual interest in the study of these systems is determined by their rather unconventional low-energy properties (see for a review [1]). An increased current activity in this field is connected with the large number of qualitatively new phenomena dominated by the quantum effects recently discovered in these systems [2,3] as well as with the opened wide prospects for use of low-dimensional magnetic materials in modern nanoscale technologies.

The spin $S=1/2$ two-leg ladders represent one, particular subclass of low-dimensional quantum magnets which also has attracted much interest for a number of reasons. On the one hand, there was remarkable progress in recent years in the fabrication of such ladder compounds [4]. On the other hand, spin-ladder models pose interesting theoretical problems, since the excitation spectrum of a two-leg antiferromagnetic ladder is gapped and therefore, in the presence of a magnetic field these systems reveal an extremely complex

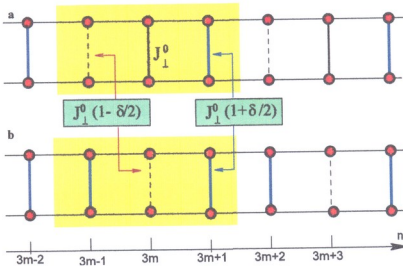


Fig. 1. Schematic representation of spin ladder with period 3 modulation of the rung exchange. Different width and color of vertical links correspond to different values of the rung exchange, indicated in the figure by arrows. Yellow blocks mark unit cells of the ladder in the case of the "saw tooth" (a) and "domain" type (b) modulation of rung exchange. The horizontal axis marks rung numbers.

behavior, dominated by quantum effects. The magnetic field driven quantum phase transitions in ladder systems were intensively investigated both theoretically [5-11] and experimentally [12-17]. Usually, these most exciting properties of low-dimensional quantum spin systems exhibit strongly correlated effects driving them toward regimes with no classical analog. Properties of the low-dimensional systems in these regimes or "quantum phases" depend in turn on the properties of their ground state and low-lying energy excitations. Therefore search for the gapped phases emerging from different sources and study of ordered phases and quantum phase transitions associated with the dynamical generation of new gaps is an important direction in theoretical studies of quantum spin systems. Particular realization of such scenario appears in the case where the spin-exchange coupling constants are spatially modulated. The spin-Peierls effect in spin chains represents a prototype example of such behavior [18]. The first studies of spin chains with trimerized exchange modulation were performed by Hida [19] and Okamoto [20] in an attempt to describe some organic compounds with periodic couplings. Later, Oshikawa and collaborators [21] undertook the first systematic study of this problem and they provided a necessary condition for the appearance of magnetization plateau in 1D spin systems. Magnetic properties of the spin $S=1/2$ ladders with alternating rung exchange has been first studied in [22, 23].

The model. In this paper we study the spin $S=1/2$ two-leg ladder with modulated rung exchange given by the Hamiltonian

$$\bar{H} = J_{\parallel} \sum_{n,\alpha} \vec{S}_{n,\alpha} \vec{S}_{n+1,\alpha} - H \sum_{n,\alpha} S_n^z + \sum_{n,\alpha} J_{\perp}(n) \vec{S}_{n,1} \cdot \vec{S}_{n,2}, \quad (1)$$

where $\vec{S}_{n,\alpha}$ is the spin $S=1/2$ operator on rung n ($n=1, \dots, N$) and leg α ($\alpha=1, 2$). The interleg coupling is antiferromagnetic, $J_{\perp}(n) > 0$ and fulfils the condition $J_{\perp}(n+3) = J_{\perp}(n)$. We restrict our consideration by the following two types of rung exchange modulation: the "saw tooth" (or the "A") type:

$$J_{\perp}^A(n) = J_{\perp}^0 \left[1 + \frac{\delta}{\sqrt{3}} \sin\left(\frac{2\pi}{3}n\right) \right], \quad (2a)$$

which corresponds to the case $J_{\perp}(3m) = J_{\perp}^0$, $J_{\perp}(3m \pm 1) = J_{\perp}^0(1 \pm \delta/2)$ (see Fig. 2.1a) and the “domain” (or the “B”) type

$$J_{\perp}^B(n) = J_{\perp}^0 \left[1 + \frac{\delta}{2} \left(\frac{1}{3} - \frac{4}{3} \cos \left(\frac{2\pi}{3} n \right) \right) \right], \quad (2b)$$

which corresponds to the case $J_{\perp}(3m) = J_{\perp}^0(1 - \delta/2)$, $J_{\perp}(3m \pm 1) = J_{\perp}^0(1 + \delta/2)$ (see Fig. 2.1b).

Derivation of the effective model. We restrict our consideration to the limit of strong rung exchange and magnetic field $H, J_{\perp}^{\pm} \gg J_{\parallel}, \delta J_{\perp}^0 \equiv \Delta$ and follow the route already used to study the standard ladder models in the same limit [7,8]. We start from the case $J_{\parallel} = 0$, where an eigenstate of \hat{H} can be written as a product of on-rung states. At each rung two spins form either a singlet state $|s_n^0\rangle$ or one of the triplet states: $|t_n^0\rangle$, $|t_n^+\rangle$ and $|t_n^-\rangle$ with energies $E_S = -3J_{\perp}^0/4$, $E_t^0 = J_{\perp}^0/4$, and $E_t^{\pm} = J_{\perp}^0/4 \pm H$, respectively. When the magnetic field, H , is small, the ground state consists of a product of rung singlet states, while at $H \approx J_{\perp}^0$ the $|t_n^-\rangle$ becomes almost degenerate with $|s_n^0\rangle$, while other states have much higher energy. Integrating out the high energy states and introducing the effective pseudo-spin $\tau = 1/2$ operators, $\bar{\tau}_n$ which acts on these states as

$$\begin{aligned} \tau_n^z |s_n^0\rangle &= -\frac{1}{2} |s_n^0\rangle, \quad \tau_n^+ |s_n^0\rangle = |t_n^+\rangle, \quad \tau_n^- |s_n^0\rangle = 0, \\ \tau_n^z |t_n^+\rangle &= +\frac{1}{2} |t_n^+\rangle, \quad \tau_n^- |t_n^+\rangle = |s_n^0\rangle, \quad \tau_n^+ |t_n^+\rangle = 0, \end{aligned}$$

we obtain the following effective Hamiltonian of the anisotropic Heisenberg chain with anisotropy parameter 1/2 in the uniform and spatially modulated longitudinal magnetic fields

$$H_{eff}^i = \sum_n \{ J_{\parallel} (\tau_n^x \cdot \tau_{n+1}^x + \tau_n^y \cdot \tau_{n+1}^y + \frac{1}{2} \tau_n^z \cdot \tau_{n+1}^z) - [h_0^i + h_1^i(n)] \cdot \tau_n^z \} \quad i = A, B, \quad (3)$$

where

$$h_0^A = H - J_{\perp}^0 - J_{\parallel}/2 - \delta J_{\perp}^0/6, \quad h_0^B = H - J_{\perp}^0 - J_{\parallel}/2, \quad (4a)$$

and

$$h_1^A(n) = \frac{1}{\sqrt{3}} \cdot \delta J_{\perp}^0 \sin \left(\frac{2\pi}{3} n \right), \quad h_1^B(n) = \frac{2}{3} \cdot \delta J_{\perp}^0 \cos \left(\frac{2\pi}{3} n \right). \quad (4b)$$

Thus, the effective Hamiltonian is nothing but the anisotropic XXZ Heisenberg chain in uniform and spatially trimerized modulated magnetic fields. The exchange anisotropy parameter of the effective model $\lambda = 1/2$, ($\lambda = -1/2$) for ladder with antiferromagnetic (ferromagnetic) legs $J_{\parallel} > 0$, ($J_{\parallel} < 0$). It is worth noting that a similar problem has been studied intensively in past years [24-26]. At $\delta = 0$, the effective Hamiltonian reduces to the XXZ Heisenberg chain in a uniform longitudinal magnetic field. The magnetization curve of this model has only saturation plateau corresponding to the fully polarized chain. At $H=0$ and $J_{\perp}^0 \gg J_{\parallel}$, spins coupled by strong rung exchange form singlet pairs and the nonmagnetic and gapped ground state of the ladder system is well described by superposition of on-rung singlets. In terms of effective τ -spin model, the ground state corresponds to the ferromagnetic order with magnetization per site $m = -1/2$. In the opposite limit of very strong magnetic field $H \gg J_{\perp}^0$, fully polarized state of the ladder with magnetization per rung $M=1$, is represented in terms of effective τ -spin chain as the fully polarized state with

magnetization per site $m = 1/2$. This gives the following relation between the magnetization per rung of the ladder system and the magnetization per site of the effective chain $m = M - 1/2$.

The performed mapping allows to estimate the critical field H_{on} corresponding to the transition from a gapped rung-singlet phase to a gapless paramagnetic phase, the saturation field H_{sat} corresponding to the transition onto the fully polarized phase as well as the critical fields H_{c1}^{\pm} and H_{c2}^{\pm} which mark borders of the magnetization plateaus at $M = M_{sat}/3$ and $M = 2M_{sat}/3$. The direct way to express H_{on} and H_{sat} in terms of ladder parameters is to perform the Jordan-Wigner transformation which maps the problem onto a system of interacting spinless fermions [27]:

$$\hat{H}_f^i = \sum_n [t(a_n^{\dagger} a_{n+1} + h.c.) + V \cdot a_n^{\dagger} a_n a_{n+1}^{\dagger} a_{n+1} - (\mu_0^i + \mu_1^i(n)) \cdot a_n^{\dagger} a_n], \quad i = A, B \quad (5)$$

where $t = J_{\parallel}/2$, $\mu_0^i = \frac{1}{2}J_{\parallel} + h_0^i$, $\mu_1^i(n) = h_1^i(n)$.

The onset and saturation critical magnetic fields. The lowest onset (H_{on}) and highest saturation (H_{sat}) critical field corresponds to that value of the chemical potential μ_0 for which the band of fermions (or holes, after the corresponding particle-hole transformation) starts to fill up. In this limit we can neglect the interaction term in (5) and obtain the model of free particles with three band spectrum. Below, in this subsection we consider only the case of "B" type of exchange modulation. Generalization of these results for the case "A" is straightforward. In this case three bands of the single particle spectrum are given by

$$\begin{aligned} E_1(k) &= -H + J_{\perp}^0 + J_{\parallel} \sqrt{1 + \gamma^2} \cos \phi(k), \\ E_2(k) &= -H + J_{\perp}^0 + J_{\parallel} \sqrt{1 + \gamma^2} \cos(\phi(k) + 2\pi/3), \\ E_3(k) &= -H + J_{\perp}^0 + J_{\parallel} \sqrt{1 + \gamma^2} \cos(\phi(k) + 4\pi/3), \end{aligned} \quad (6)$$

where $\gamma = \delta J_{\perp}^0 / J_{\parallel}$ and

$$\phi(k) = \frac{1}{3} \arccos \left(\frac{\cos(3k) + \gamma^3}{\sqrt{(1 + \gamma^2)^3}} \right), \quad (7)$$

and $-\pi/3 < k \leq \pi/3$. This gives

$$H_{on} = J_{\perp}^0 + \frac{\gamma}{6} + J_{\parallel} \sqrt{1 + \gamma^2} \cos(\phi(\pi/3) + 4\pi/3), \quad (8a)$$

in the case of antiferromagnetic legs ($J_{\parallel} > 0$) and

$$H_{on} = J_{\perp}^0 + \frac{\gamma}{6} - J_{\parallel} \sqrt{1 + \gamma^2} \cos \phi(0), \quad (8b)$$

in the case of ferromagnetic legs ($J_{\parallel} < 0$).

To estimate the critical magnetic field H_{sat} , which marks the transition into the phase with saturated

magnetization, it is useful to make a site-dependent particle-hole transformation on the Hamiltonian Eq.(5): $a_n^* \rightarrow d_n$. Up to constant the new Hamiltonian reads

$$\hat{H}_{eff} = \sum_n [-t(d_n^* d_{n+1} + h.c.) + V \cdot d_n^* d_n d_{n+1}^* d_{n+1} - (\mu_0^d + \mu_1(n)) \cdot d_n^* d_n], \quad (9)$$

where the hole chemical potential $\mu_0^d = -\mu_0 + J_{\parallel}/2$. In terms of holes, H_{sur} corresponds to the chemical potential where the band starts to fill up, and one can neglect again the interaction term. However, the effect of interaction is now included in the shifted value of the chemical potential for holes. After simple transformations, we obtain

$$\begin{aligned} H_{sur} &= J_{\perp}^0 + J_{\parallel}/2 + J_{\parallel} \sqrt{1+\gamma^2} \cos\phi(0), \quad \text{at } J_{\parallel} > 0, \\ H_{sur} &= J_{\perp}^0 + J_{\parallel}/2 - J_{\parallel} \sqrt{1+\gamma^2} \cos(\phi(\pi/3) + 4\pi/3), \quad \text{at } J_{\parallel} < 0. \end{aligned} \quad (10)$$

The spectrum of the system in the free fermion limit (6) allows also to determine two other important parameters which characterize the values of magnetization in the magnetization curve of the system in which the additional plateaus appear and the values of magnetic field which correspond to the center of each plateau. Below we consider only the case $J_{\parallel} > 0$, however extension to the case $J_{\parallel} < 0$ is straightforward. At 1/3-rd band-filling, all states in the lower band $E_3(k)$ are filled and separated from the empty at $E_2(k)$ band by the energy gap $2\Delta_1^0 = E_2(0) - E_3(0)$. Therefore, the first magnetization plateau will appear at magnetization equal to 1/3 of the saturation value. The magnetic field at the center of the plateau is given by $H_{c1} = J_{\perp}^0 + E_3(0) + \Delta_1^0$. Analogously at 2/3-rd band-filling, all states in the lower bands $E_3(k)$ and $E_2(k)$ are filled and separated from the empty $E_1(k)$ band by the energy $2\Delta_2^0 = E_1(\pi/3) - E_2(\pi/3)$. Therefore, the second magnetization plateau appears at magnetization equal to 2/3 of the saturation value and the magnetic field at the center of plateau is given by $H_{c2} = J_{\perp}^0 + E_3(0) + \Delta_2^0$. Since at finite band-filling the effect of interaction between spinless fermions cannot be ignored the width of the plateau differs from its bare value $2\Delta_j^0, j=1,2$. In the forthcoming section we use the continuum limit bosonization treatment of the effective spin-chain model (5) to determine parameters characterizing the appearance and scale of the magnetization plateaus.

Critical magnetic fields characterizing magnetization plateaus H_{c1}^{\pm} and H_{c2}^{\pm} . To determine the critical fields which mark borders of the magnetization plateaus we use the continuum-limit bosonization approach. Following the usual procedure in the low energy limit, we bosonize the spin degrees of freedom at fixed magnetization per site m as follows [28]

$$\tau_n^z = m + \sqrt{\frac{K}{\pi}} \hat{\varphi}_s \phi(x) + \frac{A}{\pi} \sin(\sqrt{4\pi K} \phi(x) + (2m+1)\pi n), \quad (11a)$$

$$\tau_n^x = e^{-i\sqrt{4\pi K} \theta} \left[1 + \frac{B}{\pi} \sin(\sqrt{4\pi K} \phi(x) + (2m+1)\pi n) \right], \quad (11b)$$

where A and B are non-universal real constants of the order of unity [29], $\phi(x)$ and $\theta(x)$ are dual bosonic



fields $\hat{c}_s\phi = \hat{c}_s\theta$ and $K(\lambda, m)$ is the spin stiffness parameter for spin chain with anisotropy λ and magnetization m . At zero magnetization $K(\lambda, 0) = \pi/2(1 - \arccos \lambda)$ and therefore for a ladder with isotropic antiferromagnetic legs $K(1/2, 0) = 0.75$, while for a ladder with ferromagnetic legs $K(-1/2, 0) = 1.5$. At the transition line into the ferromagnetic phase, where the magnetization reaches its saturation value $m_{sat} = 0.5$, the spin stiffness parameter takes the universal value $K(0.5, \lambda) = 1$ [28]. Respectively for finite magnetization, at $0 < m < m_{sat}$ and $J_{\perp} > 0$ ($J_{\perp} < 0$) the function $K(m, \lambda)$ monotonically increases (decreases) with increasing m and reaches its maximum (minimum) value at saturation magnetization $K(m_{sat}, \lambda) = 1$.

Using (11) we obtain the following continuum-limit bosonized Hamiltonian to describe infrared properties of the system at magnetization m , $H'_{bos} = H_0 + H'_m$, where

$$H'_0 = \int dx \left[\frac{1}{2}(\hat{c}_s\phi)^2 + \frac{1}{2}(\hat{c}_s\theta)^2 - h'_0 \sqrt{\frac{K}{\pi}} \hat{c}_s\phi \right], \quad i = A, B \quad (12a)$$

$$H_m^A = \frac{h_1^A}{2\pi a_0} \int dx \left[\cos(\sqrt{4\pi K}\phi + 2\pi(m + \frac{1}{6})x) - \cos(\sqrt{4\pi K}\phi + 2\pi(m + \frac{5}{6})x) \right], \quad (12b)$$

$$H_m^B = \frac{h_1^B}{2\pi a_0} \int dx \left[\sin(\sqrt{4\pi K}\phi + 2\pi(m + \frac{1}{6})x) + \sin(\sqrt{4\pi K}\phi + 2\pi(m + \frac{5}{6})x) \right]. \quad (12c)$$

Away from the commensurate values of effective chain magnetization $m = -1/6$ and $m = 1/6$ corresponding to the ladder magnetizations $M = M_{sat}/3$ and $M = 2M_{sat}/3$, respectively the sine terms in (12) are strongly oscillating and have to be neglected. In this case the system is described by the gapless Gaussian bose-field and the spin system is in the gapless paramagnetic phase with finite magnetization, which continuously increases with increasing magnetic field, till it reaches the commensurate values $m = \pm 1/6$.

At $m = -1/6$ ($m = 1/6$) the first (second) sine term in Eqs. (12.b-c) is non-oscillating and has to be retained. Up to an irrelevant shift on constant of the bosonic field, the general bosonic Hamiltonian which describes infrared properties of the ladder for both "A" and "B" type of trimerized rung exchange modulation is given by

$$H'_0 = \int dx \left[\frac{1}{2}(\hat{c}_s\phi)^2 + \frac{1}{2}(\hat{c}_s\theta)^2 - h'_0 \sqrt{\frac{K}{\pi}} \hat{c}_s\phi + \frac{\Delta'_0}{2\pi a_0} \cos \sqrt{4\pi K}\phi \right], \quad i = A, B \quad (13)$$

where $\Delta'_0 = \delta J_{\perp}^0 / \sqrt{3}$ and $\Delta''_0 = 2\delta J_{\perp}^0 / 3$. The Hamiltonian (13) can be easily recognized as the standard Hamiltonian for the commensurate-incommensurate [30] transition which has been intensively studied using bosonization approach [31] and the Bethe ansatz technique [32]. Below we use the results obtained in [31, 32] to describe the magnetization plateau and the transitions from a gapped (plateau) to gapless paramagnetic phases.

Let us first consider $h'_0 = 0$. In this case the continuum theory of the initial ladder model in the magnetic field $H = J_{\perp} + J_{\parallel}/2$ is given by the quantum sine-Gordon (SG) model with a massive term $\approx h'_{eff} \sin(\sqrt{4\pi K}\phi)$. From the exact solution of the SG model [33] it is known that the excitation spectrum of the model (13) is gapped and the value of the renormalized spin gap M_{sat} scales with its bare value as [34]

$M_{sat} \approx J_{\parallel} (\Delta / J_{\parallel})^{1/(2-K)}$. Thus for $h_{eff}^0 = 0$ the low-energy behavior of the system is determined by the strongly relevant modulated magnetic field (i.e. modulated part of the rung exchange), represented by the term $h_{\parallel} \sin(\sqrt{4\pi K\phi})$. In the ground state the field ϕ is pinned in one of the minima of the potential $\langle \sin(\sqrt{4\pi K\phi}) \rangle = -1$. In view of (7a) we conclude that this state corresponds to a long-range-ordered antiferromagnetic phase of the effective Heisenberg chain (2), i.e. to a phase of the initial ladder system, where spins on weak rungs which have a dominant triplet character and spins on strong rungs with $(n = 3m \pm 1)$ predominantly singlets. At $h_{eff}^0 \neq 0$ the very presence of the gradient term in the Hamiltonian (12) makes it necessary to consider the ground state of the SG model in sectors with nonzero topological charge. The effective chemical potential $\approx h_{eff}^0 \partial_{\phi} \varphi$ tends to change the number of particles in the ground state i.e. to create finite and uniform density solitons. However, this implies that the vacuum distribution of the field ϕ will be shifted with respect to the corresponding minima. This competition between contributions of the smooth and staggered components of the magnetic field is resolved as a continuous phase transition from a gapped state at $h_{eff}^0 < M_{sat}$ to a gapless (paramagnetic) phase at $h_{eff}^0 > M_{sat}$ [25]. The condition $h_{eff}^0 = M_{sat}$ gives two additional critical values of the magnetic field $H_{c1}^{\pm} = J_{\perp}^0 + \frac{1}{2} J_{\parallel}^0 \pm J_{\parallel}^0 (\delta J_{\perp}^0 / J_{\parallel}^0)^{1/(2-K)}$. Correspondingly the width of each magnetization plateau is given by $H_{c1}^+ - H_{c1}^- = 2C_0 J_{\parallel}^0 (\delta J_{\perp}^0 / J_{\parallel}^0)^{1/(2-K)}$. To estimate the numerical value of the spin stiffness parameter K at magnetization m and anisotropy λ , we use the following ansatz [35]

$$K(m, \lambda) = K(0, \lambda) + \frac{|m|}{m_{sat}} [1 - K(0, \lambda)]. \quad (13)$$

This ansatz gives that $K \cong 0.87$ at $J_{\parallel} > 0$ and $K \cong 1.335$ at $J_{\parallel} < 0$. It is straightforward to get that in the antiferromagnetic case the width of the magnetization plateau scales as $\delta^{1/3}$, while in the case of a chain with ferromagnetic legs it scales as $\delta^{3/2}$.

Conclusions. We have studied the effect of period three modulation of the strong antiferromagnetic rung exchange on the ground state magnetic phase diagram of a spin-1/2 ladder.

In the limit commensurate with rung exchange uniform magnetic field, we map the model to an effective XXZ Heisenberg chain in the presence of uniform and spatially modulated longitudinal magnetic fields. The anisotropy parameter of the effective chain $\lambda = 0.5$ ($\lambda = -0.5$) for a ladder with isotropic antiferromagnetic (ferromagnetic) legs, while the amplitude of the effective magnetic field modulation is proportional to the amplitude of the rung exchange modulation δ . Using the continuum-limit bosonization treatment of the effective spin-chain model, we have shown that modulation of rung exchange leads to generation of two gaps in the excitation spectrum of the system at magnetization equal to the 1/3 and 2/3 of its saturation value. As a result, the magnetization curve of the system $M(H)$ exhibits two plateaus at $M = M_{sat}/3$ and $M = 2M_{sat}/3$. The width of the plateaus is proportional to the excitation gap and scales as δ^{ν} , where the critical exponent $\nu = 1.13$ in the case of a AF legs and $\nu = 1.50$ in the case of ladder with ferromagnetic legs.

Acknowledgements. It is our pleasure to thank M. Shahri Naseri for interesting discussions. This work has been supported by the GNSF Grant no. ST09/4-447 and the SCOPES Grant IZ73Z0_128058 (NA and GIJ).

ფიზიკა

დამაგნიტებულობის პლატოები კიბის სტრუქტურის მქონე $S=1/2$ სპინურ ჯაჭვში “საფეხურის” გასწვრივ გაცვლის ტრიმერული მოდულაციის შემთხვევაში

ნ. ავლიშვილი*, გ. ჯაფარიძე**, დ. ნოზაძე†, ს. მაკლავიფარი††

* ილიას სახელმწიფო უნივერსიტეტის ხაინთრო ფიზიკის ინსტიტუტი, თბილისი

** აკადემიის წევრი, ილიას სახელმწიფო უნივერსიტეტი; ანდრონიკაშვილის სახ. ფიზიკის ინსტიტუტი, თბილისი

† მისურის მეცნიერებისა და ტექნოლოგიის უნივერსიტეტი, ფიზიკის დეპარტამენტი, მისური, როლა, აშშ

†† გილანის უნივერსიტეტის ფიზიკის ფაკულტეტი, რეშო, ირანი.

შესწავლილია სპინი $S=1/2$ ორჯაჭვიანი, “კიბის” სტრუქტურის მქონე, იზოტროპული სისტემის მაგნიტური ფაზური დიაგრამა კიბის შემადგენელ ჯაჭვებს შორის „საფეხურის“ გასწვრივ გაცვლით ურთიერთქმედების ტრიმერული მოდულაციის შემთხვევაში. მოდელი განხილულია ძლიერი „საფეხუროვანი“ გაცვლისა და (ერთგვაროვანი) მაგნიტური ველის ზღვარში, რომელშიც საწყისი ორჯაჭვიანი ამოცანა ეფექტური თავისუფლების ხარისხების ტერმინებში დაიფანება სპინი $\tau=1/2$ ანიზოტროპული ჰაინზენბერგის ჯაჭვის ამოცანაზე გარე არაერთგვაროვან მაგნიტურ ველში. ეფექტური სპინური ჯაჭვის ანიზოტროპიის პარამეტრი $\lambda=0.5$ ($\lambda=-0.5$) კიბის შემადგენელი იზოტროპული ანტიფერომაგნიტური (ფერომაგნიტური) ჯაჭვების შემთხვევაში, ხოლო ეფექტური მაგნიტური ველის მოდულაცია განისაზღვრება კიბის „საფეხურის“ გასწვრივ გაცვლის მოდულაციით. ნაწინება, რომ გაცვლის მოდულაცია განაპირობებს სისტემის აღზნებათა სექტრში ღრუჭოების განენას და ამის შედეგად ე.წ. დამაგნიტებულობის პლატოს წარმოქმნას მაგნიტური ველის იმ მნიშვნელობისას, როდესაც სისტემის დამაგნიტებულობა თავისი ნაჯერი მნიშვნელობის $1/3$ და $2/3$ აღწევს. დამაგნიტებულობის პლატოთა სიგანე შესაბამისი სექტრალური ღრუჭოს პროპორციულია, ხოლო მისი მოდულაციის ამპლიტუდაზე (δ) დამოკიდებულება მოიცემა ხარისხობრივი კანონით δ^{ν} , სადაც $\nu=1.13$ ($\nu=1.50$) ანტიფერომაგნიტული (ფერომაგნიტული) ჯაჭვების შემთხვევაში.

REFERENCES

1. U. Schollwöck, J. Richter, D.J.J. Farnell and R.F. Bishop, Ed. (2004). Quantum Magnetism. Lecture Notes in Physics, **645**. Berlin, Springer.
2. S. Suchdev (2008), Nature Physics, **4**: 173-185.
3. T. Giamarchi, Ch. Rüegg, and O. Tchernyshyov (2008), Nature Physics, **4**: 198-204.
4. E. Dagotto (1999), Rep. Prog. Phys., **62**: 1525-1571.
5. R. Chitra and T. Giamarchi (1999), Phys. Rev. B, **55**: 5816.
6. D. C. Cabra, A. Honecker and P. Pujol (1998), Phys. Rev. B, **58**: 6241.
7. F. Mila (1998), Eur. Phys. J. B, **6**: 201.
8. K. Totsuka (1998), Phys. Rev. B, **57**: 3454.
9. K. Hida, M. Shino and W. Chen (2004), J. Phys. Soc. Japan, **73**: 1587.
10. G. I. Japaridze, A. Langari and S. Mahdaviyar (2007), J. Phys.: Condens. Matter, **19**: 07620.
11. S. Mahdaviyar (2007), Eur. Phys. J. B, **55**: 371.
12. G. Chaboussant et al. (1997), Phys. Rev. B, **55**: 3046.
13. G. Chaboussant et al. (1998), Eur. Phys. J. B, **6**: 167.
14. G. Chaboussant et al. (1998), Phys. Rev. Lett., **80**: 2713.
15. D. Arcon et al. (1999), Phys. Rev. B, **60**: 4191.
16. H. Mayaffre et al. (2000), Phys. Rev. Lett., **85**: 4795.
17. B. C. Watson et al. (2001), Phys. Rev. Lett., **86**: 5168.
18. M. C. Cross and D. S. Fisher (1979), Phys. Rev. B, **19**: 402.
19. K. Hida (1994), J. Phys. Soc. Jpn., **63**: 2359.
20. K. Okamoto (1996), Solid State Commun., **98**: 245.
21. M. Oshikawa, M. Yamanaka, I. Affleck (1997), Phys. Rev. Lett., **78**: 1984.
22. G. I. Japaridze and E. Pogosyan (2006), J. Phys.: Condens. Matter, **18**: 9297.
23. G. I. Japaridze and Saeed Mahdaviyar (2009), Eur. Phys. J. B, **68**: 59.
24. F. C. Alcaraz and A. L. Malvezzi (1995), J. Phys. A: Math. Gen., **28**: 1521.
25. K. Okamoto and K. Nomura (1996), J. Phys. A: Math. Gen., **29**: 2279.
26. I. Kuzmenko and F. H. L. Essler (2009), Phys. Rev., B, **79**: 024402.
27. A. Luther and I. Peschel (1975), Phys. Rev., B, **12**: 3908.
28. D. C. Cabra and M. D. Grynberg (1999), Phys. Rev., B, **59**: 119.
29. T. Hikihara and A. Furusaki (2001), Phys. Rev., B **63**, 134438.
30. G. I. Japaridze and A. A. Nersesyan (1978), Pis'ma v JETP, **27**: 356.
31. G. I. Japaridze and A. A. Nersesyan (1979), J. Low Temp. Phys., **37**: 95.
32. G. I. Japaridze, A. A. Nersesyan and P. B. Wiegmann (1984), Nucl. Phys. B, **230**: 511.
33. A. Takhtadjan and L. D. Faddeev (1975), Sov. Theor. Math. Phys., **25**: 147.
34. Al. B. Zamolodchikov (1995), Int. J. Mod. Phys. A, **10**: 1125.
35. M. Shahri Naseri, G. I. Japaridze, S. Mahdaviyar and S. Farjami Shayesteh (2012), J. Phys. C: Condens. Matter., **24**: 116002.

Received March, 2012

Physics

Ordering Effects in the Heat Capacity of Light Rare-Earth Superstoichiometric Dihydrides. $CeH_{2.86}$

Natela Namoradze* and Ioseb Ratishvili**

* Chavchanidze Institute of Cybernetics, Georgian Technical University, Tbilisi

** Andronikashvili Institute of Physics, I.Javakhishvili Tbilisi State University, Tbilisi

(Presented by Academy Member George Japaridze)

ABSTRACT. CeH_{2+c} -type ordering hydrides are considered. Different ingredients of the total heat capacity $C(T)$ of these ordering interstitial alloys are calculated and the summary result is compared with the corresponding experimental data.

Metal-hydrogen interstitial alloys (M-H compounds) are considered usually as consisting of thermodynamically sufficiently independent following main subsystems: the lattice of metal atoms, the set of interstitial light atoms located in tetrahedral interstitial positions (tetra-positions) and octahedral interstitial positions (octa-positions), and the system of conduction electrons. It has to be taken into account that in superstoichiometric rare-earth dihydrides the subsystem of additional light atoms distributed on the set of octa-positions reveals a tendency to form ordered spatial configurations, which is associated with corresponding changes of the internal energy of light atoms. Generally, in rare-earth hydrides we have to consider as well the subsystem of local magnetic moments associated with metal ions, but in the hydrogen-rich cerium hydride magnetic interactions in the lattice we assume to be negligibly small. In such conditions the measured heat capacity $C(T)$ of the given M-H compound consists of the following main components: *a*) heat capacity caused by acoustic waves in the metal lattice, *b*) heat capacity caused by local vibrations of light interstitial atoms in tetra- and octa-interstitial positions (characterized by different local frequencies), *c*) heat capacity related to the ordering processes in the subsystem of octa-hydrogen atoms, and *d*) heat capacity induced by conduction electrons.

Basing on the standard mathematic expressions for the heat capacity ingredients mentioned above and using the set of energy constants defined in our previous article, an excellent coincidence between the calculated and measured $C(T)$ dependencies is obtained in a wide temperature range. © 2012 Bull. Georg. Natl. Acad. Sci.

Key words: rare-earth hydrides, ordering processes, ingredients of the total heat capacity.

Introduction. The ordering superstoichiometric rare-earth dihydrides were widely investigated during the 1960s-1990s. Careful measurements were made and the most significant results were summarized in a number of reviews (see e.g. [1]). Some attempts were made as well to describe the observed temperature

dependences of characteristic physical properties and, finally, to understand the nature of hydrogen-metal bonding in different metal-hydrogen compounds. In all cases it was assumed that in "heavy metal" – hydrogen alloys (M-H alloys) H-atoms occupy interstitial positions of the given symmetry and that at low

temperatures they form some spatially ordered configurations (if their number is less than the number of corresponding interstitial positions). Thus, we usually consider the M-H compounds as consisting of some, thermodynamically sufficiently independent, subsystems: metal lattice, the set of interstitial light atoms, and the system of conduction electrons. We assume additionally that even if metal ions possess some local magnetic moments, magnetic ordering in the lattice is absent (i.e. magnetic interactions in the lattice can be neglected). In such conditions the measured heat capacity $C(T)$ of a given M-H compound can be considered to contain the following ingredients: that induced by the acoustic waves in the lattice of N metal atoms (denoted as $C_{ac}(T)$), that induced by the local vibrations of N_H light interstitial atoms (denoted generally as $C_{int}(T)$), that related to the ordering processes (denoted as $C_{ord}(T)$), and that induced by conduction electrons (denoted as $C_{ac}(T)$).

It should be stressed that in the case of cerium hydrides (as well as in lanthanum hydrides) even a small number N_H of H-atoms embedded in the hcp-lattice of N metal atoms ($N_H \ll N$) form local "islands" of dihydrides MH_2 with a fcc metal lattice where H-atoms occupy preferentially tetrahedral interstitial positions. For compounds MH_{2-c} ($0 < c < 1$) it was established that N metal atoms form a fcc lattice, where $2N$ H-atoms occupy $2N$ tetrahedral interstitial positions (they are called " H_T -atoms"), while additional cN H-atoms (called respectively " H_O -atoms") are distributed among N octahedral interstitial positions and at low temperatures form spatially ordered superstructures described by two long-range-order (LRO) parameters, η_1 and η_2 . Correspondingly, we have to distinguish local vibrations of H_T -atoms and H_O -atoms, as their bonds with surrounding metal atoms are presumably different.

In our previous article [2] we considered quasi-stoichiometric dihydrides of rare-earth metals and adjusted the numerical values of characteristic parameters describing the heat capacities of different subsystems in metal-hydrogen compounds – the Debye characteristic temperature T_{Dbl} (for acoustic vibrations of metal lattice), Einstein characteristic

temperature T_E (for local vibrations of H-atoms located in tetrahedral sites of fcc metal lattice), and factor g (characterizing the electronic specific heat). Some basic mathematical relations were also presented for calculations of specific heat ingredients – $C_{ac}(T)$, $C_{op}(T)$ and $C_{el}(T)$. We shall not repeat these expressions here, and concentrate our attention on the additional ingredients of the total heat capacity in compounds MH_x ($x > 2$) induced by the set of H_O -atoms. These are the heat capacity associated with local vibrations of H_O -atoms in the ordered and disordered spatial configurations $C_{op}(H_O)$, and the heat capacity of the ordering process $C_{ord}(T)$.

Formulation of the problem. In [3] the results of low temperature heat capacity measurements taken on cerium hydride $CeH_{2.86}$ were presented, where the influence of hydrogen ordering on the temperature dependence of the total heat capacity was clearly registered. *We intend to calculate temperature dependent heat capacity of this compound, basing on the symmetry properties of the free energy function of ordering subsystem established in [4], due to which the hydrogen vacancies ordering process in $CeH_{2.86}$ can be described as the ordering of H_O -atoms in the compound $CeH_{2.14}$.*

Heat capacity of the ordering process in a system characterized by two LRO parameters. This problem was widely considered in a number of our previous articles and we shall give below only a brief summary of the main mathematical relations.

Ordering of a binary A-B alloy implies that different sites of a given crystalline lattice are characterized by different occupation probabilities of A and B components. In case of the ordering hydrogen subsystem the roles of A and B atoms are played, respectively, by H-atoms and their vacancies. It was established [5] that in superstoichiometric cerium dihydrides CeH_{2-c} the ordering of H-atoms located in octahedral positions (H_O -atoms) is characterized by two LRO-parameters $\eta_1(T)$ and $\eta_2(T)$, which provide existence of three different occupation probabilities (of octahedral interstitial positions) – n_1 , n_2 and n_3 :

$$\begin{aligned} n_1 &= c + \eta_1\gamma + 2\eta_2\gamma, & n_2 &= c + \eta_1\gamma + 2\eta_2\gamma, \\ n_3 &= c - \eta_1\gamma \end{aligned} \quad (1)$$

($\gamma = 0.25$ is a normalizing factor).

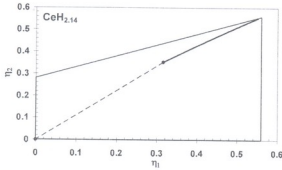


Fig. 1a. Trajectory of the ordering process in (η_1, η_2) space.

Equilibrium values of the order parameters η_1 and η_2 are determined from equations [5]

$$\ln \left[\frac{\eta_1 n_2 (1-n_1)^2}{(1-n_1)(1-n_2) n_3^2} \right] = -(V_1/T) \eta_1 \quad (2a)$$

$$\ln \left[\frac{n_1 (1-n_2) / n_2 (1-n_1)}{n_3} \right] = -(V_2/T) \eta_2 \quad (2b)$$

which can be solved only numerically (V_1 and V_2 are Fourier-components of H_0 - H_0 interaction potential taken in temperature units; they can be estimated from experimental data).

The main energy parameter of the ordering subsystem is the ratio $p = [V_2/V_1]$. In the case of CeH_x compounds $p > 1$; particularly, $p[\text{CeH}_x] = 1.25$ [5].

The ordering subsystem of H_0 -atoms is characterized by the ordering energy [5]

$$E_{\text{ord}}(\eta_1, \eta_2) = Nk_B 0.5 [V_1(\eta_1)^2 + 2V_2(\eta_2)^2], \quad (3)$$

which is zero in the disordered state and reaches its lowest value at maximum order.

Heat capacity of the ordering subsystem is determined as temperature derivative of the function

$$E_{\text{ord}}(\eta_1, \eta_2); \quad C_{\text{ord}}(T) = dE_{\text{ord}}(\eta_1, \eta_2) / dT \quad (4)$$

Numerical results for the ordering subsystem in the model compound $\text{CeH}_{2.14}$. It is known [1] that in the given compound $2N$ tetrahedral interstitial positions are filled by $2N H_1$ -atoms, while concentration of H_0 -atoms c equals $c = 0.14$. It can be estimated [4] that in cerium dihydrides for concentration $c = 0.14$ the energy parameters of the ordering subsystem V_1 and V_2 are as follows:

$$V_1[\text{CeH}_{2.14}] = -1540 \text{ K}, \quad V_2[\text{CeH}_{2.14}] = -1925 \text{ K}. \quad (5)$$

Solution of equations (2) gives us a detailed description of the ordering process presented in Figs

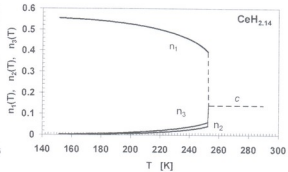


Fig. 1b. Temperature dependence of occupation numbers

1a and 1b, showing, particularly, the trajectory of the ordering process in the space of order parameters η_1 and η_2 (Fig. 1a), and temperature dependence of occupation numbers $n_1(T)$, $n_2(T)$ and $n_3(T)$ (Fig. 1b). ("Trajectory of the ordering process" is the sequence of points in the (η_1, η_2) -space denoting the set of equilibrium states at gradually varying temperature).

The ordering energy (3) and its temperature derivative (4) are given in Figs. 2a and 2b, respectively.

Numerical results for the heat capacity of compound $\text{CeH}_{2.36}$.

Using the mathematical scheme already applied to the heat capacity calculations in quasi-stoichiometric lanthanum dihydride LaH_2 [2] (where all hydrogen atoms were assumed to be located exclusively in the tetrahedral interstitial positions) and adding the heat capacity parts associated with vibrations of "superstoichiometric" H_0 -atoms and with ordering of these H_0 -atoms, we arrive at the following summary expression:

$$C(T)[\text{CeH}_{2.36}] = C_{\text{ac}}(M) + C_{\text{op}}(H_T) + C_{\text{op}}(H_0) + C_{\text{ord}}(H_0) + C_{\text{el}}, \quad (6)$$

where the first, second and last term (metal lattice acoustic waves, vibrations of H_T -atoms and electronic specific heat) were already considered in [2], while the third and fourth terms will be considered below.

As mentioned above, equations (2) can be solved only numerically and consequently analytical temperature dependences cannot be obtained either of the energy function (3), or of its derivative (4). Numerical dependence $C_{\text{op}}(H_0)$ is given in Fig. 2b, on assuming that concentration of the ordering component equals $c = 0.14$.

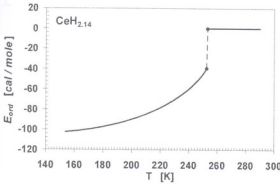


Fig. 2a. Temperature dependence of equilibrium energy of the ordering subsystem.

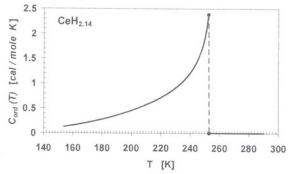


Fig. 2b. Heat capacity of the ordering subsystem.

The heat capacity related to local vibrations of H_O -atoms is proportional to the number of oscillating particles, and thus, we imply that in this case $c = 0.86$.

A few words about the electronic term which is presented usually as $C_e(T) = g T$, where g depends on the number of mobile electrons (or on the density of states at the Fermi level). It was established that during the hydrogenation process hydrogen atoms introduced in the lattice of rare-earth metals capture itinerant electrons of metal lattice and deplete gradually the conduction band [6]. In order to take this effect into account we have used the “reduced value” of factor g (determined experimentally for pure dihydride and used in [2]) on applying the relation: $g[\text{CeH}_{2,c}] = (1 - c)g[\text{CeH}_2]$. (7)

Proceeding from physical reasons we have selected the following set of parameters characterizing the metal-hydrogen system investigated in [3]:

$$T_{\text{Deb}} = 140 \text{ K}, T_{\text{Em}}(\text{tetra}) = 1240 \text{ K}, T_{\text{Em}}(\text{octa}) = 744 \text{ K}, g = 0.00028 \text{ (cal / mole K}^2\text{)}. \quad (8)$$

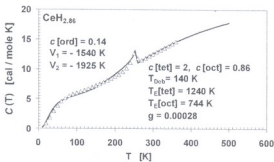


Fig. 3. Temperature dependence of the heat capacity of $\text{CeH}_{2.86}$. The sequence of triangles – experimental data [3], full line – calculated $C(T)$ curve. The numerical values of the characteristic parameters are indicated in the figure.

The results of calculations based on parameters (5) and (8) are presented in Fig.3 together with experimental points [3]. We see that general experimental $C(T)$ dependence in a wide temperature range is successfully represented by the calculated curve.

Brief comments. Agreement between the theoretical and experimental data is excellent, but there arise some doubts. We have not taken into account the hydrogen “weighting” effect induced by ordering processes [7]. Our attempts to modify parameter $T_{\text{Em}}(\text{octa})$ and to make it temperature dependent (as in the case of deuteride V_2D [7]) gave a negative result – modified $C(T)$ -curve became separated from experimental points. This apparent “anomaly” has to be considered in the future. (Perhaps the mobility of massless vacancies of H_O -atoms in the ordering $\text{CeH}_{2.86}$ is qualitatively different from the mobility of H_O -atoms in the ordering $\text{CeH}_{2.14}$).

Conclusions. In spite of the used crude assumptions the selected set of energy parameters (5) and (8) enable us to give an adequate description of the heat capacity temperature dependence of the given metal-hydrogen compound. Parameters (8) are slightly different from those used in [2], and this is a strong stimulus for further investigations aimed to understand the physical reasons of variations of the mentioned parameters induced by variations of hydrogen concentration.

Acknowledgements. The authors thank Prof. George Japaridze for supplying article [3]. Investigations were performed within the framework of the Georgia National Project GNSF/ST09-5014-280.

ფიზიკა

მოწესრიგების ეფექტები მსუბუქ იშვიათ მიწათა ზესტექიომეტრიულ დიჰიდრიდების სითბოტევადობაში. $CeH_{2.86}$

ნ. ნამორაძე*, ი. რატიშვილი**

* საქართველოს ტექნიკური უნივერსიტეტი, ჭავჭავაძის კაბერნეტიკის ინსტიტუტი, თბილისი

** ი.ჯავახიშვილის სახ. თბილისის სახელმწიფო უნივერსიტეტი, ანდრონიკაშვილის ფიზიკის ინსტიტუტი, თბილისი

(წარმოადგინა აკადემიის წევრმა გ. ჯაფარიძემ)

ნაშრომში გაანალიზებულია CeH_{2+c} ტიპის დიჰიდრიდების სითბოტევადობის ცალკეული კომპონენტი დაკავშირებული, კერძოდ, მესერის აკუსტიკურ რხევებთან, წყალბადის ატომების ლოკალურ რხევებთან, წყალბადის მოწესრიგებასთან და ლითონის გამტარებლობის ელექტრონებთან. დადგენილია ლითონ-წყალბადის მოცემული სისტემის მახასიათებელი პარამეტრები, როგორცაა დებაის ტემპერატურა წყალბადმშემცველი ლითონის მესერისთვის T_{Deb} , აინშტაინის ტემპერატურები T_{Ein} (tetra) და T_{Ein} (octa) ლითონის მესერის ტეტრა- და ოქტა-კვანთაშორისეში განლაგებული წყალბადის ატომების ლოკალური რხევების დასახასიათებლად, წყალბადის მოწესრიგებადი ქვესისტემის ენერგეტიკული პარამეტრები V_1 და V_2 , და გამტარებლობის ელექტრონების სითბოტევადობის აღმწერი პარამეტრი g . ამ პარამეტრების ქვემოთ მოყვანილი მნიშვნელობებისთვის $V_1 = -1540$ K, $V_2 = -1925$ K, $T_{Deb} = 140$ K, T_{Ein} (tetra) = 1240 K, T_{Ein} (octa) = 744 K, $g = 0.00028$ (cal / mole K^2) მიღწეულია $CeH_{2.86}$ ნაერთის სითბოტევადობის ტემპერატურული დამოკიდებულების ამსახველი ექსპერიმენტული $C(T)$ მრუდის ზუსტი აღწერა.

REFERENCES

1. P. Vajda (1995), in: Handbook on the Physics and Chemistry of Rare Earths (Eds. K.A. Gschneidner, L.R. Eyring), North-Holland, v. 20, p. 209-294.
2. N. Namoradze, I. Ratishvili (2011), Bull. Georg. Natl. Acad. Sci., 5, № 3, 51-54..
3. Z. Bieganski, W. Fesenko, B. Stalinski (1965), Bull. Acad. Pol. Scien., Ser. Scien. Chim. XIII, N3, 227-230.
4. I.G. Ratishvili, P. Vajda (1997), Journ. Alloys and Comp., 253-254: 171-174
5. I.G. Ratishvili, P. Vajda, A. Boukraa, N.Z. Namoradze (1994), Phys. Rev. B 49: 15461-15469
6. R.G. Barnes, C.-Y. Chang, M. Belhoul, et al. (1991), J. Less-Common Metals, 172-174: 411-418.
7. I.G. Ratishvili, N.Z. Namoradze (2011), Metallofiz. Noveishie Tekhnol., 33 (7): 919-936.

Received March, 2012

Physics

Application of Cherenkov Effect to Increase the Safety of Nuclear Plants

Badri Chiladze*, Nodar Lomidze*, Mikhail Nioradze*,
Alexandr Sidelnikov*, Igor Trekov*

* High Energy Physics Institute of I. Javakhishvili Tbilisi State University

(Presented by Academy Member Teimuraz Kopaleishvili)

ABSTRACT: Development of atomic power engineering with nuclear fuel cycle brings forward the requirement of the condition control of the spent nuclear fuel (SNF). First of all, these are burnup, isotope structure of nuclear materials and fission products, data on the condition of shells of fuel elements, etc. It should be noted that detailed analysis of the specified parameters is important at all stages of the nuclear fuel life cycle at the nuclear power plant and in general at plant independently of the reactor type. Various aspects of increasing the safety of nuclear plants working on thermal neutrons are discussed. A new method based on application of Cherenkov effect and optical fiber for measurement of the nuclear radiation power, identification of the spent fuel assemblies and determination of the burning factor of the nuclear fuel is considered. Knowledge of burnup depth and isotope structure is necessary for elaboration of recycling strategy or burial of radioactive wastes. It is also important to reliably identify the spent fuel assemblies (SFA) to exclude the possibility of leak of the SNF, which may be used for manufacturing weapons of mass destruction. © 2012 Bull. Georg. Natl. Acad. Sci.

Key words: Cherenkov radiation, photomultiplier, nuclear fuel, light-emitting diode.

In this work different aspects of using Cherenkov radiation to promote the increase of the nuclear safety of nuclear plants working on thermal neutrons and using water as heat carrier are considered. For this purpose to register nuclear radiation, first of all γ -radiation, a highly sensitive detector based on Cherenkov effect and fibre-optical light guide has been created.

It is known that Cherenkov radiation is generated in light-transmitting medium under the following condition: $\beta n > 1$, where n is the refractive index, $\beta = v/c$; v

is the velocity of charge particle in the medium and c - light velocity in the vacuum. For example, the threshold energy of electrons necessary for production of Cherenkov radiation in water with the refraction index of 1.33 is 0.26 MeV [1, 2].

The main advantage of the proposed system is its selective properties towards the γ -radiation sources and the lack of necessity of voltage supply to the detector in the working zone and exceptional speed of operation of the registration device (units of nanosecond).

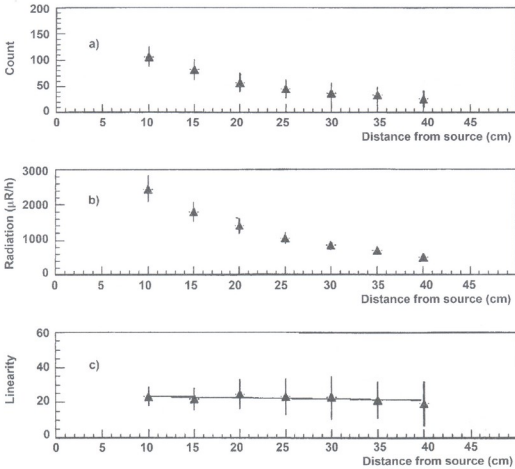


Fig. 1. Number of pulses measured by Cherenkov detector vs distance

The basic parts of the system are: a) a radiator generating Cherenkov radiation under the impact of ionizing radiation (mainly γ -radiation); b) optical fiber for signal transmission; c) detector of light radiation - a photomultiplier. Depending on the task, the radiator can be made of quartz or plexiglas and other optical transparent materials. Distilled water can be also used as a radiator.

At determining the burnup factor and identification of the SNF one deals with high levels of radiation which cannot be obtained in laboratory environment. Therefore it was necessary to find an appropriate technical solution which would allow testing the method in conditions close as possible to the real.

Since the method is based on registration of ultraviolet radiation, its check can be carried out in laboratory environment by means of an imitation of

radioactive radiation by a light source operating in ultraviolet spectrum. It is enough to use a light-emitting diode (LED) as such source, with appropriate parameters, which is fed from the pulse generator. If we pre-calibrate the system from the radioactive radiation source it is possible to imitate the radioactive radiation dose by selection of the pulse parameters submitted to the LED from generator, thereby, the laboratory conditions get as close as possible to the real. Consequently, special equipment has been constructed with the help of which the Cherenkov detector may be fixed at the required distances from the radioactive source. Radiation dose at different distances has been measured by means of a dosimeter, and then similar measurements have been carried out with Cherenkov detector which is described in [3]. The results of measurements are presented in Fig. 1.

Table 1. Results of measurements for three different emission frequencies of LED, obtained by one photomultiplier

Frequency	5-cores	10-cores	15-cores	20-cores	24-cores
30 khz	1066±15	5748±27	11530±30	14578±32	15998±32
100 khz	2888±21	17032±39	35700±52	46177±58	49855±59
200 khz	6536±33	3478 ±58	75489±65	94995±72	105847±90

Dependence of the pulse number measured by Cherenkov detector on the distance from the radioactive source is shown in Fig. 1a. Distribution of the radiation dose measured by dosimeter along the same distance is presented in Fig. 1b, and Fig. 1c shows the dependence of the ratio of the radiation dose measured by dosimeter to the pulse number measured by Cherenkov detector at different distances from the radioactive source.

As seen from Fig. 1c the number of pulses measured by the photomultiplier is proportional to the radiation dose. Consequently, it may be assumed that such proportional behavior will be valid in the range of the high radiation dose. It means that high intensity of radiation can be simulated by means of a light-emitting diode, and this method can be applied to laboratory measurements.

To identify the spent fuel assemblies, the International Atomic Energy Agency uses optical apparatus as well as night vision television cameras [4,5]. Close to SFA surveillance cameras quickly fail under the influence of radiation. Increase of the distance from SFA causes a sharp decrease of the resolution of cameras, which becomes insufficient for the full identification analysis of SFA. Besides, special monochromatic filters are required for the television cameras to observe the ultraviolet part of the spectrum. Therefore, in this case use of apparatus directly registering Cherenkov radiation is quite justified, as it does not suffer from the disadvantages mentioned above.

As is known the distribution of the radiation power of the spent fuel assembly along its length has cosine form, i.e., achieves a maximal value in the

middle. Moving the Cherenkov radiator along the full length of SFA, it is possible to determine the form of distribution of the radiation power and thereby to determine the presence of nuclear material in the assembly under examination.

It is practically impossible to create in the laboratory conditions close to those in a real reactor. Therefore to test the method an experimental device was constructed with the help of which radioactive radiation was simulated by ultra-violet LED. As shown above, it is possible to replace the radioactive radiation source with radiation of LED and to assume the number of registered pulses to be proportional to the radioactive radiation dose.

To carry out experiments a mechanical device was made representing a metal bedplate of the size of 710 mm x 300 mm. A rectangular platform of the size of 260 mm x 140 mm moves horizontally on this bedplate. The movement of the platform is carried out with the help of a micrometer screw. The screw is put in rotation by the handle supplied with a revolution counter. An optical cable with 74 cores and 300 mm in length is fixed on the platform. One end of the cable is untwisted in five plaits. The number of optical veins in plaits is 5, 10, 15, 20 and 24 respectively. Plaits are fixed on a platform by means of two interdigital-clamping laths with semi-apertures of the corresponding diameter. The distance between the centers of neighbor plaits equals 20 mm. End faces of the veins are polished and fixed on one line in horizontal plane. The opposite side of a given optical plait is also polished and connected to a light source as the ultraviolet light-emitting diode is used, which is fed from the pulse generator. Thus, each of the plaits forms a light

Table 2. Results of measurements for three different emission frequencies of LED, obtained with the start of two photomultipliers according to the coincidence circuit

Frequency	5-cores	10-cores	15- cores	20- cores	24- cores
30 khz	4±1	49±3	284±7	384±8	415 ± 8
100 khz	14±2	150±6	932±10	1285±12	1338±13
200 khz	40±3	455 ±7	2712±14	3611±18	3671±18

emitter in which the portion of general light flux is defined by the number of the used optical veins. The same optical plait with 74 cores and length of 8 m is fixed on a bedplate, opposite to the end faces of emitters. It is connected to the photomultiplier and together with it carries out the function of a light receiver. The holder design allows a precise matching of the center of the light receiver with the center of the chosen emitter radiator in a vertical plane. A transversal motion mechanism of the platform allows smooth changing of the distance between the light receiver and emitter in the range from 1 mm to 50 mm. All optical nodes of the construction are protected from external light sources by a boot made of lightproof material.

Measurements have been conducted with the help of program LabVIEW [6], which allowed obtaining results in the graphic and digital configuration. The results of measurements for three different frequencies are presented in Table 1. Data in the table are shown with a deduction of the photomultiplier background. As shown from the obtained results, the detector accurately registers the change of the radiation intensity.

Since high intensity of radiation is usual in the storehouse, it is possible to apply the coincidence scheme for unloading of the photomultiplier. For the coincidence scheme the presence of two photomultipliers is necessary. Therefore the optical plait should be divided into two identical parts, each of which is connected to its photomultiplier. In this case the influence of internal noise of photomultiplier is thus excluded, improving accuracy and expanding the measurement range. Measurements with a source

were performed using the method mentioned above with the same frequencies and the results are shown in Table 2.

As seen from the obtained results the account rate is approximately decreased by two orders. The number of Cherenkov photons is decreased (the light-emitting diode radiates more light quantum in one portion) and in this case the detector registers only intensity change. The obtained results show that by means of this method it is possible to control the condition of the SFA and, thereby, to identify the presence of nuclear material in it.

As is known, under the influence of neutrons there occurs fission of nuclear fuel in the reactor. It causes an aggregation of the decay products in the spent fuel assembly. This process is called fuel burnup. Burnup factor is defined as a ratio of the used fuel to initially loaded nuclear fuel expressed in percentage, or as a ratio of the generated energy to the mass of the initially loaded nuclear fuel:

$$B = N_{\text{dec}} / \sum_i N_i,$$

where ^{235}U , ^{238}U and ^{239}Pu are nuclei of which the nuclear fuel originally consists, and N_{dec} is number of the decay nuclei. The burnup factor defines the congestion of fission products in nuclear fuel, where ~16% is gaseous isotopes of krypton and xenon. At burnup expansion the pressure of gases under shells of the spent element grows, which can cause a breakdown of its housing. Among fission products there are also nuclides which have a great absorption cross-section of neutrons. Accumulation of these products can lead to interruption of the nuclear chain reaction. Hence the importance of knowledge of the burnup factor.

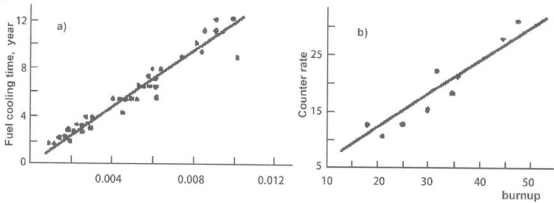


Fig. 2. a) Dependence of fuel cooling time vs I/I_0 , where I - Intensity of ^{137}Cs γ -radiation, I_0 - total intensity of γ -radiation); b) Relation between count rate of γ -radiation and burnup factor.

The larger the burnup factor the greater is the operating time of the reactor without replacement of fuel and the less requirement of a new SFA. Besides, smaller area is needed for storage of the spent fuel and the volume of transportation from the nuclear power plant to the manufacturing factory is decreased. As a result this gives improvement of the general economic indicator of the reactor operation.

In [7] the spectral analysis of the γ -radiations of an order of the 200 spent fuel assembly has been carried out and on the basis of the obtained results the following conclusions are drawn (Fig. 2):

1. Dependence of the ratio of the measured intensity of gamma radiation of isotope ^{137}Cs vs the integrated intensity of gamma radiation of the SFA (increases linearly with the storage time).

2. There is a linear dependence between the intensity of gamma radiation of isotope ^{137}Cs at the moment of shutdown of reactor and fuel burnup for all values of fuel enrichment.

These conclusions allow to offer a method of burnup factor determination, which is based on the use of Cherenkov detector. The suggested method gives a possibility to rather simply determine the burnup factor. It is important that a measurement can be carried out in parallel with the SFA inspection. Measurements can be conducted with the help of a special device, which allows the movement of Cherenkov detector along the SFA case with required step. The radiator of the detector and the part of the opti-

cal fiber adjoining it are located in a protective lead shell. By means of regulation of the gap diameter of the shell and change of distance from the detector to the SFA it is possible to allocate a small area of the SFA and, thereby, change the γ -radiation intensity incident on detector. Information transmission on photomultiplier is carried out by the optical fiber.

It is known that the neutron beams in an active zone of reactor are irregularly distributed and consequently the γ -radiation intensity along the SFA surface is changed. The ratio of the average intensity of the categorized fuel assembly (with exact information on operation, the date of stay in the storehouse and the average burnup value) and the spent fuel assembly with the same fuel cooling time allow to determine how much more or less burnup occurs in the spent fuel assembly under investigation:

$$B/B_0 = J/J_0$$

where B , B_0 and J , J_0 are the average value of burnup and intensity of the spent and categorized fuel assemblies. As mentioned in the technical quarter reports the radiation intensity has been measured with high accuracy by the Cherenkov detector. Therefore, basically the error value in the burning determination will depend on the miscalculation of the burnup factor of the categorized fuel assembly.

This work was supported by Shota Rustaveli National Science Foundation grant GNSF/ST09-1041-4-200. The authors would like to thank I. Tatisvili for his help in fulfillment of this experiment.

ფიზიკა

ჩერენკოვის ეფექტის გამოყენება ბირთვული ენერგეტიკის უსაფრთხოების ასამაღლებლად

ბ. ჭილაძე*, ნ. ლომიძე*, მ. ნიორაძე*, ა. სიდელნიკოვი*, ი. ტრეკოვი*

* ი. აკვახიშვილის სახ. თბილისის სახელმწიფო უნივერსიტეტის მაღალი ენერჯიკის ფიზიკის ინსტიტუტი, თბილისი

(წარმოდგენილია აკადემიკოს თ. კობალეიშვილის მიერ)

ნაშრომში დამუშავებულია მეთოდი, რომლის საშუალებით შესაძლებელია ნამუშევარი სითბოს გამოყოფი ელემენტების საიმედო იდენტიფიცირება და მათი გამოწვის კოეფიციენტის განსაზღვრა. ამისათვის ჩერენკოვის დეტექტორის ბაზაზე დამზადებულ იქნა ლაბორატორიული ხელსაწყო, რომელშიც გამოყენებულია რადიოაქტიური გამოსხივების იმიტაციის შესაძლებლობა ულტრაიისფერი შუქდიოდის გამოსხივებით და მიღებული სიგნალის გადაცემა შორ მანძილზე ოპტიკურ-ბოჭკოვანი კაბელით. ლაბორატორიულ ხელსაწყოზე ჩატარებულმა გაზომვებმა აჩვენა, რომ ჩერენკოვის დეტექტორის საშუალებით შედარებით მარტივად და ნაკლები დანახარჯებით შესაძლებელია როგორც სითბოს გამოყოფი ელემენტების გამოწვის კოეფიციენტის განსაზღვრა, ისე მათი საიმედო იდენტიფიკაცია.

REFERENCES

1. J. Jelly (1960), Cherenkovskoe izluchenie i ego primeneniia. M. (in Russian).
2. V. Zrelvo (1968), Izluchenie Vavilova-Cherenkova i ego primeneniie v fizike vysokikh energii. M. (in Russian).
3. N. Amaglobeli, B. Chiladze, G. Karumidze, et al. (2008), Bull. Georg. Natl. Acad. Sci., 2, 1: 73-79.
4. International Nuclear Verification (2003), Series No.1 IAEA, Vienna.
5. S. Ermakov, B. Beliaev, O. Mikhnevich, I. Khlebnikov (1989), Analysis of Hardware of Control of Nuclear Material. USSR State Committee of Atomic Energy Use. M. (in Russian).
6. A. Suranov (2005), LabVIEW 7: Spravochnik po funktsiiam. M. (in Russian).
7. O. Maslov (2007), Trudy Odesskogo Politehnicheskogo Universiteta, 2(28): 65-71.

Received April, 2011

Geophysics

Preventing Severe Convective Storm: Anticipatory Restratification of Lower Atmosphere

Irakli G. Shekrladze

Department of Hydroengineering, Georgian Technical University, Tbilisi

(Presented by Academy Member Tamaz Chelidze)

ABSTRACT. The distributed anticipatory restratification concept (DARC) points the way to prevent severe convective storm. DARC provides artificial discharge instability energy of moist unstable lower atmosphere by convective clouds proactively forced in the area to be protected. The paper discusses some problems associated with the implementation of distributed proactive forcing (DPF) (the previous scheme of DARC). It is shown that the so-called metotron, previously developed as a technical means to increase rainfall in arid areas, can be much more effective through the realization of DARC in a moist unstable lower atmosphere close to the development of severe convective storm. As follows from the simplified analysis, the required trust of the metotron and its single run time strongly depend on the distance up to the bottom of capping inversion, the other conditions being equal. This puts to the fore the implementation of the schemes with location of metotrons on mountain tops and in the marine environment. On this basis the new scheme of imported proactive forcing (IPF) is proposed. The potential applications of IPF for preventing hailstorms in the Alazani Valley (with location of the metotrons on the mountain tops) and excessive rains in Ajara (with location of the metotrons in the marine environment) are considered. The potential of DARC to prevent the development of severe tornadoes is outlined. The evaluation is made showing that the main conclusion of simplified analysis of the strong dependence of the main operating parameters on the distance up to the capping inversion will remain in force after a thorough analysis of the problem as well. © 2012 Bull. Georg. Natl. Acad. Sci.

Key words: hailstorm, capping inversion, instability energy, convective available potential energy, distributed anticipatory restratification, imported proactive forcing.

Introduction. R&D activities in the field of modification of convective clouds are mainly focused on the technology of cloud seeding to mitigate the hail impact [1-5]. There is also another approach aimed at

restriction of the development of a severe convective storm by modification of its energy basis [6].

According to generally accepted ideas, in the warm season, a severe storm depends largely on the

interaction between lower atmosphere warmed by the sun and the capping inversion [7-9]. Solar heating is a supplier of the instability energy (convective available potential energy (CAPE)) for the upcoming convective development. Capping inversion represents a remainder of a stable boundary layer formed through cooling the air by the earth surface in the night time.

After sunrise, the cool boundary layer is not completely destroyed by solar heating and gradually climbs into a capping inversion, limiting the convection height. In the daily cycle, capping inversion not only retards a lot of instability energy in the lower atmosphere, but contributes to the collection of a large amount of CAPE in a single convective cloud, supporting strongly the development of severe convective storm [6-9].

On this basis, DPF (the previous scheme of DARC [6]) points the way to prevent development of severe convective storm through discharging a great amount of CAPE, held under capping inversion, by several convective clouds, proactively forced in locations distributed across the territory to be protected.

The paper discusses the conditions for implementation of DARC. Strong dependence of the efficiency of the so-called meteoron on the distance up to the capping inversion is identified. The new scheme of imported proactive forcing (IPF) is proposed applied to the hailstorm problem in the Alazani Valley and excessive rains in the Autonomous Republic of Ajara. The potential of applying DARC to prevent strong tornadoes is outlined.

2. Conceptual basics of the study. The strength of a convective cloud depends on the instability energy involved in its development. The more CAPE is collected by the cloud, the stronger it becomes and the higher. According to [6], in pre-hailstorm situation, CAPE and absolute humidity in the lower atmosphere are more than 225 J/kg and 7×10^{-3} , respectively. Besides, "medium" hail-producing convective cloud collects CAPE at least from $1000\text{-}1500 \text{ km}^2$.

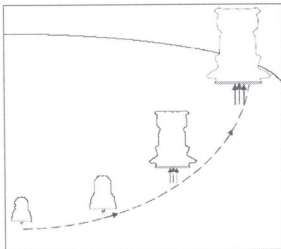


Fig. 1. A scheme of development of strong convective cloud.

A scheme of development severe storm is shown in Fig. 1. Since the first air stream breaks capping inversion, ascending air flow turns into the structure-forming dynamic core of the future convective cloud. At this point, capping inversion serves as a kind of "umbrella" collecting warm moist air in a single convective cloud from a large area.

As shown in Fig. 1, the cloud moves along the earth's surface, permanently gaining strength. In addition, the cloud gradually discharges CAPE from adjusted area and prevents other pass-through channels on a large territory. Finally, such a cloud can lead to severe storm with possible dangerous consequences, such as a tornado, hail or thunderstorm.

According to modern concepts [7-9], pass-through channel rarely results in the break of capping inversion by internal convection and is mainly caused by external forcing. Interaction of regional winds or weather fronts with local orography, development of upslope flows by solar heating of mountains or combination of these mechanisms are typical forms of forcing.

Based on these provisions, DPF offers prevention of a severe convective storm by proactive discharge of previously accumulated CAPE by several convective clouds artificially formed in capping inversion [6].

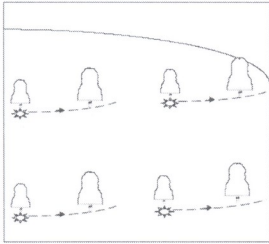


Fig. 2. A scheme of DPF moist unstable lower atmosphere using the meteotrons (eight-pointed stars).

A protection system based on DPF [6] is shown in Fig. 2. The meteotrons are uniformly distributed over the territory to be protected. When the monitoring system detects a pre-hail situation, the meteotrons are launched and a system of convective clouds is formed. After collecting the CAPE from the vicinity, a cloud can only move to an area where CAPE is already mastered by another cloud. Thus, each convective cloud remains underdeveloped with little

chance to result in a severe storm. Integral effect should be sufficient to proactively “soft” discharge CAPE above all territory.

3. Conditions of realization of DARC and associated problems. Development of severe storm requires collecting instability energy from the area greatly exceeding the cross-section of the cloud. At low values CAPE required collection route proves very long, which extremely reduces the likelihood of a severe storm. The higher is CAPE the shorter the required collection route and the higher the chance of a severe storm.

The parameters of numerous severe storms observed in the USA in 1997-1999 are presented in Fig. 3 [10]. The estimate [6] also is shown. Gaining by CAPE and wind shear the role of main influential environmental parameters fully fit in the above logic (collection route depends on regional wind). An overwhelming majority of severe storms is observed at high values CAPE (200-3,000 J/kg) in the range of wind shear 5-15 m/s. Rare severe storms, corresponding to low CAPE (0.2-100 J/kg), are observed at high wind shears (20-50 m/s), that is, they are linked to

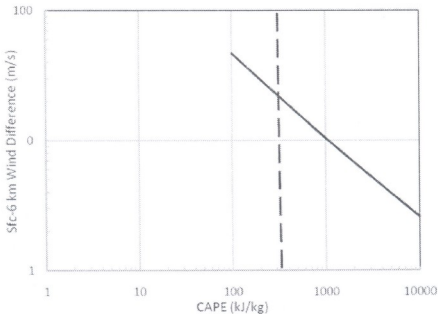


Fig. 3. The best discriminator of environmental parameters of the severe convective storms observed in the USA in 1997-1999 (sloping solid line) [10] and the estimate [6] (vertical dashed line).

long collection routes. The estimate [6] is in rough agreement with the results [10].

The estimate [6] also is roughly consistent with the analysis of convective storms observed in Europe during the warm seasons in 2006 and 2007 [11]: CAPE around 250 J/kg discriminates between thunderstorm and no thunderstorm group and predicts the probability of severe events when 500 J/kg is exceeded. Thus, proactive reduction of CAPE in the lower atmosphere may be an effective way to prevent a severe storm.

DPF should be supported by effective meteorological monitoring. Accurate identification of a pre-hailstorm situation may limit the number of startups of the protection system. The number of the meteotrons involved in a single run of the system also depends on the accuracy of the identification of a pre-hailstorm situation over the protected territory.

Another problem is prevention of a merger forced by the system clouds. According to [6] the merger can be avoided by keeping the distance between neighboring meteotrons more than 6-8 km. However, the estimate needs further validation.

4. Artificial forcing: Technical means and operational parameters. Previously, the so-called meteotron, burning petroleum products, was used to increase rainfall in arid areas [12]. Later the meteotron was improved by the use of a turbojet engine [13]. However, realized experimental systems proved insufficient for systematically obtaining precipitation in arid areas. The proposed new options with very powerful meteotrons [13] raise concerns in terms of economic feasibility.

The task is considerably simplified when implementing DARC. If in the arid zone the CAPE is about 50 J/kg [13], in the atmosphere with the potential to generate a severe storm CAPE exceeds 500 J/kg [11]. In the arid zone meteotron is to force cloud in a rather stable atmosphere, in the case of DARC the same should be done in unstable moist atmosphere close to natural initiation of cloud.

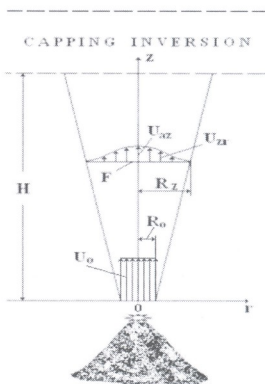


Fig. 4. A scheme of the ascending air jet between the meteotron and the bottom of the capping inversion.

In the case of mountain convection, almost every summer day, solar heating results in air updrafts that penetrate the capping inversion and contribute to forcing a convective cloud [14-15]. Acceleration of this natural cloud-forcing process by the meteotron also is obviously an easier task. A similar situation also occurs with the marine atmospheric boundary layer, where low location (800-1000 m) and relatively small thickness (200-400 m) of the capping inversions [16-17] especially eases the cloud-forcing.

Now let us look, at a first approximation, into the dependence of the development of an artificial air jet on the main parameters of the meteotron.

A scheme of the ascending air jet is presented in Fig. 4. We suppose that to overcome the capping inversion requires upward air jet with a certain specified maximum (axial) velocity (U_{alt}) at the bottom of the capping inversion. The total momentum (Q) and total kinetic energy (E) of the air mass in the jet can be equated to:

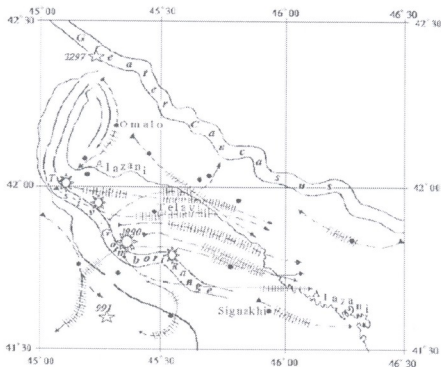


Fig. 5. The map of the Alazani Valley with natural centers forcing convective clouds (solid triangles), the most frequent hailstorm trajectories (dotted curves) and potential locations of the meteotrons (eight-pointed stars).

$$Q = \int_0^H \int_0^{R_2} \rho U_z 2\pi r dr dz \quad (1)$$

$$E = \int_0^H \int_0^{R_2} (\rho U_z^2 / 2) 2\pi r dr dz \quad (2)$$

$$U_{zs} = U_{ac} \left(1 - \frac{3r^2}{R_z^2} + \frac{2r^3}{R_z^3} \right) \quad (3)$$

$$U_{ac} = \frac{10.7U_0R_0}{z} \quad (4)$$

$$R_z = 0.22z \quad (5)$$

Here, ρ is the density of the air; H is the distance up to the capping inversion; U_z is vertical velocity of the air at the height z and the radius r ; R_z and F_z are outer radius and transverse section area of the jet at the height z , respectively.

Here, U_{ac} is vertical velocity at the axis of the jet at the height z ; U_0 and R_0 are vertical velocity and outer radius at $z=0$, respectively.

Since the jet velocity drops below 100 m/s at the height of 20 m above the meteotron [18], we neglect the momentum accumulated in this small initial section (the point $z=0$ is placed on the top of this section) and reduce the problem to propagation of the free isothermal isobaric circular jet of an incompressible fluid. Extra lift effect of heated air and the natural updrafts also are neglected. Compliance with the condition of $z/R_0 \gg 1$ along nearly the entire height allows to use the following versions of the relations [19]:

Solutions of the inner integrals from (1) and (2), respectively, are:

$$\int_0^{R_z} \rho U_{zs} \left(1 - \frac{3r^2}{R_z^2} + \frac{2r^3}{R_z^3} \right) 2\pi r dr = 0.3\pi R_z^2 \rho U_{ac} = \pi R_z^2 \rho U_{am} \quad (6)$$

$$\int_0^{R_z} (\rho U_{zs}^2 / 2) \left(1 - \frac{3r^2}{R_z^2} + \frac{2r^3}{R_z^3} \right)^2 2\pi r dr = 0.171\pi R_z^2 (\rho U_{ac}^2 / 2) = \pi R_z^2 (\rho U_{ak}^2 / 2) \quad (7)$$

Here averaged by momentum (U_{am}) and by kinetic energy (U_{ak}) cross-sectional mean velocities are equal to:

$$U_{am} = 0.3U_{ac} \quad (8)$$

$$U_{ak} = 0.414U_{ac} \quad (9)$$

It may be noted that the specific mean values (8) and (9) complement the other two mean values; they are listed in the fundamental reference book [20].

Next, we take the outer integrals and represent the final results relative to U_{aft} and H :

$$Q = \int_0^H 0.3\pi R_0^2 \rho U_{ac} dz = 0.244\rho U_0 R_0 H^2 = \\ = 0.0228\rho U_{aft} H^3 \quad (10)$$

$$E = \int_0^H 0.171\pi R_0^2 \left(\rho U_{ac}^2 / 2 \right) dz = 1.49\rho U_0^2 R_0^2 H = \\ = 0.013\rho U_{aft}^2 H^3 \quad (11)$$

Since the total momentum is roughly equal to the product of the thrust of the meteoron and its single run time, we can state a very strong dependence of the operating parameters of the meteoron on the distance H at the constant U_{aft} . Below we shall return to the issue of the validity of this conclusion when considering the implementation of a particular case of DARC.

5. Alazani Valley: potential area for application of DARC. The Alazani Valley is the heart of Georgian province Kakheti. The valley stretches about 200 km and a width of about 50 km. From the southwest it is adjacent to Tshiv-Gombori Range, from the north and north-east it is bordered by the Greater Caucasus Range. The region rather frequently is affected by hail (Fig. 5) [21].

According to [21] several mountains of Tshiv-Gombori Range are the main cloud-forcing centers providing the valley by imported convective clouds. Reproduced trajectories represent the most repetitive events. Some hailstorms have more diverse trajectories.

Pre-hailstorm situations in Alazani Valley are linked to high CAPE in lower atmosphere [21]. The role of capping inversion is particularly strongly reflected by vertical distribution of absolute humidity. It remains in the range $(7-11) \times 10^{-3}$ up to 2.5-3.0 km and decreases sharply at higher layers [21]. As for cloud-forcing, in full accordance with the above modern views, a significant role is played by the mountain upslope air flows linked to solar heating. Regional winds, cold and occluded fronts amplify the primary effects and import the arisen clouds into the valley.

In this context, the realization of DARC through the imported proactive forcing (IPF) can be proposed, reproducing in a modified form, the same natural import forced clouds.

IPF can be illustrated by the same Fig. 5. Compared to the natural base, the novelty is equipping of the same "active" mountains by the meteorons. Compared to the natural process the novelty is artificial proactive forcing of convective clouds that should repeat the natural phenomenon with one fundamental difference: it is always to be ahead and provide proactive cloud-forcing at CAPE still insufficient for severe storm.

Now let us compare the parameters of two cases of operation of the meteoron: in the Alazani Valley with a height of nearly 500 m above sea level and on the top of the mountain Tsivi with a height of nearly 2,000 m above sea level. The height of the bottom of the capping inversion can be equated to 3,500 m above sea level [21]. The required value of U_{aft} could be considered in both cases as identical.

As shown by simple calculations based on relationship (10), the required value of the product of the thrust of the meteoron and its single run time is about 15 times less during operation on the top of the mountain Tsivi ($H=1,000$ m) than in the Alazani Valley ($H=2,500$ m). It is also clear that, relative to the arid zone, such a factor of increasing the meteoron effect (FIME) will be much higher.

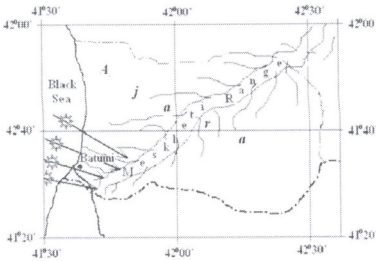


Fig. 6. Scheme of IPF aimed at reducing rainfall in Ajara with potential locations of the meteostrons (eight-pointed stars).

Now let us assess what changes this conclusion may undergo with further thorough analysis of the problem.

The first assumption made on the constancy of the required values of U_{alt} in both cases is equivalent to the assumption of the identity of the capping inversion over the mountain and the valley. Further, this assumption can be clarified only a bit toward the comparatively faster thinning the inversion over the mountain during day hours because of the natural upslope convection by solar heating. Obviously, such a clarification would increase the FIME.

The second assumption suggests the possibility of characterization of the meteostron effect only by dynamic component of the momentum, implying that the thermal component of the momentum (extra lift effect of heated air generated by the meteostron) is equally proportional to the dynamic component, both over the mountain and the valley. This assumption is quite logical and its refinement is unlikely to lead to a significant change in the FIME.

The third assumption suggests the possibility of characterization of the product of the thrust of the meteostron and its single run time only by the momentum gained below the section $z=H$. Addressing the role of the part of the total momentum gained above this section, of course, will lead to an increase of this

product. However, such an increase would likely be nearly proportional in both cases, over the mountain and the valley, with insignificant change in the FIME.

The most significant refinement of the analysis may be due to taking into account the momentum of the same natural updrafts because of the mountain natural upslope convection by solar heating (absent in the plain). Fortunately, such a clarification can only lead to a significant increase in the FIME.

Thus, we have every reason to believe that the main conclusion about the strong dependence of the main operating parameters of the meteostron on the distance up to capping inversion will remain in force after a thorough analysis of the problem as well.

6. The Problem of Excessive Rains in Ajara.

In principle, potential applications of DPF and IPF can be considered to prevent excessive rains in coastal and other areas or mitigate tornadoes.

The map of the Autonomous Republic of Ajara is presented in Fig. 6. The system Black Sea – Meskheti Range contributes to the concentration of moist air masses and intensive formation of convective clouds, turning Ajara into a region with the highest rainfall in Georgia and in the Caucasus. In this regard, reducing the intensity of rainfall would improve the benefits of the region as an important seaside resort and miti-



gate the negative environmental impact of excessive rains in mountainous Ajara.

IPF should provide proactive forcing of convective clouds over the sea at the distance ensuring the completion of the cloud life cycle (including precipitation) before reaching the shore. According to preliminary estimates, the meteotrons should operate from the positions located at a distance of 30-60 km offshore. As an alternative to the natural process, proactive forcing should result in intense rains over the sea, reducing, respectively, the "rainfall capacity" of the system sea-range.

Because of low location of the capping inversion in the marine environment (800-1000 m) [16-17], in terms of the distance H , this case turns similar to the cloud-forcing from the mountain Tsivi. At the same time, in the marine environment, capping inversion is much thinner [16-17], the overcoming of which requires much lower U_{atr} . Therefore, in the end we can expect that in this particular case the FIME relative to arid areas can reach two orders magnitude.

Consideration of the potential use of DARC to prevent the development of severe tornadoes is also of interest.

Interpretation of the final stages of tornado genesis, especially, the downdraft vertical vorticity, still encounters fundamental difficulties. Nevertheless, the initial stages are uniquely associated with a moist unstable lower atmosphere [22]. In this regard, DARC is equally applicable to any strong convective storm, including those that lead to hail or tornado.

At the same time, unfortunately, when the tornadoes are to be developed on vast plains, the use of the advantages the mountains and the marine environment is limited. Nevertheless the above conclusion remains in force the above conclusion about much more efficient operation of the meteotron in moist unstable atmosphere, compared to the arid zones.

7. Concluding Remarks.

The meteotron previously developed as a technical means to increase rainfall in arid areas can be much more effective through the prevention of the development of severe convective storm by proactive artificial discharge of instability energy in a moist unstable lower atmosphere (through realization of DARC).

Simplified analysis shows that the required trust of the meteotron and its single run time strongly depend on the distance up to the bottom of the capping inversion, the other things being same. This puts to the fore the implementation of the schemes of DARC by locating the meteotrons on the mountain tops and in the marine environment.

On this basis, the potential applications of IPF for preventing hailstorms in the Alazani Valley and excessive rains in Ajara are considered. The potential of DARC to prevent the development of severe tornadoes is also outlined.

The proposed schemes need further detailed theoretical studies, numerical modeling and field experiments.

გეოფიზიკა

მძლავრი კონვექციური შტორმის პრევენცია: ატმოსფეროს ქვედა ფენის წინმსწრები გადასტრატოფიცირება

ი. შეყრილაძე

საქართველოს ტექნიკური უნივერსიტეტი, პედროსიანენრო ლეპარტამენტი, თბილისი

(წარმოდგენილია აკადემიის წევრის თ. ჭელიძის მიერ)

არამდგრადი ატმოსფეროს წინმსწრები განაწილებული გადასტრატოფიცირების კონცეფცია მძლავრი კონვექციური შტორმის პრევენციის გზას სახავს. იგი ითვალისწინებს ატმოსფეროს ტენიანი არამდგრადი ქვედა ფენის არამდგრადობის ენერჯის ზეღონურ უზიფათო განმუხტვას დასაკაცე ზონაში წინმსწრებად ფორსირებული კონვექციური ღრუბლებით. ნაშრომში გამოკვეთილია კონცეფციის პირველადი სქემის (განაწილებული და წინმსწრები ფორსირება) რეალიზაციასთან დაკავშირებული პრობლემები. დადგენილია ე.წ. მეტეოტრონის ეფექტურობის ძლიერი დამოკიდებულება მანძილზე დამჭერი ინერსიის ქვედა ზღერამდე. აღაზნის კვლის დასეტყვასა და აჭარაში ჭარბ წვიმებთან მიმართებაში შემოთავაზებულია ახალი, იმპორტირებული წინმსწრები ფორსირების სქემა. გამოკვეთილია კონცეფციის გამოყენების პოტენციული მძლავრი ტორნადოს თუიდან აცილების მიზნით.

REFERENCES

1. I.I. Burtsev, A.I. Gaivoronsky, A.I. Kartsivadze (1974), WMO Weather Modification, N75-25408 16-47: 189-196.
2. G.K. Sulakvelidze, V.V. Tsykunov (1974), in: Weather and Climate Modification, Ed.: W.N. Hess, John Wiley and Sons, NY: 410-431.
3. E.I. Potapov, et al. (2007), Rus. Meteor. Hydrol., 32: 360-365.
4. T.W. Krauss, et al. (2009), Rus. Meteor. Hydrol., 34: 218-227.
5. G. Xueliang, Z. Guoguang (2009), Adv. Atm. Sci., 26: 240-252.
6. I.G. Shekrlidze (1992), Bull. Acad. Sci. Georgia, 146: 141-145 (in Russian).
7. D.L. Arnold (2008), Geogr. Comp., 2/1: 30-66.
8. W.R. Cotton, et al. (2011), Int. Geophysics, 99: 315-454.
9. K. Riemann-Campe, et al. (2009), Atm. Res., 93: 534-545.
10. H.E. Brooks, et al. (2003), Atm. Res., 67-68: 73-94.
11. R. Kaltenböck, et al. (2009), Atm. Res., 93: 381-396.
12. H. Dessens, J. Dessens (1965), J. Rech. Atm., 1: 158-162
13. N. I. Vul'fon, L. M. Levin (1987), Meteotron kak sredstvo vozdeistvii na atmosferu, M., 3-129 (in Russian).

14. C.B. Schaaf et al. (1988), Bull. Amer. Meteor. Soc., **62**: 272-277.
15. J.C. Demko et al. (2009), Mon. Weath. Rev., **137**: 447-468.
16. V. Manghani et al. (2000), Boundary-Layer Meteor., **97**: 411-430.
17. F.M. Ralph et al. (2000), Mon. Weath. Rev., **128**: 283-300.
18. M. Alamaro et al. (2006), J. Weath. Mod., **38**: 82-96.
19. V.A. Grigoriev, V.M. Zorin (1982), Teplo- i Massoobmen. Teplotekhnicheskii eksperiment, M.: 61 (in Russian).
20. I.E. Idelchik (1975), Spravochnik po Gidravlicheskim Soprotivleniiam, M.: 415 (in Russian).
21. V.M. Gigineishvili (1960), Gradobita v Vostochnoi Gruzii, M.: 9-122 (in Russian).
22. P.M. Markowski, Y.P. Richardson (2009), Atmos. Res., **93**: 3-10.

Received February, 2012

Geophysics

Numerical Study of the Vertical Hydrological Structure of the Black Sea under Transitive Climatic Forcing Conditions

Demuri Demetrashvili* and Diana Kvaratskhelia*

* *M. Nodia Institute of Geophysics of I. Javakishvili Tbilisi State University*

(Presented by Academy Member Tamaz Chelidze)

ABSTRACT. The paper presents the numerical investigation of the vertical structure of hydrological fields of the Black Sea for transitive (April) climatic conditions. With this purpose a 3-D baroclinic model of the Black Sea dynamics of M. Nodia Institute of Geophysics with consideration of simultaneous influence of the nonstationary atmospheric circulation and thermohaline action by both the Dirichlet and Neumann upper boundary conditions is used. The performed numerical experiment has promoted the primary role of thermohaline impact on the formation of the vertical structure of the Black Sea circulation within the upper 0-306 m layer for transitive climatic conditions. © 2012 Bull. Georg. Natl. Acad. Sci.

Key words: baroclinic circulation, numerical investigation, thermohaline fields.

Introduction. The changeability of the atmospheric processes developed above the Black Sea basin plays a significant role in the spatial-temporal changes of the hydro and thermo-dynamical parameters in the upper layer of the sea. On the other hand, the hydrophysical processes in the Black Sea directly reflect on the interaction processes between the Black Sea and atmosphere and play a significant role in the formation of the regional weather and climate.

The main goal of this paper is to investigate numerically the temporal variability of the vertical structure of circulation and thermohaline fields within the depth 0-306 m of the Black Sea for transitive seasonal conditions (April) in the inner-annual time scale. This

investigation is considered as specification of the special character of the sea circulation, which is formed under the forcing of the external perturbing factors: simultaneous influence of the nonstationarity atmospheric circulation and thermohaline action.

Description of the model. To achieve the specified goal, we used a 3-D baroclinic basin-scale z-level model (BSM) of the Black Sea dynamics [1]. It should be noted that on the basis of the high-resolution regional version [2] of this BSM, the regional forecasting system is developed for the Georgian Black Sea coastal zone with 1 km spacing, which is a part of the basin-scale Black Sea Nowcasting/Forecasting system [2, 3].

The BSM takes into account the quasi-realistic sea bottom relief, nonstationary atmospheric wind and thermohaline forcing, water exchange with the Mediterranean Sea and inflow of the Danube River, the absorption of short-wave radiation by the sea upper mixed layer, space-temporal variability of horizontal and vertical turbulent exchange. Atmospheric forcing is taken into account by boundary conditions on the sea surface considered as a rigid surface.

The model makes it possible to take into account wind-driven forcing with alternation of different climatic wind fields and the atmospheric thermohaline action by both the Dirichlet conditions through setting the temperature and salinity at the sea surface and the Neumann conditions through setting the heat fluxes, evaporation, and atmospheric precipitation.

The solution domain is covered with grid 225×111 having horizontal resolution 5 km. On a vertical the non-uniform grid with 32 calculated levels at depths: 2, 4, 6, 8, 12, 16, 26, 36, 56, 86, 136, 206, 306, ..., 2206 are considered. The time step is equal to 1 hour.

To solve this problem, we used the two-cycle method of splitting the main problem with respect to both physical processes and coordinate planes and lines [4].

Results of the numerical experiment. In the numerical experiment on simulation of transitive hydrological mode of the Black Sea the integration started on the 1st of January. The annual mean climatic fields of current, temperature, and salinity obtained by the same model were used as initial conditions [1]. Wind forcing variability was expressed as the alternation of different types of climatic wind field characterized over the Black Sea basin [5]. Atmospheric wind types differed from each other by direction, module, recurrence and duration. The duration of action of each atmospheric wind type was between 10–60 hours. When one wind type changed to another, a state to close to calm, with a wind speed of 1 m/s and wind direction corresponding to the arithmetic mean between the two consecutive wind directions, took place between these wind types.

The researches presented in this section are a continuation of the previous studies [6, 7], where the vertical hydrological structure of the Black Sea investigated for January atmospheric climatological forcing with 10 and 5 km resolutions, respectively. In [6] it was shown that the entire depth of the sea basin may be considered as consisting of some relatively homogeneous sub-layers. Within each of the sub-layers general circulation processes practically do not change qualitatively by depth, but essentially change from layer to layer. According to one of the results obtained in [7], atmospheric wind driven forcing plays an important role in the formation of the vertical structure of Black Sea circulation for winter season under both Dirichlet and Neumann upper boundary conditions for temperature and salinity.

In the present paper investigations are carried out for April climatic conditions with 5 km resolution. Besides, both the Dirichlet and Neuman boundary conditions are used to describe atmospheric thermohaline forcing. 5 km horizontal resolvability of the model has allowed us to specify the depth and location of the homogeneous sub-layers and explore their strong variability in a transitive season according to the simultaneous influence of atmospheric circulation and thermohaline impact.

In order to illustrate the vertical changeability and transformation of the Black Sea circulation during the transitive period, we chose the time interval 2684–2836 hours (April, time is accounted from the 1st January), when the atmospheric circulation was reorganized as shown in Table 1.

The same table gives the calculated locations of the homogeneous sub-layers, which are formed within the upper 0–306 m layer of the Black Sea, using both Neumann and Dirichlet conditions describing atmospheric thermohaline forcing.

The results of the numerical experiment show that when the state of the atmosphere is close to calm conditions, the character of sea circulation practically does not change by depth within 0–106 m with the use of both Neumann and Dirichlet bound-

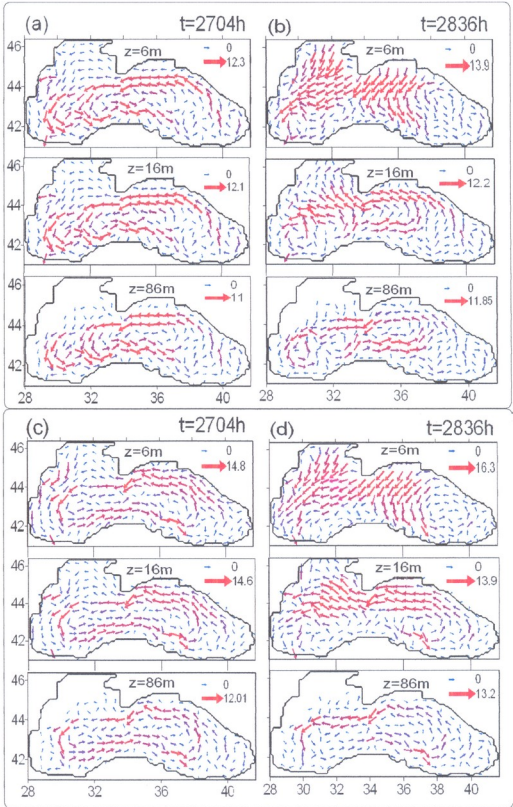


Fig. 1. Calculated current fields (cm/s) at time: $t=2704h$ and $t=2836h$ (April). Fig. 1a and 1b correspond to Neumann conditions, Fig. 1c and 1d correspond to Dirichlet conditions.

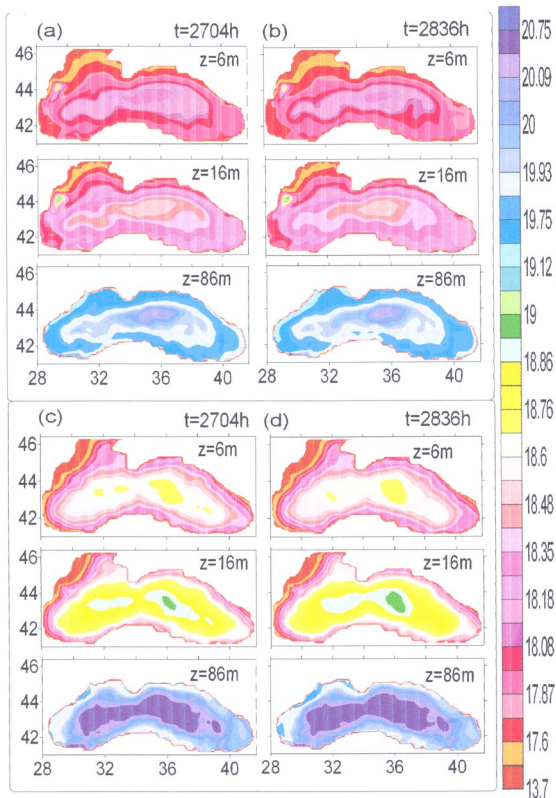


Fig. 2. Calculated salinity fields (%) at the time $t=2704h$ and $t=2836h$ (April). Fig. 2a and 2b correspond to Neumann conditions, Fig. 2c and 2d correspond to Dirichlet conditions.

Table 1. Alternation of wind types during time interval $t = 2704-2836$ hours (April) and sub-layers' location between the depth 0 – 306m.

Wind direction	Wind speed, m/s	Time interval, h	Sub-layers depth with both case Neuman and Dirichlet condition
Northwestern - north	1	2684-2704h	2-136m, 136-306m in any case
North-eastern	0-5	2704-2748h	Neum. : 2-136m, 136-306m; Dir.: 2-36, 56-136m, 136-306m.
North-western	1	2748-2772h	2-136m, 136-306m in any case.
Cyclonic	5-10	2772-2796h	Neum.: 2-12, 16- transitive layer , 16-136, 136-306m; Dir.: 2-8, 12 transition layer ,16-136m, 136-306m.
North -western	1	2796-2820h	2-136m, 136-306m in any case.
North- western	5-10	2820-2836h	Neum. : 2-12, 16-transition layer, 16-136 m, 136-306m. Dir. 2-8m; 12-16m, 26-136m, 136-306m.

ary conditions. This fact is clearly observed at $t = 2704$ h (Fig 1a and 1c) when Northwestern-north wind with speed 1 m/s was operated. The results show also that the circulating patterns received with use of two kinds of boundary conditions qualitatively differ from each other, despite their common feature - homogeneous character of vertical circulation for atmospheric calm conditions. There is a good correlation between circulation (Fig. 1a and 1c) and salinity fields (Fig. 2a and 2c), under both Neumann and Dirichlet conditions.

The observed climatic data show that generally atmospheric winds with 5-10 m/s dominate over the Black Sea during April [5]. In this case two sub-layers are formed within 0-136 m with the use of Neumann conditions and three sub-layers with the use of Dirichlet conditions (see Table 1.). This fact is illustrated in Fig. 1b and 1d, where calculated current fields are shown at $t = 2836$ h, when the north-western wind with 5-10 m/s operated. The circulation patterns presented in this Figure characterize well the peculiarities of the mentioned sub-layers. In addition, the location of sub-layers practically insignifi-

cantly depends on the method of consideration of the atmospheric thermohaline forcing, i.e. on what kind of boundary conditions are used – the Dirichlet or Neumann conditions. The uppermost sea layer with depth about 12 km is more sensitive to wind driven forcing in any case of thermohaline action and is determined by the wind type. In deeper layers below 16 m the influence of atmospheric wind forcing weakens and the structure of circulation (Fig. 1b and 1d) gradually becomes similar to that which was observed in the case of calm atmospheric conditions (see Fig.1a and 1c). This fact shows the primary role of thermohaline forcing in lower layers (see Fig. 2b and 2d respectively). Besides, in any case the level $z = 136$ m is a transition level and so it carries features of both sub-layers: 1-136 m and 136-306 m.

Conclusion. The numerical experiment carried out with consideration of alternation of atmospheric wind driven forcing and thermohaline action using both the Dirichlet and Neumann conditions has demonstrated the primary role of the thermohaline impact on the Black Sea vertical circulation within the upper 0 - 306 m sea layer for April climatic conditions.

გეოფიზიკა

შავი ზღვის ჰიდროლოგიური ვერტიკალური სტრუქტურის რიცხვითი გამოკვლევა გარდამავალი ატმოსფერული კლიმატური ზემოქმედების პირობებში

დ. დემეტრაშვილი, დ. კვარაცხელია

ი. ჯავახიშვილის სახ. თბილისის სახელმწიფო უნივერსიტეტის შ. ნოდიას გეოფიზიკის ინსტიტუტი
 (წარმოდგენილია აკადემიის წევრის თ. ჭელიძის შივრ)

სტატია ეძღვნება შავი ზღვის ჰიდროლოგიური ვერტიკალური სტრუქტურის რიცხვით გამოკვლევას გარდამავალი სეზონის (აპრილი) კლიმატური პირობებისათვის შ. ნოდიას გეოფიზიკის ინსტიტუტის შავი ზღვის დინამიკის ბაროკლინური მოდელის საფუძველზე. ატმოსფეროს თერმოპალინური ზემოქმედება გათვალისწინებულია როგორც დირიხლეს, ასევე ნეიმანის სასაზღვრო პირობებით. რიცხვითმა ექსპერიმენტმა აჩვენა თერმოპალინური ზემოქმედების პირველადი როლი შავი ზღვის ცირკულაციის ვერტიკალური სტრუქტურის ფორმირებაში აპრილის კლიმატური პირობებისათვის.

REFERENCES

1. A.A. Kordadze, D.I. Demetrashvili and A.A. Surmava (2008), Izv. RAN, Fizika Atmosfery i Okeana, **44**, 2: 227-238 (in Russian).
2. A.A. Kordadze, D.I. Demetrashvili (2011), Ocean Science, 7: 793-803.
3. G.K. Korotaev, T. Oguz, V. L. Dorofeyev, et al. (2011), Ocean Science, 7: 629-649.
4. G.I. Marchuk (1974), Chislennyye Metody Resheniya Zadach Dinamiki Atmosfery i Okeana, 303 p. (in Russian).
5. A. Kordadze, K. Tavartkiladze, and D. Kvaratskhelia (2000), J. Georgian Geophys. Soc., 5b: 28-37.
6. D.I. Demetrashvili, D.U. Kvaratskhelia and A.I. Gvlesiani (2008), Adv. Geosci., 14: 295-299.
7. D.I. Demetrashvili, D.U. Kvaratskhelia, V.G. Kukhalashvili (2011), J. Georgian Geophysical Soc., **14b**: 75-84.

Received March, 2012

Physical Chemistry

Dynamical Mechanical Properties of Boron-Doped Monocrystalline Germanium

George Chubinidze*, Ia Kurashvili*, Guram Bokuchava*,
Zurab Chachkhiani**, George Darsavelidze*

* I. Vekua Sokhumi Institute of Physics and Technology, Tbilisi

** Department of Physics, Georgian Technical University, Tbilisi

(Presented by Academy Member Givi Tsintsadze)

ABSTRACT. Microstructure, electrophysical properties and characteristics of dynamical shear modulus and microplastic deformation of boron-doped monocrystalline germanium were investigated. Bulk crystals of germanium were obtained by Czochralski method in [111] crystallographic direction. Boron concentration in monocrystals was changed in the $5 \cdot 10^{16}$ - $5 \cdot 10^{19}$ cm⁻³ interval. Dislocation density determined by estimation of the quantity of etching pits was changed from 10^3 to $5 \cdot 10^4$ cm⁻². It has been established that an increase of boron concentration in monocrystalline germanium causes a decrease of current carriers mobility and an increase of the absolute value of shear modulus in comparison with undoped specimens. After high temperature annealing tendency to increasing of current carrier mobility, dynamical shear modulus and elastic limit was revealed.

By investigations of internal friction and dynamical shear modulus amplitude dependences of boron-doped monocrystalline germanium the following results were received. The values of elastic limit, dynamical shear modulus and critical strain amplitude of Ge:B monocrystals were determined. It has been established that weakly boron-doped monocrystalline germanium is characterized by high elastic limit, critical strain amplitude and shear modulus. This is due to structure strengthening, caused by an increase of dislocation blocking by boron atoms. In the case of high concentration of boron simultaneously with the strengthening process, "softening" process has taken place. It is determined by fulfillment of broken electron bonds near to dislocation cores that has caused decrease of activation energy of dislocation motion. On the basis of changes of interaction nature of dislocations and boron atoms mechanisms of strengthening and softening processes of structure under the influence of boron were analyzed. © 2012 Bull. Georg. Natl. Acad. Sci.

Key words: germanium, internal friction, dynamical shear modulus.

The working resource and stability of characteristics of devices based on monocrystalline germanium alloys have been determined by dislocations existing in the structure. Despite this, the crystallographic and

energetic characteristics of defects, characterizing monocrystalline Ge alloys, their influence on structural-sensitive semiconducting and physical-mechanical properties have not been complexly studied.

Table. Characteristics of structure and properties of Ge:B monocrystals

Specimens	Current carriers concentration, cm^{-3} [111]	Current carriers mobility, $\text{cm}^2 \text{v}^{-1} \text{sec}^{-1}$, [111]	Shear modulus, kg/mm^2		Relative strain amplitude		Elasticity limit, kg/mm^2	
			[111]	[100]	[111]	[100]	[111]	[100]
Ge	$5 \cdot 10^{15}$	1850	3800	3600	$4 \cdot 10^{-5}$	$7 \cdot 10^{-4}$	0.15	2.66
Ge:B	$1 \cdot 10^{16}$	1600	4150	3950	$1 \cdot 10^{-4}$	$3.5 \cdot 10^{-5}$	0.41	14.5
	$5 \cdot 10^{17}$	1250	4100	3850	$8 \cdot 10^{-5}$	$2 \cdot 10^{-3}$	0.33	8.2
	$8 \cdot 10^{19}$	950	3900	3700	$7 \cdot 10^{-5}$	$1 \cdot 10^{-3}$	0.27	3.9

Investigation results of characteristics of microstructure, electrophysical properties, dynamical shear modulus and microplastic deformation of boron-doped germanium are presented in the present paper.

Bulk crystals of germanium were obtained by Czochralski method in [111] crystallographic direction. Boron concentration in monocrystals was changed in the $5 \cdot 10^{16}$ - $5 \cdot 10^{19} \text{cm}^{-3}$ range. Dislocation density on the (111) planes was determined by estimation of the quantity of etching pits. Electrophysical characteristics were determined by Hall effect in constant magnetic field.

Amplitude dependence of dynamical shear modulus was investigated by the method of torsion oscillations frequency registration. The absolute value of shear modulus was calculated by comparing the standard and test specimens [1]:

$$G = G_0 \frac{f^2}{f_0^2},$$

where G_0, f_0 are the values of shear modulus and oscillation frequency of the standard specimen (vanadium), G, f - the values of shear modulus and oscillation frequency of test crystals. The values of elastic limit were calculated from the equation: $\varepsilon = G \varepsilon_c$, where G is a value of shear modulus, ε_c - critical strain amplitude, at which distinct revealing of inelastic properties begins.

Ge:B monocrystalline specimens of [111] and [100] crystallographic orientation were studied. Crystallographic orientations were established by X-ray diffractometer DRON-3.

Characteristics of electrophysical and dynamical mechanical properties and dislocation density of

boron doped monocrystalline germanium are presented in Table.

From a comparative analysis it is shown that the absolute value of the shear modulus increased significantly with low concentration of boron. Monocrystalline germanium with high concentration of boron is characterized by a decrease of the shear modulus, though its value is high in comparison with undoped specimens.

Annealing at 600°C temperature in vacuum for 5hrs causes decrease of current carriers' concentration of the specimens, accordingly their mobility increases. Sharp increase of the shear modulus was revealed in heavily boron-doped monocrystalline germanium. Subsequent annealing at 800°C temperature causes a small increase of current carriers' concentration of the specimens. Increase of their shear modulus is insignificant.

Two regimes of thermal treatment practically do not affect the dislocation density and its distribution in the structure. It is known [2] that thermal treatment can cause significant changes in Cottrell atmospheres, formed by impurity atoms in the proximity of dislocations. At medium temperatures ($\sim 600^\circ\text{C}$) an increase of concentration of impurities and their complexes in Cottrell atmosphere is possible. Accordingly, blocking of dislocations will be increased. This circumstance causes an increase of the absolute values of structural-sensitive shear modulus. Annealing at higher temperatures (800°C) causes decomposition of complexes of germanium atoms and technological impurities ($\text{O}_2, \text{N}_2, \text{C}$), distribution of impurity atoms in crystal volume and decrease of their concentration in Cottrell atmospheres. In these condi-

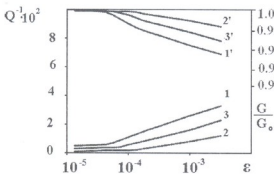


Fig. 1. Internal friction (1, 2, 3) and shear modulus (1', 2', 3') amplitude dependence of boron doped monocrystalline germanium. (1, 2, 3), $T=20\text{ }^{\circ}\text{C}$. 1, 1' - Ge: $[111]$; 2, 2' - Ge:B ($1 \cdot 10^{16}\text{ cm}^{-3}$), $[111]$; 3, 3' - Ge:B ($8 \cdot 10^{16}\text{ cm}^{-3}$), $[111]$

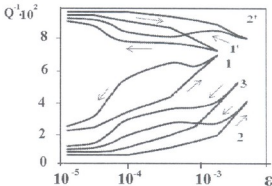


Fig. 2. (Q^{-1}) (1,2,3) and (G/G_0) (1', 2') of the monocrystalline Ge:B specimens at $550\text{ }^{\circ}\text{C}$ temperature. 1, 1' - Ge, $[111]$; 2, 2' - Ge:B ($1 \cdot 10^{16}\text{ cm}^{-3}$), $[111]$; 3 - Ge:B ($8 \cdot 10^{16}\text{ cm}^{-3}$), $[111]$.

tions a sharp increase of shear modulus is not expected. It is significant that the nature of thermal treatment effect is similar for the specimens of both $[111]$ and $[100]$ crystallographic orientations.

Internal friction (Q^{-1}) and relative shear modulus (G/G_0) amplitude dependences of boron doped monocrystalline germanium were studied at room temperature, in strain amplitude interval of $1 \cdot 10^{-5}$ - $5 \cdot 10^{-3}$ (Fig. 1).

Experimental specimens are characterized by critical strain amplitude, at which internal friction intensity begins to increase (Fig.1: 2, 2') show that weakly doping with boron significantly increases the critical values of strain amplitude. In the case of high concentration of boron, the critical strain amplitude decreases, but it remains much higher in comparison with undoped monocrystalline germanium.

The values of elastic limit were determined with the values of critical strain amplitude and shear modulus. The obtained results are presented in Table. It is experimentally established that weakly boron doped monocrystalline germanium is characterized by high values of elastic limit. In comparison with them, the values of elastic limit of undoped and heavily boron doped germanium are much lower.

Internal friction and dynamical shear modulus amplitude dependences of Ge:B monocrystals are presented in the Fig.2. Measurements were conducted at $550\text{ }^{\circ}\text{C}$ temperature, at which development

of plastic deformation in germanium is possible.

Internal friction and shear modulus amplitude dependences at $550\text{ }^{\circ}\text{C}$ temperature have a multistage character. Internal friction spectrum of the specimen with $[111]$ crystallographic orientation has three separate ranges. In the first range ($5 \cdot 10^{-6}$ - $7 \cdot 10^{-5}$) internal friction intensity is low and it increases weakly in proportion to the oscillation amplitude. Significant linear increase of internal friction intensity begins at the first critical amplitude up to the second critical amplitude. Internal friction intensity increases with the subsequent increase of amplitude (Fig. 2: 1).

The first critical amplitude corresponds to the critical strain at which breakaway of dislocation segments from the pinning points (vacancy, impurity atoms and complexes) begins. It is known [3] that up to the first critical deformation only bending of dislocation segments takes place. Irreversible increase of internal friction is observed from the second critical amplitude. Anomalous high intensity wide maximum of internal friction is revealed on the return curve.

According to the theory [3], at the second critical amplitude dislocation breakaway begins from the strong pinning centers and their motion. Generation of new dislocations is also possible. After the end of vibrations dislocation segments do not return to the initial state. This means that microplastic deformation takes place, with generation of new dislocations

and breakaway of existing dislocation segments from strong pinning points.

Analogously to undoped specimen, in the internal friction amplitude spectrum of weakly boron doped germanium two values of critical amplitude were revealed (Fig.2: 2). Both of them are increased in comparison with undoped specimens. Internal friction wide maximum was revealed on the return curve registered from the second critical amplitude, which is connected to hysteretic type oscillation energy scattering processes. On the curve of $Q^{-1}(\epsilon)$, open loop of hysteretic type is revealed, confirming development of microplastic deformation.

The $Q^{-1}(\epsilon)$ dependence of heavily boron doped germanium is characterized by two critical strain amplitudes. Their values are higher in comparison with undoped germanium, and much lower in comparison with characteristics of weakly boron doped specimens. Changes of the complex character of shear modulus of all specimens take place in a wide range of oscillation amplitude. Two critical points are revealed on the curve of the shear modulus amplitude dependence (Fig.2: 1', 2'). Microplastic deformation

is sharply revealed in the interval of high strain amplitude, in the form of an open loop.

On the basis of the results presented in Fig 2, the values of elasticity limit have been determined. It has been established that weakly boron doped monocrystalline germanium is characterized by high elastic limit, critical strain amplitude and shear modulus. This is due to structure strengthening, being caused by an increase of dislocation blocking by boron atoms.

In the case of high concentration of boron simultaneously with the strengthening process, "softening" process takes place. It is determined by fulfillment of broken electron bonds near to dislocations cores that causes decrease of activation energy of dislocations motion. All this is reflected in the decrease of mechanical characteristics of boron heavily-doped germanium.

Thus, control of changes of electrophysical and mechanical characteristics of the dislocation structure of monocrystalline germanium by boron-doping is possible. This circumstance is significant for the solution of various problems of materials based on germanium.

ფიზიკური ქიმია

ბორით ლეგირებული მონოკრისტალური გერმანიუმის დინამიკური მექანიკური თვისებები

გ. ჩუბინიძე^ა, ი. ყურაშვილი^ბ, გ. ბოკუჩავა^ა, ზ. ჩაჩხიანი^ბ,
 გ. დარსაყელიძე^ა

^ა სოხუმის ი. ვეკუას ფიზიკა-ტექნიკის ინსტიტუტი, თბილისი

^ბ საქართველოს ტექნიკური უნივერსიტეტი, ფიზიკის დეპარტამენტი, თბილისი

(წარმოდგენილია აკადემიკოს გ. ცინცაძის მიერ)

ნაშრომში გამოკვლეულია ბორით ლეგირებული მონოკრისტალური გერმანიუმის მიკროსტრუქტურა, ელექტროფიზიკური თვისებები, დინამიკური ძერის მოდულია და მიკროპლასტიკური

დეფორმაციის მახასიათებლები. გერმანიუმის მასიური კრისტალები გაზრდილია ჩოხრალსკის მეთოდით [111] კრისტალოგრაფიული მიმართულებით. მონოკრისტალებში ბორის კონცენტრაცია იცვლება $5 \cdot 10^{16}$ - $5 \cdot 10^{19}$ სმ⁻³ ინტერვალში. მოწამვლის ორმოცობის რაოდენობის შეფასებით განსაზღვრული დისლოკაციების სიმკვრივე იცვლება 10^3 -დან $5 \cdot 10^4$ სმ⁻²-მდე. დადგენილია, რომ ბორის კონცენტრაციის გაზრდით მცირდება დენის მატარებელი ხერხების ძვარადობა და იზრდება დინამიკური ძვარის მოდულის აბსოლუტური მნიშვნელობა არალეგირებულ მონოკრისტალურ გერმანიუმთან შედარებით. მაღალტემპერატურული მოწვის შემდეგ ვლინდება დენის მატარებლების ძვარადობის, დინამიკური ძვარის მოდულისა და დრეკადობის ზღვრის ზრდის ტენდენცია.

ბორით ლეგირებული მონოკრისტალური გერმანიუმის შინაგანი ხახუნისა და ძვარის მოდულის ამპლიტუდური დამოკიდებულების შესწავლით მიიღება შემდეგი შედეგები: განსაზღვრულია სხვადასხვა შედგენილობის Ge:B მონოკრისტალების კრიტიკული ამპლიტუდური დეფორმაციის, დინამიკური ძვარის მოდულისა და დრეკადობის ზღვრის მნიშვნელობები. დადგენილია, რომ ბორით სუსტად ლეგირებული მონოკრისტალური გერმანიუმი ხასიათდება ძვარის მოდულის, კრიტიკული ამპლიტუდური დეფორმაციისა და დრეკადობის ზღვრის მაღალი მნიშვნელობებით. ეს გარემოება განპირობებულია გერმანიუმის სტრუქტურის განმტკიცებით, რასაც იწვევს ბორის ატომებით დისლოკაციების ბლოკირების გაძლიერება. ბორის მაღალი კონცენტრაციების შემთხვევაში განმტკიცების პროცესთან ერთად მიმდინარეობს “დარბილების” პროცესი. ეს უკანასკნელი გამოწვეულია ელექტრონული გაწვევითი კავშირების შვესებით დისლოკაციების ბირთვების მახლოვლობაში, რაც თავის მხრე განაპირობებს დისლოკაციების მოძრაობის აქტუაციის ენერჯის შემცირებას. დისლოკაციებისა და ბორის ატომების ურთიერთქმედების ბუნების ცვლილების გათვალისწინებით გაანალიზებულია ბორის გაელენით სტრუქტურის განმტკიცებისა და “დარბილების” მექანიზმები.

REFERENCES

1. M.A. Krishtal, S.A. Golovin (1978), Internal Friction and Structure of Metals. M., 380p. (in Russian).
2. S. Gan, L. Li, and R.F. Hieks (1998), Appl. Phys. Lett., 73, 8:1068-1070.
3. A. Pushkar (2005), Internal Friction in Metals and Alloys. London, 640p.

Received March, 2012

Chemical Technology

Study of the Process of Obtaining Metal Chlorides from Materials Containing Tungsten

Zurab Mirijanashvili*, Giorgi Tavadze**, Vazha Gharibashvili*,
Alexandre Kandelaki*

* Ferdinand Tavadze Institute of Metallurgy and Materials Science, Tbilisi

** Academy Member; Ferdinand Tavadze Institute of Metallurgy and Materials Science, Tbilisi

ABSTRACT. Technological parameters of simultaneous production of pure tungsten hexachloride (WCl₆) and a complex salt (NiFeCl₄) have been established by the study of the basic kinetic characteristics of the chlorination process of tungsten-containing waste. The process of chlorination is possible in an autothermal mode. © 2012 Bull. Georg. Natl. Acad. Sci.

Key words: waste, chlorination, tungsten chloride, complex salt.

The capacities of the well-known methods of processing of the residue containing tungsten are limited. Particularly, the schemes of processing of oxide raw materials involve significant waste of scarce reagents and repetitive cycles: annealing, alkali treatment, sedimentation, evaporation, neutralization, filtering etc. Residues, containing tungsten and other elements, can be processed like metals via the following methods: oxidization of tungsten carbide by sodium hypochlorite solution; dissolving metals by mineral acids; thermal annealing and processing of the successive solution in an autoclave chamber [1-4].

The above-mentioned methods turned out to be inappropriate for application in manufacturing, which can be explained by: complexity of their control; low speed of interaction of solid residue reagents; technology staging; implication of the massive complex non-standard equipment, etc.

The residues containing tungsten and waste materials (unfit anti-tank missile cores, metal junk of hard alloys and worn screw-cutting metal tools) that have simple chemical composition should be taken into special consideration. Besides the basic metal – tungsten, they contain cobalt, nickel and iron.

High reactivity of chlorine makes it possible to transform efficiently the metals, enclosed in the raw material, into chlorides. Chlorination products – metal chlorides appear to be transitional products for manufacturing of a wide range of pure metals and alloys [5-6].

The most essential for obtaining metals in the form of chlorides from anti-tank missile-cores and ensuring the optimal technological parameters is the study of the basic kinetic characteristics of chlorination processes.

One of the stages of the technological process of chlorination of piercing anti-tank missile cores is their

crushing/disintegration. This is accomplished via their detonation inside the metal cylindrical ampoule/cartridges with explosive material. Initiating the explosive material by the detonator causes propagation of the detonation waves that are later transformed into the shock wave. In the process of its propagation through the armor material the latter is broken into particles of different fractions. Larger one (>5 mm) is subject to further exploding.

Thermographic studies revealed the characteristics of thermal effects of chlorination of various metals in missile cores, the differential curves for their temperatures being provided in Fig. 1. In all cases the chlorination reactions were of exothermal character hence they might be accomplished in the auto-thermal regime.

Nothing is observed below 350°C on the temperature differential curve (curve d) of the thermogram of missile-core chlorination. Though in the case of chlorination of iron, contained in the alloy, its chlorination effect should have been observed at 185°C (curve c).

Chlorination process of missile cores is characterized by much stronger exothermal features than chlorination of each metal element contained in it. The temperature is self-rising up to 680°C in the reaction zone, due to the great heat release. Endo-thermal effects are also detected at the temperature of about 350-680°C, namely, the evaporation of formed WCl_6 and $FeCl_3$ ($t_{b,WCl_6}=348^\circ C$; $t_{b,FeCl_3}=320^\circ C$), therefore the chlorination effect of missile cores is a combined phenomenon, where the exothermic effect prevails over endothermic ones and so the exothermic effect is reflected on the thermogram below 350°C.

Chlorination products include the smelt of nickel and iron chlorination, condensed tungsten hexachlorides and non-chlorinated mass of the furnace-charge.

The study of disintegrated missile-core chlorination processes was performed in horizontal, as well as in vertical non-standard quartz chlorinators. The equipment consisted of the following units: horizon-

tal and vertical quartz chlorinator; chlorine distillation system, furnace, tungsten hexachloride condenser and waste gaseous chlorine neutralizer.

The reason for the chlorination of the furnace burden in different chlorinators, was to identify the possibility of separation and production of simultaneously formed flux and evaporable chlorides. The results of the experiment lead to the design of a new universal hermetic chlorinator framework.

Prior to the experiment the chlorinator was "washed" with argon and a specific fraction of chlorination material was loaded in it. Upon reaching a fixed temperature, gaseous chlorine (argon), purified from presumed humidity, was put into the chlorination unit. Chlorine supply measure was controlled via a rheometer and was regulated via a special reduction regulator.

During the chlorination process the mixture of volatile chlorides and superfluous chlorine was directed to the condenser, where the temperature was regulated by either the temperature of vapor-gas mixture or using a heating spiral coiled around it. Temperature in the condenser should not exceed the tungsten chloride boiling temperature. The superfluous gas chloride was sparged/flushed in 30% NaOH solution, where it was fully neutralized.

Shortly after achieving a fixed temperature and at a certain interval after the experiment the chlorinated mass was cooled in chlorine atmosphere. Then, in order to eliminate soluble chlorides, the chlorinated material was washed with warm water, filtered, the sediment was dried up in the vacuum drier stove and weighed. The chlorination degree of burden/charge was determined according to the weight loss.

In order to determine the optimal fraction for the chlorination of disintegrated missile cores, experiments were made over the following fractions: <2.0-3.0 mm; 3.5-5.0 mm; 5.5-8.0 mm. Chlorination process of the furnace-charge loaded into the chlorinator was performed for 30 minutes at 800°C. The pace of chloride delivery was constant and it did not exceed 0.20 l per min.

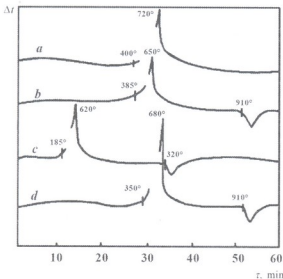


Fig. 1. Differential curves of material chlorination.
 a) W-Cl₂; b) Ni-Cl₂; c) Fe-Cl₂; d) W-Ni-Fe-Cl₂.

Under the above-mentioned conditions the chlorination level of missile core fractions below 2-5 mm were found to change insignificantly, reaching 52-55%. Further increase of fraction from 5.5 to 8.0 mm caused a decrease of the furnace-charge chlorination level to 42 – 47 %. Two controversial factors acted in this case – increase of gas propagation degree of furnace-charge and decrease of the surface area. In the case of 2-5 mm fraction, the former factor is dominant, which explains the increase of chlorination levels. Increasing the fraction to 8 mm, reduction of the surface area of furnace-charge becomes a limiting factor, which leads to the reduction of the speed and the quality of the chlorination process.

In the case of reduction of the supply pace of gaseous chloride, secondary reactions take place, producing FeCl₂, WCl₄ or WCl₅. These hardly evaporable chlorides enclose the surface of burden, impede penetration of chlorine and ultimately hamper the chlorination process.

Probing of the optimal rate for chlorine supply (0.1; 0.20; 0.25; 0.30 and 0.40 L/min) was accomplished via chlorination of the furnace-burden at temperature of 800°C for 30 minutes. Increase of the chlorine supply rate from 0.15 to 0.40 L/min significantly raises the degree of the furnace-burden chlorination. The

optimal rate for chlorine supply can be regarded as 0.25 L/min. In this case the existence of less volatile iron and tungsten chlorides is not detected in the chlorinated products.

Through the study of the influence of chlorine concentration changes (100%Cl₂; 75%Cl₂ – 25%Ar; 50%Cl₂-50%Ar) on the chlorination degree of crude in a mixture of chlorine-argon gases, it was detected that while delivering the chlorine concentration of 75% in the gas mixture, the degree of chlorination does not differ notably from supplying of chlorine of 100% (Fig. 2). Further reduction of the chlorine concentration causes the decrease of chlorination degree of crude.

In order to determine the optimal temperature and time for the chlorination process, experiments were held at the temperatures of 700°C, 750°C and 800°C with duration of 30, 60, 90, 120 and 189 minutes (Fig. 3). At all the aforesaid temperatures the chlorination process proceeds efficiently and completely, but to different extents. At the temperature of 700°C the chlorination level of missile cores reaches its maximum efficiency (98-99%) within 180 minutes; at 750°C - in 120 minutes and at 800°C - in 90 minutes.

Designing major units for a chlorinator construction, we took into account the peculiarities of the chlorination process, related to chlorination of materials containing tungsten. In particular, it was detected that while chlorinating the disintegrated material at 700-800°C in the horizontal type chlorinator, less volatile chlorides (NiCl₂, FeCl₂) are created, which surround non-chlorinated surface and prevent further penetration of chlorides into the material. This phenomenon might be avoided either by implementing the chlorination process of the furnace-charge via sparging (flushing) of gaseous chlorine in the fused salt mix (e.g. in eutectic smelt of NaCl-KCl, the melting temperature of which does not exceed 425°C), or via permanently extracting fused salt mix (NiCl₂, FeCl₂) from the reaction zone.

The chlorination process of the furnace-burden in a vertical chlorinator is implemented quickly and

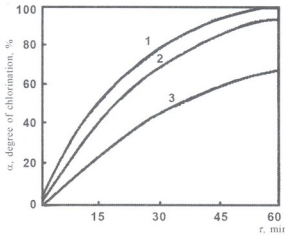


Fig. 2. Influence of chlorine concentration changes on chlorination degree of core. 1) 100%Cl₂; 2) 75%Cl₂ - 25%Ar; 3) 50%Cl₂-50%Ar. α - degree of chlorination, %.

efficiently. The mix of molten salts detaches from the surface of the recuperating furnace-burden and the gaseous chlorine is permanently in contact with the surface of the burden.

In the former case the contact of chlorine with a chlorinating material is enhanced, though a mix of buffer salts (NaCl-KCl) is added to one of the chlorination products (NiFeCl₄). This salt-mix is not an impediment in the case of metal thermal recuperation as it can be eliminated via distillation or hydrometallurgical re-processing of by-products; but it is unacceptable in the case of a hydrogen-thermal process, as it is virtually impossible to separate it from the ultimate product.

In the latter case it is necessary to design such a construction of the chlorinator hearth that provides continuous outflow of molten salts from the reaction zone, with proper vacuum-tightness.

We consider that the most optimal case is integration of both above-mentioned options – accomplishing the chlorination process in the molten salt mix - NiCl₂-FeCl₂ (T_{mb} = 672°C) or NiCl₂-CoCl₂ (T_{mb} = 680°C), which contains salts (“primary salt solution”) of metals - ingredients of substance for chlorination. The produced excessive mix of molten salts should be permanently removed from the reaction zone. Tungsten hexachloride, produced in the system of mixed salts of this kind, does not react with molten

salts, easily escapes the reaction zone and the evaporated tungsten hexachloride transfers towards the condensers as a chlorine-gaseous flow.

It is acknowledged that even a small amount of impurities significantly degenerates metal tungsten properties. For example, 0.01% of iron alloy in tungsten powder causes its fragility. So, spectrally pure tungsten hexachloride must be used in order to produce tungsten powder.

Alkaline soil salt chlorides are utilized for purification of tungsten hexachlorides from the admixtures. They produce easily fusible and less volatile chemical combinations with iron chlorides, as MeFeCl₄. At the same time tungsten hexachloride does not interact with alkali soil salt chlorides.

A diagram of the unit in which tungsten hexachloride was purified from iron contaminants is shown in Fig.3. The mixture of gaseous chloride and argon, emerging from the chlorinator was directed towards a unit made of a quartz tube (length - 650 mm, diameter - 40 mm), containing 10-20 mm pieces of sodium chloride (common salt) or potassium chloride. The quartz tube was heated to the temperature of 350-370°C using a spiral wrapped around it. In these conditions gas-chloride mixture interacted with the sodium chloride and a less volatile substance (NaFeCl₄)

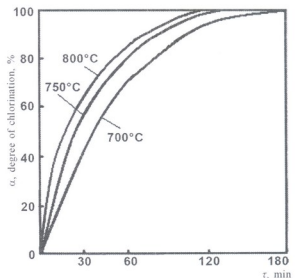


Fig. 3. Influence of temperature and duration on chlorination degree of core. α - degree of chlorination, %.



was produced. Tungsten hexachloride steam purified from admixtures flowed towards the second unit, where it was recuperated to metal tungsten in a counter-flow of hydrogen at temperatures of 700-950°C. In this case the amount of iron impurities in the ultimate product was significantly reduced and did not exceed 0.003%.

Thus, the study of the basic kinetic properties of the chlorination process of the remains containing tungsten revealed optimal technological parameters for producing pure tungsten hexachloride and concurrently fused salts (NiFeCl_4). The result served as a basis for the construction of a universal vacuum-proof chlorinator and its core units. Its novelty is in the separation of concurrently produced chlorination substances – molten and evaporated chlorides and in their production in pure form.

Conclusions:

1. The chlorination process of armor-piercing missile cores is characterized by strong exothermal features and great heat release, which results in the spontaneous rise of temperature in the reaction zone. Thus the chlorination process can be handled in autothermal mode;

2. The degree of chlorination of disintegrated missile cores reaches its maximum level in the case of 2-5 mm fraction being chlorinated. Further increase of the fraction up to 6.0-10.0 mm causes reduction of

the degree of furnace-charge chlorination;

3. The optimal supply rate of chlorine in the chlorination process might be considered as 0.25 liters/min. At this point the existence of less volatile iron and tungsten chlorides (FeCl_2 , WCl_4 , WCl_6) is not detected in chlorination products.

4. In the mixture of gases (100% Cl_2 ; 75% Cl_2 -25%Ar; 50% Cl_2 -50%Ar) the degree of chlorination while supplying chlorine of 75% concentration is not essentially different from the case of supply of chlorine of 100%. Further reduction of the chlorine concentration causes the decrease of the chlorination degree of the raw material.

5. The chlorination process is performed efficiently and completely within temperatures of 700°C-800°C, though at different degrees. Namely, at a temperature of 700°C the chlorination degree of missile core reaches its maximum value (98-99%) in 180 minutes; at 750°C - within 120 minutes and at 800°C - in 90 minutes.

6. Study of the basic kinetic properties of the chlorination process of tungsten-containing remains revealed optimal technological parameters for simultaneous production of pure tungsten hexachloride along with salt fuse (NiFeCl_4).

Acknowledgement. The work is supported by Shota Rustaveli National Science Foundation (Grant # GNSF/ST 1-7/87)

ქიმიური ტექნოლოგია

ვოლფრამის შემცველი მასალებიდან შემადგენელ ლითონთა ქლორიდების მიღების პროცესის კვლევა

ზ. მირიჯანაშვილი*, გ. თაყაძე**, გ. ღარიბაშვილი*, ა. კანდელაკი*

* ფერდინანდ თავაძის მეტალურგიისა და მასალათმკვლევების ინსტიტუტი, თბილისი

** აკადემიკოსი; ფერდინანდ თავაძის მეტალურგიისა და მასალათმკვლევების ინსტიტუტი, თბილისი

ვოლფრამშემცველი ნარჩენების ქლორირების პროცესის ძირითადი კინეტიკური მახასიათებლების კვლევით დადგინდა სუფთა ვოლფრამის პექსაქლორიდის (WCl_6) და კომპლექსური მარილის ($NiFeCl_4$) ერთდროული მიღების ტექნოლოგიური პარამეტრები. ქლორირების პროცესის წარმართვა შესაძლებელია ავტოთერმულ რეჟიმში.

REFERENCES

1. G.V. Samsonov (1970), Tugoplavkie metally. M. (in Russian).
2. G.V. Samsonov, G.Sh. Upadkhaya, I.S. Neshpor (1974), Fizicheskoe materialovedenie karbidov (Physical Chemistry of Carbides), Kiev: Naukova Dumka.
3. A.I. Nikolaev, V.G. Maiorov (2007), Tekhnologiya pererabotki otkhodov tverdosplavnogo materiala s polucheniem soedinenii kobalta i volframa. J. Information of IREM (in Russian).
4. A.V. Chub, A.V. Gorshkov (2007), Method izvlecheniia volframa iz volfram-soderzhashchikh materialov. Information of the Solikamsk Manganese Plant (in Russian).
6. I.S. Morozov (1966), Primenenie khloro v metallurgii redkikh i tsvetnykh metallov. M. (in Russian).
7. A.A. Furman (1980), Neorganicheskie khloridy. M. (in Russian).
8. A.A. Furman, B.G. Rabovskii (1970), Osnovy khimii i tekhnologii bezvodnykh khloridov. M. (in Russian).

Received February, 2012

Geology

Duration of Mesozoic Orogenies (on the Example of Georgia)

Ferando D. Maisadze

Academy Member; A. Janelidze Institute of Geology, I. Javakishvili Tbilisi State University, Tbilisi

ABSTRACT. On the basis of litho-facies analysis of Mesozoic deposits that accumulated during the development of orogenies (phases of folding), the processes of sedimentation accompanying these phases of folding as well as some paleogeographic and structural changes have been considered. Each phase of folding was accompanied mainly by synorogenic regressive formations. They were a direct consequence and criterion of manifestation of the tectonic movements. The most important among the manifested orogenies in the considered territory in the Mesozoic was the Chegem orogeny. It formed the main morphostructural units and mostly predetermined the character and appearance of present-day structure of the region. With due regard to the age of regressive deposits and geochronological data the first attempt to determine the duration of each orogeny was made. As to the Cenozoic orogenies, they will be discussed in a separate article of the same journal. © 2012 Bull. Georg. Natl. Acad. Sci.

Key words: orogeny, phases of folding, regressive formation, paleogeography.

The deposits accompanying the phases of folding are represented mainly by regressive synorogenic formations that were a consequence and criterion of the duration of intensification of tectonic movements. On the territory of Georgia, it was illustrated with the example of Okriba (Western Georgia) and the Southern slope of the Greater Caucasus for the Chegem [1] and then for the Late Pyrenean [2] phases of folding, respectively (Fig. 1).

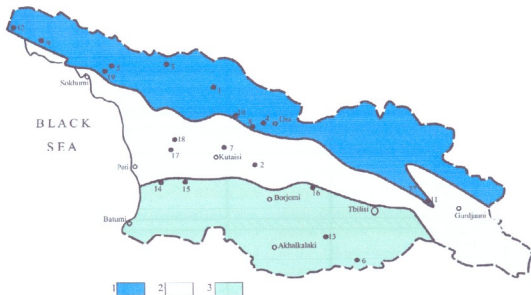
In the paper, based on litho-facial analysis of the Mesozoic sediments in the light of recent actual material and "plate tectonics", those facies and palaeogeographic changes that accompanied the orogenies are considered and to the possible extent the time of their manifestation is specified. According to geologic time-scale [3] the duration of each orogeny is defined (Fig. 2).

Before turning to the problem, it should be noted that in the study area, in the Mesozoic-Cenozoic time all the orogenies (except the Savian) distinguished by H.Schtille [4] as well as three new ones – the Donetsk, Chegem and Early Pyrenean (Trialetian) have been established.

Old Cimmerian Orogeny

The judgment on Old Cimmerian (Hindustani) folding that manifested itself before the Liassic is connected with considerable difficulties, first of all because of the fact that the deposits of the Triassic age are preserved only in two areas.

According to the existing concepts in the Triassic time in the Caucasus, two separated basins existed – the Greater Caucasian in the north and the Armenian in the south [5]. While in Georgia from the first basin



1 - Foldsystem of the Greater Caucasus; 2 - Transcaucasian intermountain area; 3 - Foldsystem of the Lesser Caucasus

Fig. 1. Scheme of tectonic zoning of the territory of Georgia (I. Gamkrelidze, 2000)

• location of some geographical names mentioned in the text.

only the Dizi series and “lower tuffites” (the *Narula suite*) are preserved, in the Lesser Caucasus sediments of this age are more widely represented.

Triassic deposits of Georgia by nature (petrographically, by the degree of metamorphism) are more closely related to the Paleozoic than to the Jurassic formations.

The *Dizi series*, the age range of which is Upper Paleozoic - Triassic developed in Chkhalta-Layli subzones of the Main Range zone. It is exposed in the upper reaches of the rivers Enguri and Tskhenistskali (Fig. 1, dot 1) composing the cores of the echelon-like arranged Upper Svaneti and Lower Svaneti anticlines. They are composed of relatively deep formations of the continental slope and its foot, which underwent regional and contact metamorphism [6].

Triassic age of the upper part of the *Dizi series* is defined mainly according to its stratigraphic position between the faunally dated Upper Permian and Lower Liassic.

In the *Dizi series* several suites were distinguished by different authors. The Triassic part is allocated under the name of Gvashkhara [7], or Gvadarash [8] suite.

The second, southern outcrop of Triassic formations, as already mentioned, is preserved in the Dzirula subzone of the South Caucasus intermountain area in the south-western periphery of the Dzirula crystalline salient (Fig. 1, dot 2). These formations, known as the “lower tuffites” [9], are exposed in the Narula, Kvirila, Glinavisgele, Kotorula and Macharula river gorges. Later on, they were identified as the *Narula suite* [10]. The *Narula suite* is exposed most completely on the river Narula, where it transgressively overlies crystalline rocks of the basement with basal conglomerates (10 m).

The age of *Narula suite* remained controversial for many years. Until now, it was defined as the Lower Liassic due to the transgressive bedding of Pliensbachian or Sinemurian rocks on the sediments of the *Narula suite* and fossil plant data [11]. Recently, on the basis of review and synthesis of the whole Triassic-Bajocian paleobotanical material, an opinion in favor of the Upper Triassic age (Norian and Rhaetian stages) of the *Narula suite* was expressed [12].

Thus, it can be inferred that the Old Cimmerian orogeny was manifested rather strongly causing regression and extensive pre-Liassic erosion. That is

Period	Epoch	Age	Foldsystem of the Greater Caucasus	Transcaucasian Intermountain area	Foldsystem of the Lesser Caucasus	Duration (Ma)	Folding phases	
E	E ₁	Tha				5-6	VII	
		Dan						
K	K ₂	Maa				11-12	VI	
		Cmp						
		San						
		Con						
		Tur						
	K ₁	Cen					4-5	V
		Alb						
		Apt						
		Brm						
		Hau						
		Vlg						
		Ber						
J	J ₃	Tth				5-6	IV	
		Kim						
		Oxf						
	J ₂	Civ				3-4	III	
		Bth						
		Baj						
		Aal						
	J ₁	Toa				3-14	II	
		Plb						
Sin								
		Het						
Tr			?	?	?	?	I	

Folding phases: I - Early Cimmerian; II - Donetsk; III - Chegem (Bathonian); IV - Andean; V - Austrian; VI - Subhercynian; VII - Laramide;  - regressive deposits.

Fig. 2. Time and duration of manifestation of Mesozoic folding phases by regressive deposits

why the Triassic formations are preserved only in two areas. The latter does not allow to judge the character and duration of Old Cimmerian folding (Fig. 2).

Donetsk Orogeny

Before the Liassic, as a result of Old Cimmerian folding, paleogeographic reconstructions took place. By the beginning of the Liassic in the considered terri-

tory from the north to the south the following principal structural and sedimentary units were formed: 1) the Greater Caucasus island arc, 2) marginal sea or an intra-arc basin (remainder of the Tethys basin) and 3) the South Caucasian (Transcaucasian) island arc.

The first unit corresponds to the contemporary zone of the Greater Caucasus Main Range, the sec-

ond – to the northern part of the Southern Slope zone of the Greater Caucasus and the third – to the Gagra-Java zone, the Southern Caucasus intermountain area, the Achara-Trialeti and Artvin-Bolnisi zones.

In the Early Liassic, a large-scale transgression involved the greatest part of the territory under consideration, indicating the beginning of a new stage of geological evolution of the region.

Between the Middle and Late Liassic in the Donetsk basin, the Donetsk phase of folding was established. According to M.G. Lomize and D.I. Panov [13], based on the analysis of manifestations of magmatism during the Late Aalenian-Early Bajocian the Dzirula phase of folding was established in the North Caucasus. It was earlier distinguished in the South Caucasus intermountain area [14]. Because of lack of indication of specific sites and sections, where the angular unconformity between the Aalenian and Bajocian is recorded, it is impossible to discuss the nature and extent of manifestations of the Dzirula phase of folding within the limits of Georgia.

In the territory of Georgia, in contrast to the North Caucasus, the Donetsk orogeny was not so extensive and it was manifested in different ways. According to I.R. Kakhadze [15], the stratigraphic range of manifestation of the Donetsk orogeny corresponds to the interval from the Early Aalenian to the upper part of the Early Bajocian.

For the central part of the marginal sea of the Southern slope of the Greater Caucasus, according to magmatism [16], at the end of the Liassic and in the beginning of the Bajocian the following consistency of tectonic implications was determined: tension of the Earth's crust in the Late Pliensbachian with the eruption of tholeiitic magma, then the compression of the Earth's crust in the Toarcian-Early Aalenian and a complete cessation of volcanism (corresponding to the manifestation of Donetsk orogeny), then retension (Late Aalenian-Bajocian) and the resumption of tholeiite-basalt magmatism. In the eastern part of the marginal sea (east of the river Enguri) the Upper Liassic is represented by argillo-arenaceous

rocks. In vertical direction an increase of sandstones and appearance of conglomerate packets is observed. Along with this, the content of plant residues also increased [17]. Together with the above-mentioned, that points to the regressive nature of these deposits induced by the Donetsk phase of folding.

In the western part of the marginal sea (North Abkhazia) in the Liassic clayey-volcanogenic-sandy formations of the *Lashipse* (Sinemurian), *Avadkhara* (Lower Pliensbachian-lower part of Upper Pliensbachian), *Atsgara* (Upper Pliensbachian-Lower Toarcian) and the *Achaeon* (Toarcian) suites were deposited [18]. In the *Achaeon suite* the increased number of sandstones points to the beginning of the regression. In the same suite the sections with the Upper Liassic clayey-sandy deposits contain stretched (over 2.5 km) lenses of granular crystalline limestones, pointing to the shallowing of the sea (the rivers Vostochnaya Gumista, Kelasuri, pass of Sanchar, etc.). In the upper reaches of the river Kodori (Fig. 1, dot 2), above these limestones there follow limestone breccias and conglomerates (up to 100 m) containing debris and pebbles of underlying limestones [9].

On the Southern slope of the Greater Caucasus (Gagra-Java zone), after deposition of Middle Liassic clay rocks, delivery of sandy material abruptly increased, causing the deposition of flyschoid *Sori suite* (Toarcian-Aalenian) with thickness 1,000-1,300 m. It is best represented in the basins of the middle course of the rivers Kodori (Fig. 1, dot 5) and Rioni (Fig. 1, dot 4) and is divided into two parts: the lower – alternation of medium- and thick-layered sandstone, argillites and aleurolites, and the upper part – massive and thick-layered sandstones with intercalations of argillites. All this undoubtedly points to the regressive nature of the *Sori suite*. The increase of psammitic material is observed both in the vertical direction and from north to south towards the Dzirula crystalline massif [16].

In the Southern Caucasus intermountain area tectonic movements of the Donetsk orogeny were most obvious within the limits of the Dzirula crystal-

line massif. In its greater part (except the north-east) an unconformity between the Bajocian and more ancient rocks, including the Toarcian and Aalenian, is observed. In the north-eastern part of the massif uninterrupted sections are observed, where the Aalenian gradually passes into the Bajocian. Here, the Toarcian-Aalenian deposits are represented mainly by clayey-sandy facies, in the upper part of which sandstones and conglomerates occur [15], indicating regression.

In the Loki-Karabakh zone, the Donetsk orogeny was expressed as a regression and also in the form of stratigraphic and angular unconformity. Within the limits of the Loki crystalline massif (Fig. 1, dot 6) sedimentation of the flyschoid *Jandara suite* took place during the Toarcian-Aalenian. It is built up of argillites, aleurolites and sandstones. As a result of regression and shallowing of the sea, the upper part of the suite is represented by coarse-grained sandstones, gravelites and conglomerates (the river Gorastskali). At the same time there occur sections (right bank of the river Akhkerphay), where the red zoogenic limestones of the Aalenian pass upwards (in complete conformity and gradually) into the porphyritic series of the Bajocian [20].

Chegem Orogeny

The considered orogeny in the Caucasus was established by A.N. Gerasimov [21] at first as a Chegem folding and then as an Adyghe one. In Georgia, this folding was identified as the Bathonian [1], but in the literature it was more known as the Chegem orogeny. Its age was defined as the pre-Callovian.

The Chegem folding in the territory under study was one of intense orogenies. It caused significant changes in the structural-facial as well as in the palaeogeographic sense. After its manifestation the main morpho-structural units were formed. Later on, they largely determined the character of the geological development of the region.

One of such phenomena was the formation of the transverse-uplift of Svaneti, dividing the marginal sea of the Southern slope of the Greater Caucasus into

two parts: the Abkhazian in the west and the Rachatiani in the east [15]. Along with the facial changes, the Chegem orogeny caused partial inversion of the geotectonic regime and overall uplifting of the central parts of the Greater Caucasus and of the Georgian block, reflecting the tendency to transverse uplifting of the whole Caucasus [17].

On the territory of Abkhazia the formation of Akhtsu-Katsirkha cordillera took place, located along the southern periphery of the Western marginal sea associated with the Chegem orogeny. To the south of the cordillera, after the formation of volcanogenic-terrigenous sediments of the Upper Bajocian, in the Bathonian age the marine environment was gradually replaced by the continental-marine and continental environment, where the regressive *Betagian suite* represented by the alternation of sandy aleurolites and graywacke sandstones with rare interbeds of sandy limestones was deposited. The upper part of the suite comprises layers of microconglomerates and conglomerates composed of fragments of the Bajocian porphyritic series [19]. Regression and palaeogeographic reconstructions caused by the Chegem orogeny, determined the development of a coal-bearing formation and coal deposits (Bzibi, Tkvarcheli).

A distinct manifestation of the Chegem phase of folding was illustrated by A.I. Janelidze [1, 22] in Okriba (Western Georgia). The structural-facies analysis of Middle Jurassic deposits and their thicknesses has shown that the deposits accompanying the Chegem (Bathonian) folding are represented mainly by regressive synorogenic formations.

At the end of the Bajocian abrupt weakening of volcanic activity took place. By the beginning of the Bathonian age, in Okriba (Fig. 1, dot 7) low anticlinal uplifts (Bziauri, Shkmeri, Sori) appeared. They caused the formation of the Okriba lagoon. As a result of ongoing tectonic movements the Bziauri anticline turned into land and divided the Okriba lagoon into two separate lake-lagoons: the Gelati in the south and Tkibuli in the north, later turning into areas of coal accumulation [1].

Further to the east, in the Racha-Tianeti basin (Eastern marginal sea), where from the Liassic to the Late Eocene inclusive uninterrupted sedimentation took place, the Chegem orogeny was manifested in the formation of separate cordilleras and of corresponding regression. In Upper Racha, Bathonian formations are represented by the regressive "Talakhiani horizon" (in the north) and volcanic-terrigenous "diabase horizon" (in the south). Due to the Chegem folding, in the greatest part of the Eastern marginal sea, cordilleras appeared along its southern edge, creating a cordillera zone. Later on it played (Late Jurassic - Late Eocene) an important role in supplying flysch (in the North) and epicontinental (in the South) basins with terrigenous and detrital material. This cordillera zone was first distinguished by P.D. Gamkrelidze [23] and is known as the Gagra-Java cordillera [24], or the Racha-Vandam [25] cordillera zone, which is now completely covered with flysch formations overthrusting from the north.

The first signs of manifestation of Chegem folding, as already mentioned, appeared in the Late Bajocian, when intensive volcanic activity had stopped and sedimentation of arkose sandstones started. In the Bathonian age they were replaced also by regressive paper shales and a coal formation, which as thought earlier [20], accumulated during the Bathonian age. Then follow a transgression and unconformable bedding of Callovian sediments with conglomerates in the base. Based on these facts (villages of Tsesi, Sori, Zhoshkva, the Baklanovka river-gorge, Tskhanari syncline, etc.), the age of the Chegem folding was defined as the pre-Callovian. However, new factual material [26] requires a new approach to the question of the upper boundary of regressive deposits and respectively to the age of Chegem folding.

In uninterrupted sections of the Middle Jurassic (upper reaches of the rivers Psou and Gega, Okriba, Racha) the boundary between the Bathonian and the Callovian was usually drawn according to lithological features, in particular in the base of rudaceous rocks (mainly conglomerates) attributed to the lowermost

Callovian. However, in the village of Tsesi (Racha) in the rocks related to the Lower Callovian (40 m) ammonite fauna of the Upper Bathonian was found [20]. On this basis, the age of regressive formations and duration of the Chegem orogeny according to new concepts covers the stratigraphic range from the Late Bajocian to Middle Bathonian inclusive. How this inference can be applied to the entire region, depends on the results of a critical review of the factual material.

Andean Orogeny

The Andean orogeny was manifested before the Tithonian and was much weaker than the previous one, although it covered a significant part of the territory. Western and Eastern marginal seas, from the Late Jurassic to Late Eocene inclusive turned into areas of accumulation of flysch formations.

In the Western flysch basin (upper reaches of the rivers Psou and Gega) flysch formations of the Upper Oxfordian-Tithonian follow above the Callovian-Lower Oxfordian *Aibgin suite*. Lithologically they are divided into two parts: the lower - terrigenous and the upper - carbonate [19]. The lower, terrigenous part (argillites, aleurolites with intercalations of graywacke sandstones and marls) located between the carbonate rocks (Upper Oxfordian sediments as well as the Tithonian are represented by limestones), by stratigraphic position corresponds to the Kimmeridgian and is represented by regressive formations.

In the Eastern flysch basin (to the east of the river Enguri), where deposition of flysch began from the Late Jurassic, any facies changes pointing to the regression is not observed, except for the presence of intraformational conglomerates (lower part of the *Tsipori suite*) confined to intrabasin cordilleras appearing due to the Andean orogeny [20].

Southwards of the flysch basins (Gagra-Java zone) due to the Andean orogeny a barrier, mainly coral reefs, was formed [20]. They developed around the cordilleras (Akhtsu-Katsirkha, Racha-Vandam cordillera zone), restricting the flysch basins from the south.



On the territory of Abkhazia, most of the reef structures formed in the Late Oxfordian-Kimmeridgian, with the exception of separate areas (the western slope of mountain Akhi-bakh), where reef-formation continued in the Early Tithonian [27]. To the south and east of limestone facies of the Upper Jurassic as a result of Andean orogeny the depressions formed that are most distinct in Western Georgia (Racha and Bzyb bays) and in the South Caucasus intermountain area (town of Tkvarcheli, vil. Okumi, the river Tshenistskali, Okriba, Racha, Lechkhumi, etc.), where from the end of the Oxfordian sedimentation of freshwater formations of the "variegated suite" began. Lithologically they are represented by alternation of sandstones, clays, limestones, dolomites and marls, having variegated coloring and containing plant residues. In the Kimmeridgian part of the suite, an increase of the terrigenous component and emergence of gypsum interlayer are observed, pointing to its regressive nature.

In the Tithonian age, despite the cessation of folding, in separate parts of lagoons, apparently the preceding facies conditions were preserved and the "variegated suite" continued to settle. In the Neocomian it is replaced with arenaceous and brecciated limestones. In the territory of the Kaldakhvara ridge (Abkhazia) (Fig. 1, dot 9), Oxfordian arenaceous limestones were replaced by variegated sandstones and clays, alternating with sandy limestones, dolomites and marls of the Kimmeridgian [15]. In the western part of the Racha syncline, the "variegated suite" is overlapped by the transgressive sandy-carbonate stratum of the Late Tithonian age. In the central part of this structure (Fig. 1, dot 10) Neocomian carbonate deposits are transgressed on the Lower-Middle Kimmeridgian and Upper Oxfordian-Lower Kimmeridgian (village of Chibrevi) rocks of the "variegated suite" [28].

In some sections (west of the village Tsesi, in Okriba and further to the west) the "variegated suite" transgressively and with angular unconformity overlies the Middle Jurassic formations, contrary to Late Oxfordian-Kimmeridgian regression. According to A.I. Janelize [1], this inconsistency was a result of

ingression conditioning transgressive bedding of regressive formations.

Age of the "variegated suite" remained disputable for many years and various authors interpreted it in different ways: the Kimmeridgian [1, 15], the Kimmeridgian-Tithonian [20], the Callovian-Tithonian [29, 28], the Middle Oxfordian-Middle Tithonian [28]. Thus, it is impossible to judge the duration of the Andean orogeny according to the "variegated suite". Considering the palaeogeographic situation induced with the Andean and Chegem phases of folding, the "variegated suite" in my opinion, has lower and upper boundaries moving from the Callovian to the Tithonian inclusive. Based on this assumption, the formations under consideration represent a facies of "variegated deposits" without strictly defined stratigraphic boundaries, which does not allow distinguishing them as a suite.

As to the duration of the Andean folding, according to the available data it should cover a stratigraphic range from the Oxfordian to the Kimmeridgian inclusive (Fig. 2).

Austrian Orogeny

The exact age of Austrian folding is disputable due to the lack of angular unconformity between the Lower and Upper Cretaceous.

In the Western flysch basin (Abkhazia) mainly identical sediments (sandy marls, carbonate clays) were deposited in the Aptian and Albian and any signs of regression are missing.

In the Eastern flysch basin (east of the river Enguri) sandstone-aleurite flysch was deposited in the Aptian. It is known as the *Dgnali (Tetrakhevi) suite*. The above following Albian deposits are represented also by sandy-aleuritic flysch (*Pavleuri or Navtiskhevi suite*), consisting of alternating sandstone-, gravelite- and aleurolite-bearing turbidites and pelagic argillites and marls. Sandstone turbidites in the upper part of the suite are more coarse-grained and multiple [20]. Among them interlayers of sandy and organogenic-detrital limestones and volcano-genic-terrigenous rocks also occur [30].

The age of the *Dgnali (Tetrakhevi)* suite is defined as the Aptian-Lower Albian, of the *Pavleuri suites (Navtiskhevi)* – as the Middle and Upper Albian [31.32]. Along with regressive character, the Albian sediments differ from the Aptian ones in multicoloring. Regression, which began from the Late Albian, continued in the Early Cenomanian, as shown by the lithologic character of the Lower Cenomanian sandy-aleurolitic *Ukughmarti suite* composed of alternating sandy-aleurolitic, rarely gravelite-bearing turbidites and pelagic argillites. The sandstones contain glauconites in places. In the Kakheti region (the Cheremi syncline) (Fig. 1, dot 11) the *Ukughmarti suite* consists of thick-layered gravelites and coarse-grained sandstones with intercalations of argillites and conglomerates. The suite is crowned by the layer of conglomerates containing Upper Jurassic zoogenic limestone debris [33]. In the southern facies of the flysch (Zhinvali-Gombori subzone), the *Ukughmarti suite* is built up of breccia-conglomerates and sandstones (sometimes containing glauconite), interlayers of volcanic rocks occur rarely.

Thus, the Austrian orogeny in the Eastern flysch basin was manifested in the form of regression, which lasted from the Late Albian to the Early Cenomanian inclusive.

In the epicontinental basin, particularly in its western part (the rivers Arkva and Psou) Aptian and Albian rocks are built up of marls with rare intercalations of argillaceous limestones. Further to the south (village of Khashupse) (Fig. 1, dot 12) the Aptian is represented by brecciated limestones and the Albian comprises marls with interlayers of sandstone (upper part of the section).

In the territory of the Dzirula salient of the crystalline basement the Aptian is represented by limestones and marls and the Albian – by clays, marls, carbonate-bearing and glauconitic sandstones. The thickness of the latter in the upper part of the section reaches 1.5-2 m. They are unconformably overlain by quartz-glauconitic limestones of the Cenomanian [34].

At the same time, here (the northern periphery of the massif), as well as in the Eastern flysch basin, the regression continued in the Cenomanian, as indicated by the pre-Turonian break in sedimentation [20].

In the western and northern parts of Okriba (villages of Gordi, Kinchkha, etc.), among the Albian marls, lenses and intercalations of conglomerates with fragments of underlying marls appear. In the uninterrupted sections (southern limb of the Racha-Lechkhumi syncline, the western part of Okriba) deposits of the Cenomanian conformably follow above the Albian rocks and are represented by glauconitic sandstones, rarely by glauconitic limestones

Against the general background of the Albian-Early Cenomanian regression in some parts of the territory transgression took place (city of Kutaisi, the river Kvirila, Southern Okriba, Dzirula massif, etc.), which spread locally. As a result of transgression, at places Albian and Aptian deposits are missing (town of Chiatura, vil. Chkhari) (Fig. 1, dots 13,6). Similar movements took place in Southeastern Georgia (Khrami and Loki crystalline massifs), where at different stratigraphic levels of the Upper Cretaceous separate transgressions and regressions are observed.

Among the folded structures formed due to the Austrian folding, a Satsalike anticline separating the Racha-Lechkhumi syncline (in the north) from the Dzirula massif should be distinguished. Another anticline, formed on the southern periphery of the mentioned massif, separated the Kharagauli (in the north) and Molisi (in the south) synclines.

A significant episode, presumably taking place in the Albian age, was the appearance of the Black Sea - Achara-Trialeti rift zone in the central part of the Southern Caucasus island arc earlier subject to wash-out. In the eastern part (in the contemporary Achara-Trialeti zone) thick (up to 2000 m) volcanogenic formations accumulated during the Albian [34]. Due to the appearance of an intra-arc rift the South Caucasian island arc was divided into the northern and southern parts.

Sub-Hercynian Orogeny

The sub-Hercynian orogeny was manifested before the Maastrichtian and it completed the Mesozoic cycle of orogenesis. Its first impulses on the Southern slope of the Greater Caucasus and in the Achara-Trialeti zone were observed already before the Late Santonian [20].

In the Eastern flysch basin, this folding is fixed mainly in the areas of cordilleras and submarine uplifts. In the Shovi-Pasanauri subzone the Campanian is represented by clastic-limestone *Tsitiani suite* of flysch (limestones, marls, argillites), in the upper part of which at places (the village of Sakobliano in Kakheti) material of the eroded Upper Cretaceous flysch is attested [33]. In Kakheti (the village of Cheremi), angular unconformity is observed also under the Maastrichtian *Sabue (orbitoid) suite* [20]. In the synclinal structures, where the Campanian (*Jorchi suite*) gradually passes into the Maastrichtian (*Sabue suite*), between them signs of regression are not observed (Daradavi syncline in the Zhinvali-Gombori subzone). At the same time, in the section of the river Mejuda, the *Jorchi suite* is composed of clastic and biomorphic-detrital greywacke-sandy turbidites and shaly marls.

To the south, in the epicontinental basin in the Campanian age descending movements caused the contraction of Dzirula land and its gradual overlap by the younger members of the Campanian. These descending movements went on concurrently with Sub-Hercynian folding taking place in adjacent tectonic zones (Southern Slope of the Greater Caucasus and Achara-Trialeti zone). In the rest of the epicontinental basin sedimentation of shallow water limestones and marls took place.

In the Achara-Trialeti zone pre-Maastrichtian movements are well recorded in the northwestern part of the Trialeti Range, causing erosion and deposition of coarse-grained material. Deep washouts took place in the northern part of the Achara-Trialeti zone (town of Lanchkhuti, village of Dapnara) (Fig. 1, dots 14, 15), where the Maastrichtian (*Kheoba suite*) with

a basal conglomerate overlies the rocks of the Campanian age. In some sections, as a result of pre-Late Santonian washouts (Gorisjvari-Khvedureti anticline) (Fig. 1, dot 16), Campanian deposits and in some places the Maastrichtian ones unconformably overlie the older rocks. Washouts are evidenced on the river Tedzami as well and they all associate with the Sub-Hercynian movements [20].

It should be noted that the Sub-Hercynian folding is connected with the tendency to overall compression taking place at that time in the Mediterranean belt, when splitting of the African-Arabian continent and the development of rifts of the Red Sea and Gulf of Aden began [35].

Laramide Orogeny

The Laramide folding involved the greater part of the territory under consideration. As a result of this folding, a remarkable reduction of the Eastern flysch basin (the Enguri and Liakhvi interfluvium) took place and it turned into a part of the Greater Caucasian land.

The considered phase of folding caused an overall regression, which began from the end of the Maastrichtian and lasted during the Early Paleocene (Danian). Lithologically, the regression was manifested in the replacement of the Cretaceous carbonate sedimentation (limestones) by more terrigenous (clays, marls) in the Paleocene.

In the Eastern flysch basin the regression most distinctly manifested itself in the Zhinvali-Gombori subzone, where the regressive part of the Maastrichtian, occupying the upper horizons of the clastic-limestone *Sabue (orbitoid) suite* is represented by rudaceous facies - conglomerate-breccias and olistostromes composed of rubble and boulders of underlying flysch rocks and rocks of the Gagra-Java zone, in particular, of the products of erosion of the Racha-Vandam cordillera zone. Olistostromes of the Upper Maastrichtian (rivers Sakanapeskhevi, Mejuda, Ksani, Aleura, etc.) by their structure and appearance are similar to those of the Upper Eocene formations of the Southern slope of the Greater Caucasus [25].

In the deepened areas of flysch basin, where uninterrupted sedimentation took place, facies changes indicating regression are still observed. In the Daradavi syncline the *Sabue suite* is represented by the alternation of sandstone- and gravelite-bearing turbidites and pelagic limestones and clays. In the upper part of the suite an increased number of turbidites and, instead of limestones, deposition of sandstones or microconglomerates took place [33].

In the epicontinental basin (the Gagra-Java zone) the regression is manifested in replacement of carbonate sedimentation by carbonate-terrigenous one. The Abkhazian part of the basin was an exception, where in the Maastrichtian (*Mokvi suite*), as well as in the Danian age (*Tsebelda suite*), sedimentation of limestones continued. In this part of the basin signs of regression are observed in the sections of the Eki and Nokalakevi anticlines (Samegrelo) (Fig. 1, dots 17, 18), where in the *Mokvi suite* terrigenous material in the form of quartz and limestone fragments was attested [33]. In the vicinity of the village of Tsebelda (river Kodori) (Fig. 1, dot 19) in the upper part of

Maastrichtian limestones a considerable amount of quartz-arkose material is observed—a product of erosion of the Kelasuri granitoid massif. Terrigenous component in limestones increased in vertical direction and they are replaced by carbonate quartz-arkose sandstones. In the Achara-Trialeti zone the *Zguderi suite* of the Santonian-Maastrichtian age developed; it is built up of limestones with marl intercalations. In the upper part of the suite intraformational conglomerates are present, pointing to the activation of tectonic movements in the Late Maastrichtian. Here, as in the Dzirula subzone, due to the regression from the end of the Maastrichtian and throughout the Danian, “variegated marls” accumulated instead of limestones. As a result of Laramide folding, folded structures in the form of Tsiteltskaro, Satskhenisi, Gorisjvari, Khvedureti and other cordilleras appeared for the first time in the Achara-Trialeti rift basin [34]. Thus, according to the regressive deposits the time of development of Laramide folding was determined within the interval of Late Maastrichtian-Early Paleocene (Danian) inclusive.

გეოლოგია

მეზოზოური ოროგენული ფაზისების ხანგრძლივობა (საქართველოს მაგალითზე)

ფ. მაისაძე

აკადემიის წევრი; ი. ჯავახიშვილის სახ. თბილისის სახელმწიფო უნივერსიტეტი, ა. ჯანელიძის გეოლოგიის ინსტიტუტი, თბილისი

ოროგენული (დანაოჭების) ფაზისების დროს წარმოქმნილი ნალექების ლითო-ფაციესური ანალიზის საფუძველზე განხილულია იმ დროის სედიმენტაციური პროცესები, პალეოგეოგრაფიული და სტრუქტურული ცვლილებები. დანაოჭების ყველა ფაზისს თან ახლდა სინოროგენული რეგრესიული წარმონაქმნები, რომლებიც ტექტონიკური მოძრაობების გააქტიურების პირდაპირ

შედგეს და დროში მათი ხანგრძლივობის საზომს წარმოადგენს. საქართველოს ტერიტორიაზე დადგენილ მეზოზოურ ოროგენულ ფაზისებს შორის ყველაზე მნიშვნელოვანი ჩვეუური დანაოჭება იყო. მის შედეგად ჩამოყალიბდა ის ძირითადი მორფოტრუქტურული ერთეულები, რომლებმაც შემდგომში მნიშვნელოვნად განაპირობეს რეგიონის თანამედროვე გეოლოგიური აგებულების ზასიათი. რეგრესიული ნალექების ასაკისა და გეოქრონოლოგიური მონაცემების გათვალისწინებით აღნიშნულ სტატიამ პირველად განისაზღვრა მეზოზოური ოროგენული ფაზისების სავარაუდო ხანგრძლივობა.

REFERENCES

1. A.I. Janelidze (1940). Geologicheskie nabludeniia v Okrube v smezhnykh chastiakh Rachi i Lechkhumi. 408p. (in Russian).
2. F.D. Maisadze (1984). Izvestiia AN SSSR. Ser. Geol., 7: 148-152 (in Russian).
3. International stratigraphic chart (2000). International Union of Geological Sciences. Trondheim.
4. H. Stille (1924). Grundfragen der vergleichenden Tektonik. Berlin. 443.
5. A.L. Tsagareli, M.S. Eristavi (1960). Mezhdunarodnyi geologicheskii Kongress. XXI sessiia. Problema 12: 130-137 (in Russian).
6. Sh.A. Adamia (1968). Trudy GIN AN GSSR. Nov. Seriia, vyp. 16: 249 (in Russian).
7. V.I. Slavin, M.L. Somin. (1962). Trudy VAGT i MGU, 3: 315-335 (in Russian).
8. M.L. Somin, A.A. Belov (1967). Bull. MOIP. Sec. geol. 1: 40-48 (in Russian).
9. P.D. Gamkrelidze, S.S. Chikhelidze (1932). Bull. GIN AN GSSR, 1, 3: 81-105 (in Russian).
10. E.K. Vakhania (1976). Trudy VNIGNI, vyp. 207, 413 s. (in Russian).
11. Ts.I. Svanidze (1971). Trudy TSU, 21(141): 165-169 (in Russian).
12. Ts.I. Svanidze, Z. Lebanidze (2000). Geologica Balcanica, 30, 1-2: 19-24.
13. M.G. Lomize, D.I. Panov (2001). Geotektonika, 4: 78-92 (in Russian).
14. A.L. Tsagareli (1980). Tektonika. Geologiiia Af'pid "Tetiskogo" proiskhozhdeniia, 187-192 (in Russian).
15. I.R. Kakhadze (1947). Trudy GIN AN GSSR. Ser. geol., III (VIII), 371 s. (in Russian).
16. M.A. Beridze (1983). Trudy GIN AN GSSR. Nov. Seriia, 80: 182s. (in Russian)
17. P.D. Gamkrelidze (1960). Mezhdunarodnyi geologicheskii kongress, XXI sessiia. Problema 193-203 (in Russian).
18. M.V. Topchishvili (1996). Trudy GIN AN GSSR. Nov. Seriia, vyp. 108: 216 s. (in Russian).
19. Voprosy geologii NW chasti Abkhazii (1972). Tbilisi, 238 s. (in Russian).
20. Geologiya SSSR (1964). X. Georgia: 655 s. (in Russian).
21. A.P. Gerasimov (1928). Izvestiia Geol. Komiteta. XLVII, 4: 327-360 (in Russian).
22. A.I. Janelidze (1940). Sovetskaiia Geologiiia, 5-6: 172-174 (in Russian).
23. P.D. Gamkrelidze (1970). Tezisy dokladov. Tbilisi, 3-5 (in Russian).
24. P.D. Gamkrelidze, I.P. Gamkrelidze (1977). Trudy GIN AN GSSR. Nov. Seriia, 57: 80 (in Russian).
25. F.D. Maisadze (1994). Stratigrafiia. Geologichskaia korrelatsiia, 2, 1: 95-102 (in Russian)
26. I.D. Tsereteli (1978). Soobshch. AN GSSR, 92, 1: 117-120 (in Russian).
27. Z.M. Lebanidze (1998). Proc. Georg. Acad. Sci.: 29-36 (in Russian).
28. V.A. Todria (2000). Trudy GIN AN GSSR. Nov. Seriia, 115: 36-47 (in Russian).
29. N.G. Khimshiasvili (1957). Verkhneirskaia fauna Gruzii. M., 313 s. (in Russian).
30. I.G. Chechelashvili, E.V. Varsimashvili (1981). Trudy GIN AN GSSR, 72: 84-129 (in Russian).
31. V.P. Rengarten (1932). Trudy VGRO, 148: 78 (in Russian).
32. E.V. Kotetishvili (1986). Trudy GIN AN GSSR. Nov. Seriya, 91: 160 (in Russian).
33. R.A. Gambashidze (1984). Trudy GIN AN GSSR. Nov. Seriia, 82: 111 (in Russian).
34. P.D. Gamkrelidze (1949). Geologicheskoe stroenie Adjaro-Trialetskoi skladchatoi sistemy. 508 s. (in Russian).
35. I.P. Gamkrelidze (1976). Trudy GIN AN GSSR. Nov. Seriia, 52: 225 (in Russian).

Received March, 2012

Plant Growing

Natural Zeolite – One of the Possibilities of Transition from Chemical to Biological Agronomy

Teimuraz Andronikashvili*, Marine Zautashvili**, Luba Eprikashvili**,
Nino Burkiashvili**, Nino Pirtskhalava**

* Academy Member; P.Melikishvili Institute of Physical and Organic Chemistry, I.Javakishvili Tbilisi State University, Tbilisi

** P. Melikishvili Institute of Physical and Organic Chemistry, I. Javakishvili Tbilisi State University, Tbilisi

ABSTRACT. Some aspects of transition from chemical to biological agronomy are discussed in the article. Attention is focused on the questions of use of natural zeolites of sedimentary origin in practice of plant growing. On the basis of the researches carried out at the end of the 20th and at the beginning of the 21st centuries, positive influences of the natural zeolites on its physical and chemical properties, biological activity and efficiency are established. © 2012 Bull. Georg. Natl. Acad. Sci.

Key words: soil, properties, clinoptilolite-containing tuff, organo-zeolitic fertilizer.

In the nearest future the danger of losing agricultural soils arises in the world because of global natural cataclysms and irrational activity of man [1]. One of the reasons of the development of the negative processes in the soil is the increasing utilization of mineral fertilizers and pesticides. All these cause an increase in crop yield but at the same time create the danger of the contamination of the environment by toxic substances.

Therefore, development of new solutions becomes necessary in order to feed the growing world population and maintain a safe environment at the same time.

In the middle of the past century, calls for renouncing chemical (industrial) arable farming and moving to its biological counterpart appeared in scientific journals. However, in many scientists' opinion, not

absolute rejection of mineral fertilizers and pesticides but "balanced utilization of agro techniques, agrochemical and biological methods together with the system of integral plant protection" is more reasonable [2]. G. Kahnt, a German scientist, holds this opinion and advances three main factors for transition to biological arable farming:

1. Transition of nitrogen of the air into plant protein by means of bean culture and specific soil bacteria, but not by means of synthetic nitrogen fertilizers.

2. Loosening and aggregation of the soil by means of plant roots, small soil-inhabiting animals and soil microorganisms, but not by means of tools and mechanisms.

3. Struggle against weeds, plant diseases, and pests is to be carried out by means of proper alternation of crop-rotation of cultures, choice of species

and sorts applicable to specific conditions and methods of activation of natural enemies of pests; but not at the expense of application of chemical against (herbicides, insecticides, fungicides, etc.).

In this case, biological arable farming does not exclude utilization of mineral fertilizers: - "goal-directed tilling of the soil, crop rotation, fertilization by manure (organic), and harmonic addition of mineral nutritious substances are the prerequisites for good harvest" [2].

At present, natural zeolites of sedimentary origin are widely used in plant-growing [3-7]. Their application in the soil (both individually and in combination with minerals and organic fertilizers) not only increases the capacity of the crops but also improves their qualitative indices [8].

Zeolites belong to a special class of crystalline alumo-silicate minerals and are characterized by their inherent alkaline reactions [9]. Combination of well-defined adsorption and ion-exchange capacity with considerable biological activity is a specific characteristic of zeolites [9]. Furthermore, the cation-exchange capacities of zeolites are one order higher than those for any other types of soils [10, 11].

It is due to this specificity that addition of zeolites to the soil improves its physical and chemical properties.

At present, more than forty types of zeolites are known but only the following zeolites of sedimentary origin have practical utilization: clinoptilolite, heulandite, mordenite, phillipsite, faujasite, laumontite, analcime, chabazite and erionite. Industrial deposits of these zeolites, with the main mineral content above 50-60% in rocks, are widely represented on all the continents of our planet. They are inexpensive, easily accessed for extraction and exploration [9-10].

According to the specificity of these minerals, their utilization is more reasonable for acidic (infertile) soil, but this does not exclude the possibility of their use for other types of soils as well. Acidic soil (podzolic, soddy podzolic, gray forest, boggy, peat, red, yellow) are widely distributed on all the continents and are characterized by high acidity (pH of

water extracts of these soils ranges from 3-3.5 up to 4.6-6.0) [12]. Such soils are useless for growing the majority of the crops successfully grown on neutral soils (pH=7 for the soil solution). The method of liming [12] is used in the practice of plant-growing in order to decrease the acidity and increase the fertility of such soils. This method is based on the enrichment of soil exchangeable complex with cations of calcium characterized by clearly shown alkaline reaction. However, already at the end of the past century, it appeared that natural zeolites can fulfill this positive role [5]. Effects of zeolites on pH of soil solutions are mainly noticed for acidic soils, depending on the doses of the applied minerals.

Laboratory experiments showed that application of 2% zeolite-bearing rocks (deposits of Bulgaria) to weakly alkaline soils of that country changes pH of the surrounding only by 0.44 units; for weakly acidic soils of Central Greece – by 0.44 units as well [13]. Identical results were obtained in the case of application of 1% clinoptilolite-bearing tuff (Ai-Dag deposit, Azerbaijan) to weakly cultivated soddy podzolic soils (Moscow region) where alkalinity also increased only by 0.3 units [14].

The experiments, carried out in Georgia [15], proved that application of clinoptilolite-bearing tuffs to red and podzolic soils in the amount of 0.5% did not change the pH of the medium; only application of 1.0-1.5 % of zeolites increased alkalinity by 0.2-0.3 units. Appreciable results were obtained by enrichment of this soil with 15% zeolites. On red soils alkalinity increased by 2.5 units but that on podzolic soil by 2.4 units, i.e. became neutral (pH=6.8-7.4). Similar results are given in [14] according to which application of zeolites in the amount of 5 and 10 % increases alkalinity by 2.3 and 3.0 units respectively for the first year and preserves that effect for the following two years.

Field experiments carried out in Ukraine and Yakutia fully confirmed the experiments done in laboratory conditions. So, application of clinoptilolite-bearing tuff to soddy podzolic soils (Ukraine) in the amount of 30 t/ha (against the background of NPK)

increased the pH of the water extraction from 5.3 to 6.7, i.e. by 1.4 units [16].

Introduction of calcium forms of zeolite (Khonguru deposit, Yakutia) into podzolic, sandy loam (against the background of NPK) in the amount of 50 t/ha increased alkalinity by 0.6 units, from 5.2 to 5.8; but enrichment of the boggy-high soil of South Yakutia with the same type of zeolites in the amount of 100 t/ha contributed to an increase in pH by 1.6 units, from 5.2 to 6.8 [17]. It has been established by the field experiments that the change in pH is preserved for a long time (2-3 years) after a single application of zeolite [16]; according to other data - for 4-5 years [18]. Thus, a new possibility of reclamation of acidic soils without liming has become available.

Other important properties of zeolites, such as ability to adsorb a lot of quantity of moisture and retain it in their pores at increased temperature attracted the attention of growers.

In [19-20] carried out in Azerbaijan on chestnut soils of Karabakh steppe it has been found that introduction of clinoptilolite-bearing tuffs of a local deposit (Ai-Dag) into the soil increased the water-content in the latter.

In this case, moisture of the soil in an arable layer (a month prior to the harvesting) changed in a wide range depending on the dose of the applied zeolite. On non-irrigated plots of these soils, moisture in the control against the background of NPK totaled 8.26 %, enrichment of the soil by zeolite in the amount of 5, 10 and 20 t/ha has led to the increase in moisture up to 11.50; 15.38 and 21.79% respectively. The same regularity was observed on irrigated plots: 12.99%, 18.56%, 22.12%, 20.80%. On the average, over three years of use of the same doses of zeolites on non-irrigated plots, the moisture of soil increased from 21.2% up to 24.0; 25.4; and 27.8%; and on irrigated - from 25.3 up to 29.6; 30.5; and 32.2%.

A similar fact is observed on soddy-podzolic soils of Ukraine [16]. On the average over five months of the vegetative period (1980), application of zeolites in the amount of 10; 20; 30 and 50 t/ha against the

background of NPK, moisture of soil exceeded that of the control by 6.7; 13.3; 9.2 and 10.8 %. Increase in norms of zeolites up to 30 and 50 t/ha has not led to an adequate change in moisture compared to 10 and 20 t/ha. It should be noted that the positive influence on the increase of water-content in soils and their retention capacity is evidenced with all types of soil.

Application of zeolites to the soil promotes improvement of some of its physical and chemical properties. So, it is shown [21-22] that as a result of enrichment of serozemic-meadow soil of Shirvan steppes (Azerbaijan) with clinoptilolite-containing tuff, granulated in 0.5-1.0 mm, in a dose of 5 t/ha, contributed to the improvement of such indices of soil as aggregation, swelling, and filtration capacity. The quantity of agronomically valuable aggregates of 1-10 mm size in an arable layer has increased up to 75.25 % in comparison with the control (51.08 %); but aggregates of greater sizes <25 mm – 96.13 % (in the control – 81.62 %), attesting to the aggregation (structuration) of the soil.

The size of swelling in an arable layer, on the contrary, has decreased to 6.9 % (in the control 8.9 %), filtration capacity has increased within 9 min from 13 ml (in the control) to 23.7 ml. The same effect was obtained by application of clinoptilolite-containing tuff to the chestnut soil of Azerbaijan in the amount of 5, 10 and 20 t/ha [22]. Thus, positive influence of zeolites is more clearly shown on non-irrigated soil than on its irrigated counterpart and depends on the dose of zeolites used. The amount of water-stable micro aggregates of 1.0–0.25 mm in size has noticeably increased, and the difference between the contents of these aggregates in the control and non-irrigated plots amounted to 5.7 %; but that on irrigated one to only 1.9 % (the norm of the used zeolite – 10 t/ha). On non-irrigated plots the swelling decreased from 8.5 % (in the control) to 5.5 %, and that on irrigated one from 11.6 up to 7.8 %. Filtrational properties of the arable layer have noticeably improved. Thus, whereas on the non-irrigated plots it amounted to 21.3 ml/10 min, after application of zeolites it increased up to 39 ml/10 min. A similar pic-



ture was observed on irrigated plots as well: a maximal increase of these parameters (from 43.6 ml/10 of min up to 65.2 ml/10 min) took place.

The researches carried out in Georgia established that application of clinoptilolite-containing tuffs to acidic soil, characteristic of the humid subtropics of Western Georgia, contributed to the formation of giant (up to 50-60 mk) amoebas, being an indirect evidence of the increase in porosity of soil and improvement of its structure [15]. In a later work [23], it has been shown that enrichment of acidic soil of Kolkheti lowland (belonging to the category of light-clay) by natural zeolite - laumontite (20 t/ha) reduces the content of physical clay from 62 % to 58 %, transferring it to the category of heavy loam. The factor of structure formation in this case increases from 76.9 up to 80.6 %; but the total porosity of the test plots from 52.3 % up to 55.5 %.

Bulgarian scientists [24] made an attempt to recultivate yellow and green clay by means of clinoptilolite-containing tuffs. By laboratory experiments, it has been established that the total porosity increased from 43 up to 49.6 % and approached the control variant - 51.80 (humus layer of soil without fertilizers).

Fertility of soils in many respects depends on the exchange-absorption capacity of the arable layer (absorbing complex). In the scientific literature the terms "absorbing capacity", "cation-exchange capacity" [11, 12] and sometimes "capacity of base exchange" [25] are used for its designation. These terms imply the total amount of all absorbed (exchange) cations which can probably be ejected from soil. This index is expressed in milligram-equivalents per 100 gram of soil. Reaction of soil solution, dispersity of soil, aggregation ability, and stability of an absorbing complex to the destructive action of water in the process of soil formation depends on the composition of the absorbed cations. The absorbed H^+ , Al^{3+} and especially Na^+ contribute to destruction of the absorbing complex, reduction of the ability of retention and fixation of humus substances. Saturation of the absorbing com-

plex by calcium, on the contrary, provides favorable conditions for plants by protecting the absorbing complex from destruction, promotes its aggregation and fixation of humus in it. Therefore, calcium is called "guard" of fertility [11]. As the cation composition of zeolites is identical with the cations of the absorbing complex of soil in composition, its enrichment with zeolite-containing rocks seems advisable. Utilization of zeolites with prevailing Ca^{+2} composition, (for example heulandites or laumontite) is desirable. In the case of utilization of clinoptilolite for this purpose, samples differing by high content of Ca^{+2} and K^+ and absence or negligible content of Na^+ should be selected. Thus, application of zeolites to the soil: in the first place, increases many times its cation capacity and in the second place enriches it with "useful" Ca^{+2} . In 1975-1976, the first studies were carried out in Ukraine on soddy-podzolic sandy and sandy loam, for which the absorbing capacity varied within the limits of 3-4 mg-eq/100g soil for sandy and 5-7 mg-eq/100g for sandy loam. Introduction of clinoptilolite-containing tuff to such soil in the amount of 15-30 t/ha increases the content of exchangeable cations and absorbing capacity by 15-25 % which is stably observed for five years [25]. In this case, enrichment of the absorbing complex occurs at the expense of calcium, potassium and magnesium. In [14], carried out on soddy-podzolic soils under influence of 10 % zeolite, cation exchangeable capacity increased from 15.2 up to 34.6 mg-eq/100g of soil (more than twice), and the sum of the absorbed bases - from 6.5 up to 15.8 mg-eq/100g of soil. The calcium content in the soil increased 2-3 times, but magnesium content decreased 5-8 times.

The same effect was observed by application of the calcium form of natural zeolite khongurin in acidic, podzolic, sandy loam and boggy-upper soils of Yakutia [17]. In the first case, at application of zeolite in the amount of 50 t/ha against the background of NPK, the sum of the exchangeable cations increased from 15 (in the control) to 24.2 mg-eq/100g of soil, the amount of calcium has increased 2.5 times. In the second case, with application of 100 t/ha khongurin

the sum of exchangeable cations increased from 35.3 to 69.8 mg-eq/100g of soil, and the amount of calcium and magnesium – 2.0 and 2.3 times. Such positive effect is observed independently of the type of soil. Thus, application of zeolite in the amount of 10 t/ha to chestnut soils of Azerbaijan led to an increase of the sum of the absorbing bases in comparison with the control; but further increase in doses of zeolites does not exert an influence on this index [22].

Application of zeolite-containing rocks exerts a certain influence on the content of such nutritious elements as NH_4^+ and K^+ . At application of clinoptilolite-containing tuffs to soddy-podzolic soils, an increase in the fixed ammonium (~77 %) and creation of the best conditions for its assimilation by plants is observed; the process of nitrification is slowed down; loss of nitrogen by washing away and denitrification is reduced [16]. Introduction of zeolite-containing rocks in the amount from 5 up to 15 t/ha in meadow, grey, heavy-loamy soil of the Far East contributed to the adsorption of ammonium on the average more than 50 % in comparison with the control (untreated plots) [26]. By laboratory studies it has been established that at introduction of 15 % clinoptilolite-containing tuff to red and podzolic soils of Georgia, the absorption capacity of potassium increases almost three times [14].

Microorganisms, living in the soil, considerably contribute to soil fertility. Accumulation of organic substances, formation of humus in the arable layer depend on the number of these microorganisms and their composition. Activity of microorganisms is determined by a number of factors, such as: humidity, temperature and acidity of the soil, and so on. Application of mineral, and especially organic, fertilizers exerts a certain influence on the increase of their number in the soil [27]. In the second half of the last century, biological activity of zeolites was also revealed. It was shown that their application to the soil increased the number of microbial coenosis [15]. A number of studies were carried out in this direction.

In the laboratory investigations carried out in 1984, the dynamics of the variation of the number and biomass of microorganisms in acidic soil under the influence of clinoptilolite-containing tuff and peat [28] was studied. Duration of the experiment: 22 days. The best results were obtained for the mixture soil+clinoptilolite in the ratio 8.5/1.5. The weight of the formed bacteria for this period of time amounted to 5.32 mg/g. The weight of the bacteria in the control (on pure soil) was 2.69 mg/g. The increase in number of microorganisms has pulsating character. Such fluctuations are probably caused by periodic reproduction and necrosis of microorganisms during the experiment.

Biological activity of zeolites became apparent in the process of their impact on the decomposition of organic substances in soil (red) [29, 30]. To determine the dynamics of decomposition of organic substances in the soil, such highly informative index as rate of release of CO_2 from the surface of the soil in a unit of time, so-called respiration of soil, has been used [11]. Laboratory studies [29, 30] established that application of clinoptilolite-containing tuff to an acidic soil in the amount of 10-20 % sharply increased the intensity of decomposition of organic substances in comparison with the control (soil without fertilizer) 3.2-5.0 times and thus worsened the agronomical properties of the soil. Application of the same amount of peat practically does not exert any influence on this process. At application of a mix of clinoptilolite (20 %) and peat (20 %), the intensity of the process of decomposition of organic substances in the soil increased only 1.8 times in comparison with the control. This contributed to more regular decomposition of organic substances and created favorable conditions for growth and development of plants.

The positive effect of zeolites on the increase of the number of microorganisms in the soil depends on the type of the latter as well. Application of 10 % clinoptilolite-containing tuff to humus-carbonated soil even causes slight decrease in the number of the microflora to 880 thousand/g of soil (in the con-



trol 890 thousand/g of soil). Application of the same doses of zeolites to podzolic and red soils doubled the number of the microorganisms in the soil in comparison with the control 1646 and 1642 thousand/g of soil (in the control 830 and 820 thousand/g of soil) [30].

In the presence of natural zeolites in the soil, not only an increase in the number of microorganisms but also change of their qualitative composition have been observed. Thus, in acidic soils containing 15 % clinoptilolite, mycolytic bacteria dominate, inducing lysis (eating up mold fungi) and reducing their content 2-3 times [15]. Almost threefold increase in the number of actinomyces that have bacterial activity and therefore contribute to the sterilization of soil from undesirable microflora has also been noted. The fact of positive influence of zeolites on the increase in the number of blue-green algae and azotobacter in soils, which play an important role in atmospheric nitrogen fixation and their conversion into forms that are available for plants has been established also. Only in acidic soils the number of azotobacter increased by 30-40 % [15].

Similar field experiments fully confirmed the laboratory study of change in the qualitative composition of microflora under the influence of natural zeolites.

By the experiments carried out in Azerbaijan [31] in 1985-1987, it was shown that application of 10 t/ha clinoptilolite-containing tuff to mountain-gray-brown soils increased the number of microorganisms from 5707 thousand/g soil in the control (soil without fertilizer) up to 6901 thousand/g soil; and the number of actinomyces increased 1.4 times. The same effect was observed on soddy podzolic soils of Ukraine [16]. After application of 10 t/ha zeolite-containing tuff to this soil only once, increase in the number of microorganisms from 3844 thousand/g soil in the control against a background of NPK and manure up to 6139 thousand/g soil took place even in the third year of the experiment. It is necessary to note that the number of actinomyces increased 2.5 times, and

the number of ammonium fixators was doubled compared to the control.

By the field experiments carried out on the grey-brown soils of Eastern Georgia in 1989-1992, [30] it was established that introduction of organo-zeolitic fertilizers (a mixture of clinoptilolite-containing tuff and fresh poultry manure) in the ratio 1:1 also contributed to the increase in the number of such microorganisms as nitrogen fixers. From the obtained results it follows:

1. Introduction of these fertilizers in the amount of 20-40 t/ha into soils increases the number of nitrogen fixers to a greater extent than utilization of mineral fertilizers ($N_{60}P_{60}K_{15}$ kg/ha);
2. Increase in the doses of the applied organo-zeolitic fertilizers contributed to the increase in the number of microorganisms in the soil;
3. Vital activity of nitrogen fixers in the autumn-winter period is noticeably decreased in the control soil and in soils with mineral fertilizers that takes place with application of organo-zeolitic fertilizers but to a lesser extent.
4. Considerable effect of the after-action in the case of utilization of organo-zeolitic fertilizers has been noted: in 1991, the number of microorganisms almost doubled in comparison with that in 1990.

A similar regularity was observed in the case of application of organo-zeolitic fertilizers in acidic soils characteristic of humid subtropics of Western Georgia in 1989-91 [32]. The total number of microorganisms increased 1.5-2.0 times in comparison with the control against a background of mineral fertilizers $N_{60}P_{60}K_{45}$.

At present, there are a few works about the possibility of utilization of natural zeolites to combat diseases, pests and weeds of crops. However, the necessity of development of this direction is seen to be prospective in some of them.

In the work of Russian scientists [33] it has been shown that application of natural zeolites to soil prevents disease of the root system of plants and holds back the development of diseases. Vegetative laboratory tests have shown that zeolites reduce lesion of sprouts of ginseng and purple coneflower with

root rots. Application of zeolites in the amount of 2 t/ha (in field conditions) led to the decrease in the number of sick plants in comparison with the control by 30 % for ginseng and 15 % for coneflower. This is apparently related to the fact that zeolites increase the physiological and biological activity of soils, their aeration and normalization of water balance. Also it has been found that growing of seeding of common valerian on a substratum-containing zeolite, decrease lesion of plants by root rots up to 4.9 %; in the control (sand-peat-soil) it amounted to 14.8 %.

In Italy [10] natural zeolites have been used as dusting agents to kill aphids affecting fruit trees. The mechanism of this reaction is not known: the zeolite could act as a desiccant, although it is almost completely saturated with water before use, or its highly alkaline character in water could simply kill individual insects that come in contact with it.

Laboratory investigations have been carried out in Georgia to study the influence of natural zeolites on germination of seeds of wheat and weeds, characteristic of this culture [34]. In vegetative vessels filled with podzolic soil (control) and the same soil enriched with finely ground clinoptilolite-containing tufts in the amount of 5, 10, and 15 %, were sown with wheat and weeds. Germination of weeds in the control was found to be 100 %, and that of wheat - 91%. Along with enrichment of the soil with zeolite, the germination of weeds decreased to 77.5 %, while the germination of wheat increased up to 97 %.

Thus, from the analysis of numerous studies of the utilization of natural zeolites in plant-growing it follows that all the three propositions presented in the monograph of G.Kahnt [2] in many cases can be carried out by means of natural zeolites of sedimentary origin - an inexpensive and available mineral raw material.

მემცენარეობა

ბუნებრივი ცეოლითები - ქიმიური აგრონომიიდან ბიოლოგიურზე გადასვლის ერთ-ერთი შესაძლებლობა

თ. ანდრონიკაშვილი*, მ. ზაუტაშვილი**, ლ. ეპრიკაშვილი**, ნ. ბურკიაშვილი**, ნ. ფირცხალაუა**

* აკადემიკოსი; თ. ჯგერაძის სახ. თბილისის სახელმწიფო უნივერსიტეტი, პ. მელიქიშვილის ფიზიკური და ორგანული ქიმიის ინსტიტუტი, თბილისი.

** თ. ჯგერაძის სახ. თბილისის სახელმწიფო უნივერსიტეტი, პ. მელიქიშვილის ფიზიკური და ორგანული ქიმიის ინსტიტუტი, თბილისი.

სტატიაში განხილულია ქიმიური აგრონომიიდან ბიოლოგიურ მიწათმოქმედებაზე გადასვლის ზოგიერთი ასპექტი. დიდი ყურადღება ეთმობა მემცენარეობის პრაქტიკაში სედიმენტაციური წარმოშობის ბუნებრივი ცეოლითების გამოყენებას. XX ს-ის ბოლოს და XXI ს-ის დასაწყისში ჩატარებული კვლევების ანალიზის საფუძველზე დადგენილია ნიადაგში შეტანილი ბუნებრივი ცეოლითების დადებითი ზეგავლენა მის ფიზიკურ-ქიმიურ თვისებებზე, ბიოლოგიურ აქტიურობასა და პროდუქტიულობაზე.



REFERENCES

1. W.E.H. Blum, S. Nortcliff (2011), *Annals of Agrarian Science*, **9**, 4: 9-15.
2. G. Kahnt (1988), *Biologicheskoe rasteniyevodstvo: vozmozhnosti biologicheskikh agrosistem*, 209 (in Russian).
3. M.A. Kardava, G.V. Tsitsishvili, T.G. Andronikashvili (1988), *Primenenie klinoptilolitsoderzhashchikh tufov v rasteniyevodstve*, Tbilisi, 34-61 (in Russian).
4. B.P. Loboda (2000) *Agrokimiya*, 6: 78-91 (in Russian).
5. D.W. Ming, E.R. Allen (2001), *Rev. Mineralogy and Geochemistry*, 45: 615-654.
6. P.S. Leggo, B. Ledesert (2009), in: *Fertilizers: Properties, Applications and Effects*. Nova Science Publishers USA, New York, 223-239.
7. T.G. Andronikashvili, T.F. Urushadze (2008), *Chemical and Environmental Research*, **17**, (3-4): 311-339.
8. T.G. Andronikashvili, T.F. Urushadze (2010), *Annals of Agrarian Science*, **8**, 2: 8-19.
9. G.V. Tsitsishvili, T.G. Andronikashvili, G.N. Kirov, L.D. Filizova (1992), *Natural Zeolites*. Ellis Horwood, England, 295.
10. E.A. Mumpton (1999), *Proc. Nat. Acad. Sci., USA*, 96, 3463-3470.
11. G.D. Belitzina, V.D. Vasiljevskaya, L.A. Grishina et al. (1988), *Pochvovedenie*, Ch. I, Moscow, 400 (in Russian).
12. *Agronomiya* (1982), Moskva, 574 (in Russian).
13. E.G. Filcheva, G.D. Tsadilas (2002), *Communications in Soil Science and Plant Analysis*, **33**, 3-4: 595-607.
14. Nguen Van Bo (1988), *Doklady VASKhNIL*, 12: 39-40 (in Russian).
15. M.K. Gamisonia, T.G. Andronikashvili, A.V. Rusadze (1988), *Primenenie klinoptilolitsoderzhashchikh tufov v rasteniyevodstve*, Tbilisi, 85-116 (in Russian).
16. A.I. Kisel (1985), *Zemledelie*, Kiev, 22-27 (in Russian).
17. A.P. Chevichelov, A.K. Konorovskiy, D.R. Shindler (1993), in: *Perspektivy primeneniia tselolitovykh porod mestorozhdeniia Khonguruu, Iakutsk*, 47-57 (in Russian).
18. G.V. Mazur, G.K. Medvid, T.I. Grigora (1984), *Pochvovedenie*, 10: 73-78 (in Russian).
19. I.Sh. Iskanderov (1979), *Pochvovedenie*, 10: 126-129 (in Russian).
20. I.Sh. Iskanderov, S.N. Mamedova (1989), in: *Occurrence, Properties and Utilization of Natural Zeolites*. Akademiai Kiado, Budapest, Hungary, 717-720.
21. I.Sh. Iskanderov, S.N. Mamedova, A.N. Yusifov (1989), in: *Materiyaly Vsesoyuznoi nauchno-tekhnicheskoi konferentsii po dobyche, pererabotke i primeneniui prirodnykh tselolitov*, Tbilisi, 288-290 (in Russian).
22. S.N. Mamedova (1984), *Abstract of a Doctoral thesis*. Baku, 22 (in Russian).
23. L. Gvasalia (2006), *Abstract of a Doctoral thesis*. Tbilisi, 71 (in Russian).
24. K.D. Dimitrov, P.T. Treikiashki, K.I. Chakalov (1986), In: *Trudy 4-yogo Bolgarsko-Sovetskogo Simpoziuma po prirodnykh tselolitam*. Burgas 1985, BAS: 379-384 (in Russian).
25. T.I. Grigora (1985), *Zemledelie*, Kiev, 31-35 (in Russian).
26. E.N. Iakovlev, A.M. Rubtsov, V.P. Basisty, A.A. Fedorov (1991), *Ispol'zovanie prirodnykh tselolitov v narodnom khoziaistve*, Novosibirsk, 110-118 (in Russian).
27. Ye.N. Mishustin, V.T. Yemtsev (1978), *Mikrobiologiya*, M., 368 (in Russian).
28. G.V. Tsitsishvili, T.G. Andronikashvili, M.K. Gamisonia, et al. (1985), *DAN SSSR*, **284**, 4: 983-985 (in Russian).
29. G.V. Tsitsishvili, T.G. Andronikashvili, M.K. Gamisonia, et al. (1984), *Vestnik AN GSSR. Biological series*, **10**, 5: 356-359 (in Russian).
30. T.G. Andronikashvili, G.V. Tsitsishvili, M.A. Kardava, M.K. Gamisonia (1999), *Proc. Georg. Acad. Sci., Chem. series*, **25**, 3-4: 243-252.
31. Ya.Ch. Mustajafayev (1990), *Abstract of a Doctoral thesis*. Baku, 20 (in Russian).
32. T.G. Andronikashvili, M.A. Kardava, M.K. Gamisonia (1997), *Natural Zeolites - Sofia'95*, Pensoft: Sofia-Moscow, 111-112.
33. G.P. Pushkina, P.M. Lyan, L.M. Bushkovskaia, L.I. Krimova (1996), *Khimiko-Farmatsevticheskii Zhurnal*, 9: 24-26 (in Russian).
34. T. Oglishvili, I. Shatirishvili, T. Andronikashvili (1998), *Bull. Georg. Acad. Sci.*, **152**, 2: 300-302.

Received February, 2012

Biochemistry

Isolation and Biochemical Characterization of Mannose-Specific Lectin from Georgian Endemic Plant *Polygonatum obtusifolium* Misch. rhizomes

Nino Dumbadze*, Nugzar Aleksidze**, Giorgi Alexidze*

* St. Andrew the First-Called Georgian University of the Patriarchy of Georgia, Tbilisi

** Academy Member; St. Andrew the First-Called Georgian University of the Patriarchy of Georgia, Tbilisi

ABSTRACT. From the Georgian endemic medicinal plant *Polygonatum obtusifolium* Misch. rhizomes hemagglutinin (lectin SABA-1) was separated and partially purified. It was revealed that minimal hemagglutinating activity of lectin is 0.01 mg/ml. SABA-1 is a thermostable protein and maintains hemagglutinating activity during 15 min incubation at 60°C. Hemagglutinating activity of lectin SABA-1 is inhibited by mannose, α -methylmannopyranoside and N-acetyl-D-glucosamine. Lectin SABA-1 belongs to the mannose-specific lectins class. © 2012 Bull. Georg. Natl. Acad. Sci.

Key words: lectins, *Polygonatum obtusifolium* Misch. rhizomes, mannose-specific lectin.

Introduction. It is well known that biologically active compounds are widely used in biology, medicine, agriculture and in other fields of science. The available literature shows that most important class of these compounds is information carrier and information decoding – carbohydrate contains biomolecules (glycoproteins, glycolipids, glycolipoproteins, etc.) and carbohydrate binding proteins – lectins [1].

The first plant lectin was discovered in 1888 by H. Stillmark. To date hundreds of plant lectins have been isolated and biochemically characterized. Because of the unique property (specifically binding to carbohydrates and carbohydrates containing biomolecules) of lectins they are successfully used as exploration tools, affinity adsorbents for the isolation of various glycoproteins, cells and organelles.

Lectins as specific biological probes have found much use in studies of the membrane carbohydrate topography, in medicine and criminalistics as a diagnostic means [1]. Special interest of scientists was stirred by the ability of lectins for cell proliferation, having hormonal, toxic, immunomodulatory, antitumor, antiviral and other functions [2-4]. Thus, isolation of new plant lectins and ascertaining their biological role still remains one of the topical biomedical problems. Therefore, we carried out experiments to identify lectins from the Georgian endemic medicinal plant *Polygonatum obtusifolium* Misch. and study some of their biochemical properties.

Material and Methods.

The underground parts of rhizomes of *Polygonatum obtusifolium* Misch., which is extensively used in folk

medicine due to their essential medicinal properties, served as the object of this study. With the aim of lectin extraction the plants rhizomes were homogenized. For extraction PBS solutions of different composition were used:

- 1) 0.9% NaCl, 40 mM K⁺-phosphate buffer, pH 7.4
- 2) 0.9% NaCl, 40mM K⁺- phosphate buffer 0.1% b-mercaptoethanol (β-M), pH 7.4
- 3) 0.9% NaCl, 40mM K⁺- phosphate buffer, 1% polyvinylpyrrolidon (PVP), pH 7.4;
- 4) 0.9% NaCl, 40mM K⁺- phosphate buffer, 0.5 mM phenylmethylsulfanylfluoride (PMSF), pH 7.4.

To choose the optimal extraction conditions we took into account the ratio of crude material and extraction solution (w/v=1/5; 1/10; 1/20), pH (5.0; 6.0; 7.0; 7.4; 8.0; 9.0) and incubation time (15; 30; 45; 60 min). The homogenate was placed on magnetic stirrer in accordance with the extraction time at room temperature. The mixture was filtered using cheese cloths and the filtrate was centrifuged at 16 000 g/min for 15 min. For partial purification the supernatant was fractionated with ammonium sulfate under 0-20, 20-40, 40-60, 60-80, 80-100% saturation. The separate suspension was centrifuged at 10 000 g for 20 min at +4°C ("Beckman" SW-27 rotor). The precipitate was dissolved in a minimal volume of extraction solution, was homogenized and centrifuged at 5 000 g (centrifuge TY5.375-4172-78, rotor PY180) for 15 min. The supernatant was filtered through Whatman CF/C and sinpor-0.45-0.22 mkm filter and ammonium sulfate was removed with dialysis on G-10 Sephadex column (50x2.7 cm). Extracts were stored at +4°C.

Lectin activity was determined visually using 96-well immunological microtiter U-plates using a hemagglutination test on rabbits trypsinized erythrocytes with the method of Takatsy [5]. Lectin hemagglutinating activity (HA) was estimated according to that minimal protein concentration (mg/ml) which shows full agglutination of rabbits trypsinized erythrocytes. In order to estimate lectin activity we used also a specific activity (ml/mg) which is its inverse value and reflects the minimal concentration

which still causes agglutination: $SA = T^{-1} \times C^{-1}$, where T⁻¹ (titer) is the degree of minimal protein concentration in which agglutination is still noticeable (6), C is protein concentration expressed in mg/ml. Lectins content was judged by the ratio of overall protein content to lectin activity (conventionally agglutination unit, hemagglutination unit – HU) or by the formula $GAA = 1/Tm$ (T - titer of lectin hemagglutinating activity; m - mass of the used fragment of *Polygonatum obtusifolium*).

Lectin activity kinetics was measured in hemagglutination medium by the photocolometric method, at 670 nm light, a 200 μl 2% suspension of trypsinized erythrocytes was introduced into the control and testing cuvettes. Lectin fraction was added into the testing cuvette and PBS of the same volume to the control one. In the control cuvette of light transmission at 670 nm was considered as 100% and variation of this index was fixed with an automatic recorder connected with a photo colorimeter (KФК-3). The influence of H⁺ ions concentration on lectins hemagglutinating activity was studied in the pH 2.0 – 10.0 ranges PBS, at 1 unit intervals. The extracted protein was titered according to a decreasing concentration on immunological plates, in the relevant pH of PBS. Agglutination was studied in 2% suspension of rabbit's trypsinized erythrocytes that had been prepared on pH changed buffer.

To study lectin thermostability the purified protein fractions were incubated in a water bath at the temperature 20, 40, 60, 80 and 100°C for 10 min. The thermally treated samples were cooled in the ice bath (15min) and centrifuged in order to remove the denatured protein sediment (1500 g/15min). Hemagglutinating activity was measured in supernatants at room temperature.

Lectin specificity in relation to carbohydrates was studied by means of the hapten-inhibitory method [7]. For the analysis we used 0.6 M solution of monosaccharide prepared on PBS. In the experiments 18 different carbohydrates were used: D-galactose, methyl-D-galactose, α-methylmannopyranoside, D-

Table 1. The influence of extraction time and different extraction solutions on the protein concentration and hemagglutinating activity of *Polygonatum obtusifolium* rhizome extracts

Composition of PBS	Time (min)	Titer	Protein concentration (mg/ml)	Lectin activity (mg/ml)	Specific activity (ml/mg)
PBS 0.9%NaCl + 40mM KH ₂ PO ₄ pH 7.4	15	2 ³	0.720	0.023	11.1
	30	2 ³	0.752	0.024	10.6
	45	2 ³	0.816	0.026	9.8
	60	2 ³	0.832	0.026	9.6
PBS 0.9%NaCl + 40mM KH ₂ PO ₄ 0.1% β-M pH 7.4	15	2 ⁴	0.976	0.015	16.4
	30	2 ⁵	1.264	0.010	25.3
	45	2 ⁵	1.408	0.011	22.7
	60	2 ⁵	1.648	0.013	19.4
PBS 0.9%NaCl + 40mM KH ₂ PO ₄ 1% PVP pH 7.4	15	2 ⁴	0.992	0.016	16.1
	30	2 ⁵	1.336	0.010	24.0
	45	2 ⁵	1.352	0.011	23.6
	60	2 ⁵	1.344	0.010	23.8
PBS 0.9%NaCl + 40mM KH ₂ PO ₄ 0.5mMPMSF pH7.4	15	2 ⁴	0.872	0.013	18.3
	30	2 ⁴	1.072	0.016	14.9
	45	2 ⁴	1.160	0.018	13.8
	60	2 ⁴	1.208	0.019	13.2

p<0.01

mannose, D-raffinose, D-glucose, D-ramnose, N-acetyl-D-glucosamine, N-acetyl-D-galactoseamine, D-galacturonic acid, D-fructose, L-inositol, D-arabinose, L-ribose, Melibiose, D-lactose, D-cellobiose, Saccharose.

Sugar solution was titrated from 200 mM with decreasing concentration, on the immunological plates. Equal concentration of 1:4 titer lectin solutions was introduced in all cells of the plate. Hapten specificity was estimated by that minimal concentration of sugar (mM) which resulted in inhibition of lectin hemagglutinating activity. Protein concentration was measured by the method of Lowry, et al. [8].

Results and Discussion

In the first series of experiments we studied the effect of different solutions, widely varying the composition and extraction time on hemagglutination activity of extracts from *Polygonatum obtusifolium* rhizome lectin - SABA-1. As seen from Table 1, hemagglutinating activity of lectin -SABA-1 is completely extracted by PBS (0.9% NaCl, 40 mM K⁻ phosphate buffer 0.1% β-mercaptoethanol (β-M), pH 7.4), extraction time was 30 min, the minimal concentration of protein causing agglutination was 0.01 mg/ml, its

specific activity index was highest 25.3 ml/mg. Introduction of PMSF into extraction solution did not alter the extract's hemagglutination and specific activity, suggesting stability of SABA-1. Introduction of PVP into extraction solution did not change hemagglutinating activity of SABA-1.

As seen from Table 1, in the case of PBS use of (0.9%NaCl + 40mM KH₂PO₄ 0.1% β-M pH 7.4) as extraction solution (extraction time 30 min) there occurs maximal separation of the protein with lectin activity.

It is known from the literature that during visual determination of lectin activity, by the Takatsy microtitration method, apparent hemagglutination is frequently recorded. Namely, it is known that this kind of artefacts may be elicited by polysaccharides, phenol compounds and also by damaged immunological plates. In order to avoid this, we have used the photocolorimetric method to determine the kinetics of the hemagglutination process.

Fig. 1 shows that in control (erythrocytes without lectin) and in testing (erythrocytes in the presence of lectin) erythrocytes sedimentation kinetics is of reciprocal character. In particular, in testing

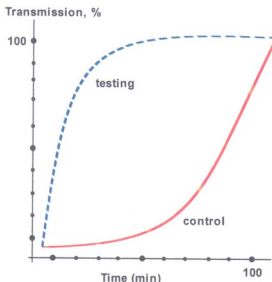


Fig. 1. Kinetics of SABA-1 lectin hemagglutinating activity.

Control: trypsinized erythrocytes without lectin;
Testing: trypsinized erythrocytes in presence of lectin.

transmission rises rapidly and achieves maximum (100%) after 40 min, in control, the same index is recorded only after 90 min, this is induced by a fast agglutination of erythrocytes by SABA-1, as a result sedimentation and transmission are rapidly increased.

In the next series of experiments we studied the influence of different extraction solution volumes (crude material/PBS – 1/5, 1/10, 1/20) on the lectin SABA-1 content in *Polygonatum obtusifolium* rhizome extracts (Table 2).

The results presented in Table 2 show that the most optimal ratio between the weight of *Polygonatum obtusifolium* rhizome and extraction solution volume is 1/20 (g/ml). With the use of extraction solution of this ratio one can fix the highest indices of lectin content in extracts of plant tissue (0.0156).

Lectin activity is changed depending on a wide

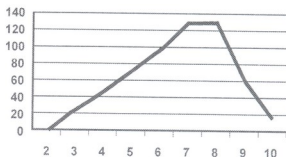


Fig. 2. The influence of H^+ ion concentration on lectin SABA-1 hemagglutinating activity. On ordinate – hemagglutination titer. On abscissa – pH

range of pH. We have experimentally studied the effect of various pH on SABA-1 lectins hemagglutinating activity within 2.0-10.0 range of pH (Fig. 2).

As seen from Fig.2, at pH 7.0-8.0 range the highest hemagglutinating activity of lectin SABA-1 is recorded.

In parallel the effect of temperature on lectin SABA-1 specific activity was investigated (Fig. 3). As reported in the literature, as a rule, most lectins are thermostable and they are used for their purification because lectin stability facilitates their separation from the relatively thermolabile proteins.

As evident from Fig. 3 SABA-1 maintains activity at +60°C under 15 min incubation. With a further rise in temperature there occurs a gradual inactivation of lectin, while at 100°C its hemagglutinating activity becomes completely inhibited (Fig.3). Thus, the results obtained indicate that SABA-1 belongs to the thermostable class of proteins.

Next series of experiments was aimed at partial purification of SABA-1 by ammonium sulfate under varying saturation (Fig.4).

As seen from Fig. 4, the highest specific activity of SABA-1 is recorded in the fractions obtained by

Table 2. The effect of *Polygonatum obtusifolium* rhizome weight and extraction solution volume ratio on the lectin content in plant tissue extracts

Crude material/PBS (g/ml)	Titer	m – mass fragment of the used <i>Polygonatum obtusifolium</i>	Lectin content (GAA=1/Tm)
1:5	2 ⁸	1g	0.0039
1:10	2 ⁸	1g	0.0078
1:20	2 ⁸	1g	0.0156

p<0.01

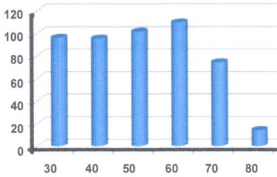


Fig. 3. The effect of temperature on lectin SABA-1 hemagglutination specific activity. On ordinate – specific activity. On abscissa – temperature in °C.

ammonium sulfate saturation from 20-40 to 40-60%. The results indicate that maximal sedimentation of lectin SABA-1 from the extracts of *Polygonatum obtusifolium* rhizome occurs under 0-60% saturation of ammonium sulfate.

In a special series of experiments we studied SABA-1 specificity in relation to carbohydrates (Table 3). To obtain full-value characteristics of lectin it is necessary to ascertain lectin specificity to carbohydrates. Lectins are known to bind with carbohydrates specifically and inhibit lectin-induced hemagglutination. As shown in Table 3, 18 different

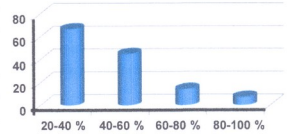


Fig. 4. Fractionation of the extracts from *Polygonatum obtusifolium* rhizome with ammonium sulfate under different saturation. On ordinate – specific activity of SABA-1. On abscissa – ammonium sulfate saturation

carbohydrates were tested in an initial concentration of 200 mM.

The data presented in the table demonstrate that lectin SABA-1 hemagglutinating activity is inhibited only in the presence of mannose, α -methylmannopyranoside and N-acetyl-D-glucosamine. The data obtained indicate that lectin SABA-1 isolated from *Polygonatum obtusifolium* rhizome is attributed to the mannose-specific lectin class.

Conclusion

Lectin SABA-1 has been isolated from the Georgian endemic medicinal plant *Polygonatum obtusifolium*

Table 3. Specificity of lectin SABA-1 to carbohydrates

Carbohydrates (Initial concentration 200 mM)	Inhibition of hemagglutinating activity	Minimal inhibiting concentration (mM) of a carbohydrate
D-galactose	–	
α -methyl-D-galactose	–	
α -methylmannopyranoside	+	25
D-mannose	+	50
D-raffinose	–	
D-glucose	–	
D-rhamnose	–	
N-acetyl-D-glucosamine	+	75
N-acetyl-D-galactosamine	–	
D-galacturonic acid	–	
D-fructose	–	
L-inositol	–	
D-arabinose	–	
L-ribose	–	
Melibiose	–	
D-lactose	–	
D-cellobiose	–	
Saccharose	–	

+ Inhibition of hemagglutinating activity.

– Noninhibition of hemagglutinating activity.

rhizome and has been partially purified. Minimal hemagglutinating activity of lectin SABA-1 is 0.01mg/ml. SABA-1 belongs to the thermostable class of proteins, its specific inhibitors of hemagglu-

tion activity are mannose, α -methylmannopyranoside and N-acetyl-D-glucosamine. Lectin SABA-1 belongs to the mannose specific class of lectins.

ბიოქიმია

საქართველოს ენდემური მცენარე სვინტრიდან (*Polygonatum obtusifolium* Misch.) მანოზა-სპეციფიკური ლექტინის გამოყოფა და ბიოქიმიური დახასიათება

ნ. ლუმბაძე*, ნ. ალექსიძე**, გ. ალექსიძე*

* საქართველოს საპატრიარქოს წმინდა ანდრია პირველწოდებულის სახ. ქართული უნივერსიტეტი, თბილისი
** აკადემიის წევრი; საქართველოს საპატრიარქოს წმინდა ანდრია პირველწოდებულის სახ. ქართული უნივერსიტეტი, თბილისი

საქართველოს ენდემური მცენარე *Polygonatum obtusifolium* Misch.-დან პირველადაა გამოყოფილი და ბიოქიმიურად დახასიათებული მანოზა-სპეციფიკური ლექტინი SABA-1. ლექტინი SABA-1-ის მინიმალური ჰემაგლუტინაციური აქტივობა შეადგენს 0.01 მგ/მლ-ს. SABA-1 თერმოსტაბილური ცილაა და ლექტინურ აქტივობას ინარჩუნებს 15 წუთის განმავლობაში 60 °C-ზე თერმული დამუშავების პირობებში. SABA-1-ის ჰემაგლუტინაციური აქტივობა ინჰიბირდება მანოზით, α -მეტილ-მანოპირანოზიდით და N-აცეტილ-D-გლუკოზამინით. გაკეთებულია დასკვნა, რომ SABA-1 განეკუთვნება მანოზა-სპეციფიკური ლექტინების კლასს.

REFERENCES

1. A. Pusztai (2008). Plant Lectins (Chemistry and Pharmacology of Natural Products). Cambridge University Press, 263 p.
2. R. Hamid and A. Masood (2010). Plant Lectins: A Biochemical study. Lap Lambert Acad. Publishing, 232 p.
3. C.H. Astoul, J.W. Peumans and V. Danime (2000). Biochem. Biophys. Res. Commun., 274: 455-460.
4. S.K. Lam and T.B. Ng (2011). Journal of Phytotherapy & Phytopharmacology, 7: 14-35.
5. I. Liener (1976). Ann. Rev. Plant Physiol., 27: 291-319.
6. G. Takatsy (1967). Symp. Series Immunobiol. Standard, 4: 275-280.
7. T.P. Novak, S.H. Barondes (1975). Biochim. et Biophys. Acta, 393:115-123.
8. H. Lis, N. Sharon (1986). Ann. Rev. Biochem., 55:35-67.
9. O.H. Lowry, N.J. Rosebrough, A.L. Far, R.J. Randall (1951). J. Biol. Chem., 193(1): 265-271.

Received February, 2012

Zoology

New Data on Georgian Species of Freshwater Horsehair Worms (Nematomorpha: Gordiida)

Oleg Gorgadze*, Andreas Schmidt-Rhaesa**, Nunu Kintsurashvili*

* Institute of Zoology, Ilia State University, Tbilisi

** Zoological Museum, University of Hamburg, Hamburg, Germany

(Presented by Academy Member Irakli Eliava)

ABSTRACT. The results of the taxonomic studies of the freshwater hairworms spread at present in Georgia are given in the work. Based on the light and electron microscopic studies species *Gordionus violaceus* Baird, 1853 from the *Gordionus* genus is described for Georgia for the first time. © 2012 Bull. Georg. Natl. Acad. Sci.

Key words: nematomorpha, hairworm, Gordiida, Gordionus, cuticle, areole.

Introduction. Several species of hairworms (Nematomorpha: Gordiida) are described from the Georgian fauna belonging to the three genera: *Gordius*, *Chordodes* and *Spinochordodes*. These species are *Gordius villoti* Rosa, 1882 [1], *Gordius georgiensis* Kirjanova, 1955 [2], *Chordodes oscillatus* Kirjanova, 1953 [3], *Spinochordodes baeri* Kirjanova, 1950 [4], *Gordius* sp. Gorgadze and Kintsurashvili, 2002 [5], *Spinochordodes* sp. Gorgadze, et al., 2008 [6], *Chordodes parabipilus* Kintsurashvili, et al., 2011 [7]. Representatives of the genus *Gordionus* have not been found in Georgia to date.

Material and methods. Hairworms were collected in different localities of Georgia. They were fixed in 70% ethanol. Measurements of the body were taken after fixation of material and cuticle prepara-

tions were prepared for light microscopy studies. Studies of the preparation were performed under a binocular microscope at 100 X 10 magnification: binocular microscope PH 100. Pieces of the cuticle and the posterior end (about 1-2 mm from the terminal tip) were prepared for Scanning Electron Microscopy (SEM). Pieces were dehydrated in an increasing ethanol series, critically point dried and coated with gold in a sputter coater. Observation took place using a LEOSEM 1524 under 10 kV. Digital images were taken.

Results

Gordionus violaceus Baird, 1853

Type locality. One male specimen of the hairworm was collected together with its insect host in a field near a stream, on the territory of Borjomi – Kharagauli National Park (territory of the Romanov's Park). The host insect is *Carabus septemcarinatus* (Coleoptera,

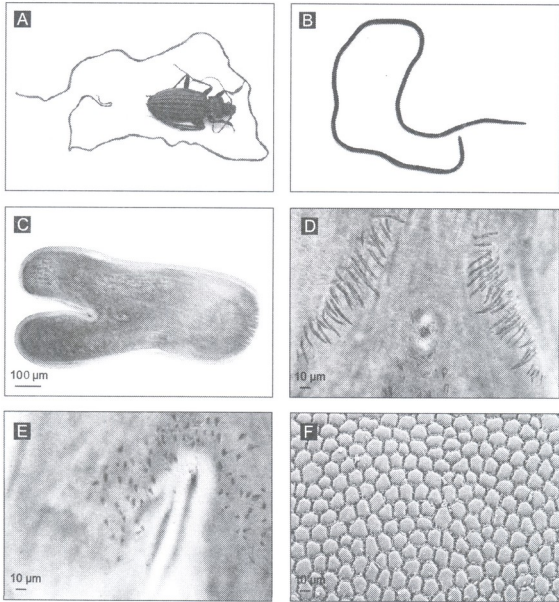


Fig. 1. A. *Gordionus violaceus*. The male specimen together with its insect host (Photo by G. Chaladze). B. Female Specimen. C. Terminal end of the body male. D. Prelocaal rows of spines of the male. E. Conical spines posterior of the cloacal opening. F. Overview of the cuticle with one type of the areoles

Carabidae). A second male specimen was collected from the same location. The host is unknown. Female specimens were collected in a stream, in Borjomi-Kharagauli National Park, Likani village, the host is unknown.

Description. Male. (Fig. 1.A). The length of the body is 235 mm. The body is narrow towards the anterior part. The width is 340 µm. The body widens towards

tail and its maximum width is 1 mm. The body is dark brown. The exception is the anterior part, where the body is whitish. Mouth opening is located in the centre of the apex. Posterior end of the body is divided into two parts and forms two lobes (Fig. 1, C). Tail lobes are longer (300 µm) than their width (213 µm). Cloacal opening is oval. The diameter of the long side of the cloacal opening is 67 µm and of the short side 33 µm. The distance between the cloacal

opening and the base of the lobes is 87 μm . Above the cloaca, a pair of precloacal rows of long spines is arranged on both sides of the middle line of the body (Fig. 1,D). At the beginning, the distance between the two rows is about 75 μm . The rows gradually separate from one another and end in a lateral position. The number of spines in each row is 27-28, the length of spines is 12.5-42.5 μm . Precloacal rows of spines are spread below the cloaca, not reaching the base of the tail lobes (at the level of lobe division). The surface of the hairworm body posterior to the cloacal opening is covered with numerous spines (Fig. 1,E). These are short, sharpened, conical spines 2.5-12.5 μm in length. Postcloacal spines occur in several clusters. They are located immediately below the cloaca and spread on the surface of the tail lobes. Immediately below the cloaca the number of conical spines is about 55-60, 26-30 on each lobe. Conical spines are localized on the medial part of the tail lobes but they are not spread on the terminal part of the tail lobes, conical spines are absent around the cloaca as well.

The cuticle is composed of one type of areoles (Fig. 1,F). Areoles are polygonal in shape and are characterized by some variations depending on the difference in the length and number of facets in them. Areoles in the cuticle are in the form of quadrangles, pentagons and hexagons; they fuse to form one whole layer of the cuticle. The size of areoles varies significantly. The diameter of the long side of the areoles is about 9-24 μm . Areoles are well-defined from each other by interareolar furrows, though in

some cases limits between two areoles are almost indistinguishable. The width of the interareolar furrows is about 2 μm . Sometimes cuticular areoles arrange according to some order and form longitudinal strings. During the examination under the light microscope small, spherical granules and outgrowths surrounding areoles are noticeable. The surface of the areoles is smooth.

Female. (Fig. 1, B). Body colour is brown. Body length of the first specimen is 315 mm, width at the anterior end is 600 μm , the maximum width is 1.6 mm, and at the posterior end of the body it is 600 μm . The length of the second specimen is 165 mm, the width at the anterior end is 180 μm , the maximum width is 1.1 mm and at the posterior end it is 320 μm . The cloacal opening is located at the posterior end. Cuticle structure of the female is identical with that of the male.

Diagnosis. The presence of bilobed terminal end, two fences of long bristles on the precloacal area, fields of numerous, short, conic, spines behind the cloaca and interior to the lobes of the tail side not reaching the tail tips, although cuticle with one type of the irregular, polygonal areoles, the presence of well defined outgrowths and short spines in interareolar furrows in male enables to identify the described specimen of the hairworm as *Gordionus violaceus*.

Acknowledgement. We would like to thank Research Assistant of Ilia State University Giorgi Chaladze for providing material.

ზოოლოგია

ახალი მონაცემები საქართველოს მტკნარი წყლის ბეწვეურების (Nematomorpha: Gordiida) შესახებ

ო. გორგაძე*, ა. შმიდტ-რეაზა**, ნ. კინსურაშვილი*

* ილიას სახელმწიფო უნივერსიტეტი, ზოოლოგიის ინსტიტუტი, თბილისი

** კამბურგის უნივერსიტეტი, ზოოლოგიის მუზეუმი, კამბურგი, გერმანია

პირველად, საქართველოს ფაუნადან რეგისტრირებულია მტკნარი წყლის ბეწვეურების (Nematomorpha: Gordiida) გვარი *Gordionus*. სინათლის და ელექტრონული მიკროსკოპული გამოკვლევის საფუძველზე იდენტიფიცირებულია ამ გვარის ერთ-ერთი სახეობა *Gordionus violaceus* Baird, 1853.

REFERENCES

1. L. Camerano (1896), Monografia del Gordii R. Acad. Torino, 2: 247-419.
2. E. Kirjanova (1955), Trudy Zool. Inst. AN SSSR, 21: 152-160 (in Russian).
3. E. Kirjanova (1953), Soobshcheniia AN Gruz. SSR, 14:101-103 (in Georgian).
4. E. Kirjanova (1950), Trudy Zool. Inst. AN SSSR, 9: 255-280 (in Russian).
5. O. Gorgadze, N. Kintsurashvili (2002), Proc. Inst. Zool. of Georgia, 21: 68-70 (in Russian).
6. O. Gorgadze, A. Schmidt-Rhaesa, N. Kintsurashvili (2008), Bull. Georg. Natl. Acad. Sci., 2, 4: 131 -133.
7. N. Kintsurashvili, A. Schmidt-Rhaesa, O. Gorgadze (2011), Verh. Naturwiss. Ver. Hamburg, 46: 235-241.

Received December, 2011

Parasitology and Helminthology

Arginase in the Organs of Water Snake (*Natrix tessellata*, Laurenti, 1768) and Cestode (*Ophiothaenia europaea*, Odening, 1963) Parasitizing in it

Ketevan Nikolaishvili*, Tsitsino Lomidze*, Lali Murvanidze*

* *Institute of Zoology, Ilia State University, Tbilisi*

(Presented by Academy Member Irakli Eliava)

ABSTRACT. The activity of arginase in the organs of water snake (*Natrix tessellata*) and cestode (*Ophiothaenia europaea*) inhabiting its intestine was determined. pH optimums are established. It was shown that the greatest activity of arginase in water snake was noted in kidneys and the least activity was in the liver. No arginase was detected in the intestine. Considerable activity of the arginase of the parasite is established.

The role of biochemical adaptation of arginase in the system parasite-host is discussed. © 2012 Bull. Georg. Natl. Acad. Sci.

Key words: *Natrix tessellata*, *Ophiothaenia europaea*, arginase.

Studies of adaptational reactions in parasite worms to the habitation medium, have always interested the researchers dealing with biochemistry of helminths [1-3]. Helminths of warm-blooded and cold-blooded animals have often been the object of study. However, these processes have hardly been investigated in the endogenous parasites of snakes and their hosts. Detection of the peculiarities of metabolism in the above animals is very important for comparative biochemistry, biochemistry of helminths and system parasite-host formation. We focused attention on arginase enzyme. A number of studies are devoted to arginase from different tissues of vertebrate animals. It is also found in the body of helminths of different classes and some

researches connect the role of this enzyme with adaptation to parasitizing [2-5].

Proceeding from the integral system parasite-host we considered it to be necessary to determine the activity of arginase of both components using the example of water snake (*Natrix tessellata*, Laurenti, 1768) and cestode (*Ophiothaenia europaea*, Odening, 1963) parasitizing in its intestine. We aimed to find the values of enzyme activity in the organs of host and parasite. The peculiarities revealed are very important for a deeper understanding of interrelations in the system parasite-host.

Materials and Methods. The liver, kidneys and intestines of water snakes and cestodes *O. europaea*

served as material for the investigation. 5 exemplars of water snakes were brought from the territory close to Tbilisi water reservoir and 3 exemplars from the environs of Rustavi.

The animals caught near the water reservoir were all infected with cestodes (invasion intensity is 3-9 pieces), and animals brought from the environs of Rustavi were free of cestodes.

Out of fresh-frozen organs of water snakes and cestodes 2.5% and 5% water homogenates were prepared. After extraction in cold conditions homogenates were centrifuged at 3000 rev/min for 10 min. Sediment was thrown away and supernatant served as a source of enzyme.

The activity of arginase was determined according to the method of Khramov and Galaev [6]. The calculation was done by a calibration curve, constructed on dissolving the standard solution of urea. Specific activity was expressed in μg of urea per mg of protein for 1 hour at 37 °C.

Protein was determined by Lowry [7].

Results and Discussion. In homogenates of tissues of water snake and cestodes *O. europaea* arginase activity was revealed. Arginase helps to decay arginine to ornithine and urea. Enzyme activity is evaluated by the quantity of the latter. The results of evaluation are presented in Table 1. They show that maximal activity was detected in kidneys of the water snake ($197.5 \pm 13.84 \mu\text{g}$ of urea/mg of protein/hour).

Arginase was absent in the intestine and its activity in the liver was quite low, totaling $7.31 \pm 0.89 \mu\text{g}$ of urea/mg protein/hour. Comparing the values of enzyme activity in the liver and kidneys of the snake one may say that high-active arginase is located in the kidneys. Abundant blood circulation ensures both their excretory function and intensive metabolism. Low activity of arginase in liver of the water snake can be explained by the fact that snakes and birds have no system of ureogenesis. Adaptation of these animals to the surface life led to the creation of uricotelism and formation of uric acid as the final product of protein metabolism.

Table 1. Activity of arginase in the organs of water snake and cestode *Ophiothoena europaea* (at pH 9.5)

Object of investigation	Activity of arginase in μg of urea/mg protein/hour
Kidney	197.5 ± 13.84
Intenstine	not revealed
Liver	7.31 ± 0.89
<i>O. europaea</i>	35.95 ± 6.24

Low activity value of arginase in the liver of water snake agrees with the data for arginase of chicken's liver obtained by Sokhina and Koloskova [2]. It should be assumed that liver arginase *N. tessellata* refers to the type of non-ureotelic arginases, which take part in the process of rendering ammonia harmless. Such arginase is an evolutionarily more ancient enzyme with a function independent of ureotelism. Some authors consider that while establishing the "ureotelism" in the liver of amphibians the specific ureotelic arginase is induced, which functions together with the present philogenetically more ancient non-ureotelic arginase [8,9]. Comparing the values of the activity of arginase of liver of the water snake and snake's cestode with the data for arginase of the chicken's liver and her parasite *Ascaridia galli* [2], we noted that these values are very close to each other (Table 2).

From this example we can see that arginine decay in the liver of birds and snakes occurs almost with equal intensity and their arginases possibly fulfill analogous functions. Adaptation of these animals to the medium with limited water content occurred in similar conditions and was reflected on nitrous me-

Table 2. Arginase activity in the liver of water snake and chicken, nematodes *Ascaridia galli* and cestodes *Ophiothoena europaea*

Object of investigation	Activity of arginase in μg of urea/mg protein/hour
Liver of water snake	7.31 ± 0.89
*Liver of chicken	8.62
<i>Ophiothoena europaea</i>	57.05 ± 7.97
* <i>Ascaridia galli</i>	50.51

* According to Sokhina and Koloskova [2]

tabolism. Parallely to this the process of biochemical adaptation of intestine helminths parasitizing in these animals took place. The above mentioned arginase activity and uric acid as the final product of nitrous metabolism can serve as confirmation of this. The latter is produced as a result of purine decay in cestodes [18].

The study of the influence of the concentration of hydrogen ions on the activity of arginase of the water snake organs and *O.europaea* allowed to establish pH optimum of enzymes. For liver arginase it was equal to 7.5 (activity 18.39 μg of urea per mg protein/hour). A similar value of pH optimum was determined for one of the isoforms of arginase plerocercoid *Ligula intestinalis* from fishes [11]. It is known that pH optimum range of arginase can vary from 9 to 10.5. For kidney arginase of water snake it was 9.5 (activity 197.5 μg urea/mg protein/hour).

This value is close to the values of pH optimum of arginases of vertebrate animals [12-14] and some other helminths [11, 15-17]. Arginase activity of cestodes at pH 9.5 was 5.5 times lower than the activity of kidney enzyme and at the same time it almost 5 times increased the level of arginase activity in the liver of water snake. Unlike arginase of liver and kidneys of water snake pH arginase optimum *O.europaea* shifted to more alkalinity and was equal to 10.5, and activity totaled already 57.05 μg urea/mg protein/hour. Such difference in activity at different values of pH, probably points to the change of ionization state of different ionizing enzyme groups, which then influence on catalytic center of the latter.

Comparing enzyme activity in the organs of water snake at optimum value pH, it is shown that high-active arginase is localized in kidneys. It exceeds 27 times the liver enzyme activity. Thus, it is evident that intensity of arginine decay in different organs of water snake differs, taking into account intestines. Products of protein hydrolysis and aminoacids are actively absorbed by mucous membrane of the intestine, then they pass into blood taking part in metabolism of those organs and tissues which have argin-

ase. Adaptation to the medium with abundant quantity of food substances in cestodes inhabiting intestine found reflection not only on their morphology (absence of digestive system) but on metabolism as well. Arginine is easily accessible for *O.europaea*. Arginase activity in hosts intestine was not revealed. Parasite's own arginase activity was significant (Table 1) and almost 8 times exceeded the enzyme activity of water snake's liver. It should be noted that earlier we have revealed acid and alkaline phosphatases in homogenates of water snake cestode. Their activity three times exceeded the level of activity of those enzymes in tapeworm of African hieroglyph python [10]. We suppose that high activity of phosphatase and arginase in *O. europaea* is the reflection of intensity of metabolic processes characterizing the given type of cestode and adaptation to habitat.

It is quite difficult to determine the role of the investigated enzymes, as non-ureotelic arginases have many other functions. They participate in the regulation of a definite quantity of urea, arginine and other guanidine compounds, in proline formation. The latter is involved in biosynthesis of polyamines necessary for division and differentiation of cells [19]. Similar synthetic processes may take place in hosts and their parasites. According to the data by Lee [20] and Brand [21] the function of the arginase of parasite worms is to provide them with proline which is used in collagen cuticle formation. Polyamine synthesis in helminths does not occur and requirements in these substances are completely fulfilled on the host's account [22]. Their fast growth, reproduction system development and great fecundity are probably provided in this way.

At arginine hydrolysis in water snake kidneys and cestode body both in host and parasite considerable quantity of urea and ornithine must be accumulated. It is known that in reptiles and birds osmoregulation occurs via uric acid. Urea as low molecular substance in helminths inhabiting the intestines of sea fishes performs an important function of osmoregulation on cellular level [3,4]. We are not quite



sure about it as to *O. europaea* and water snake, but we suppose that the formed urea might be an agent additional to uric acid, which strengthens osmoregulation process in both host and parasite.

Arginase also takes an active part in adaptation processes in both vertebrate animals (tailless amphibians) at some stages of ontogenetic development [23,24] and in helminths with formation of arginase isoenzymes [5, 25]. Correlation between kinetic and thermodynamic parameters of arginases in nematodes and their hosts [2,3], temperature optimums and thermostability of fishes cestode arginase with temperature homeostasis of host [2,26,27] is also an evidence of adaptation.

On the basis of the above-said we can conclude that non-ureotelic arginases play an important and

diverse role in metabolism emerging as an adaptive factor.

The results of our work showed that arginase activity of water snake is connected with the intensity of arginine decay in the organs in which they are localized. At the same time the level of activity of cestode enzyme attests to the high level of biochemical adaptation of *O. europaea* metabolism to the conditions in the water snake intestine ensuring metabolic balance in the interrelationship of parasite and host.

Acknowledgement. The authors express their gratitude to A.Pataridze and D.Bekoshvili the collaborators of the Institute of Zoology of Ilia State University, for help in collection and delivery of the material.

პარაზიტოლოგია და ჰელმინთოლოგია

წყლის ანკარას (*Natrix tessellata*, Laurenti, 1768) ორგანოებში და ცესტოდაში (*Ophiothaenia europaea*, Odening, 1963) ფერმენტ არგინაზას აქტივობის შესახებ

ქ. ნიკოლაიშვილი*, ც. ლომიძე*, ლ. მურვანიძე*

* ილიას სახელმწიფო უნივერსიტეტი, ზოოლოგიის ინსტიტუტი, თბილისი

(წარმოდგენილია აკადემიის წევრის ი. ელაიასს მიერ)

წყლის ანკარას ორგანოებში და მის ნაწლავში მობინადრე ცესტოდაში განსაზღვრულ იქნა ფერმენტ არგინაზას აქტივობა და დადგინდა pH ოპტიმუმი. ნაჩვენებია, რომ წყლის ანკარას თირკმელებში ფერმენტი აუღენს მაღალ აქტივობას, ღვიძლში – შედარებით დაბალს. ნაწლავში არგინაზა არ იქნა გამოვლენილი. აღინიშნა აგრეთვე პარაზიტის არგინაზას მნიშვნელოვანი აქტივობა. განხილულია მოცემულ პარაზიტ-მასპინძლის სისტემაში ფერმენტ არგინაზას ბიოქიმიური ადაპტაციის როლი.

REFERENCES

1. *FF. Soprunov* (1971), Trudy VIGIS, 17: 9-14 (in Russian).
2. *L.I. Sokhina, T.G. Koloskova* (1978), Trudy GELAN SSSR, 28: 104-108 (in Russian).
3. *O.A. Shishova-Kasatochkina, Z.K. Leutskaia* (1979), in: Biokhimicheskie aspekty vzaimootnoshenii gelmintov i khozaiina, M. 279 p. (in Russian).
4. *O.A. Shishova-Kasatochkina, L.I. Sokhina, T.G. Abramova* (1974), Trudy GELAN SSSR, 24: 250-255 (in Russian).
5. *A.A. Dubovskaia, A.D. Mamatsashvili* (1988), Trudy GELAN SSSR, 36: 85-88 (in Russian).
6. *V.A. Kharamov, Iu. Galaev* (1969), Voprosy meditsin. khimii, 15, 4: 435-439 (in Russian).
7. *O.H. Lowry; N.J. Rosenrough, A.L. Farr, et al.* (1951), J. Biol. Chem., 193:265-275.
8. *M.A. Davtian* (1968), in: Voprosy biokhimii mozga, 4: 237-266, Yerevan (in Russian).
9. *M.A. Davtian, L.A. Petrosian* (1970), Biolog. Zhurn. Armenii, 23, 6: 99-101 (in Russian).
10. *Ts.V. Lomidze, K.G. Nikolaishvili, L.P. Murvanidze, N.O. Melashvili* (2009), in: Actual problems of parasitology in Georgia. X: 12-17, Tbilisi (in Georgian).
11. *A. Mamatsashvili* (2009), Abstract of Doctoral Thesis, Tbilisi (in Georgian).
12. *K.T. Kossmann, K. Lange, F. Menne* (1964), Hoppe-Seyler's Z. Physiol. Chem., 335, (2-6): 250-254.
13. *M.A. Davtian, G.Kh. Buntiatian* (1970), Biokhimiia, 5: 412-415 (in Russian).
14. *I. Gasiorowska, Z. Porembska, J. Iachimowicz, I. Mochnacka* (1970), Acta Biochim. Pol., 17: 19-30.
15. *W.P. Rogers* (1952), Austr. J. Scientif. Research. Ser. B. Biol. Sciences, 5, 1: 210-222.
16. *J.W. Campbell* (1963), Comp. Biochem. Physiol., 8, 1: 13-27, 29-38.
17. *K.G. Nikolaishvili* (1974), Abstract of Candidate Thesis, M. (in Russian).
18. *J.D. Smyth, D.P. McManus* (1989), The Physiology and Biochemistry of Cestodes. Cambridge University Press, 398 p.
19. *O. Heby* (1981), Differentiation, 19: 1-20.
20. *D.L. Lee* (1965), The Physiology of Nematodes. Edinburgh-London, 4-13.
21. *Th. Brand* (1973), Biochemistry of parasites. New York, Academic Press, 499 p.
22. *V. Sharma, B.L. Tekvani, J.K. Saxena, et al.* (1991), Exp. Parasitol., 72, 1: 15-23.
23. *G.W.Jr. Brown, P.P. Cohen* (1959), in: Symposium on the Chemical Basis of Development. Baltimore, Maryland, 495 p.
24. *E.M. Egizarian, E.Kh. Barsegian, M.A. Davtian* (2009), Izv. Agrarnoi nauki, 7, 2: 123-126.
25. *A. Mamatsashvili, N. Melashvili* (2009), Proc. Georg.Natl.Acad.Sci. Ser.Biol., 7, 1-2: 110-115.
26. *A.A. Dubovskaia* (1982), Parasitologiia, 16, 6: 494-497 (in Russian).
27. *A.A. Dubovskaia* (1984), in: Gelminty sel'skokhoziaistvennykh i okhotnich'e-promyslovyykh zhivotnykh, 5-10 (in Russian).

Received April, 2012

Genetics and Selection

“Gorda”- a New Short-Stemmed Botanical and Genetic Variety of Soft Wheat (*Triticum aestivum* L.) Obtained by Induced Mutagenesis

Petre Naskidashvili*, Gulnari Chkhutlashvili**, David Bedoshvili **, Maka Naskidashvili**

* Academy Member; Georgian Agrarian Academy, Tbilisi

** I. Lomouri Institute of Agriculture of the State Agrarian University of Georgia, Tserovani

ABSTRACT. Short-stemmed super dwarf wheat “Gorda” is obtained via treating seeds of the French-bred winter variety “Ducat” (released for distribution in Georgia) by 0.01% solution of chemical mutagenic NMU – nitrosomethylurea. “Gorda” is a mutant form of winter wheat. The plant is bunch forming with reduced numbers and lengths of internodes and its maximal height is 26-27 cm. The leaves are broad and erect. The stems are short, firm and they hardly bend. The spikes are awnless, short (4-5 cm), flat and dense, in which grown underdeveloped florets are densely arranged on the spike rachis. The glumes of the spikelet are convex. “Gorda” is a late variety for as many as 10-12 days as compared to the regular local check varieties. It is susceptible to leaf rust and powdery mildew. Grain is shriveled and therefore the mass of its thousand kernels does not exceed 30 g. Grain raw gluten content is about 27-28%. “Gorda” represents breeding material of new inheriting property, which can be used as initial material for developing short-stemmed varieties with 2-3 height reducing genes. © 2012 Bull. Georg. Natl. Acad. Sci.

Key words: induced mutation, mutant, short-stemmed plant.

Cultivated species of wheat (*Triticum* L.) underwent significant modifications outside the genetic centre or their origin as a result of domestication, but complete reconstruction of plants of each species (variety) was performed by means of natural and artificial, close and remote hybridization of different varieties, sorts, forms and landraces, via possible recombination, interaction of characters of paternal forms and also by means of induced mutagenesis.

The idea of reducing the stem length of soft wheat (*T. aestivum* L.) was first proposed by the famous Italian breeder Nazareno Strampelli nearly 80 years ago [1]. His contribution to this objective is enormous and the first commonly accepted short-stemmed

selection variety of soft wheat (“Ardito” as well as others) was developed by him.

The problem of obtaining short-stemmed and comparatively early sorts of soft wheat was solved by N. Strampelli by crossing Italian and West European high stemmed sorts with Japanese short-stemmed and early sorts. Further significant scientific and practical results in this direction were achieved in Japan, Argentina, Canada, Mexico, as well as in Georgia and its neighbouring countries [2-5].

Versatile scientific investigations and practice have proven that potential capacity for increasing the grain yield of wheat is to a great extent dependent on the reduction of stem height and obtaining

the corresponding short-stemmed varieties.

Scientific investigations and practice clearly demonstrate that 70-90 cm should be assumed as the most favourable height for wheat species. Such height of stem provides not only resistance of a plantation to lodging but also efficient kernel formation.

In parallel to developing short-stemmed wheat species by the method of hybridization plant selection practice successfully applies the method of induced mutagenesis. Hundreds of initial selection materials of cereals, legumes, melons and gourds, technical, forage, vegetable, ornamental and other crops have been obtained by means of affecting seeds and plants with physical and chemical mutagens. On the basis of this material many varieties and hybrids checked (approved) for distribution have been obtained and their number increases annually.

Applying the methods of hybridization and induced mutagenesis, Georgian breeders (L. Dekaprevich, M. Sikharulidze, E. Chernysh, P. Naskidashvili, S. Tedoradze, O. Liparteliani, G. Khutishvili, Z. Jincharadze, G. Chkhutishvili, A. Mdivani, N. Rusitashvili, V. Sukhishvili, I. Saatashvili, A. Makharoblidze, and others) have developed donor varieties which bear valuable economic and biological features and obtained sorts and hybrids which are approved for distribution.

The present work deals with breeding and research of super-dwarf "Gorda" – a completely new donor cultivar, genetic source for breeding of intensive type wheat, winter, spring and facultative wheat cultivars, which can be sown in two terms.

Initial material and methods. Intensive type French-bred variety of winter soft wheat "Ducat" has been chosen as initial material for obtaining the mutant by means of induced mutagenesis. Initial seed material was provided by the germplasm depository of the Department of Genetics and Selection of the I. Lomouri Institute of Farming. Seeds of the mentioned variety were treated with the 0.01% solution of NMU - nitros methyl urea. Seed treatment with the mutagen, sowing, care for the planted site, monitoring of the plot, plant scoring and harvesting were performed according to the commonly accepted methods.



Fig. 1. Super dwarf plant.

Results and discussion. Study of mutants revealed in M_1 has shown that it is constant and sharply differs by features from the initial variety "Ducat"; it retained only the vegetation pattern – it is winter sowing and even by this character is late for as many as 10-12 days as compared to the initial variety.

Super dwarf form "Gorda", obtained via treating seeds of approved for distribution in Georgia French-bred variety of winter soft wheat "Ducat" with 0.01% solution of NMU represents a completely new variety of soft wheat and it was named as "var. Dekaprevichii" (Naskidashvili) in honor of Leonid Dekaprevich - the founder of genetic and selection studies in the Caucasus.

Plant of the super dwarf "Gorda" is bunch forming (Fig. 1), half-prostrate. Number of internodes is 3-4, with sharply reduced lengths of internodes.

Plant stem is very short, its maximum height attains 21-27 cm. Stem cross-cut (between the spike basis and upper stem node) is filled in with parenchyma, firm and hard bending (Fig. 2). Leaf is wide, erect. Heading (ear forming) time (emergence of the first ears in 50% of plants) occurs as many as 10-12 days later as compared with initial and regular checked varieties. Spike (ear) is short (4-5 cm), strongly dense and compact, of light straw colour, without awn and awn-like appendix (Fig. 3). Spike lower glume arm (in the middle third of the spike) is wide. Lower spikelet glume (in the middle third of the spike) is convex. Tooth of the lower spikelet glume (in the middle third of the spike) is moderately bent.

Kernel is white, shriveled, mass of 1000 kernels makes 30 g (Fig. 4, 5). Content of gluten in the kernel is 27-28%, being by 10-12% higher than in the initial variety.



Fig. 2. Plant stem and spike



Fig. 3. Spike



Fig. 4. Spike rachis and spikelet



Fig. 5. Spikelet, glume and grains (kernels)

Thus "Gorda" represents a new genetic source, new initial material for breeding, donor-variety for obtaining low height varieties with 2-3 stem reducing genes. Information on the new cultivar of soft wheat unknown to science – the Dekaprelevichi (Naskidashvili) is being published for the first time. Below is given a brief description of a new variety: var. Dekaprelevichi (Naskidashvili), var. nova is late winter variety of wheat, bunch-forming, short-stemmed (10-12 cm). Leaves wide, erect, without villi. Spike short (4-5 cm), flat, awnless. Spikelets without villi. Kernel white, corneous in consistence. The cultivar has been developed at the I. Lomouri Institute of Farming by means of treating seeds of French bred variety of winter soft wheat "Ducat" with 0.01% solution of NMM (authors: G. Chkhutiashvili, G. Khutsishvili, P. Naskidashvili, N. Japaridze, N. Sokhashvili). var. Dekaprelevichi (Naskidashvili), var. nova. planta est *Triticum autumnale serotinum typo frutex, stipula brevis* (10-12 cm). habet folia lata verticalia

sine villis. spica brevis (4-5 cm) *plana sine arista. spicula sine villis. granum album consistentia cornuosa. prodicitur in instituto explorationis scientificae agriculturae Georgiae. admittitur pro semente segetis per praeparationem granum speciei gallici (francesi).*

Conclusions

1. Obtaining of a completely new super dwarf wheat variety "Gorda" as a result of treatment with 0.01% solution of NMM of seeds of French bred variety of winter soft wheat "Ducat", approved for distribution in Georgia, proves again the significance for the process of emergence of new forms of induced mutations together with spontaneous hybridization, which provide rich material for artificial and natural selection.

2. Super dwarf wheat variety "Gorda" developed by means of application of the chemical mutagen is an important achievement in terms of breeding varieties resistant to lodging for irrigated agriculture.

გენეტიკა და სელექცია

რბილი ხორბლის (*T. aestivum* L.) ინდუცირებული მუტაგენზით მიღებული მოკლელეროიანი ახალი ბოტანიკური და გენეტიკური ფორმა „გორდა“

პ. ნასყიდაშვილი*, გ. ჩხუტიაშვილი**, დ. ბედოშვილი**, მ. ნასყიდაშვილი**

* აკადემიის წევრი; საქართველოს აგრარული აკადემია, თბილისი

** საქართველოს აგრარული უნივერსიტეტის ი. ლომოურის მიწათმოქმედების ინსტიტუტი, წეროვანი

მოკლელეროიანი სუპერჯუჯა „გორდა“ მიღებულია საქართველოში გასაერცვლებლად დაშვებული ფრანგული სელექციის, საშემოდგომო რბილი ხორბლის ჯიშ „დეუკატი“-ს თესლზე ქიმიური მუტაგენის NNU 0,01%-იანი ხსნარის ზემოქმედებით.

„გორდა“ საშემოდგომო რბილი ხორბლის მუტანტური ფორმაა. მცენარე არის ბუჩქის ტიპის, მკვეთრად შემცირებული მუხლთშორისების სიგრძით, რომლის მაქსიმალური სიმაღლე შეადგენს 26-27 სმ. ფოთოლი ფართო, ვერტიკალურად მდგომი; ღერო მოკლე, მტკიცე, ძნელად იღუნება. თავთავი უფხო, მოკლე (4-5 სმ), ბრტყელი, მკვეთრად მკვრივი, რომელშიც გაზრდილი განუვითარებელი თავთუნების რაოდენობა მჭიდროდ განლაგებულია თავთავის ღერაკზე, თავთუნების კილები გამობერილია. ჯიშში „გორდა“ 10-12 დღით საგვიანოა სტანდარტულ ჯიშებთან შედარებით. მარცვლი ბჟირია, რის გამოც 1000 მარცვლის მასა შეადგენს 30 გ. მარცვლის ნედლი პროტეინის შემცველობა შეადგენს 27-28%.

„გორდა“ არის ახალი მემკვიდრეობის მქონე სასელექციო საწყისი მასალა სელექციური მოკლელეროიანი (2-3 გენით) ჯიშების გამოსაყვანად.

REFERENCES

1. L.L. Dekaprevich (1929) Sluchai voznikoveniia mutsii sredi chistoj linii pshenitsy. Zapiski Nauchno-Prikladnykh Otdelov Tiflisskogo Botanicheskogo Sada. Iss. VI, Ed. L.L. Dekaprevich, Tiflis (in Russian).
2. N. Stampelli (1932), Origini, sviluppi, lavori e risultati. Roma (in Italian).
3. G. Inazuka (1971), Norin, a Japanese semi-dwarf wheat variety. WIS, 32.
4. N.E. Borlaug (1958), Acad. Sci. Trans., 20: 278. NY.
5. P.P. Lukyanenko (1965). Agrobiologiya. 163, 2, (in Russian).
6. S. Borovnich (1979), Genetika, IX, 11: 15-25, November, Moscow (in Russian).
7. P. Naskidashvili, M. Sikharulidze, E. Chernysh (1983), Khorblis selektsia sakartveloshi [Selection of wheat in Georgia]. Tbilisi, 340 p. (in Georgian).

Received March, 2012

Palaeobiology

The Comparison of the Results of Palynological and Microfaunistical Investigations of the Sarmatian Deposits of Eastern Georgia

Irina Shatilova*, Lamara Maissuradze*, Irma Kokolashvili**,
Kakhaber Koiava†

* Georgian National Museum, L. Davitashvili Institute of Paleobiology, Tbilisi

** Georgian Technical University, Tbilisi

† A. Janelidze Institute of Geology, I. Javakishvili Tbilisi State University

(Presented by Academy Member Abesalom Vekua)

ABSTRACT. The results of palynological and microfaunistical investigations of the Sarmatian deposits of Eastern Georgia are given. The similarity in dynamics of terrestrial and marine biocenosis is established. © 2012 Bull. Georg. Natl. Acad. Sci.

Key words: Eastern Georgia, Sarmatian, flora, microfauna, stages of development.

Sarmatian deposits are widely distributed on the territory of Eastern Georgia. By faunistical data they are divided into three substages: Volhinian, Bessarabian and Khersonian (Fig. 1). In most cases the Lower Sarmatian is conformably bedded on the Konkian deposits and is represented by coastal-shallow and deep-sea sediments. The thickness of Lower Sarmatian is 50-90 m in coastal regions and 250-350 m in the central part of the basin. The sections are dated by micro-macrofauna (*Quenqueloculina*, *Nonion*, *Elphidium*, *Porosonion*, *Donax*, *Maetra*, *Ervilia*) [1-3].

By data of Koiava [3], the thickness of Lower Sarmatian deposits, poorness of fauna indicate the existence of a large, shallow, brackish basin. North-

southward of this basin mountain ranges of latitudinal direction were situated.

At the beginning of the Middle Sarmatian the paleogeographical situation was unchanged. Only the retreat of the sea northwards had taken place, that found reflection in the transgressive bedding of Middle Sarmatian deposits of the south wing of the Kakhetian range. The deposits of Middle Sarmatian mainly are represented by blue-grayish clays with rich fauna. The thickness of the Middle Sarmatian is changed from 100 to 1000 m [1,3].

In Kartli to the Upper Sarmatian belongs the thick series of continental deposits of the so-called Natskhorian suite, whose thickness changes from 300 to 2500 m. This suite is widely distributed on

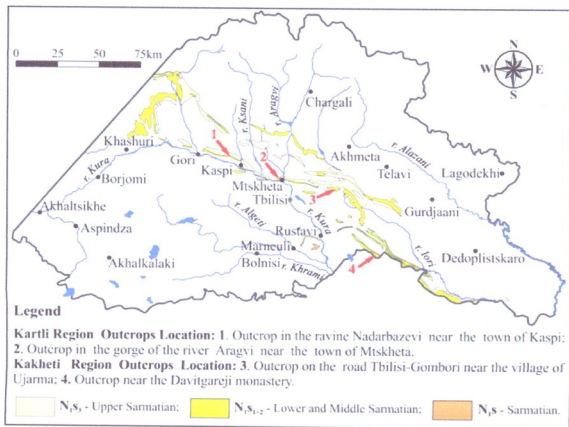


Fig. 1. Map of distribution of Sarmatian deposits of Eastern Georgia together with outcrops location (according to Gudjabadze, 2003).

slopes of Kartli depression, where it takes part in the building of most anticline and syncline folds. In some sections it is divided into two parts: lower - clayey-sandstone and the upper built by the sandy clay deposits [1].

In Kakheti the Upper Sarmatian is somewhat different. Here in north-eastern part of the region it is represented by continental sediments of Eldarian suite with tests of freshwater and terrestrial gastropods. To the south-eastwards the character of deposits is changed and clays of the lower part of Eldarian suite are replaced by marine deposits with fauna of *Maetra*. The presence of the "marine series" in the area of the Iori river is confirmed by micropaleontological investigations of core material from boreholes of Taribani and Eldari [4].

Until recently the knowledge about the Sarmatian flora and vegetation was based on macrobotanical remains from deposits of Lower and Middle substages

[5,6]. Palynologically Sarmatian deposits were not studied. There was only one work devoted to study of core material from boreholes of the central part of Kartli depression [7]. In spite of poorness of palynoflora (28 forms) the assemblages of three stages of Sarmatian were distinguished. Now we possess rich palynological material [8-10] from outcrops on the territory of Kartli (Aragvi, Nadarbasevi) and Kakheti (Davitgareji, Gombori). In the composition of flora about 200 forms belonging to 130 genera and 88 families are determined. Besides, palynomorphs were seen in deposits of the entire Sarmatian. So, the use of palynological method broadens the outlook both about the composition of flora and dynamics of the vegetation cover. On the basis of this material a palynological diagram was built, which reflects the changes of percentage contents of separate groups of plants, joined according to their ecological - climatic requirements.



The analysis of the diagram allows to trace the dynamics of vegetation directed mainly to the reduction of forests and the expansion of woodless areas. These changes were connected with the decrease of humidity. This process acquired the most distinct character in Late Sarmatian, especially in Kartli. In Kakheti (area of Gombori) it was not so drastic.

The changes in composition of pollen assemblages allow to distinguish 5 phases in dynamics of vegetation, which are represented completely in Aragvi section [9].

Phase I corresponds to the upper part of the Early Sarmatian. It is represented in Aragvi and Nadarbazevi sections and probably in Gombori. In this time on the territory of Eastern Georgia the polydominant forest predominated. In its composition were pine, thermophilic conifers and leaf-bearing trees, among which the subtropical plants and plants of warm-temperate climate had an equal part. In comparison with the following stretch of time the humidity was somewhat lower, being indicated by high percentage contents of pollen grains of pine and grasses.

Phase II corresponds to the lower part of the Middle Sarmatian and is represented in all outcrops studied. Most completely it is reflected by pollen assemblages of the Nadarbazevi section. In the II phase the area of subtropical ferns and trees expanded noticeably, whose systematical composition was very rich. The role of pine and xerophytes was decreased. The II phase can be considered as climatic optimum, with comparable high humidity.

Phase III, which in the sections of Aragvi and Davidgareji corresponds to the middle part of the Middle Sarmatian significantly differed from the previous one. The composition of thermophilic conifers, leaf-bearing trees and ferns was impoverished; the territory of their distribution was also reduced. The role of pine and the area of xerophytic vegetation were increased. These changes were probably connected with the process of xerophytisation, which had oscillating character. This is confirmed by the composition of the vegetation of the next phase.

Phase IV of development of flora and vegetation was distinguished in the sections of Aragvi, Nadarbazevi and Davidgareji, where it corresponds to the uppermost part of the Middle Sarmatian. During this time the role of thermophilic trees rose again but on the whole the flora was impoverished.

Phase V corresponds to the lower part of the Late Sarmatian when, by the data of Buleishvili [1], on the territory of Eastern Georgia continued to preserve water basins. The sea divided into separate small lakes, poorly connected with each other. Such supposition is confirmed by data of palynology. The Upper Sarmatian deposits of the sections studied contain a great enough number of palynomorphs, whose accumulation was possible only in water conditions. Phase V is characterized: by a sharp increase of the role of xerophytes in the composition of vegetation; by reduction of leaf-bearing plants and conifers, among which the pine predominated. We suppose that the subtropical plants whose pollen grains occur in palynological assemblages of Upper Sarmatian deposits were represented by shrub forms. *Disanthus cercidifolius* Maxim. var. *minor* Shat. et Mched. [11] can be cited as an example. The pollen grains of this form are of much smaller sizes than those of the species *Disanthus cercidifolius* Maxim. Probably, it was a shrub that developed under the influence of dry climate, unfavorable for this plant.

The Sarmatian deposits of Eastern Georgia were studied by the micropaleontological method [2,3, 12,13]. In the lower part of Early Sarmatian the foraminiferal assemblages are characterized by *Quingueloculina*, *Sinuloculina*, *Varidentella*, *Affinetrina*, *Nontion*, *Elphidium*, *Porosonion* and *Ammonia*. *Bolivina*, *Discorbis*, *Bulimina*, *Cibicides* and *Fissurina* are relatively rare. Their morphology does not differ noticeably from that displayed by their Middle Miocene ancestors. These forms are also characterized by small sizes, and sometimes, transparent walls. The lower part of Early Sarmatian is distinguished as the layers with *Varidentella reussi*. They reflect the first phase of development of foraminifera.

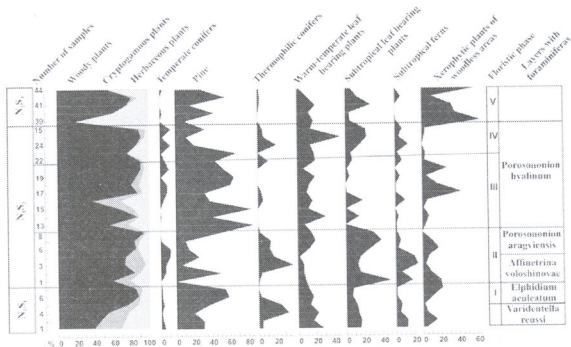


Fig. 2. Comparison of flora and microfauna development phases during the Sarmatian on the territory of Eastern Georgia.

Assemblages from the upper part of Early Sarmatian are characterized by reduced diversity because of the disappearance of *Bolivina*, *Discorbis*, *Cibicides*. Nevertheless, a large number of genera survived and adapted to the new environment. They are characterized by strong intraspecific variability and a potential for a speciation. The upper part of Early Sarmatian is distinguished as the layers with *Elphidium aculeatum*. They reflect the second phase of development of Early Sarmatian foraminifera.

By the data on microfauna the Middle Sarmatian is divided into three parts. The first is characterized by foraminiferal assemblages very different from those observed in the Early Sarmatian. The new genera, such as *Dogielina*, *Meandroloculina*, *Sarmatiella*, contributed a considerable number of species. Foraminifers of these assemblages are characterized by comparatively large sizes.

The richest assemblages of endemic foraminifera characterize the second part of the Middle Sarmatian, with the number of individuals and new species and their size reaching the maximum.

The third part of the Middle Sarmatian is distin-

guished for a decrease in the abundance of foraminiferal genera, species and individuals. Because of the worsening of biogenic conditions only very few representatives of most euryhaline families survived: *Elphidium*, *Porosonion*, *Ammonia* and very seldom *Affinetrina* and *Varidentella*. Among them *Porosonion* is characterized by large size and additional ornamentations on very coarse walls of tests. The lower part of the Middle Sarmatian is identified as layers with *Affinetrina voloshinovae*; the middle part - as layers with *Porosonion aragviensis* and the upper - as layers with *Porosonion hyalinum*.

Some species of genera (*Elphidium*, *Nonion*, *Porosonion*, *Ammonia*) of Middle Sarmatian assemblages also occur in Upper Sarmatian. These forms show deformation, irregular cameras or immature shell development and are presented only in some parts of the Late Sarmatian basin. The above-mentioned anomalies of shells point to the existence of nonoptimal conditions for foraminifera.

The phase of development of flora and vegetation of Eastern Georgia during the Sarmatian were

compared with those of foraminifera (Fig.2). In sections Nadarbazevi and Aragvi the I - floristic phase corresponds to the deposits directly underlying the Middle Sarmatian. On the basis of this we correlate it with the second phase of development of Early Sarmatian foraminifera. The conditions of this time were not optimal, either for flora, or for foraminifera.

In the development of flora and foraminifera during the Middle Sarmatian three phases are distinguished but in terms of time they do not coincide completely. The appearance of new taxa and increase of test sizes served as the common sign of the first and second phases of development of foraminifera. In the second phase these phenomena were more distinct, indicating the existence of optimal conditions. We correlated both microfaunistic phases with phase II of development of flora and vegetation, which reflects the conditions of climatic optimum.

Phases III-IV, when the impoverishment of Middle Sarmatian flora took place, can be correlated with the third phase of development of Middle Sarmatian foraminifera. It was characterized by a decrease of the number of genera, species and individuals.

The V - floristic phase, in our opinion, corresponds to the lower part of the Upper Sarmatian. It was characterized by sharp changes in the composition of marine and terrestrial biocenoses and in the conditions of their existence. Similar phenomena happened also in other regions of Eastern Paratethys. The sections of Azerbaijan, South Ukraine, the Crimea and some other regions of the Pre-Caucasus are characterized only by euryhaline forms: *Ammonia*, *Elphidium*, *Nonion* indicate the brackish conditions of Late Sarmatian basins [2].

The paleofloristic data also indicate changes of environmental complex in Upper Sarmatian on the territory of South-western Ukraine. Here began the formation of steppes, which periodically gave way to forest landscape [14]. The flora of South-eastern Ukraine and of the south part of the Russian plain was also impoverished. In the opinion of Ananova [15] here in Late Sarmatian and Meotian began the

phase of "borealization" of Miocene flora but the main time of disappearance of most of thermophilous and hygrophilous plants was the Middle Sarmatian.

Thus, the use of the palynological method allows to trace the history of the flora, vegetation and climate of Eastern Georgia during the Sarmatian and distinguish the phases of their development. The main signs, used by us as the basis were: the reduction of forest areas; the decrease of the part of hygrophilous subtropical plants in the composition of the flora; the expansion of woodless areas. The climate was the main factor influencing the development of flora and vegetation. Xerophytisation, which began in the Middle Sarmatian, acquired a more drastic character in the Late Sarmatian, when the predominance of xerophytic vegetation began in the larger part of Eastern Georgia.

The comparison of floristic phases with phases of development of foraminifera revealed a definite similarity in the dynamics of terrestrial and marine biocenoses, connected, mainly with the deterioration of habitation conditions both for thermophilous and hygrophilous plants and foraminifera. Probably, the main reason was the changes in the paleogeographical situation. As a result of tectonical movements on the boundary of the Middle and Late Sarmatian the Transcaucasus depression transformed into dry land with two great regions, divided by the Dzirulian Block. On the West, in the Colchis refugium, the humid and warm climate, favorable for development of subtropical flora was preserved. In the East began the process of xerophytisation, connected with common phenomenon that took place beyond the boundaries of the Caucasus. The decrease of sea and the appearance of freshwater basins was fatal for foraminifera, the main part of which became extinct on the boundary of the Middle and Upper Sarmatian nearly in the whole Eastern Paratethys.

The identified phases of development of flora and foraminifera can be used for division of the Sarmatian deposits of Eastern Georgia into small stratigraphic units.

პალეობიოლოგია

აღმოსავლეთ საქართველოს სარმატული ნალექების პალინოლოგიური და მიკროფაუნისტური კვლევის შედეგების შეპირისპირება

ი. შატილოვა*, ლ. მაისურაძე*, ი. კოკლაშვილი**, კ. ქოიავა†

* საქართველოს ეროვნული მუზეუმი, ლ. დავითაშვილის პალეობიოლოგიის ინსტიტუტი, თბილისი

** საქართველოს ტექნიკური უნივერსიტეტი, თბილისი

† ი. ჯავახიშვილის სახ. თბილისის სახელმწიფო უნივერსიტეტი, ა. ჯანელიძის გეოლოგიის ინსტიტუტი, თბილისი

(წარმოდგენილია აკადემიის წევრის ა. ვეკუას მიერ)

აღმოსავლეთ საქართველოს სარმატული ნალექების პალინოლოგიური მეთოდით შესწავლამ შესაძლებელი გახადა თვალი გავადევნოთ ფლორის მცენარეულობისა და კლიმატის ცვალებადობის ისტორიას და გამოვყოთ მათი განვითარების ეტაპები სარმატული საუკუნის განმავლობაში. ეტაპების დასადგენად ძირითად კრიტერიუმად გამოყენებულია მცენარეულობის შემადგენლობაში ტყის ფორმაციების და ტენიანობის მოყვარული სახეობების რაოდენობის შემცირება, რაც უტყეო სივრცის არეალის გაფართოებას იწვევდა.

ფლორისა და მცენარეულობის განვითარებაზე გავლენის ძირითად ფაქტორად ითვლება კლიმატური პირობები. დადგინდა, რომ შუასარმატულის ბოლოს იწყება ქსეროფიტიზაციის პროცესი, რომელმაც შედარებით მკვეთრი ხასიათი მიიღო გვიანსარმატულში. ამ პერიოდში აღმოსავლეთ საქართველოს ტერიტორიის დიდ ფართობზე ქსეროფიტული მცენარეულობა გაბატონდა.

ფლორისტული ეტაპების შეპირისპირებამ ფორამინიფერების განვითარების ეტაპებთან გამოვლინა გარკვეული მსგავსება ხმელეთისა და ზღვის ბიოცენოზების დინამიკაში, განსაკუთრებით გარემოს გაუარესების პირობებში. ცნობილია, რომ შუა და ზედასარმატულის საზღვარზე განვითარებულმა ოროგენეტიკურმა პროცესებმა შეცვალა პალეოგეოგრაფიული გარემო ამიერკავკასიაში. საქართველოს ტერიტორია ძირულის მასივით ორ დიდ რეგიონად გაიყო. დასავლეთით (კოლხეთის რეფუგიუმში) შენარჩუნდა თბილი და ტენიანი ჰავა, რამაც განაპირობა სუბტროპიკული მცენარეულობის გადარჩენა. აღმოსავლეთით კი დაიწყო ქსეროფიტიზაციის პროცესი (რომელმაც მოიცვა კავკასიის ჩრდილოეთით მდებარე ტერიტორიები). ზღვის ფართობის შემცირებამ და ცალკეული განმარბილიანებული დახშული აუზების გაჩენამ დამლუპველი პირობები შეუქმნა ფორამინიფერებს, რამაც შუა და ზედასარმატულის საზღვარზე ფორამინიფერების დიდი უმრავლესობის ამოწვდომა გამოიწვია.

ხმელეთისა და ზღვის ბიოცენოზების დადგენილი ეტაპები შეიძლება გამოყენებული იყოს აღმოსავლეთ საქართველოს სარმატული ნალექების უფრო დეტალურ სტრატეგრაფიულ ერთეულებად დანაწილებისათვის.

REFERENCES

1. D. Buleishvili (1960), Geologia i neflegazonosnost' mezhgornoi vpadiny Vostochnoi Gruzii. Leningrad, 368 s.
2. L. Maissuradze, K. Koiava (2011), Bull. Georg. Natl. Acad. Sci., 5, 1: 143-151.
3. K. Koiava (2000), Abstract of Ph. Thesis, Tbilisi (in Georgian).
4. L. Maissuradze, K. Koiava (2006), Sakartvelos navtobi da gazi [Oil and Gas of Georgia], 19: 48-61 (in Georgian).
5. M. Uznadze (1965), Neogenovaia flora Gruzii. Tbilisi, 180 s. (in Russian).
6. L. Chelidze (1987), Postmiotsenovaia flora i rastitel'nost' Zakavkaz'ia. Tbilisi, 112 s. (in Russian).
7. P. Mchedlishvili, N. Mchedlishvili (1953), DAN SSSR, XCI, 3: 621-623 (in Russian).
8. I. Kokolashvili, I. Shatilova (2009), Proc. Georg. Acad. Sci. Ser. B, 7, 1-2: 85-89.
9. I. Shatilova, N. Mchedlishvili, I. Kokolashvili (2010), Bull. Georg. Natl. Acad. Sci., 4, 2: 165-171.
10. I. Shatilova, I. Kokolashvili (2011), Proc. Georg. Acad. Sci. Ser. B, 9, 1-4: 65-71.
11. I. Shatilova, N. Mchedlishvili (2011), Bull. Georg. Natl. Acad. Sci., 5, 1: 139-143.
12. K. Koiava (2006), Sakartvelos navtobi da gazi [Oil and Gas of Georgia], 17: 38-43 (in Georgian).
13. I. Shatilova, L. Maissuradze, N. Mchedlishvili, et al. (2009), Proc. Georg. Acad. Sci. Ser. B, 7, 1-2: 90-109.
14. N. Shekchina (1979), Istoriia flory i rastitel'nosti iuga evropeiskoi chasti SSSR v pozdnem neogene. Kiev, 196 s. (in Russian).
15. E. Ananova (1974), Pyl'tsa iz neogenovykh otlozhenii yuzhnoi chasti russkoi ravniny. Leningrad, 196 s. (in Russian).

Received February, 2012

Medical Sciences

Brain Structural-Hemodynamic Changes in Patients with Potential Cardiac Source of Embolism

Fridon Todua* and Dudana Gachechiladze**

* Academy Member, Research Institute of Clinical Medicine, Tbilisi

** Research Institute of Clinical Medicine, Tbilisi

ABSTRACT. The aim of our study was to evaluate the brain structural and haemodynamic changes in patients with potential source of cardiogenic embolism.

In the period of 2002-2007 116 patients with carotid system severe and chronic dyscirculation were investigated. Patients age varied between 42-76 years.

The patients were divided into 2 groups. Group I - 56 patients (mean age 62 ± 7.3 yr) with potential source of cardiogenic embolism (PCSE) (atrial fibrillation, endocarditis, aortic or mitral valve calcinosis, postinfarct aneurism). Source of embolism was defined by corresponding diagnostic tools: ECG, 24 h, Holter monitoring, echocardiography. Patients with extra-intracranial artery haemodynamically or embologenous pathology were excluded from group I. Group II: 60 patients (mean age 61 ± 8.4 yr) with lack of PCSE and with evidence of carotid artery atherosclerotic disease (CAD). All patients underwent routine neurologic examination, functional status study by Rankin scale, brain computed (CT) or magnetic resonance tomography (MRI), extra-intracranial artery Color Doppler, MDCT or MR-angiography.

Examination revealed prevalence of symptomatic cerebral ischemia in group I. In comparison, in group II cases of chronic cerebral dyscirculation was noted.

By CT and MRT images of infarction were divided into 5 subtypes: total, cortical/subcortical, deep, small cortical, lacunar infarctions. In the PCSE group in 39 (69%) cases the presence of infarctions was noted. From them in 24 cases total or cortical/subcortical infarctions were present. In the CAD group non-focal changes (diffuse, atrophy changes) prevailed 31 (52%).

In the CAD group in 49 (82%) cases atherosclerotic stenosis of the internal carotid artery (ICA) was revealed. Patients had a higher frequency of moderate stenosis of the symptomatic internal carotid artery (ICA) side 28 (58%) and lower frequency of severe stenosis 5 (8%) and occlusion 3 (5%). Potential embologenous atherosclerotic plaques were defined in 28 (47%) cases. By TCd-embolodetecting cerebral emboli was defined in 13 (72%) of 18 PCSE patients and 11 (65%) of 17 CAD patients.

Transcranial Doppler examination revealed flow decrease in middle cerebral (MCA), and anterior cerebral arteries (ACA) in PCSE patients. In cases of large infarction flow velocity at the MCA was 32.6 ± 4.8 cm/s. In comparison, in the CAD group flow parameters in the anterior circulation arteries were at normal levels. Only in the cases of ICA severe stenosis or occlusion flow decrease in the ipsilateral MCA and ACA was noted.

Our data show that PCSE has a tendency to have a larger infarction, combined superficial and deep territorial, bilateral involvement, high recurrence rate. Cardioembolic stroke is associated with a worse outcome than other stroke subtypes. In patients with carotid artery atherosclerotic changes the main reason of brain infarction may be atherothromboembolism from nonstable carotid atherosclerotic plaque. The diagnosis of cardiogenic or large artery stroke relies on detection of potential emboligenic sources in the absence of other etiology of equal or greater plausibility. Early application of modern neuroimaging techniques raises the diagnostic accuracy in the evaluation of patients at risk for cerebrovascular



disease. In patients with a potential source of cardiogenic embolism careful complex examination of the cardiac status and extra-intracranial blood flow conditions is quite important. © 2012 Bull. Georg. Natl. Acad. Sci.

Key words: stroke, brain, cardiogenic embolism.

Stroke is a common cause of death and an important cause of morbidity in industrialized countries, imposing an enormous economic burden. The overall incidence of stroke is estimated as 127 000/ year in Germany, 112,000/ year in Italy, 101,000/year in UK (1) of which 75% are first strokes. These figures are likely to raise overall stroke incidence, ¾ of which falls to developing countries. The high case-fatality rate and morbidity associated with stroke make substantial demands on healthcare resources [1,2].

Ischemic stroke occurs in 80% of all stroke cases. While the aetiology of ischemic stroke is often found in the cervicocranial vasculature, approximately 20-25% result from high-risk cardiac abnormalities – cardiogenic embolism. In elderly rate of cardiogenic reason of stroke rise to 1/3. Cerebral blood supply strictly depends on cardiac status. Cardiac pathology can cause brain symptomatic ischemia by two main pathogenetic mechanisms: 1. Brain hypoperfusion; 2. Cardiogenic embolism [3-5].

Patients with cardioembolic cerebral infarction have a poorer prognosis than those with atherothrombotic cerebral infarction. One of the reasons for the poorer prognosis is the recurrence of embolisation. For the high incidence, poor outcome and high mortality the problem of CE is of considerable importance [6].

The aim of our study was to assess brain structural-hemodynamic changes in patients with potential cardioembolic source of symptomatic cerebral ischemia (Transient ischemic attack (TIA) or stroke);

Subjects and Methods. 116 patients, 49 women and 67 men aged 42-76 years (mean age 63.2±11.2 years) with symptomatic cerebral ischemia were investigated;

All patients underwent a careful neurological examination, brain CT or MRT, 3D TOF-MR-angiography or CT-angiography and Color Doppler of extra-intracranial vessels.

MR imaging was performed by using a 1.5-T unit (Magnetom Avanto) and 3 T whole-body system Magnetom Verio (Siemens Medical Systems, Erlangen, Germany). Flow territory imaging was achieved by using a regional perfusion imaging sequence. Contrast enhancement by 5% Magnevist (Schering) was used. Evaluation of intracranial vessels was performed by ToF-fl3d-multiple-tra TR 56ms, TE 10.4ms, F.A.40 programs, for the extracranial vessels tof-fl2d-tra-tra-w-sat. TR 52ms, TE 10ms, F.A. 70 program was used.

Brain CT and multidetector CT-angiography (MDCT) was performed on Siemens unit Somatom Definition AS 128 sl. and Toshiba unit Aquillion ONE 640sl. Contrast enhancement by 5% Ultravist (Schering) was used.

Color Doppler ultrasonography (CDUS) of the extracranial carotid and vertebral arteries was performed on the unit Toshiba Aplio XG and Acuson X 300, with 5-10MHz linear probe. Carotid artery disease was assessed and defined according to standardized criteria. Transcranial color Doppler sonography (TCCD) was performed on the same units with 2.0-2.5 MHz probes.

TCD embolodetection (ES) monitoring was performed using the Nicolett Pioneer TC 8080 system. Insonation, using the temporal acoustic window, was performed at a depth of 50 to 60 mm using a 2-MHz pulsed Doppler transducer.

Patients were categorized into two groups; 56 patients (mean age 62±7.3 years) with potential car-

Table 1. The baseline characteristics of the PCSE and CAD patients

	PCSE n=56(9%)	CAD n=60(9%)
Women	24(43)	24(40)
Men	32(57)	36(60)
Age	62±7.3y	60.7± 8.4y
Clinical sign		
Stroke	31(55)*	28(47)
TIA	25(45)	32(53)

* – statistical significance, $p < 0.05$

diac source of embolism (PCSE). Presence of a probable or certain source of cardiac emboli was defined, including a) valvular heart disease $n=21$, b) cardiac arrhythmias such as atrial fibrillation, $n=26$, c) myocardial infarction and postinfarction aneurism, $n=7$. In all cases the source of CE was defined by several cardiologic investigations, as ECG, 24 hour Holter monitoring, EchoCG. Patients with high-grade stenosis of extracranial arteries or carotid embologenous atherosclerotic plaque were excluded from this group.

Another 60 patients (mean age $60.7 \pm 10.2y$) were identified to have anterior circulation ischemia, lack of PCSE and with evidence of carotid artery atherosclerotic disease (CAD).

Groups were compared by age, gender, clinical symptoms of ischemia, ischemia outcome, size and localization of infarction area, cerebral hemodynamic parameters. In acute stroke the patient was defined by Glasgow Coma scale.

Results. The baseline characteristics of the PCSE and CAD patients are compared in Table 1. Distribution of patients by gender showed prevalence of men. A significantly higher proportion of the PCSE patients had stroke, while majority of CAD expired TIA.

Evaluation of the severity of stroke by Glasgow coma scale ($M \pm \sigma$) showed that patients with PCSE had poorer prestroke status, more severe neurologic deficits at the time of stroke onset compared with CAD patients (PCSE- 11.8 ± 3.6 ; CAD 13.9 ± 3.1).

Using brain CT or MR images the vascular topography, the site and size of infarctions were classified: Total anterior circulation infarction (TACI), Cor-

tical/subcortical, Deep, Small cortical, Lacunar infarction.

Of the 56 patients of PCSE group more than half 39(69%) had infarction on the symptomatic side; 6(11%) lacunar, 15 (27%) cortical-subcortical, 9(16%) territorial. The analysis of CT/ MRT images showed that large single cortical-subcortical lesion and multiple lesions were significantly linked with CE. The proportion of LI and non-focal, atrophic changes was comparatively low. Combined anterior and posterior circulation involvement, or bilateral hemispheric involvement was more frequent in the PCSE group than CAD group (Fig. 1). The CT/MRT lesions of the PCSE group also showed more frequent involvement of simultaneous superficial and deep Middle Cerebral artery (MCA) territories than CAD group (Table 2).

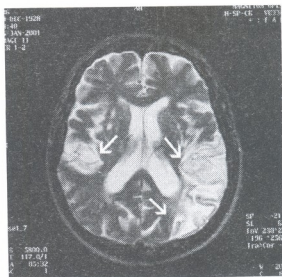


Fig. 1. Multiple infarctions at bilateral temporal and left occipital lobes; MR-T2 tse image. ●

Table 2. Topographic patterns in patient with PCSE and CAD

Brain changes	PCSE n=56	CAD n=60
Atrophy	7(13)	11(18)
Leukoaraiosis	8(14) *	13(22)
Total infarction	9(16)**	1(2)
Cortical/ subcortical Infarction	15(27)*	9(15)
Deep infarction	5(9)	4(7)
Small cortical infarction	4(7) *	7(12)
Lacunar infarction	6(10.7)*	15(25)
Bilateral anterior circulation	8(14) **	2(3)

* – significance, $p < 0.05$

On the other hand, in the CAD group the prevalence of small single cortical/subcortical infarctions and LI was marked. Infarctions more frequently involved only superficial territories. In 24(40%) cases brain diffuse, non-focal changes, as leukoaraiosis and cortical atrophy was found. We can suggest that because of the prevalence of large, territorial and multiple infarctions Cardioembolic stroke is associated with a worse outcome than other stroke subtypes.

18 patients with PCSE were investigated by TCD-embolodetecting within 48 hours of the symptomatic event. Microemboli were found in 13 (72%) of 18 observed patients. Emboli were seen in 3 of 5 patients with valvular heart disease, 4 of 6 AF, and 2 patients with past myocardial infarction. Patients with emboli had a significantly higher prevalence of prior cerebrovascular symptoms.

As was mentioned above, patients with high-grade CA stenosis and CA occlusion were excluded from the PCSE group. Of the 60 patients of CAD group, 49(82%) had more than 40% ICA atherosclerotic stenosis estimated by Color Doppler sonography; Patient had a higher frequency of moderate stenosis of the symptomatic internal carotid artery (ICA) side 28 (58%) and lower frequency of severe stenosis 5 (8%) and occlusion 3 (5%).

Several studies have demonstrated that about 50% of all cerebral ischemic events, whether permanent or transient, are due to the thrombotic and embolic complications of atheroma, which is a disorder

of large and medium-sized arteries. Large-artery atherothrombosis causes not only brain hypoperfusion, but also artery-to-artery embolism [1,7].

We have analysed the structure and stability of atherosclerotic plaques by high-resolution ultrasound images. Plaque tissue components, such as non-homogeneity, lipid-rich core, hemorrhage, irregular or ulcerated surface, loose matrix, were defined as potentially embologenous and prone to arterio-arterial embolism.

In 28 cases atherosclerotic plaques were classified by ultrasound criteria as unstable, embologenous. Of these 17 patients were studied by TCD embolodetecting within 48 hours of symptomatic

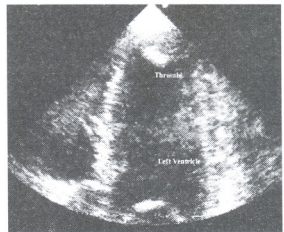


Fig. 2-a. Left ventricle postinfarction aneurism. Transthoracic EchoCG Apical two-chamber view. At the LV apex hyperchogenic thrombotic masses are located.

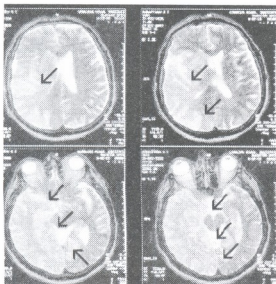


Fig. 2-b. Right circulation Total infarction. MR-T2 tse axial images. At the right parieto-temporal and occipital lobes diffuse hypointense area-infarction is marked

ischemia. Microemboli were detected in 11 of 17 patients (65%). 4 of the emboli-positive patients had had a high-grade carotid stenosis, and 3 patient had a mild (<50%) carotid stenosis. No microemboli were detected in the 3 patients with carotid occlusions.

We can suggest that prevalence of large/total infarctions in the PCSE patients and comparatively small lacunar, cortical/subcortical infarctions in CAD patients can be explained by the larger size of cardiogenic emboli than arterio-arterial emboli. So cardiogenic emboli cause brain large-sized artery occlusion, and give rise to large to total brain infarction (Fig 2 a-c).

By TCCD examination we studied flow parameters of arteries of the circle of Willis. Blood flow velocities (Vcm/s) in the middle, anterior, posterior cerebral arteries (MCA, ACA, PCA) and pulsatile indices (PI) were measured (Table 3).

In the majority of patients with PCSE tendency of decreased blood flow at the ipsilateral ACA and predominantly MCA was revealed; In patients with large to total brain infarctions significant decrease of blood flow at the MCA was detected - V mean-

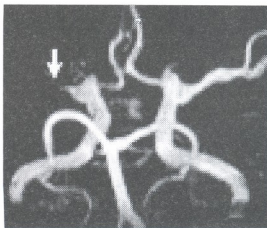


Fig. 2-c. Right MCA occlusion. 3D- tof MRA

32.8±8.3cm/s. In two patients from 3 with hemispheric total infarctions occlusion of MCA 1 segment was marked, and in one patient - postocclusive-collateral flow in the MCA - V mean-22cm/s.

In contrast, in CAD group patients blood flow parameters seemed to stay normal or were slightly decreased. Only in 5 cases of ICA high-grade stenosis or occlusion significant asymmetry on the affected side was revealed.

In patients both with PCSE and CAD with brain small cortical infarctions, lacunar infarctions or subcortical leucoencephalopathy hemodynamic changes were not impaired - V mean MCA-41.5±9.2cm/s.

Cardiac diseases affect the brain in two different ways; by pump and perfusion failure, and by embolism. Cardiogenic stroke accounts for approximately one in six ischemic strokes. Many different cardiac sources can give rise to emboli. About 20 different nosologies are associated with the CE. Cardiac emboli may be composed of thrombus, calcific particles, tumor, air, fat, foreign bodies [6-9].

Different size of brain infarctions in CE patients

Table 3. Mean flow velocity rates in Circle of Willis arteries

Artery	PCSE n=56 V, cm/s	CAD N=60 V, cm/s
MCA	37.6±11.3	47.7±8.5
ACA	34.3±6.8	45.7±8.5
BA	26.6±8.3	27.9±9.2
PCA	30.4±8.9	33.7±7.5

(different size of emboli) can be the result of cardiac chamber and valvular concomitant pathologies. Endocardial damage and cardiac chamber pathology provides circulatory stasis and formation of intracavitary thrombosis. The low shear rate that exists in areas of stasis promotes activation of the coagulation cascade rather than platelets, leading to thrombus formation. This process leads to formation of large-sized red, fibrin thrombus, which can be the reason of large/total brain infarction.

Valvular heart disease carries the greatest risk of embolism of any cardiac condition. Activation of Thromboxan A1 leads to form thrombocyte-monocyte, comparatively small-sized "white" thrombus formation. Most emboli from damaged (calcinated or mixomatous) cardiac valves are small and lead to lesser mortality but higher morbidity [6,10-12].

Recent studies by TCD embolotetection have revealed the presence of thrombocyte aggregated small thrombus in patients with cardiac valvular changes, that lead to the formation of small multiple brain infarctions [13,14].

Clinical presentation is imperfect in differentiating cardioembolic from noncardioembolic stroke. Cardiogenic brain embolism characteristically presents with neurologic deficits that are maximal at onset, reflecting sudden interruption of blood flow. While insensitive, the most specific features for cardioembolism are infarcts in multiple territories and concurrent systemic embolism [15,16].

Recent studies showed that cerebral infarctions due to CE occurs most frequently in MCA supply territory. The location of infarcts in MCA territory differs between the two groups. Superficial infarcts were more frequent to CAD group (arterio-arterial embolism), whereas combined superficial and deep territory infarct were more frequent in embolism with PCSE. Although the nature of the embolic substances for arterio-arterial embolism and PCSE is quite heterogeneous, more recently it has been proposed that embolism from large vessels is primarily caused by white thrombus (platelet aggregates), and that embolism from the heart is mainly caused by red thrombus (platelet and fibrin aggregates) [6,11,12].

In conclusion, our data shows that PCSE has a tendency to have a larger infarct, combined superficial and deep territorial, bilateral involvement, high recurrence rate. The rate of emboli formation might be different in various cardiac diseases. So cardioembolic stroke is associated with a worse outcome than other stroke subtypes. In patients with carotid artery atherosclerotic changes main reason of brain infarction may be atherothromboembolism from nonstable carotid atherosclerotic plaque. The diagnosis of Cardiogenic or Large artery stroke relies on detection of potential emboligenic sources in the absence of another etiology of equal or greater plausibility. Early application of modern neuroimaging techniques stands to raise diagnostic accuracy in the evaluation of patients at risk for cerebrovascular disease.

სამედიცინო მეცნიერებათა

თავის ტვინის სტრუქტურულ-ჰემოდინამიკური ცვლილებები კარდიოგენული ემბოლიის წყაროს მქონე პირებში

ფ. თოდუა*, დ. გაჩეჩილაძე**

* აკადემიკოსი; კლინიკური მედიცინის ს/კ ინტიტუტი, თბილისი

** კლინიკური მედიცინის ს/კ ინტიტუტი, თბილისი

კვლევის მიზანს წარმოადგენდა თავის ტვინის სტრუქტურულ-ჰემოდინამიკური მდგომარეობის შეფასება საყარაულო კარდიომოლოგიური დისპემიის მქონე პირებში.

მასალა და მეთოდები. შესწავლილ იქნა 116 პაციენტი კაროტიდულ აუზში განვითარებული თავის ტვინის სისხლის მიმოქცევის როგორც მწვავე, ისე ქრონიკული მოშლით. პაციენტთა ასაკი მერყეობდა 42-76 წლების ფარგლებში

პაციენტები დაყოფილ იქნა 2 ჯგუფად; I. 56 პაციენტი (საშ. ასაკი 62 ± 7.3 წ.) კარდიოგენული ემბოლიის პოტენციური წყაროთი (მოციმციმე არითმია, ინფექციური ენდოკარდიტი, აორტის ან მიტრალური სარქველის კალცინოზი, მარცხენა პარკუჭის პოსტინფარქტული ანევრიზმა). ყველა შემთხვევაში ემბოლიის პოტენციური წყარო იდენტიფიცირებულ იყო შესაბამისი ინსტრუმენტული კვლევებით: ეკგ-თი, პულტრის მონიტორირებით, ექოკარდიოგრაფიით. ამ ჯგუფში არ გაერთიანდნენ პაციენტები თანდართული ექსტრა-ინტრაკრანიალური არტერიების ჰემოდინამიკურად ან ემბოლოგენურად მნიშვნელოვანი პათოლოგიებით. II ჯგ. 60 პაციენტი (საშ. ასაკი 60.7 ± 8.4 წ.), საძილე არტერიების ათეროსკლეროზით, რომელთაც არ აღენიშნებოდათ კარდიომოლოგიური რისკი.

ყველა პაციენტს ჩატარდა რუტინული ნეუროლოგიური კვლევა, თავის ტვინის კომპიუტერული ან მაგნიტურ-რეზონანსული ტომოგრაფია, მაგისტრალური ექსტრაკრანიალური და ინტრაკრანიალური სისხლძარღვების დუპლექს-სკანირება მრავალშრიანი კტ- ან მრ-ანგიოგრაფია, ტრანსკრანიალული დოპლერგრაფიული (ტკდ) ემბოლოდეტექცია.

I ჯგუფში პრევალირებდა სიმპტომატური იშემიის შემთხვევები, მაშინ როცა, II ჯგუფში უპირატესად აღინიშნა ქრონიკულად მიმდინარე დისცირკულაციის შემთხვევები. თავის ტვინის კტ- ან მრ-ტომოგრაფიების მიხედვით გამოყოფილ იქნა ინფარქტის 5 ქვეტიპი: ტოტალური, კორტიკალურ-სუბკორტიკალური, დრმა, მცირე კორტიკალური და ლაკუნური.

I ჯგუფში უმეტეს ნაწილში - 39 (69%) გამოვლინდა ინფარქტები. მათგან 24 ტოტალური, ან კორტიკალურ/სუბკორტიკალური. II ჯგუფის პაციენტებში წინა პლანზე არაკრონიკული ცვლილებები - საერთო ჯამში 31 (52%) პაციენტი.

II ჯგუფის პაციენტთაგან გამოკვლეულთაგან 49 (82%) პაციენტს აღენიშნებოდა შიგნითა საძილე არტერიის სტენოზი. ზომიერი სტენოზი გამოვლინდა 28(58%) შემთხვევაში. კრიტიკული სტენოზი და ოკლუზია შებამისად გამოვლინდა 5(8%) და 3(5%) შემთხვევაში. 28 შემთხვევაში ათეროსკლეროზული ფოლაქი ჩაითვალა ემბოლოგენურად.

ტკდ-ემბოლოდეტექციამ I ჯგ. 18 პაციენტიდან 13 (72%) შემთხვევაში და II ჯგ. 17 პაციენტიდან 11 (65%) შემთხვევაში გამოავლინა მიკროემბოლიების არსებობა; ტკდ-მ I ჯგ-ს პაციენტებში გამოავლინა ნაკადის დაქვეითების ტენდენცია როგორც დაზიანების იმპლეტერალურ წინა და უპირატესად შუა ცერებრულ არტერიაში; განვითარებული ინფარქტის მქონე პირებში ადგილი

ჰქონდა ნაკადის მკვეთრ დაქვეითებას შუა ცერებრულ არტერიაში- 32.6 ± 4.8 მმ/წმ.

განხილული I დეკუმენტაციის, II დეკუმენტაციის ინტრაკრანიალ კარდიოიდულ სისტემაში ნაკადის პარამეტრები პრაქტიკულად ნორმის ქვემო საზღვარზე რჩებოდა. მხოლოდ იმ შემთხვევებში, სადაც გამოვლინდა საძილე არტერიის უნილატერალური კრიტიკული სტენოზი, ან ოკლუზია, აღინიშნა პათოლოგიის იპსილატერალურად ნაკადის დაქვეითება.

თავის ტვინის მწვავე თუ ქრონიკულად მიმდინარე დისცირკულაციის მქონე პირებში კარდიოლოგიური პათოლოგიის შეუფასებლობამ შესაძლოა გამოიწვიოს კარდიოგენული ემბოლიის გენეზით განვითარებული პირველადი თუ განმეორებითი ინსულტის განვითარება და პაციენტის მდგომარეობის საგრძნობო გაუარესება. ჩვენი აზრით, კარდიოლოგიური დაავადებების მქონე პაციენტებში განსაკუთრებული ყურადღებით უნდა მოხდეს კარდიოგენული ემბოლიის რისკის მქონე პირების გამოვლენა და მის მიხედვით ადეკვატური მკურნალობის ტაქტიკის შერჩევა.

REFERENCES

1. J.M. Valdueza, S.J. Schreiber, J.E. Rozohl, R. Klingebiel (2008), Neurosonology and Neuroimaging of Stroke. Thieme, NY., 383 p.
2. C. Argentine, M. Prencipe (2000), In: C. Fieschi, M. Fisher, Eds., Prevention of Ischemic Stroke, 1-5, London, Martin Dunitz.
3. C.P. Warlow, M.S. Dennis, J.M. Bamford, G.J. Hankey, J. van Gijn, P.A.G.Sandercock, J. Wardlaw (1998), Stroke. A Practical Guide to Management. John Wiley&Sons, Jan 6, 672 p.
4. V. Smirnov, L. Manvelov (2001), Stroke. Suppl. J. Neurol. and Psych., 2: 19-25 (in Russian).
5. American Heart Association. Heart and stroke statistics: 1997 statistical supplements. Dallas: American Heart Association 1997
6. G.W. Petty, R. D. Brown, J. Whisnart et al. (2000), Stroke, 31: 1062-1068.
7. F. Todua, R. Shakarishvili, D.Gachechiladze (2007), Noninvasive radiodiagnosics of cerebrovascular pathologies. Tbilisi (in Georgian).
8. N.I. Vereshchagin, V.A.Morgunov, T.S.Gulevskaia (1997), Brain Changes at Atherosclerosis and Arterial Hypertony. M. (in Russian).
9. D. Gachechiladze (2005), Doctoral Thesis. Tbilisi (in Georgian).
10. A.A. Kuznetsov, A.V. Foniakin, Z.A. Sustina (2003), Clinical Medicine, 4: 34-38 (in Russian).
11. E. Doufekias, A. Segal, J. Kizer (2008), J. Am. Coll. Cardiol., 51:1049-1059, doi:10.1016/j.jacc.2007.11.053.
12. D.C. Park, H.S. Nam, S.R. Lim et al. (2000), Yonsei Medical Journal, 4: 431-435.
13. A.D. Mackinnon, R. Aaslid, H.S. Markus (2004), Stroke, 35: 73-78.
14. S. Gao, K.S. Wong, T. Hansberg, et al. (2004), Stroke, 35: 2832-2836.
15. F. Todua, D. Gachechiladze, M. Akhvediani (2004), Angiology and Vascular Surgery, 1: 70-75 (in Russian).
16. V.A. Shakhnovich, G.E. Mitroshin, D.Yu. Usachev et al. (2003), J. Neurol. and Psych., Neurodiagnostics, 3, 1: 47-52 (in Russian).

Received May, 2012

Archaeology

Uruk Migrants in the Caucasus

Konstantine Pitskhelauri

Academy Member; Department of Arts and Sciences, Ilia State University, Tbilisi

ABSTRACT. At the end of the 5th and in the 4th millennia B.C. large masses of Uruk migrants had settled in the South, and later in the North Caucasus. Assimilation of cultures of the newcomers and residents, as a result, caused their “explosive” development paving the way to the formation of the Maikop culture in the North Caucasus and the Kura-Araxes culture in the South Caucasus. © 2012 *Bull. Georg. Natl. Acad. Sci.*

Key words: *Uruk migrants, Uruk culture, Maikop culture, Kura-Araxes culture.*

The period between the 4th and 3rd millennia B.C. was the time of great cataclysmic events in the Caucasus; its cultural advances were influenced by changes within its boundaries as well as interactions with the outside world.

The most significant occurrence of this epoch was the appearance of a large number of peoples of Mesopotamian cultural identity who contributed to speeding up the rhythm of its cultural development, adding “explosive” character to its progress.

Researchers have been arguing about the problems of the local culture of this period and many of its aspects are still unresolved. However, a more or less acceptable concept of it has been already formulated. It assumes the existence of two chronologically contiguous and genetically interrelated cultures in the central area of the Southern Caucasus. Those are Sioni Late Neolithic monuments, which are adequate to the contemporaneous similar materials of Western Georgia and Tsopi Late Neolithic culture, which is spread over large territories of Eastern and Southern

Georgia as well as of the Northern Caucasus [1-5]. It is hypothesized that there was still another, not yet determined developmental stage between the above-mentioned two cultures. It is believed also that there must have been a transitional phase from the culture of Tsopi and the following early Bronze Age of Kura-Araxes culture, since in ceramic artefacts of Tsopi one can see only indications but not well recognizable forms of the latter [6:41; 5: 68].

During this period the South Caucasus experienced two powerful waves of Middle Eastern expansion: the first at the time of Late Neolithic culture of Sioni in the 4th-5th millennia B.C., and the second at the period of Tsopi culture in the Late Neolithic Age, at the end of the 5th and the first half of the 4th millennium B.C., which is known as the Uruk expansion era. Later, in the second half of the 4th and throughout the 3rd millennium B.C., during the Early Bronze Age the Kura-Araxes culture of the Caucasus spread throughout the greater part of the Caucasus, Eastern Anatolia, northern parts of Iran, Middle East and even Europe.



In my opinion this was the outcome of mutual absorption and integration of the Uruk and local cultures. During this period the central area of the South Caucasus became a new stage of mostly external influences and is referred to as the Bedenic culture. On the basis of its many characteristic features, it is considered to be of northern origin [7], however, it is a special topic of discussion and will not be touched upon here.

In this paper I would like to discuss only the penetration of large masses of people from the Uruk culture into the Caucasus. I suggest that the advanced traditions of the newcomers played an extremely important role in the formation of the local culture, fundamentally changing its character and directing the economic and social development of the host society along a radically new and progressive path.

Signs of a foreign cultural penetration into the South Caucasus at the end of the 5th and 4th millennia B.C. were noticed in the archaeological finds of the Qvirila gorge, and in the caves of Samertskhle and Samele k'ide (rock). Specifically, imported clay vessels, made on a potter's wheel, are of essentially high quality and differ from local artefacts [8]. Similar items were later identified at the Tsopi settlement of the Aeneolithic Age [9: 28-32, Fig.9]. They were found in the 1950s [5; 10] but this novelty was not yet fully understood and no opinion was formulated about its origin. Later, similar ceramic artefacts were discovered at the well-stratified settlement sites of Berik'ideebi under the earlier Kura-Araxes cultural layer and they were dated to the end of the 5th and the first half of the 4th millennia B.C.

Material of this kind was known only from the archaeological finds of the Qvirila gorge cave cultural layers which closely resembled the remarkable pottery of Maikop culture. These finds led to the conclusion that it was necessary to review and pre-date the well-known Maikop culture as belonging to an earlier period [11; 12.] This data became the firm basis for adjusting the chronology frame of archaeological finds of the 4th and 3rd millennia B.C. through-

out the Caucasus. By now, we have a specific chronology established by means of more than one radiocarbon analysis, which gave it greater credibility [13; 14: 74,75; 15]. This does not mean, however, that the coexistence of these two cultures should be moved to a later period of their development. There are enough data to support this view (newcomers from Uruk apparently did not leave the South Caucasus).

These new ideas concerning the archaeological finds in the South Caucasus were given greater attention after it had been established that there were similarities between metal and ceramic items of the Maikop culture found in the North Caucasus and those found in Mesopotamia [16]. In fact, this has become the starting point for redirecting the studies of archaeological finds in the Caucasus in connection with Mesopotamian civilization and is frequently used today [17-25].

In this context, recent archaeological finds in the Southern and Northeastern Caucasus gave yet another, entirely new nuance to scientific researches into the ancient past of the Caucasus. They made it clear that incursion of these peoples into the Caucasus was not a onetime event, but continued for a significantly long period. Reasoning by the topography of the archaeological finds in Mesopotamia, it becomes clear that large masses of migrant settlers from that area did not move straight along the route to Transcaucasia in order to reach the destination faster. Actually, they settled down in every region of the Caucasus, in the mountains and flatlands, in areas where they could maintain a lifestyle familiar to them.

It seems obvious that from that period on, two cultures of the Caucasus that had been at different stages of development could coexist peacefully on the basis of their mutual participation in metallurgical manufacturing; it was this type of communal economy that gave impetus to a speedy development of the local culture. This is well illustrated by the metallurgical items of the Kura-Araxes culture, which is significantly more advanced in comparison with the pre-Aeneolithic culture.

Presumably, the main purpose of Uruk migrants' exodus from Mesopotamia was the search for resources of metal – copper, gold, silver [26: 9; 27: 46]. I personally doubt that this could be the only reason for large masses of people to abandon their established settlement locations and move away across large distances. Most probably, they must have had another, more considerable motive, e.g. problem of overpopulation or something else. However, specific interest in metallurgical manufacturing certainly was not of secondary importance for communities whose lifestyle and cultural development was basically stimulated precisely by this type of economy [26]. Such interest of Mesopotamian communities in the Caucasus, the ancient center of metallurgy [28-32], seems quite natural to me. The archaeological discoveries made in the mountainous region of the western part of the South Caucasus, the central area of North Ossetia, along the Caucasus mountain range and at the high altitude mountainous cave cultural layers of the river Araks, all may support this assumption. The items found there were high quality ceramic vessels, made on the potter's wheel [33-39] and in one case metal artefact as well [8], all bearing characteristic features of Uruk origin. Thus, it cannot be excluded that the migrants were, indeed, metal seekers, or metal workers. Hence, it would be hard to believe that people of such highly developed culture originally belonged to the cave communities.

Initially, it was considered that this wave of Mesopotamian migrants were representatives of the Ubeid culture [40], and for quite some time this was an accepted view among scholars. Today, they are determined, and rightly so, as belonging to a later, Uruk period [21; 26; 27] when the Mesopotamian culture spread wider in the western and north-eastern direction. The data obtained in the Caucasus area confirm movement of migrants in large masses and rather intensively to the north as well.

One can identify two basic routes of Uruk migrants' movements. One started from East Anatolia along the upper reaches of the river Euphrates,

crossed Arslan Tepe region initially following the left side of the river Mtkvari (Kura) valley and after Akhaltsikhe-Abastumani went directly to the north. Then via Bagdadi-Kutaisi territory it reached the river Rioni; here it moved along its upper reaches and after traversing the Mamisoni pass reached the main area of Maikop culture distribution - the western part of the North Caucasus. This data is supported by the archaeological material with distinctly Uruk features that we have discovered along the route: Abastumani [41], Orchoshani [42-44], Dzudzuana cave [33; 34], White cave [36; 37], multilayered cave in Darkveti [35], the Samelekide and Samertskhleklde [8]. The entire material has been already published [45].

In the eastern region of the South Caucasus numerous and impressive archaeological monuments are found pointing to characteristic Uruk style material. On the basis of these finds, one can identify a credible outline of the route along which Uruk migrants moved from the northern part of Iran along the Caspian Sea shore and towards the north-east Caucasus. These are ancient settlement sites of Leilatepe, Beiu-Kesik, Poilo I and II, Misharchaia, Alikemektepes, Alkhantepe, Chinar tepe, Abdal Aziz Tepe, Shomul Tepe, Adsiz Tepe, Agil Tepe, Khodjasan and others [13; 14; 46-55]; burial mounds in the Absheron peninsula – Uch-Tepe, Soyug-Bulag [56-60]. Material closely resembling artefacts of the Maikop culture [64] is found in Se Girdan burial mound in north-west Iran [27, 61-63; references according to Akhundov, Mahmudova and Narimanov; Akhundov and Aliev]. A whole series of settlement sites and burial mounds have been found throughout Dagestan's mountainous and Caspian shore areas, from Samur all the way to Sulaka: Ginchi, Velikent, Toprak-kale, New Gaptakhm Serzhen-lurt, Ust Dzegutinsk, Gorodskoe, Beliaevo, Serker, Tepe, Miatl, Miskin Bulak, Diubend, Seidlar and others; they all are a part of the same route (the information is based on the maps attached to the manuscript [55] and articles [27; 65; 66]). It is believed that the influence of the Uruk culture covers the entire North Caucasus

and spreads from the Caspian Sea shore to the west all the way to the area of the Maikop culture [22; 27].

In a discussion concerning the movement of Uruk migrants from the South to the north, it is hardly possible to ignore the variety of data that points at the Jvari Pass as one of the segments of their routes [39; 67-69].

In order to have a clear idea about the settlement of Uruk migrants throughout the Caucasus territory, we should list all the known sites in the central part of the South Caucasus, where material, specific to their culture has been found. Undoubtedly, there must have been many more similar sites, but, as we will demonstrate further down, even the data available today is sufficient for forming a definite opinion concerning the matter. One of the most important among them is a burial mound with a large catacomb-like grave that was discovered on the Iori plateau near Dedoplistsqaro. Although it had been damaged by treasure hunters, it was possible to establish that the site represented a collective grave with ceramic vessels typical for the Kura-Araxes culture [70: 7-24]. The particularly significant item was an oblong stone insignia with circular cross-section, and with an image of an animal's head on one of its sides. Similar items have been found among other typically Uruk style material in the burial mounds around lower parts of the river Mtkvari (Kura) [50: Tabs. 28, 30, 35; 60:78; 71: Fig. 4]. This item was found among the material dug up by grave robbers, but this fact hardly puts under suspicion that it has been a part of the gravesite paraphernalia. A similar insignia was accidentally found also near the village Cheremi, on the Gombori mountain range in the South central Caucasus (it is preserved in the depository of the Georgian National Museum in the city of Gurjaani.)

With regard to Uruk migrants, a particularly noteworthy location is the Tsopi settlement where high quality ceramic vessels of apparently Uruk origin were found *in situ* in the cultural layer among local pottery [72: 55; 5]. One can say the same about the multilayered settlement Berikldeebi that allowed us to deter-

mine the chronological relationship of this culture with the local Kura-Araxes culture [11; 12]. It is also important that at this site among the finds of contemporaneous nature there was a quadrangular religious structure, the only one in the Caucasus, that is believed to have had originated in Southwest Asia [73: 34, 35]. Another exceptionally significant site was discovered near the village Kavtiskhevi in the area of the river Mtkvari flatlands; it is a large burial mound containing specifically Uruk style ceramic vessels [74]. It is also remarkable that items of this type were also found at the Tetristsqaro settlement site where fragments of a potter's wheel have been discovered as well [75: 56, 59, 71]. Similar high quality ceramic vessels were found in the western part of Tbilisi, in the cultural layer of the Delisi settlement [76: 31; 77]. We should mention as well the presence of similar material in the Tekhut settlement in the Ararat valley [78] and in the upper horizon of the cultural layer of the cave Areni I near the estuary of the river Araks [38]. These two points represent medial segments connecting Mesopotamia to the Caucasus and therefore they deserve particular attention in studies related to this problem.

In the past centuries, large masses of migrants left a strong positive or negative trace along the path of their movement. Their consequences must definitely be taken into consideration in order to get a clear picture of the indigenous population's past. According to our data the wave of Uruk migrants moving from the south to the north covered the entire territory of the Caucasus in the 4th millennium B.C. It seems that at the very outset, they settled all over the South Caucasus, acclimatized to local conditions, assimilated with the local population and jointly continued their customary activity. Probably in search of predominantly metal works, they gradually got acquainted with the main mountain range of the Caucasus, traversed it to the north Caucasus either through passages across it or along the sea shore strip and spread throughout both its highlands and valleys. It is quite possible that it was they, the bear-

ers of advanced culture of Mesopotamia, who had a deep impact on the development of local cultures of the Caucasus, speeded up its development and gave it “explosive” character. It is believed that precisely this integration of indigenous and incoming cultures made possible the emergence of the so-called magnificent Maikop culture in the north-western part of the Caucasus. It is possible that a similar process was simultaneously developing in the South Caucasus as well, where it left a noticeable trace. The transformation was so significant that it is reasonable to presume that Uruk migrants together with the local population participated in the creation of the powerful Kura-Araxes culture in the South Caucasus of the Early Bronze Age.

There are differing views concerning the direction of the routes along which large masses of migrants moved on the territory of the South Caucasus in the 4th-3rd millennia B.C., and accordingly, we have different interpretations of the relevant transformative processes.

Some scholars do not deny the fact of Uruk migration to the north across the South Caucasus. In their opinion, these migrants traversed the Greater Caucasus range to the north and contributed to the formation of the magnificent Maikop culture. Later, however, some of them, already naturalized Maikop inhabitants, returned to the South Caucasus and finally settled in the area of the lower reaches of the river Mtkvari [52; 55; 71]. In support of the theory about the southbound movement of the migrants back from the north, the authors point at a single proof, the burial mounds containing Uruk artefact that have been discovered in the South Caucasus. They consider that Uruk migrants had learned in the north how to build this type of burial mounds and brought the acquired tradition back to the South Caucasus.

There are other opinions concerning the routes of Uruk migrants’ entry into the Caucasus and their movements through the territory. For example, some believe that one group of these migrants entering the

Caucasus from Anatolia, moved along the upper stream of the Mtkvari, then followed the river Rioni to the north towards the Kuban area. The second group crossed Shida Kartli from the basin of the rivers Rioni and Qvirila and settled in the eastern part of the Kvemo Kartli valley [79: 182-186]. It is not clear to me, why those researchers did not choose eastern track of Uruk migrants which started from Northern Iran, passed through the eastern side of the South Caucasus and the west coast of the Caspian Sea, and crossed the North Caucasus [80: 341]. This route is more real and better confirmed with finds. However, it looks like even in this case they do not exclude the possibility of the reverse movement of the integrated migrant population after the formation of the Maikop culture since in their opinion the Maikop artefact reached the south across the Greater Caucasus passes [79:190,191]. It is possible that both these views have accepted *a priori* the idea concerning the north-south interaction and the tradition of the specific structure of the burial mounds was brought from the north; they particularly stress the superior influence of the northern steppe traditions in the South Caucasus. Up to now these views were believed to be an indisputable truth. Understandably, the scientists had enough ground to formulate their conviction. From the start they supported this assumption by the fact that the burial mounds were typical of the ancient pit-grave culture and already present throughout the northern steppe zone in the 4th millennium B.C., whereas there were no mounds of such construction in Southwest Asia. This was why they assumed that even the magnificent Maikop culture absorbed the technique of building this type of burial mounds as a result of its contacts with the steppe area cultures [81: 75].

At present the situation has changed drastically. On the basis of a whole series of radiocarbon analyses, it has been proved [15; 82] that burial mounds of the ancient pit-grave culture are of a significantly later period in comparison with Maikop archaeological sites. This allows scholars to assume that the tradition of

building this type of burial mounds emerged precisely in the Maikop culture. Its ties with Levant and Mesopotamian antiquities point to its earlier origin [15: 97]. At the same time, a whole range of chronological data obtained with radiocarbon analysis has established that the settlements and burial mounds of the South Caucasus containing Uruk artefact are coexistent with the Maikop culture [13: 149-153] and, accordingly, the ancient pit-grave culture and its burial mounds belong to a later period. Therefore, today we cannot possibly ascribe the emergence of this kind of burial mounds in the Maikop culture as well as similar contemporaneous sites in the South Caucasus to the influence of the steppe zone cultures. Moreover, there were no adverse conditions that would have prevented emergence of this type of burial mounds in the Caucasus itself.

The custom of constructing such burial mounds continued even in a later period. Researchers discern two groups of burial mounds in the 3rd millennium B.C. [83]. The first group is represented by large, individual burial mounds containing items belonging to the final phase of the purely Kura-Araxes culture [84: 29; 31], while artefacts typical of the north are seldom found [84: 31]. The second group of burial mounds of the same period is represented by grave sites of the so-called Bedenic culture containing material distinctly different from that of the South Caucasus. In the central and eastern part of the South Caucasus the type of burial mounds remained of traditional form even in the first half of the 2nd millennium B.C. and became quite rare in the later periods.

In connection with the given issue, we should set apart one particular group of mounds from those of the 3rd millennium B.C. These are especially rich burial mounds of the Kura-Araxes culture in its final

stage of development known as the Martqopi period. Among them large burial mounds on the left bank of the river Alazani merit particular attention. Their remarkably strong stone armour mounds are often 20-25 meter high and 200-300 meter in diameter. They contain especially rich artefacts, among them gold and silver jewelry [28: 235; 85].

I believe, this was the final stage of the integration of the Uruk migrants into the Kura-Araxes culture when their social and economic development reached its zenith. It is natural that such thoroughly settled migrants influenced the languages of the communities living in the Caucasus [86: 38-155; 87: 22-26; 88: 29-39].

It needs to be clarified why Uruk migrants left their distinct imprint on the Maikop culture, while we do not see similar signs in the Kura-Araxes culture. I suggest that the main reason of it is the fact that so far the problem of fusion of Uruk migrants in the culture of the South Caucasus has not been sufficiently studied. It should be also taken into consideration that the inhabitants of the Kura-Araxes area did not lose their already well defined cultural identity thanks to their powerful energy of inherent development. Nevertheless, the consequences of their interaction are well discernible in the “explosive” nature of the development of the Kura-Araxes culture in its final phase.

Thus, we offered here a model of development of the Kura-Araxes culture in its final, “explosive” phase and participation of Uruk migrants in this process. However, this is only a tentatively posited scientific problem. In order to arrive at a final conclusion it is necessary to make a thorough study and every detail from various aspects, which goes beyond the framework of the present article.

არქეოლოგია

ურუქელი მიგრანტები კავკასიაში

კ. ფიცხელაური

აკადემიკოსი; ილიას სახელმწიფო უნივერსიტეტი, მეცნიერებათა და ხელოვნების ფაკულტეტი, თბილისი

ძვ. წ. V ათასწლეულის მიწურულსა და ძვ. წ. IV ათასწლეულში, ვერ სამხრეთ, შემდეგ ჩრდილოეთ კავკასიაში კომპაქტურად საზღვრავდა ურუქელ მიგრანტთა დიდი მასები. უცხო და დამხვედური მოსახლეობის კულტურების შერწყმის შედეგად განსაკუთრებით წინაურდება ბრინჯაოს მეტალურგია, რაც “ფეთქებადი” განვითარების საფუძველი ხდება. შედეგად, ჩრდილოეთ კავკასიაში ფალიბდება მაიკოპის, ხოლო სამხრეთ კავკასიაში – მტკვარი-არაქსის კულტურა.

REFERENCES

1. T. Kiguradze (1976), Periodization of the Early Agricultural Culture of Eastern Trans-Caucasia. Tbilisi, 176 p., 60 tab. (in Georgian).
2. T. Kiguradze (1986), Neolithische Siedlungen von Kvemo-Kartli, Georgien. Materialien zur Allgemeinen und Vergleichenden Archäologie, Band 29. München, 116 p., 4 tabs.
3. M. Menabde, T. Kiguradze (1981), Sioni Archaeological Monuments. Tbilisi, 122 p., 19 tabs. (in Georgian).
4. L. Nebieridze (2001), Settlement Sioni – A Late Aeneolithic Monument of Eastern Georgia. Dzeblani. Journal of the Georgian Archaeology/Georgian National Museum, 7: 5-13. Tbilisi (in Georgian).
5. L. Nebieridze (2010), Tsopi Aeneolithic Culture. Tbilisi, 256p. (in Georgian).
6. T.N. Chubinishvili (1971), K drevnei istorii luzhnogo Kavkaza. Tbilisi, 169p., Tab.I(in Russian).
7. K.K. Pitskhelauri (2012), In: Problems of History and Archaeology of Georgia and the Caucasus. Tbilisi (in Georgian).
8. L. Glonti, A. Javakhishvili, G. Javakhishvili, et al. (1968), Vestnik Gosudarstvennogo Muzeia Gruzii, XXV-B: 3-14. Tbilisi (in Russian).
9. K.Kh. Kushnareva, T.N. Chubinishvili (1970), Drevnie Kul'tury luzhnogo Kavkaza (V-III tys.do n.e.), Leningrad, 187 p. (in Russian).
10. L. Nebieridze, N. Tskvitinidze (2011), in: Arkheologia, Etnologia, Fol'kloristika Kavkaza, 178-180, Tbilisi (in Russian).
11. L. Glonti, A. Javakhishvili (1987), Kratkie Soobshcheniya Instituta Arkheologii, 192: 80-86. M. (in Russian).
12. A. Zavaxivili (1998), Ausgrabungen in Berikldeebi (Sida Kartli), “Georgica”. Zeitschrift für Kultur, Sprache und Geschichte Georgiens und Kaukasiens. Heft N 21: 7-20. Konstanz.
13. N. Museibli (2007), Chalcolite settlement Beyuk-Kesik, Baku, 227 p. (in Russian and English).
14. N. Aliev, I. Narimanov (2001), Kul'tura severnogo Azerbaidzhana v pozdnem Eneolite. Baku, 142 p. (in Russian).
15. E.N. Chernykh, L.B. Orlovskaya (2004), Rossiiskaia Arkheologia, 1: 80-99. M. (in Russian).
16. M.V. Andreeva (1977), Sovetskaia Arkheologia, 1: 39-56, M. (in Russian).
17. V.A. Trifonov (1987), Kratkie Soobshcheniya Instituta Arkheologii, 192: 18-26. M. (in Russian).
18. I.M. Mziev (1990), Sovetskaya Arkheologiya, 4: 131-137. M. (in Russian).
19. R.M. Munchaev (1994), Maikopskaia Kultura, Arkheologia, Ranniaia i Sredniaia Bronza Kavkaza, 158-225. M. (in Russian).



20. R.M. Munchaev (1996), in: Mezhdru Aziei i Evropoi. Kavkaz v IV-I tys. do n.e. Materialy konferentsii posviashchennoi 100-letiiu so dnia rozhdeniia A.A.Iessena. 37-38, Spb. (in Russian).
21. R.M. Munchaev (2005), Rossiiskaia Arkheologiya. 1: 13-24. M. (in Russian).
22. R.M. Munchaev, Sh.N. Amirov, R.G. Magomedov (2010), in: Issledovaniia pervobytnoi arkheologii Evrazii. 316-334. M. (in Russian).
23. S.N. Korenevskii (1993), Drevneishee oseedloe poselenie na srednem Tereke. M. 167p. (in Russian).
24. S.N. Korenevskii (2004), Drevneischie zemledel'tsy i skotovody Predkavkaz'ia. 113 p. 122 figs. 19 tabs. M. (in Russian).
25. S.N. Korenevskii (2007), in: Arkheologiya, Etnologiya, Fol'kloristika Kavkaza, 58-59. Makhachkala (in Russian).
26. R.M. Munchaev (2007), in: Arkheologiya, Etnologiya, Fol'kloristika Kavkaza, 89. Makhachkala (in Russian).
27. R.M. Munchaev, Sh.N. Amirov (2009), in: Kavkaz – Arkheologiya, Etnologiya. Materialy Internatsional'noi Konferentsii, 41-52. Baku (in Russian).
28. I. Gambashidze, G. Mindaishvili, G. Gogochuri, K. Kakhiani, I. Japaridze (2010), Ancient Metallurgy and Mining in Georgia at 6th-3rd Millennium B.C. Tbilisi, 592 p. (in Georgian).
29. G. Inanishvili, B. Maisuradze, G. Gobejishvili (2010), Mining and Metallurgical Activity in Ancient Georgia (3rd-1st millennia B.C.), Tbilisi , 224 p. (in Georgian).
30. Ts. Abesadze (2011), Towards the History of the Metallurgy in Georgia. Tbilisi, 398 p. (in Georgian).
31. A.Ts. Gevorkyan (1980), Iz istorii drevneishei metallurgii Armianskogo nagor'ia. Yerevan, 127 p. (in Russian).
32. K. Pitschelauri (1997), Waffen der Bronzezeit aus Ost-Georgien. Archäologie Eurasien, Band 4, 87 p. 116 tabs., Berlin.
33. D. Tushabramishvili (1971), Archaeological Research in Georgia in 1969. 5-7. Tbilisi (in Georgian).
34. D. Tushabramishvili (1972), Archaeological Research in Georgia in 1971. 4-5. Tbilisi (in Georgian).
35. L. Nebieridze (1978), Darkveti Multilayer Rockshelter. Tbilisi, 105 p. 12 tab. (in Georgian).
36. A. Kalandadze, K. Kalandadze, A. Ioseliani, et al. (1976), Polevye Arkheologicheskie Issledovaniia v 1974. 7-10. Tbilisi (in Russian).
37. A. Kalandadze, K. Kalandadze, M. Gabunia, et al. (1979), Polevye Arkheologicheskie Issledovaniia v 1975. 8-9. Tbilisi (in Russian).
38. D. Zardaryan (2011), in: Arkheologiya, Etnologiya, Fol'kloristika Kavkaza. 123-124. Tbilisi (in Russian).
39. N.I. Gijrati, D.F. Rostunov (1993), in: Kavkaz i tsivilizatsiia Vostoka v drevnosti i srednevekov'e. 75-99. Vladikavkaz (in Russian).
40. I. Narimanov (1985), Vsesoiuznaia Arkheologicheskaia Konferentsiia „Dostizheniia Sovetskoi Arkheologii v XI Piatiletke“. Tezisy dokladov, 71-72. Baku (in Russian).
41. K. Kalandadze (1974), Polevye Arkheologicheskie Issledovaniia v 1973. 11-12. Tbilisi (in Russian).
42. L. Jibladze (2005), in: Arkheologiya, Etnologiya, Fol'kloristika Kavkaza, 100-101. Baku (in Russian).
43. A. Orjonikidze (2005), Dzebani. Journal of the Georgian Archaeology/Georgian National Museum, 15-16, 69-73. Tbilisi (in Georgian).
44. G. Pkhakadze (2009), In: Annals, 5: 222-241. Tbilisi (in Georgian).
45. G.G. Pkhakadze (1988), Sovetskaia Arkheologiya. 2: 43-57. M. (in Russian).
46. A. Agalarzade (2009), in: Kavkaz – Arkheologiya i Etnologiya. Materialy Internatsional'noi Nauchnoi Konferentsii. Shamkir, 2008. 83-88. Baku (in Russian).
47. Kh. Alamedov (2009), in: Kavkaz – Arkheologiya i Etnologiya. Materialy Internatsional'noi Nauchnoi Konferentsii. Shamkir, 2008. 89-95. Baku (in Russian).
48. T. Akhundov (2001), Severno-Zapadnyi Azerbaidzhan v Epokhu Eneolita i Bronzy. Baku. 331 p. (in Russian).
49. T. Akhundov (2005), in: Archaeologiya, Etnologiya, Folkloristika Kavkaza. 52-53. Baku (in Russian).
50. T. Akhundov, F. Mahmudova (2008), Iuzhnyi Kavkaz v kavkazsko-peredneaziatskikh etnokulturnykh processakh v IV tys.do n.e. Baku , 197 p. (in Russian).
51. T. Akhundov (2007), in: Arkheologiya, Etnologiya, Fol'kloristika Kavkaza, 61-64. Makhachkala (in Russian).
52. T. Akhundov (2010), in: Arkheologiya, Etnologiya, Fol'kloristika Kavkaza. Tbilisi (in Russian).
53. F. Guliyev (2005), in: Arkheologiya, Etnologiya, Fol'kloristika Kavkaza. 82. Baku (in Russian).
54. N. Museibli (2010), in: Arkheologiya, Etnologiya, Fol'kloristika Kavkaza. 208-211. Tbilisi (in Russian).
55. I. Narimanov, T. Akhundov, N. Aliev (2007), Leilatepe (Poselenie, traditsiia, etap v etnokul'turnoi istorii Iuzhnogo Kavkaza). Baku, 128 p. (in Russian).
56. N.G. Aliev (2005), in: Arkheologiya, Etnologiya, Fol'kloristika Kavkaza. 34. Baku (in Russian).
57. A.A. Yessen (1965), Materialy po Arkheologii SSSR, 125: 153-194, M.-L. (in Russian).
58. N. Museibli (2005), in: Arkheologiya, Etnologiya, Fol'kloristika Kavkaza. 135-138. Baku (in Russian).
59. N. Museibli (2005), in: Kavkaz – Arkheologiya i Etnologiya. Materialy Internatsional'noi Nauchnoi Konferentsii. Shamkir, 2008. 53-63. Baku (in Russian).
60. B. Lyonnet (2009), in: Kavkaz – Arkheologiya i Etnologiya. Materialy Internatsional'noi Nauchnoi Konferentsii. Shamkir, 2008. 69-78. Baku (in Russian).

61. *O.W. Muscarella* (1969), The Tumuli at Segirdan. A Preliminary Report. Metropolitan Museum Journal 1969, II.
62. *O.W. Muscarella* (1971), The Tumuli at Segirdan: Second Report. Metropolitan Museum Journal 1971, IV.
63. *O.W. Muscarella* (2003), The Chronology and Culture of Segirdan. Ancient Civilizations from Scythia o Siberia.
64. *V.A. Trifonov* (2000), Kurgany Maikopskogo tipa v Severno-zapadnom Irane. 244-264, S.-Pb (in Russian).
65. *M. Gajiyev* (1966), Kratkie soobshcheniia Instituta Arkheologii. 108, M. (in Russian).
66. *R.G. Magomedov* (2007), in: Arkheologia. Etnologia. Fol'kloristika Kavkaza, Makhachkala (in Russian).
67. *G. Gogochuri, V. Rostunov, G. Chikovani* (1996), International Conference "The Caucasus in the Context of World History", Abstracts of Papers. Tbilisi.
68. *V. Rostunov* (2005), in: Arkheologia. Etnologia. Fol'kloristika Kavkaza, Baku (in Russian).
69. *S. Korenevskiy* (1996), New settlement Redant near Vladikavkaz. Abstracts of Papers of the International conference "The Caucasus in the Context of World History", Tbilisi.
70. *I. Varazashvili* (2008), "Amirani" - Bulletin of the International Caucasological Research Institute, XIX: 7-24, Tbilisi-Montreal (in Georgian).
71. *T. Akhundov, K. Alamedov* (2009), South Casasia in the Neolithic to Early Bronze Age (Central and Eastern Regions). ALBEW. TKTD "FG" IS.
72. Archaeology of Georgia, II, (1992), Tbilisi, 124-151. (in Georgian).
73. *G. Kipiani* (1997), Bulletin of the Georgian State Museum, XI,II-B, 13-57. Tbilisi (in Georgian).
74. *Z. Makhharadze* (2007), In: B.Lyonnet (ed.), Les cultures du Caucase (VI^e-III^e millénaires avant notre ère). Leurs relations avec le Proche-Orient. Paris, pp.123-131.
75. *G. Gobejishvili* (1978), Settlement Tetrtskaro, Tbilisi, 118 p. (in Georgian).
76. *R. Abramishvili* (1978), Settlement Delisi. Collection of Works, I, 28-33, Tbilisi (in Georgian).
77. *E. Gogadze* (2003), Dzicbani. Journal of the Georgian Archaeology/Georgian National Museum, Additions, X, 27-29, Tbilisi (in Georgian).
78. *R. Torosyan* (1976), Early Agricultural Settlement Tekhuta. Yerevan, 142 p. (in Armenian).
79. *O. Japaridze* (2011), Researches in Archaeology of Georgia, 20, 178-196. Tbilisi (in Georgian).
80. *R.M. Munchaev, N.Ya. Merpert, Sh.A. Amirov* (2010), Research of Primitive Archaeology of Eurasia. 335-343, Makhachkala (in Russian).
81. *A.D. Rezepkin* (1991), International Symposium-Colloquium "Caucasus in the System of Palaeometal Cultures of Eurasia", 72-79, Tbilisi (in Russian).
82. *E.N. Chernykh, L.B. Orlovskaya* (2007), In: Arkheologia. Etnologia. Fol'kloristika Kavkaza, 10-28, Makhachkala (in Russian).
83. *Z. Makhharadze, A. Orjonikidze* (2007), Archaeology, Ethnology, Folklore of Caucasus, 83-84, Makhachkala (in Russian).
84. *O. Japaridze* (1988), Proc. Georg. Acad. Sci. Ser. Archeology, Ethnography and History of Arts, 4, Tbilisi (in Georgian).
85. *K. Pixelauri, W. Orthmann, D. Qvavadze* (1994), Neue archäologische Funde in Kachetien. in: Georgica, Heft 17: 9-13, Konstanz.
86. *R. Gordeziani* (2007), Mediterranea – Kartvelica, I, Origins, Tbilisi, 209 p. (in Georgian).
87. *N. Khazaradze, K. Topuria* (2000), In: Issues of the International Symposium on the Development of Natural and Engineering Sciences, 22-26, Tbilisi (in Georgian).
88. *G. Giordadze, N. Khazaradze* (2002), In: Ethnogenesis of the Georgians. 29-39, Tbilisi (in Georgian).

Received May, 2012

Economics

Impact of the Average Tax Rate on the Aggregate Demand (Keynesian Models)

Iuri Ananiashvili* and Vladimer Papava**

* I. Javakishvili Tbilisi State University, Tbilisi

** Academy Member, P. Gugushvili Institute of Economics, I. Javakishvili Tbilisi State University, Tbilisi

ABSTRACT. Based on an analysis of a modified version of the standard Keynesian Model of a product market, it is shown that a change in the average tax rate has a complex effect on aggregate demand. Depending on the marginal propensity of households to consume and the marginal propensity for government purchases, an increase in the average tax rate may lead to either a decrease or an increase in aggregate demand. In this case, since the parameter of marginal propensities to purchase is easily regulated, by selecting its appropriate value the government can purposefully use a tax increase to stimulate or to reduce aggregate demand. © 2012 Bull. Georg. Natl. Acad. Sci.

Key words: Keynesian model of aggregate demand, average tax rate, marginal propensity to consume, marginal propensity to public purchases.

Since the 1930s, after John Maynard Keynes proposed the concept of government regulation of the economy, economists' interest in taxes has grown considerably. As we know, in this concept, taxes, along with government purchases and transfer payments, are supposed to play a significant role in regulating aggregate demand and, through aggregate demand, in solving problems of employment, inflation, and economic growth.

In contemporary macroeconomics, the interrelation of taxes and aggregate demand is ambiguously defined: it is thought that increasing taxes has a negative effect on aggregate demand and that lowering them has a positive effect, since the main element of aggregate spending – the amount of household consumer spending – decreases in the former case and

increases in the latter [1, ch. 3; 2, ch. 9; 3, ch. 12; 4, ch. 5]. However, because every phenomenon, including a change in taxes, has two sides – positive and negative – by considering the relationship between taxes and aggregate demand only in this context, we significantly simplify the existing reality. It can be shown that, in a certain situation, a tax increase causes an increase in aggregate demand and a tax cut causes a decrease [5]. We will consider this question in greater detail.

Version I of the Keynesian Model. The explanation of the mechanism and pattern of the average tax rate's influence on aggregate demand is traditionally based on using a modeling method. We will turn to this method and first consider the simplest standard

Keynesian Model of equilibrium in the market for goods and services, which can be written as follows [1-4]:

$$E = C + I + G + NX, \quad (1)$$

$$C = a + b(Y - T), \quad (2)$$

$$I = I_0, \quad G = G_0, \quad NX = NX_0, \quad (3)$$

$$T = T(Y), \quad (4)$$

$$Y = E, \quad (5)$$

where E is aggregate spending; C is household consumption; I is gross domestic private investments; G is government purchases; NX is net exports; a is autonomous consumption; b is marginal propensity of households to consume, $0 < b < 1$; T is net taxes (the difference between taxes and transfers); and Y is gross domestic product (GDP).

In this system, conditions (1)–(4) determine aggregate spending. According to (2), the element C of this spending is a linear function of current disposable income $(Y - T)$. As for the remaining three elements, I , G , and NX , for the sake of simplicity it is understood that they are given exogenously in the model and fixed at the levels I_0 , G_0 , and NX_0 , respectively, as indicated in (3).

The condition corresponding to net taxes (4) requires special scrutiny. Traditionally, in a simple model such as (1)–(5) it is either accepted that taxes are of a lump-sum nature (or fixed), and $T = T_0$, where T_0 is a fixed amount, or a linear taxation system is considered, in which T is defined as a linear function of Y . In the latter case, depending on what form of taxation $T(Y)$ describes, three possible versions can be considered: functions corresponding to proportional, linearly progressive, and linearly regressive taxation. We should point out that in model (1)–(5), the consideration of any of the functions given here in the role of $T(Y)$ makes it possible to draw almost the same conclusions. Therefore, we will dwell on just one of them, for example,

$$T(Y) = tY. \quad (6)$$

Henceforth we will call the system (1)–(6) *Version 1 of the Keynesian Model*.

Taking into account conditions (2), (3), and (6), in (1) we get:

$$E = b(1-t)Y + I_0 + G_0 + NX_0 + a.$$

With a fixed level of prices (which takes place in the model under consideration), E , which is determined by the given equation, can be regarded as the value of aggregate demand. As we see, E depends on the aggregated average tax rate t and, all else being equal, decreases in relation to the latter. In turn, in model (1)–(6), for a given fixed level of prices, the output (supply) of GDP amounts to Y . This implies that it is completely determined by aggregate demand.

In such conditions, the value of equilibrium GDP is determined from the equilibrium equation of the market for products and services (5):

$$Y = \lambda_1 A_1, \quad (7)$$

where A_1 is the amount of autonomous spending:

$$A_1 = a + I_0 + G_0 + NX_0, \quad (8)$$

and λ_1 is autonomous spending multiplier:

$$\lambda_1 = \frac{1}{1 - b(1-t)}. \quad (9)$$

Since the multiplier λ_1 decreases in relation to t , (7)–(9) formally lead to the following conclusions:

1. For given autonomous spending (all else being equal), equilibrium output is a decreasing function of t . At the same time, if we assume that t can take extreme values from 0 to 1, then the equilibrium output is maximum when $t = 0$ and minimum when $t = 1$. In particular, $Y_{\max} = A_1 / (1 - b)$ and $Y_{\min} = A_1$.
2. For given autonomous spending, the net budget revenues (net taxes T) corresponding to equilibrium output are an increasing function of t . T is maximum when $t = 1$ and minimum when $t = 0$. In this case, $T_{\max} = A_1$ and $T_{\min} = 0$.

3. For given t , the equilibrium output and corresponding budget revenues increase (or decrease) when there is an increase (or decrease) in autonomous spending A_1 , of which one of the elements is government purchases G_0 .

We should point out that a change, an increase, for example, in A_1 causes simultaneous upward movement of the curves corresponding to T and Y .

With aggregate supply that does not depend on t , which takes place in model (1)–(6), the relationship between the average tax rate, equilibrium output, and budget revenues can be considered true only when government purchases G_0 and net taxes T do not depend on each other. Naturally, in such conditions, when the average tax rate rises and G_0 is fixed, there is an outflow of some funds from economic circulation, which, all else being equal, has a negative effect on the amount of aggregate demand and causes a contraction of equilibrium output.

However, in reality, T and G are quantities that depend on each other. In practice, the value of G is generally planned, for the most part, depending on what the expected net tax revenues T are. Furthermore, the need for changes in the average tax rate t is determined precisely by the steady growth of government purchases. According to Wagner's law, demand for public goods rises faster than demand for private goods, which is gradually saturated [6]. Therefore, consumers are willing to give up more and more of their income as taxes funding the production of public goods [7, p. 390]. Hence, in the model of aggregate demand, G and T should be considered not as isolated from each other – as in (1)–(6) – but as related to each other.

Version II of the Keynesian Model. We now consider the connection between government purchases (G) and net taxes (T) using an equation for the government's budget:

$$D = G + rB_{-1} - T = (G - T) + rB_{-1}, \quad (10)$$

where B_{-1} is the amount of government debt or government assets at the beginning of the period (in the

case of debt, $B_{-1} > 0$; in the case of assets, $B_{-1} < 0$); r is the averaged rate based on which interest payments are made at the expense of debt or assets. Consequently, rB_{-1} represents the amount of debt service ($rB_{-1} > 0$) or interest income ($rB_{-1} < 0$) received from payments out of assets; and D is a quantity representing the budget's deficit or surplus. If $D = 0$ in (10), then the budget is balanced. If $D < 0$, then the budget has a surplus. And finally, if $D > 0$, then the budget has a deficit.

In the case of a deficit budget, tax revenues are not enough to cover spending. Therefore, the government is forced to borrow an appropriate amount from the private sector, international financial organizations, other countries, or the central bank. Borrowing from the private sector is particularly common. This process is carried out directly by the state treasury, whose securities are sold to individuals, firms, commercial banks, and other financial institutions. The money obtained in this way at the expense of the state treasury is used, just the way tax revenues are, to cover government spending. Financing a deficit with credit from the private sector (*debt financing*) is the basic form of deficit financing and is widely used in most countries in the current conditions. However, there are individual exceptions, especially in developing countries, when the treasury borrows from the central bank to finance a deficit. In this case, the central bank actually purchases an appropriate part of the treasury's debt and creates "high-efficiency money" [3, ch. 9]. As we know, such financing is called *monetization of the deficit*. Without dwelling here on the positive and negative points of financing a budget deficit in these ways, we only point out that a budget cannot be constantly in deficit. There are periods when it is in surplus. In such cases, the government uses the surplus to repay or reduce the accumulated debt, or to create a reserve fund.

For simplicity, in what follows we use D to represent a deficit and B to represent government debt. At the same time, if necessary, we will specify the content of these quantities more precisely.

Equation (10) shows that the total budget deficit D is divided into two parts. One of them $(G - T)$ is called a *primary deficit* when it is positive, and a *positive primary balance* when it is negative; and the other, rB_{-1} , is net interest payments [1, ch. 16]. Representing the deficit in this form emphasizes the special significance of government debt service in budget spending. If there is debt, the interest payments necessary to service it may be so high that the budget as a whole is in deficit, even in the case of a positive primary balance.

As we see, the amount of government debt at the beginning of the period determines how much the current budget is in deficit. For its part, the budget deficit is also a basis for the origin and growth of debt. Or rather, a budget deficit in the current period fosters the growth of government debt at the beginning of the next period. In general, the following relationship is valid [4, p. 557]:

$$B = B_{-1} + D,$$

where B_{-1} and B are the values of government debt at the beginning and end of the period, respectively.

In this relationship we take into account the value of D from (10). Using simple operations, we get an equation that can be used to determine government debt based on the primary budget deficit as:

$$B = (G - T) + (1 + r)B_{-1}. \quad (11)$$

We will assume that B_{-1} in (11) is fixed and is a given quantity. This is a natural assumption, since the amount of B_{-1} is completely determined by decisions that the government has made in past periods. We will also assume that the value of the debt B at the end of the period is exogenously planned in the government budget and, if necessary, can be changed by taking on new debt or reducing current spending. As for government purchases G , they are tied to T and are determined from (11) as follows:

$$G = T + (B - (1 + r)B_{-1}). \quad (12)$$

Consequently, we understand that the amount of government purchases is determined, on the one

hand, by net tax revenues T and, on the other hand, by the policy that is conducted in relation to government debt. In other words, a change in G cannot be isolated – in the form in which it is traditionally considered in simple Keynesian Models, including the model (1)–(6) – and it is always associated with a change in taxes or debt (or both at the same time).

We replace the condition $G = G_0$ in model (1)–(6) with (12), and we call the system modified in this way *Version II of the Keynesian Model*. The equation for calculating equilibrium output will take the following form for this model:

$$Y = \lambda_2 A_2, \quad (13)$$

where

$$A_2 = a + (B - (1 + r)B_{-1}) + I_0 + NX_0, \quad (14)$$

$$\lambda_2 = \frac{1}{1 - b(1 - t) - t}. \quad (15)$$

Consequently, in (13)–(15), in contrast to (7)–(9), what determines autonomous spending A_2 , along with other elements, is not total government purchases G_0 , but only the part of them made at the expense of government debt incurred in the current period $(B - (1 + r)B_{-1})$. According to (11), this quantity is determined by the primary budget deficit $(G - T)$. Moreover, in Version II of the Keynesian Model, the autonomous spending multiplier λ_2 has a completely different form. While in conditions (7)–(9) the multiplier λ_1 diminishes in relation to t , the opposite situation takes place in this case, and the multiplier λ_2 increases in relation to t . This circumstance leads to the following conclusions for Version II of the Keynesian Model:

1. All else being equal, the creation or growth of government debt (creation or growth of a primary budget deficit $(G - T)$) has a positive effect on equilibrium output, while reduction of government debt or growth of government assets (creation or growth of a primary budget surplus $(T - G)$) has a negative

effect. It is obvious that this situation is completely consistent with traditional Keynesian theory.

2. All else being equal, equilibrium output is an increasing function of the average tax rate t : $dY/dt > 0$. For given positive autonomous spending: $Y_{min} = A_2/(1-b)$, when $t=0$; and $Y_{max} = \infty$, when $t=1$. This result, which is not the customary one for Keynesian theory, is interesting from the point of view that, according to Version II of the Keynesian Model, in conditions of insufficient autonomous spending, one of the most important ways of increasing aggregate demand and boosting economic activity is to increase the average tax rate.

3. All else being equal, net budget revenues are an increasing function of t , and for given $A_2 > 0$: $T_{min} = 0$, when $t=0$; and $T_{max} = \infty$, when $t=1$.

We dwell further on an interesting result that follows from the relationship (13)–(15). In characterizing the effectiveness of fiscal policy tools, researchers often turn to the theorem of the well-known economist Trygve Haavelmo [8; 9, p. 95]. Based on a simple Keynesian Model in which taxes are determined independently of Y , the theorem asserts that the balanced budget multiplier is equal to zero. In other words, according to this theorem, if the government increases its purchases and taxes by the same amount $\Delta G = \Delta T$, then output will rise by the same amount, that is, the equality $\Delta G = \Delta T = \Delta Y$ will be fulfilled. It can be shown that this theorem is also valid in Version II of the Keynesian Model (It is not possible to prove the validity of this theorem based on Version I of the Keynesian Model, or model (1)–(6), since government purchases and taxes are not a priori interrelated in it).

Consequently, according to Version II of the Keynesian Model, all else being equal, a tax increase fosters growth of output, but the overall effect obtained in this way is used only to provide for government purchases (the amount of household consumption remains unchanged, in spite of the growth of output; and investments and net exports are also

unchanged, since, according to the assumption, these characteristics are given exogenously in the model and they are fixed).

To clarify why equilibrium output is increasing in relation to the tax rate in Version II of the Keynesian Model, we will first explain the principle of operation of the multiplier λ_2 . We will use the standard method and consider a situation in which the amount of autonomous spending A_2 increases by one unit. This change will cause a multistage process in each stage of which the equilibrium output and the income corresponding to it will grow by a certain amount. In keeping with these stages, we will designate the value of the corresponding increases as $\Delta Y^{(1)}$, $\Delta Y^{(2)}$, $\Delta Y^{(3)}$, and so on.

It is clear that for the first stage $\Delta Y^{(1)}=1$. From this unit increase of income, $(1-t)$ will remain in the private sector, and the other part (t) will go to the government's budget in the form of taxes.

In the second stage, households use the part $b(1-t)$ of their disposable income $(1-t)$ for consumption, which leads to growth of equilibrium output by the same amount. In parallel, the revenue t that the budget receives goes out into the market for goods and services and increases the equilibrium output by the amount t . So in the second stage the total increase in equilibrium output will be $\Delta Y^{(2)} = b(1-t) + t$. It should be noted that, as follows from what was said above, $[b(1-t) + t]$ expresses spending by households and the government to purchase products and services from a unit of income additionally created in the economy. Therefore, $[b(1-t) + t]$ represents the joint marginal propensity of households and the government to purchase products and services.

Considering this circumstance, it is easy to see that for the third stage:

$$\Delta Y^{(3)} = [b(1-t) + t]\Delta Y^{(2)} = [b(1-t) + t]^2.$$

The increments of equilibrium output corresponding to subsequent stages are obtained analogously. Therefore, we will finally write:

$$\Delta Y = \Delta Y^{(1)} + \Delta Y^{(2)} + \Delta Y^{(3)} + \dots =$$

$$= 1 + [b(1-t) + t] + [b(1-t) + t]^2 + [b(1-t) + t]^3 + \dots$$

In a normal situation, $0 < b < 1$ and $0 < t < 1$. On the strength of this,

$$0 < [b(1-t) + t] = [b + (1-b)t] < [b + (1-b)] = 1.$$

Consequently, the derived series is an infinitely decreasing geometric progression, and the following equality is valid:

$$\Delta Y = [1 - b(1-t) - t]^{-1} = \lambda_2.$$

As we see, the main role in the multiplier process of creating equilibrium output is played by the joint marginal propensity of households and the government to purchase goods and services $[b(1-t) + t]$. This parameter is the weighted value of two types of marginal propensity. One of them $-b-$ is the marginal propensity of households to consume, and the other is the marginal propensity of the government to purchase products and services. In the model under consideration, the latter is equal to one, since, according to (12), each additional unit of net tax revenue is fully spent on government purchases. The two values of marginal propensity (b and 1) are weighted according to $1-t$ and t . Since the marginal propensity for government purchases of products and services is greater than b ($0 < b < 1$), the greater the value of t , the higher the joint marginal propensity $[b(1-t) + t]$ will be. And this means that, in the case of a high average tax rate, a large part of the income goes into the market in the form of spending and, all else being equal, the level of equilibrium output is also high.

From what has been said, it follows that when the marginal propensity of households to consume is low in a country, and government purchases are planned in accordance with (12), then to stimulate aggregate demand and increase equilibrium output, it is advisable to raise the average tax rate. At the same time, it should be taken into account that implementing this measure will not affect the total amount of household consumption and will only increase the part of output that will go to providing for government purchases.

Version III of the Keynesian Model. We consider one more version of the Keynesian Model, which differs from Version II given above in how it describes the correlation between G and T . In particular, suppose that only a certain part of the net taxes going to the budget is used for purchases, and the rest is used to service government debt and create a reserve fund. In addition, we will assume that part of the government purchases is determined exogenously and does not depend on taxes. In such conditions, the correlation between G and T can be expressed by the following linear function:

$$G = gT + \tilde{G}_0, \quad (16)$$

where \tilde{G}_0 is the autonomous value of government purchases the amount of which does not depend on taxes and is determined exogenously. In conditions of insufficient tax revenues, this part of purchases can be made through borrowing; and g is the marginal propensity for government purchases. This parameter should be seen as exogenously regulated. Based on the situation existing in the economy, the government can increase or decrease the value of g , but in any case the marginal propensity to purchase must satisfy the condition $0 \leq g \leq 1$, which is a fairly natural requirement.

In model (1)–(6), we replace the condition $G = G_0$ with (16) and call the system thus obtained *Version III of the Keynesian Model*. It is easy to establish that, according to this version, equilibrium output is determined by the following equation:

$$Y = \lambda_3 A_3, \quad (17)$$

where:

$$A_3 = a + I_0 + \tilde{G}_0 + NX_0, \quad (18)$$

$$\lambda_3 = \frac{1}{1 - b(1-t) - gt} = \frac{1}{(1-b) - t(g-b)}. \quad (19)$$

As we see, in this model it is not the total amount of government purchases G that participates in the

creation of autonomous spending A_3 , along with the elements a , I_0 , and NX_0 , as is traditional in the Keynesian Model of aggregate demand, but a part of this amount \bar{G}_0 : autonomous government purchases, that is, purchases whose amount does not depend on net taxes going to the budget. Consequently, the autonomous spending multiplier λ_3 is also different. The latter is determined by the joint marginal propensity of households and government to purchase products and services $[b(1-t) + gt]$, which is the weighted average of b and g . Comparing (9), (15), and (19), we notice that the multipliers λ_1 and λ_2 are particular cases of λ_3 . Specifically, λ_1 is derived from λ_3 in the case when g – the marginal propensity for government purchases – is equal to zero (zero marginal propensity to purchase does not mean that no purchases are made); and if $g = 1$ in (19), then λ_3 turns into λ_2 .

Previously, when considering Versions I and II of the Keynesian Model, it was shown that changes in the average tax rate t affect equilibrium output differently in the cases when $g = 0$ and $g = 1$. Generalization of this fact gives us (17)–(19), from which it follows that in the Keynesian Model the role of the average tax rate is determined by the relationship between the marginal propensity to consume b and the marginal propensity for government purchases g . When $b > g$, a rise in the average tax rate lowers the joint propensity of households and the government to purchase products and services $[b(1-t) + gt]$.

Therefore, all else being equal, an increase in t causes a reduction in equilibrium output. And in the opposite case (i.e., when $b < g$), an increase in the average tax rate causes growth of the joint marginal propensity of households and the government to purchase products and services, which, all else being equal, is a condition that fosters the growth of aggregate demand and, consequently, equilibrium output. And finally, when $b = g$, then both the joint marginal propensity of households and the government to purchase products and services and aggregate demand are indifferent to t .

From the analysis done using the versions of the Keynesian Model examined above, we can draw the following conclusion. The effect of an increase (or decrease) in the average tax rate and taxes as a whole on aggregate demand is not unequivocally negative (or positive), as it is customarily presented in canonical form in contemporary macroeconomics [1, ch. 3; 2, ch. 9; 3, ch. 12; 4, ch. 5]. Depending on what the values of the marginal propensity to consume b and the marginal propensity to purchase g are, in the general case a tax increase can cause either a reduction or growth of aggregate demand. At the same time, since g is a parameter that the government can easily regulate, by selecting its appropriate value the government can purposefully use a tax increase to conduct a stimulating or inhibiting economic policy.

კონომიკა

გასაშუალოებული საგადასახადო ტვირთის ზეგავლენა ერთობლივ მოთხოვნაზე (კეინზიანური მოდელები)

ი. ანანიაშვილი*, ვ. პაპაია*

* ი. ანანიაშვილის სახელობის თბილისის სახელმწიფო უნივერსიტეტი, თბილისი

** აკაღმის წერილი: ვ. გუგუშვილის კონომიკის ინსტიტუტი, ი. ანანიაშვილის სახელობის თბილისის სახელმწიფო უნივერსიტეტი, თბილისი

სტატიაში საქონლის ბაზრის სტანდარტული კეინზიანური მოდელების გარდაქმნილი ვარიანტის ანალიზის საფუძველზე დასაბუთებულია, რომ ერთობლივ მოთხოვნაზე საშუალო საგადასახადო განაკვეთის და მთლიანობაში გადასახადების ზრდის (კლებების) ზემოქმედება ისე ცალსახად უარყოფითად (დადებითად) არ არის განსაზღვრული, როგორც ეს კანონიკური სახით თანამედროვე მაკროეკონომიკაშია მიღებული. იმაზე დამოკიდებულებით, თუ როგორია მოხმარებისადმი შინამეურნეობების მიდრეკილების და შესყიდვებისადმი სახელმწიფოს მიდრეკილების მნიშვნელობები, გადასახადების გადიდება ზოგად შემთხვევაში შეიძლება გამოიწვიოს ერთობლივი მოთხოვნის როგორც შემცირება, ისე გადიდება. ამასთან, რადგანაც შესყიდვებისადმი ზღვრული მიდრეკილება სახელმწიფოს მხრიდან თავისუფლად რეგულირებადი პარამეტრია, ამიტომ მისი შესაბამისი მნიშვნელობის არჩევით გადასახადების ზრდა მთავრობის მხრიდან მიზანმიმართულად შეიძლება გამოყენებულ იქნას როგორც წამახალისებელი, ისე დამუხრუჭებელი ეკონომიკური პოლიტიკის გასატარებლად.

REFERENCES

1. R. Dornbusch, S. Fisher (1990), *Macroeconomics*. New York: McGraw-Hill Publishing Company.
2. N. G. Mankiv (1992), *Macroeconomics*. New York: Worth Publishers.
3. J. D. Sachs, F. Larrain B. (1993), *Macroeconomics in the Global Economy*. Englewood Cliffs, N.J.: Prentice Hall.
4. O. Blanchard (2009), *Macroeconomics*. Upper Saddle River, N.J.: Prentice Hall.
5. I. Ananiashvili (2008), Tax Impact on Aggregate Demand. *Economics and Business*, 3 (in Georgian).
6. B. Akitoby, B. Clements, S. Gupta, G. Inchauste (2006), Public Spending, Voracity, and Wagner's Law in Developing Countries. *European Journal of Political Economy*, 22, online at http://www2.warwick.ac.uk/fac/soc/economics/ug/modules/3rd/ec320/details/wagners_law.pdf.
7. M. G. Kolosnitsina (2003), *Ekonomika obshchestvennogo sektora: gosudarstvennye rashody* [Economics of the Public Sector: Government Spending]. *Ekonomicheskii Zhurnal VShE* [The HSE (Higher School of Economics) Economic Journal], 3 (in Russian).
8. L. Matthiessen (1966), A Note on the Haavelmo Theorem. *The Swedish Journal of Economics*, 68, 4.
9. H. Herr, M. Kazandziska (2011), *Macroeconomic Policy Regimes in Western Industrial Countries*. Oxon: Routledge.

Received March, 2012

Economics

Capitalization of Mineral Commodities – World and Georgian Experiences

Alexander Tvalchrelidze* and Avtandil Silagadze**

* *Georgian Academy of Natural Sciences, Tbilisi*

** *Academy Member; Georgian National Academy of Sciences, Tbilisi*

ABSTRACT. The recent world economic crisis had a huge impact on Georgia's social & economic framework. The sole possibility to avoid the negative influence of global deteriorating economic tendencies is to base economic and, first of all, industrial development of the country on national natural resources and commodities. However, extensive use of Georgia's mineral commodities is slowed down due to lack of possibility to capitalize them at early stages of exploration. The present article proposes a new economic method, which allows computing the Net Present Value of an eventual mining enterprise at the early stage of exploration. In turn, such analysis provides indicators not only for assessment of the volume of possible venture investment in exploration but also for immediate capitalization of eventual commodities on international commodity markets. © 2012 Bull. Georg. Natl. Acad. Sci.

Key words: capitalization, mineral resources, Net Present Value (NPV).

The recent world economic crisis had a huge impact on Georgia's social & economic framework: the rate of economic development and volume of direct foreign investments significantly decreased; on the contrary, the inflation rate, volume of foreign debts, number of population under the poverty line increased dramatically [1]. Within the given realms the sole possibility to avoid negative influence of global deteriorating economic tendencies is to base economic and, first of all, industrial development of the country on national natural resources and commodities [2]. It should be noted that the same problem arose by the end of the 19th century, and the well-known national public leader Niko Nikoladze proposed the same remedy [3].

However, extensive use of Georgia's extremely rich natural resources [2] and, first of all, of mineral commodities is slowed down due to lack of the possibility to capitalize them at early stages of feasibility studies and exploration, namely, in case of so-called "greenfields", e.g. areas where deposits of mineral resources are still undiscovered but which according to geological criteria are prospective on certain kinds of mineral commodities. Thus, a mining company always has to solve a dilemma – either to perform a venture investment in regional exploration or to abandon a greenfield. Econometrics of venture investments in exploration was thoroughly investigated by P. de Verte Harris [4] and other researchers. However problems of capitalization of these poten-

tial commodities are still unexplored.

In this article we will try to solve the mentioned problem.

Any mining enterprise performs capitalization of their mineral resources pro rata the Net Present Value (NPV) of eventual mining activity [5-6]. According to the classical definition [7], NPV may be computed by the following equation:

$$NPV = \int_{n=1}^t \alpha_n \frac{\partial P^n}{\partial t}, \quad (1)$$

where NPV means Net Present Value, α_n is discounting factor, P^n is annual nominal net profit of the year n , t - term of mining activity.

It is clear from the equation (1) that in a classical case computing of NPV is possible only in terms of feasibility studies and, according to the existing financial theory, is impossible for greenfields. That is why early exploration of greenfields is a venture business and its financial viability greatly depends on the experience of the exploration team. Hence, there is a possibility to discount NPV even at the early stage of exploration. In this case calculations could be based on the so-called Price Index (I_p), which was introduced in 1995 [8]:

$$I_p = P_s Q_0, \quad (2)$$

where P_s is specific price of 1 unit (e.g. t or m³) of a commodity, Q_0 - resources of commodities.

Then

$$P_s = \sum_i P_i C_i k_{Ei} - K_0, \quad (3)$$

where P_i is specific market price of i constituent of ores, C_i is its grade in ores, K_{Ei} its extraction factor from ores, and K_0 operational cost of ore processing chain ranging from ore mining to production of the market commodity.

In this case

$$NPV = \int_{n=1}^t \alpha_n \frac{\partial I_p^n}{\partial t}, \quad (4)$$

In course of economic assessment of greenfields all

resources of neighboring mineral deposits should be thoroughly registered. But in this case the reliability of estimated resources must be taken into account [9]:

$$Q_i = \sum_j Q_{ij} + k_{In} Q_{In} + k_{If} Q_{If} + k_{Sp} Q_{Sp}, \quad (5)$$

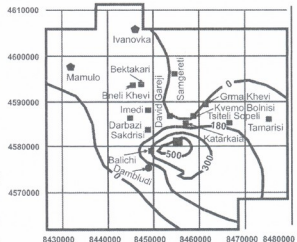
where k_{In} k_{If} k_{Sp} are confidence factors of indicated, inferred and speculative resources, Q_{In} Q_{If} Q_{Sp} - amount of indicated, inferred and speculative resources of the ores' constituent i .

Now, for processing these primary data the Kriging method may be used [10]:

$$Q_{i+1}^{X,Y} = Q_i^{X,Y} + a(Q_i^{X,Y})^{-1} + b(Q_i^{X,Y})^{-2} + \dots + n(Q_i^{X,Y})^{-n}, \quad (6)$$

where $Q_{i+1}^{X,Y}$ = resources in $i+1$ point, $Q_i^{X,Y}$ = resources in i point, X, Y - coordinates' matrix:

$$X, Y = \begin{pmatrix} x_1 y_1 & x_1 y_2 & \dots & x_1 y_n \\ x_2 y_1 & x_2 y_2 & \dots & x_2 y_n \\ \dots & \dots & \dots & \dots \\ x_n y_1 & x_n y_2 & \dots & x_n y_n \end{pmatrix} \quad (7)$$



Type of mineralization

- Madneuli Mine
- Epithermal Au-Cu-Pb-Zn
- Vein Au-Cu-Pb-Zn
- ★ Porphyry Cu

Fig. NPV per Square Kilometer in Bolnisi Mining District, USD Million

This method may be used for computing NPV per square kilometer. Let us consider, for example, the case of Bolnisi Mining District where a number of gold-bearing polymetallic deposits is known but exploration of greenfields is not yet scheduled. Computing resources of gold, silver, copper, lead and zinc in each deposit according to formula (5), identifying the specific price of each deposit according to formula (3), then, extrapolating the resources in two-dimensional space according to formula (6) and computing NPV in each x_n, y_n point according to equation (4), one would

be able to provide a picture of NPV per square kilometer for the whole mining district. This information is provided in Figure.

Analysis of these data calls for exploration of the south-eastern part of the district, which has never been the subject of specific interest of the exploration teams. In addition, such analysis provides indicators not only for assessment of the volume of possible venture investment in greenfields but also for their immediate capitalization on international commodity markets.

ეკონომიკა

მინერალური ნედლეულის კაპიტალიზაცია – მსოფლიო და ქართული გამოცდილება

ა. თვალჭრელიძე*, ა. სილაგაძე**

* საქართველოს საბუნებისმეტყველო აკადემია

** აკადემიის წევრი, საქართველოს მეცნიერებათა ეროვნული აკადემია

ბოლო წლების მსოფლიო ეკონომიკურმა კრიზისმა მძიმე გავლენა იქონია საქართველოს სოციალურ-ეკონომიკურ გარემოზე. ერთადერთი შესაძლებლობა, დაძლეულ იქნას ნეგატიური მსოფლიო ეკონომიკური ტენდენციები, — ქვეყნის ეკონომიკური და, უპირველეს ყოვლისა, სამრეწველო განვითარებისთვის ეროვნული ბუნებრივი რესურსებისა და ნედლეულის რაციონალური გამოყენებაა. ამასთან, საქართველოს მინერალური ნედლეულის ინტენსიურ გამოყენებას ხელს უშლის ძიების ადრინდელ ეტაპებზე მათი კაპიტალიზაციის შეუძლებლობა. ნაშრომში შემოთავაზებულია ახალი ეკონომიკური მეთოდი, რომელიც შესაძლებლობას იძლევა გამოითვალოს დასაპროექტებელი სამთო საწარმოს დისკონტირებული ღირებულება ძიების ადრინდელ ეტაპებზე. გარდა ამისა, შემოთავაზებული მეთოდი შეიცავს ინდიკატორებს არა მხოლოდ ძიებაში ვენჩურული ინვესტირების მოცულობის შესაფასებლად, არამედ მსოფლიო სანედლეულო ბაზრებზე აღმოსაჩენი ნედლეულის დაყოფილებული კაპიტალიზაციისთვის.

REFERENCES

1. A. Tvalchrelidze and A. Silagadze (2011), Central Asia and the Caucasus, **12**, 4 : 110-127.
2. A. Tvalchrelidze, A. Silagadze, G. Keshelashvili and D. Gegia (2011), Sakartvelos sotsialur-ekonomikuri ganvitarebis programa [Georgia's social & economic development program]. Tbilisi, 312 p. (in Georgian). English version available at <http://www.ifsdeurope.com/presentation.html>.
3. N. Nikoladze (1960-1962), Collected works. Vol. 1, 2. Tbilisi, (in Georgian).
4. P. de Verte Harris (1984), Mineral Resources Appraisal: Mineral Endowment, Resources, and Potential Supply Concepts, Methods, and Cases. London, 445 p.
5. The Economics of Primary Commodities: Models, Analysis, Policy (1994), David Sabsford (ed.), University of Liverpool, 192 p.
6. Y. Chen and K. Rogoff (2003), Journal of International Economics, **60**, 1: 133-160.
7. M.Y. Khan and P.K. Jain (1999), Theory and Problems in Financial Management, Boston, 441 p.
8. A.G. Tvalchrelidze (1995), Development of a Geological-Economic System for Governmental Management of Georgian Mineral Resources. Tbilisi, 87 p.
9. A.G. Tvalchrelidze (2006), Poleznye iskopaemye i mineral'naia resursnaia baza Gruzii [Mineral Resources and the mineral resource base of Georgia]. Moscow, 320 p. (in Russian).
10. J. Sacks, W.J. Welch, T.J. Mitchell, and H.P. Wynn (1989), Statistical Science, **4**, 4: 409–435.

Received April, 2012

History

The Byzantine Thema of Soteroupolis-Anakopia in the 11th Century

Werner Seibt

Austrian Academy of Sciences, Department for Byzantine Research, Vienna, Austria

(Presented by Academy Member Thomas V. Gamkrelidze)

ABSTRACT. A Byzantine Thema was established in Georgian Abkhazia ca. 1033, when the second wife of the Georgian king Giorgi, Elda or Alde, donated her *apanage* to the emperor Romanos III Argyros. Soteroupolis is surely a mediaeval name for Pityous/Bičvinta/Picunda. Probably also the palace of Likhni belonged to this Thema.

About 1044-1045 the Georgian king Bagrat laid siege to Anakopia but could not conquer it. About this time a certain Nicholas with the Title of Protospatharios was Strategos of the Thema. Only ca. 1074 the Georgians seem to have regained Anakopia and the rest of the Thema. © 2012 Bull. Georg. Natl. Acad. Sci.

Key words: Byzantine history (11th century), Georgian history (11th century), Abkhazia (11th century), Anakopia, Soteroupolis/Bičvinta.

In the 11th century the Byzantine expansion in the East extended all the way to the modern Georgian province of Abkhazia. No war of aggression was necessary, for it was by good fortune that the emperor was able to take possession of an important part of this region.

The Georgian king Giorgi (1014-1027) was married to Mariam, the daughter of the Armenian king Senek'erim Yovhannēs of Vaspurakan, his ally, when he planned a war against the Byzantine emperor Basil II. But Giorgi was defeated before the allies could bring support in 1022. Senek'erim lost his kingdom [1, 2], Giorgi lost only small territories but presumably was forced to divorce Mariam and to marry a daughter of the king of Alania as his second wife,

who was probably called Elda (in Greek Ἀλδή; in the old Alanic Narten-epos we find the form Elda, Osetian variants are Aldä, Āldi, in Georgian Alda, Aldi, Alde) [3]; Ioannes Skylitzes says only Ἀλδή ... τοῦ γένους οὔσα τῶν Ἀλανῶν [4], but the Georgian source Matiane Kartlisa specifies her as "daughter of the king of the Osetians" [5: Georg.295,6f. Cf.; Rus.47; Germ.368], using in a misleading way one and the same denomination for Alans and Osetians [6].

Giorgi had a son with this Elda, Demetre, but apparently after some time (Basil had passed away in 1025), Mariam returned to her husband. When Giorgi died (1027) Elda was living in her *apanage* in Abkhazia in the region of Anakopia (near the modern town New Athon) with her small son, far from the

court, but Mariam became regent in the Georgian realm in the name of her son Bagrat, who was only then nine years old.

Given the weak position of the Georgian monarchy in relation to the power of the *didebulis*, the big landlords, any alliance of dissenting lords were in a position to choose Demetre as a rival candidate to the throne and consequently his presence on Georgian territory was a threat to king Bagrat.

Whether such an enterprise was set in motion or only prepared, Elda nevertheless left Georgia together with her son circa 1033 and travelled to Konstantinople, where she was welcomed by emperor Romanos III Argyros (1028-1034). Elda donated her possessions to the emperor, who bestowed the title *Magistros* on Demetre. The Byzantine historian Ioannes Skylitzes mentions only Anakopia as the new Byzantine stronghold [4:48f.], and the Georgian source, Matiane Kartlisa, corroborates only this [5: Georg. 295,6-12]. So these sources cannot yield more information about the borders of this new Byzantine realm.

Under these conditions it was a happy circumstance that some years ago a Byzantine lead seal was found in Bulgaria mentioning a certain Nicholas with the Title “imperial Protospatharios of the Chrysotriklinos” and the command of a “Strategos of Soteroupolis and Anakoupia”. On both sides of the seal only the inscription: Κ(ύρι)ε β(σι)ήθ(ε)ι Νικολάω (πρω)τοσπαθ(αρίω) ἐπὶ τοῦ χρ(υσο)(τρι)κλ(ι)ν(ου) | (καί) στρατηγ(ῶ) Σ(ωτηρ)ουπόλ(εως) (καί) Ἀν(α)κουπί(ας).

The object dates from about the middle of the 11th century [7]. The seal provides definitive proof that there was established a real Byzantine Thema in this region, and that Soteroupolis belonged to it.

Though there is some discussion about the localization of Soteroupolis (some scholars mixed it up with the other Soteroupolis/Bourzo on the Çoruh, scil. Borçka, modern Yeniyol [8], others searched for it near Batumi [9], there can be no doubt that it is identical with Bičvinta/Picunda, the old town of Pityous, north of Anakopia. And taking into account

that the palace of Likhni/Lykhny [10] lies between these two centres we may assume that also this place was integrated into the Byzantine hegemony. It would have been strategic nonsense to combine Anakopia in Abkhazia with a place upstream on the Çoroh so far away, not even situated on the seashore! And it is well known that Soteroupolis in Abkhazia was an archbishopric of the Oecumenical Patriarchate of Constantinople from the time of the 10th century, very often combined with the metropolis Alania since the early 12th century [11].

About 1044-1045 the Georgian king Bagrat attacked the Byzantine realm in Abkhazia and laid siege to Anakopia. In these years the Byzantine reputation in the East was damaged, as its armies had great difficulties in occupying Greater Armenia after the death of king Yovhannēs Smbat and his brother Ašot IV (1041), who had been forced in 1022 to accept the Byzantine emperor as their heir. Michael Isaites, the military commander of the Byzantine Ducate Iberia (established in 1000 after the death of Davit Kuropalates of Tao, a vast territory reaching as far as Mantzikert in the south), was ordered to occupy Greater Armenia with his forces, but he failed. As a consequence of the usurpation of Georgios Maniakes and the civil war that followed there were no new Byzantine initiatives against Armenia, where a new Armenian king was established, Gagik II. Only in 1044 was the war against Armenia resumed under the command of Michael Isaites and Nicholas, the *Domestikos* of the East (a kind of *Generalissimus*); in the spring of 1045 the Byzantine forces could enter Ani, the capital of Greater Armenia, but the problems did not end with this success, as there followed a war against the former ally Abu’l Aswār, the Kurdish Emir of Dvin [2: 154-158; 12]. The role of the Georgian king in these wars is not quite clear, but it seems that his troops occupied some northern Armenian places at least for some time, presumably in cooperation with the Armenian leader Sargis Bestes [2: 158f.; 13].

About this time Bagrat laid siege to Anakopia. But, according to the official version in the Georgian

Chronicle, he hurried away to Tbilisi when he was informed about the death of the Emir Jafar, seeing in this circumstance a chance to gain control of this Emirate (ca. 1046), leaving behind in front of Anaḱopia Otayo, the son of Ḳaḱa Kuabulel, but it all was in vain [5: 6-10]. After a lapse of time surely Byzantine reinforcements had arrived in Abkhazia and the Georgian troops resigned. Perhaps Nicholas was precisely at this time Strategos of Anaḱopia and the seal originates from a letter to the Dux of Paristrion/Paradounabon informing him about the arrival of a strong Georgian army and asking for assistance.

After the retreat of the Georgian army the Byzantines started to renovate damaged buildings, and some inscriptions give us information about that; as they were re-edited recently [14: 209-224; 268f.] there is a good foundation for further research. On an inscription from the church of St. Theodore on the top of the Anaḱopia fortress we learn about the restoration of a cistern in February 1046 (not 1047! [14: 269, "in February, 1074]); the emperor Konstantine Monomachos is mentioned, and we read also δηḱ συνδὸρμηḱ Εὐγενίου προτωσπαθαρῖου ὁ τοῦ δεσπότης κῆ Θεοδῶρου ταξιάρχου Κασῆς τοῦ Βιḱάντη [14: 215; Plates, Fig. 3]. Despotēs is surely not the surname or family name of Eugenios, the well-known Byzantine formula ὁ τοῦ can mean "nephew of a despotēs", yet despotēs can also be a bishop or archbishop, e.g. the one of Soteroupolis! I would prefer to see in Eugenios a landlord in the Byzantine realm in Abkhazia, rather than the Strategos, as Vinogradov proposed. Theodoros on the other hand was a military commander, but perhaps only temporarily detached to strengthen the troops in the Thema, coming from the Thema Kassenon north-east of Kaisarēia [15]. A Turma Κασῆς is already mentioned in *De administrando imperio* [16, 17]. The family name is not so clear; is it a special form of Balantes, Balantios, Abalantes etc.?

And there is another inscription from March 1046, mentioning again Eugenios, whose title is reduced to Αḱ (for προτωσπαθαρῖου), followed by ὁ τοῦ δ[...];

after that the editors want to read the name Alda, but the letter vestiges to my mind do not support this hypothesis; then we read again κῆ Θεοδῶ[ρου] τα[ξι]άρχου Κασῆς τοῦ Β[...]; it is not so clear if after the last Beta follows Alpha or Iota [14: 217; Plates, Figs 4,5, 16,40]. A third inscription mentions the re-consecration of the church of St. Theodore by Michael, archbishop (probably of Soteroupolis) on April 16. Vinogradov wants to read 2nd indiction (dating the inscription to 1049), but that is not for sure [14: 218f; Plates, Figs 4,6,41].

In the following years there was peace on the Byzantine-Georgian border in Abkhazia till the early 70s of the 11th century. After the catastrophe of Mantzikert (1071) the Byzantine position in the East was again extremely damaged. About 1074 the Georgians seem to have regained Anaḱopia and the rest of this Thema, and also Byzantine possessions in Northeast Anatolia, including the city of Kars [18, 19], but this one only for a limited number of years, because here the Georgians were again expelled by a Seljuk army under Emir Aḱmad ca. 1080; afterwards Kars came again under Byzantine control under the Dux Georgios Alousianos Protonobellissimos [15: 20f; 20]. In the last chapter of Matiane Kartlisa we read that the Georgian king Giorgi II (1072-1089) was able to regain the Georgian cities occupied by the Byzantines, and as most importantly Anaḱopia is mentioned there [5: Georg.317,16; Rus. 61; Germ.394].

On maps of Historical Geography the "new" Thema should be considered in the future. The important new Georgian *Sakartvelos istoriis atlasti* [21: 22f.] does not yet consider it, and so too the map B VII 16 of the "Tübinger Atlas des Vorderen Orients", titled "Armenien und Georgien im 10. und 11. Jahrhundert" [22]. In the new atlas "Armenia. A Historical Atlas" R. H. Hewsen notes the "Byzantine enclave" on map 105, "The Third Byzantine Expansion into Armenia, 966-1064" [23], but in a wrong place, situating it in the vicinity of Sebastoupolis/Suchumi, a region which did not in fact belong to this Thema.

ისტორია

სოტერუპოლის-ანაკოფიის ბიზანტიური თემა XI საუკუნეში

ვ. ზაიბტი

ავტორის შეცნობებითაა აკადემია, ბიზანტიური კვლევების ლუბარტამენტი, ვენა, ავსტრია

(წარმოდგენილია აკადემიკოს თ. გამყრელიძის მიერ)

ბიზანტიური თემა საქართველოს აფხაზეთში ჩამოყალიბდა დაახლოებით 1033 წელს, როცა საქართველოს მეფის, გიორგის, მეორე მეუღლემ, ელდამ ან ალდემ, თავისი აპანაჟი ძღვნად მიართვა იმპერატორ რომანოს III არგიროსს. სოტერუპოლისი უნდა იყოს პიტიუნტ-ბიჭვინთა-პიცუნდის სახელი შუა საუკუნეებში. საყარაულოდ, ლიხნის სასახლეც ამ თემს ეკუთვნოდა.

დაახლოებით 1044-1045 წლებში ქართველთა მეფე ბაგრატმა ალფა შემოართვა ანაკოფიას, მაგრამ ვერ მოახერხა მისი აღება. ამ პერიოდში თემის სტრატეგოსი იყო პროტოსპატარიონი ნიკოლოზი. მხოლოდ 1074 წლისთვის ქართველებმა, როგორც ჩანს, შესძლეს ანაკოფიისა და თემის დანარჩენი ნაწილის დაბრუნება.

REFERENCES

1. *W. Seibt* (1978), Die Eingliederung von Vaspurakan in das Byzantinische Reich (etwa Anfang 1019 bzw. Anfang 1022). *Handes amsoya*, 92: 49-66, esp. 58-63.
2. *W. Felix* (1981), Byzanz und die islamische Welt im früheren 11. Jahrhundert (Byzantina Vindobonensia, 14). Vienna, 139f.
3. *S. Fritz* (2006), Die ossetischen Personennamen (Iranisches Personennamenbuch III/3). Vienna, 10, 30, 90.
4. *Skyllitzes* (ed. Thurn), A Synopsis of Byzantine History, 389.
5. *Matiane Kartlisa* [Chronicle of Kartli] (ed. Quakhchishvili, in: *Kartlis Tskhovreba* I, Tbilisi 1955), 295, 6f. (in Georgian); cf. also the Russian translation by M. D. Lordkipanidze (Tbilisi 1976), 47, and the German translation by G. Pättsch (Leipzig 1985), 368.
6. *W. Seibt* (2012), Die orthodoxe Metropolis „Kaukasos“, in: J. Tubach, S. G. Vashalomidze, M. Zimmer (edd.), *Caucasus during the Mongol Period – Der Kaukasus in der Mongolenzeit*. Wiesbaden, 244f.
7. *W. Seibt, I. Jordanov* (2006), Στρατιωτὸς Σοτηροπόλεως καὶ Ἀνακοπιᾶς. Ein mittelbyzantinisches Kommando in Abchazien (11. Jahrhundert). *Studies in Byzantine Sigillography*, 9 (München–Leipzig), 234f.
8. *Iskusstvo Abkhazskogo tsarstva VIII-XI vekov. Khristianskie pamiatniki Anakopiiskoi kreposti* (2011). St. Petersburg, 264 (in Russian).
9. *B. Martin-Hisard* (2000), Constantinople et les archontes du monde caucasien dans le *Livre des cérémonies*, II, 48. *Travaux et Mémoires*, 13, esp. 530.
10. *L. G. Khrushkova* (1998), Lykhny. Srednevekovyi dvortsovyi kompleks v Abkhazii. Moscow (in Russian).
11. *O. Kresten* (2002), Die Affäre des Metropoliten Symeon von Alania im Spiegel des Patriarchatsregisters von Konstantinopel. *Anzeiger d. phil.-hist. Klasse (d. Österr. Akademie d. Wissenschaften)*, 137, esp. 11-14.
12. *W. Seibt* (2009), Das byzantinische Militärkommando „Iberia“. In: *Scientific Paradigms*. Tbilisi, 151f.

13. E. Honigmann (1935), Die Ostgrenze des Byzantinischen Reiches von 363 bis 1071 nach griechischen, arabischen, syrischen und armenischen Quellen (A. A. Vasiliev, Byzance et les Arabes, vol. III). Brussels, 174-176.
14. A. In. Vinogradov (2011), Epigrafika. Nadpisi s Anakopiiskoi gory. In: Iskusstvo Abkhazskogo tsarstva VIII-XI vekov. Khristianskie pamiatniki Anakopiiskoi kreposti. St. Peterburg, 209-224 (in Russian); English abstract 268f.
15. W. Seibt (2011), Zukunftsperspektiven der byzantinischen Siegelkunde – Auf welchen Gebieten sind die bedeutendsten Wissenszuwächse zu erwarten? In: Ch. Stavrakos, B. Papadopoulou (edd.), Πρακτόνδε. Proceedings of the 10th International Symposium of Byzantine Sigillography (Ioannina, 1-3 October 2009). Wiesbaden, 24f.
16. De administrando imperio (ed. G. Moravcsik, Washington, D.C. 1967), 50, 110.
17. F. Hild – M. Restle (1981), Kappadokien (Kappadokia, Charsianon, Sebasteia und Lykandos). Tabula Imperii Byzantini, vol. II. Vienna, 202, s. v. „Kasē“.
18. W. Seibt, I. Jordanov (2006), Strategos Soteroupoleos 238.
19. W. Seibt (2012), Byzantine Imperialism against Georgia in the Later 10th and 11th Centuries? Tbilisi (in print).
20. W. Barthold, C. J. Heywood, Kars. EI IV (1978) 697.
21. D. Muskhelishvili, Edit.(2003), Sakartvelos istoriis atlati [Atlas of Georgian History].Tbilisi, 22f. (in Georgian).
22. R. H. Hewsen (1988), TAVO B VII 16.
23. R. H. Hewsen (2001), Armenia. A Historical Atlas. Chicago-London, 125.

Received June, 2012

მეზუური ავტორთათვის

1. წარმოდგენილი სტატია დაბეჭდილი უნდა იყოს A4 ფორმატის თეთრ ქაღალდზე ორი ინტერვალით, ზედა და ქვედა არეები – 20-20 მმ, გვერდითი არეები - 30-30 მმ. სტატიის სიგრძე არ უნდა აღემატებოდეს 12 ნაბეჭდ გვერდს, ფორმულების, ცხრილებისა და სურათების ჩათვლით.

2. სტატია წარმოდგენილი უნდა იყოს ინგლისურ ენაზე მთავარი რედაქტორის სახელზე. სტატიას უნდა ახლდეს აგრეთვე:

- ცნობები ავტორის (ავტორების) შესახებ, მოცემულ შრომაში მისი წვლილის აღნიშვნით;
- აკადემიის წევრის წარდგინება ან ორი კვალიფიციური რეცენზია სხვადასხვა ინსტიტუტიდან (თუ ავტორი არ არის აკადემიის წევრი); მიმართვა რედაქციის სახელზე გამოქვეყნების თხოვნით იმ დაწესებულებიდან, სადაც შესრულებულია შრომა;

სტატიას განიხილავს სარედაქციო საბჭო და გადაწყვეტს მისი გამოქვეყნება-არაგამოქვეყნების საკითხს.

3. სტატია უნდა გაფორმდეს შემდეგი სახით:

- მეცნიერების დარგი;
- სტატიის სათაური;
- ავტორის (ავტორების) სრული სახელი, გვარი;
- სამუშაო ადგილი, საფოსტო მისამართი, ელექტრ. ფოსტა;
- ნაშრომის წარმომდგენი აკადემიის წევრის გვარი;
- რეზიუმე;
- საკანძო სიტყვები;
- ტექსტი. ტექსტის ბოლოს დაფინანსების წყაროს და მადლობების ჩამონათვალი;
- ინგლისური ტექსტის შემდეგ რეზიუმე ქართულ ენაზე (გაფორმებული იმავე თანმიმდევრობით, როგორც ინგლისური ტექსტი), მოცულობა ერთ გვერდამდე;
- დამოწმებული ლიტერატურის სა უნდა დალაგდეს ტექსტში ციტირების მიმდევრობის მიხედვით (ლიტერატურა ტექსტში აღნიშნული უნდა იყოს ციფრებით კვადრატულ ფრჩხილებში);

- ნახაზები და ცხრილები მოცემული უნდა იყოს ცალკე გვერდებზე. ფოტოები – ორიგინალის სახით;

- სურათებს უნდა ახლდეს წარწერები;

სტატიის ბოლო გვერდზე უნდა იყოს ყველა ავტორის ხელმოწერა (გარკვევით).

4. ელექტრონული ვერსია: CD-ROM, შრიფტი Times New Roman. ტექსტი: Supply – Word, Word Perfect, RTF. ცხრილები და ნახაზები წარმოდგენილი უნდა იყოს ცალკე ფაილად, ნახაზები უნდა შესრულდეს TIFF, EPS, მაღალი ხარისხის PDF, JPEG, ცხრილები: Word, Word Perfect, RTF. ფორმულები Equation 3.0, Equation 5.0;

5. სტატიის ტიპოგრაფიული თუ ელექტრონული სახით გამოქვეყნებაზე ავტორმა უნდა განაცხადოს თანხმობა;

მიღებული სტატიის გასწორებული ვერსია, ან დაწუნებული ნაშრომი ავტორს არ უბრუნდება.

სარედაქციო საბჭო არ განიხილავს ნაშრომს, რომელიც მოთხოვნების მიხედვით არ იქნება გაფორმებული.

ავტორს შეუძლია ნიმუშად გამოიყენოს ჟურნალის რომელიმე ნომერი.

6. რუსული ტექსტის ტრანსლიტერაცია მოცემულია ლათინური ასოებით კონგრესის ბიბლიოთეკის სისტემის მიხედვით.

7. ნაშრომის გამოქვეყნება უფასოა.

GUIDE FOR AUTHORS

Manuscripts should be presented in the following form:

1. Two double-spaced copies of the manuscript, printed on a white paper A4, marginated 20 mm below and above, 30 mm on the sides, must be provided. The length of the manuscript should not exceed 12 printed pages, including all text with figures, tables, and equations.

2. Manuscripts should be written in English and sent to the Editorial Board. Attached to the manuscript should be:

- Short information about the research work by the author(s), including specific contribution to the published work;

- Qualified references from different Institutions;

Articles will be evaluated by the Editorial Board and may be rejected or subjected to further review.

3. Manuscript order:

- Classification;

- Title;

- Full name(s), surname(s) of the author(s);

- Affiliation(s), postal address, e-mail;

- Abstract;

- Key words;

- Text, including acknowledgements and funding sources;

- References in the order of citation (square brackets used);

- Figures and Tables must be given on separate pages. Pictures and photos must be original;

- Figure legends;

- The last page of the manuscript must be signed by the author(s).

4. Electronic version: CD-ROM in Times New Roman. Text: Supply Word, Word Perfect, RTF.

Figures and Tables must be submitted as separate files, not imbedded in manuscript text. Provide figure images in TIFF, EPS, high resolution PDF, JPEG. Tables: Supply Word, Word Perfect, RTF. Include one Table per file. Do not use tabs or spaces to separate columns in Word or Word-Perfect Tables.

5. The author will be asked to give consent to publish the manuscript in print and electronic version. Corrected version is not returned to the author(s). The Editorial Board reserves the right not to consider the paper, if the instructions are ignored. For symbols and style conventions, authors should consult current issues of the Journal.

6. Transliteration of the Russian text into Roman letters should be given according to the LC system.

7. Publication is free of charge.

*Starting with the year 2009 each Volume of the
Bulletin of the Georgian National Academy of Sciences
appears in three Issues annually*


Subscription Information:

Correspondence regarding subscriptions and manuscript publications should be sent to:

Georgian National Academy of Sciences,
52, Rustaveli ave, 0108 Tbilisi, Georgia
Phone: +995-32 99-75-93
Fax/Phone: +995-32 99-88-91
E-mail: Bulletin@science.org.ge

The online edition of the *BULLETIN* is available
from the website of the Academy at:
<http://www.science.org.ge>
<http://www.science.org.ge/moambe/moambe.html>

© საქართველოს მეცნიერებათა ეროვნული აკადემიის შიდაგეგმა, 2012
Bulletin of the Georgian National Academy of Sciences, 2012

GEORGIAN NATIONAL ACADEMY OF SCIENCES  საქართველოს მეცნიერებათა ეროვნული აკადემია

0108 Tbilisi, Georgia
52 Rustaveli ave
Tel.: (+995 32) 2 99 88 91;
Fax/Tel.: (+995 32) 2 99 88 23
E-mail: bulletin@science.org.ge
academy@science.org.ge

0108 თბილისი,
რუსთაველის პროსპ. 52
ტელ.: 2 99 88 91; ფაქსი: 2 99 88 23
ელ. ფოსტა: bulletin@science.org.ge
academy@science.org.ge